UNIVERSITY OF SOUTHAMPTON

FACULTY OF PHYSICAL SCIENCES AND ENGINEERING

Department of Physics and Astronomy

Dynamic AdS/QCD: A holographic approach to asymptotically free gauge theories.

by

Marc Alexander Scott

A thesis submitted in partial fulfilment for the

degree of Doctor of Philosophy

September 2016

UNIVERSITY OF SOUTHAMPTON

Abstract

FACULTY OF PHYSICAL SCIENCES AND ENGINEERING

PHYSICS

Doctor of Philosophy

Dynamic AdS/QCD: A holographic approach to asymptotically free gauge theories.

by

Marc Alexander Scott

Dynamic AdS/QCD is a bottom-up model inspired from top-down, probe-brane extensions to the renowned AdS/CFT correspondence. The AdS/CFT correspondence states that there is an equivalence in the physics describing an $\mathcal{N} = 4$ super-Yang-Mills gauge theory and that pertaining to a type IIB superstring theory on an $AdS_5 \times S^5$ background. Moreover, the duality between the two theories in a particular limit requires that the gauge theory be strongly coupled when the superstring theory is weakly coupled. From this, we have a tool for studying strongly coupled gauge theories in a physically equivalent gravitational description. Using the AdS/CFT correspondence as a springboard, relationships between more complex superstring constructions on varying backgrounds have been studied to push the dual gauge theory to be more like those of QCD. In this thesis, we use one such bottom-up model, Dynamic AdS/QCD, to probe the behaviours of strongly coupled, asymptotically free gauge theories, including QCD. We show that the model correctly describes the hyperscaling relations of quark masses and the condensate, the behaviours expected of the scalar, vector and axial meson spectra in theories with infrared fixed points and how the condensate is affected by temperature and magnetic field in such theories. We finally go on to show that it is possible to describe QCD-like theories with a Lorentz-symmetry breaking vacuum, e.g. a striped condensate, and follow up with the cosmological ramifications of such a proposal and conclude that outside of a totally disconnected dark sector, this behaviour is highly constrained.

Contents

List of Figures xiii

List of Tables xv

Declaration of Authorship xvii

Acknowledgements 1

I Part One: Foundations 3

1 AdS/QCD: A History 5

1.1 The road to 1974 . . . 5

1.2 To the present day . . . 9

2 Introduction 11

2.1 Chiral symmetry and its breaking . . . 11

2.1.1 Spontaneous symmetry breaking . . . 11

Coleman's theorem & Goldstone's theorem . . . 13

2.1.2 Chiral Quantum Chromodynamics . . . 14

The chiral Lagrangian . . . 14

Explicit symmetry breaking by mass . . . 16

Chiral symmetry breaking and the chiral condensate . . . 18

Effective chiral Lagrangian . . . 20

2.2 Asymptotically free gauge theories . . . 22

2.2.1 Renormalization . . . 22

2.2.2 The beta function & the running coupling . . . 23

Walking & the conformal window . . . 26

2.2.3 Anomalous dimension . . . 27

2.2.4 Representation of the matter fields . . . 29

2.2.5 Large-N_c expansion . . . 30

2.3 String theory . . . 33

2.3.1 Bosonic string action . . . 35

Mode expansions . . . 37
Quantisation . . . 38
2.3.2 Superstring theory . . . 40
Open superstrings - Type I . . . 41
Closed superstrings . . . 42
Gliozzi-Scherk-Olive projection & type IIA/B . . . 43
2.3.3 Type IIB low-energy action . . . 44
String coupling and the dilaton . . . 44
Supergravity limit . . . 45
Type IIB supergravity action . . . 45
2.4 D-branes . . . 46
T-duality and D-branes . . . 46
2.4.1 The Dirac-Born-Infeld action . . . 49
Chan-Paton degrees of freedom . . . 50
2.5 Gauge/Gravity duality . . . 50
2.5.1 AdS/CFT correspondence: Motivation . . . 51
A useful analogy . . . 51
Interpretation I . . . 51
Interpretation II . . . 53
2.5.2 AdS/CFT correspondence: A statement . . . 55
2.5.3 AdS/CFT correspondence: Parameter matching . . . 55
2.5.4 Forms of the correspondence . . . 56
2.5.5 The conformal boundary of AdS space . . . 57
2.5.6 The holographic principle . . . 58
2.5.7 Field-operator map . . . 58

3 Holographic QCD **61**
3.1 Towards holographic QCD . . . 61
3.1.1 Top-down *versus* bottom-up approaches . . . 62
3.2 Top-down models . . . 62
3.2.1 Introducing flavour . . . 63
D7-brane metric . . . 64
D7-brane embedding . . . 65
3.2.2 Constable-Myers and dilaton flows . . . 68
3.3 Bottom-up models . . . 70
Hard-wall *versus* soft-wall . . . 71
3.3.1 Dynamic AdS/QCD . . . 72
Understanding g_5 . . . 73
The vacuum structure . . . 74
Breitenlohner-Freedman bound . . . 76

Meson spectra . . . 77
Adding temperature and magnetic field . . . 78
3.4 A few questions . . . 81

II Part Two: Research **83**

4 HyperScaling Relations in the Conformal Window **85**
4.1 Dynamic AdS/QCD . . . 88
4.2 Scaling behaviour of the quark condensate . . . 91
4.2.1 Infrared fixed point behaviour . . . 93
4.2.2 The large quark mass limit . . . 95
4.2.3 Numerical solutions for the full running theory . . . 97
4.3 Bound state masses . . . 99
4.3.1 Linearized fluctuations . . . 100
4.3.2 Bound states of the $N_c = 3, N_f = 12$ theory . . . 101
4.3.3 $N_c = 3$, $N_f = 13, 15$ mesons . . . 104

5 Meson Spectra of Asymptotically Free Gauge Theories **107**
5.1 A top-down model . . . 109
5.1.1 Constable-Myers geometry: A recapitulation . . . 110
5.1.2 Analysis . . . 111
5.2 Dynamic AdS/QCD . . . 115
5.2.1 The running of γ . . . 116
5.2.2 Linearized fluctuations . . . 116
5.2.3 Meson spectra results . . . 117
Quenched fundamental representation . . . 118
Fundamental representation . . . 119
Other representations . . . 123
5.2.4 The scalar glueball . . . 127

6 Inverse Magnetic Catalysis **133**
6.1 Dynamic AdS/QCD in the context of finite temperature & magnetic field strength . . . 135
6.1.1 Meson melting . . . 137
6.2 The Dynamic AdS/QCD model at finite temperature . . . 139
6.3 Magnetic fields in Dynamic AdS/QCD: Introduction and analysis . . . 141
6.4 Non-zero quark masses . . . 148

7 Translational Symmetry Breaking & Striped Condensation **149**
7.1 Effective Higgs theories . . . 152
7.2 A holographic model . . . 155

7.3 Striped phases and the cosmological constant in R^2-gravity 160

8 Concluding Remarks **165**

Appendices **167**

A Parity doublets of chiral symmetry **169**

B U(1)$_A$ anomaly **171**

C UV expansion of $L(\rho)$ **175**

D Expanding the Dynamic AdS/QCD action **179**

E Vector-field equation of motion **181**

F Derivation of $\langle\bar{q}q\rangle^*$ **183**

G Derivation of fixed point mass and condensate **185**

H Derivation of k **187**

I The Banks-Casher Relation **189**

J Vafa-Witten Theorem **195**

List of Figures

1.1 [**top**] Gell-Mann octet of mesons. They are grouped such that the horizontal layers each have the same strangeness quantum numbers, i.e. the same number of strange quarks inside, and the diagonal lines connect mesons of like charges. The singlet η' is missing from the diagram. [**bottom**] The same categorisation for the octet and decuplet of the baryons. . . . 8

2.1 A) The potential with global minimum occurring at $|\phi| = 0$ exhibiting a global U(1) symmetry. B) The old minimum becomes an unstable extremum of the potential. The new global minimum is a set of solutions at fixed $|\phi| \neq 0$ – there is a non-zero vacuum expectation value of the field ϕ. 12

2.2 When quark-antiquark pairs are condensed out of the vacuum they must have zero net momentum and angular momentum. This leaves us with two quark fields; one right-handed quark field (a) and one antiparticle of a left-handed quark field (b) or *vice-versa*. 19

2.3 a) The beta function for $\beta_0 > 0$ and $\beta_1 > 0$ (top) with the running of the coupling (bottom). b) The beta function for $\beta_0 > 0$ and $\beta_1 < 0$ (top) with the running of the coupling (bottom) c) The beta function of $\beta_0 < 0$ and $\beta_1 < 0$ (top) with the running of the coupling (bottom). 24

2.4 Experimental verification of the asymptotically free nature of the strong coupling parameter [48]. 25

2.5 Plot of $\alpha_s(\mu)$ for the case $\alpha_s^* > \alpha_s^\chi$. The critical coupling is met at the scale, Λ_χ, triggering chiral symmetry breaking and generating a dynamic mass for the quarks of order this scale. Below Λ_χ, the quarks decouple and the theory then runs into the IR as '$N_f = 0$'. The scale Λ_1 can be seen as the UV boundary of the walking regime and it dictated by the scale generated by the one-loop running. 27

2.6 A cartoon showing the different phases of an SU(3) gauge theory with N_f fundamental flavours. 28

2.7 The $N_c - N_f$ phase space for the fundamental representation, adapted from [44]. Region A is where asymptotic freedom is lost. Region B is the conformal window. Region C is where walking regimes will occur since the beta function displays an NTIR fixed point but chiral symmetry is broken. Region D has only one trivial UV fixed point. 28

2.8 The $N_c - N_f$ phase space for the fundamental representation (black), the adjoint representation (green), the two-index symmetric representation (red) and the two-index antisymmetric representation (blue), adapted from [44]. 30

2.9 The double line notation for a) a gauge field propagator, b) a three point gauge field vertex and c) a matter field interacting with a gauge field. . 32

2.10 The lower genus diagrams in the double line notation dominate over higher genera. All diagrams of the same genus are proportional to the same power of N_c and so, to leading order, only the planar $g = 0$ diagrams, proportional to N_c^2 need be considered in the $N_c \to \infty$ limit. . . 33

2.11 D-branes as hyperplanes over which Dirichlet strings can move freely, spanning the dimensions (or a subset thereof) of the target spacetime along which the string is Neumann. x_D are the dimensions in the target spacetime where the shown string ends are fixed. String A shows an open string with two Dirichlet ends stretched between two different D-branes, string B shows a string attached at both ends on the same brane and string C shows a string with one Dirichlet end (fixed to the D-brane) and one free-to-move Neumann end. 47

3.1 The D3/D7-brane set-up allows for fundamental fields e.g. quarks. Multiple D7-branes allows for different flavours of quarks. E.g. string a) pertains to a red up-type quark and string b) pertains to a red down-type quark. 3-3 strings generate the $\mathcal{N} = 4$ SYM theory, 3-7 strings realise quark-like fields and 7-7 strings represent mesons. 64

3.2 10d spacetime set-up of the D3/D7 system. The most stable configuration of the D7 brane might have a non-trivial relation between L and ρ (as seen on the left plot). 65

3.3 Plot of $L(\rho)$ for SU(3) with $N_f = 3$ in the fundamental representation. The plot shows the chiral embedding, i.e. the profile asymptotes as $\langle\bar{q}q\rangle/\rho^2$ as $\rho \to \infty$ ($\gamma \to 0$ in the field theory). Here the boundary condition on the beta function is imposed as $\alpha(0) = 0.14$. 76

4.1 An example of the running in the conformal window. The value of the coupling at the IR fixed-point is below the critical coupling to trigger SχSB. The scale Λ_1, set by the perturbative *one-loop* log-running of α_s roughly separates the fixed-point regime from the perturbative regime. Quarks with masses $m > \Lambda_1$ don't see the IR fixed point behaviour whereas as much lighter quarks will be affected by its presence. 86

4.2 Profile for $L(\rho)$ living only at scales above Λ_1 (i.e. outside the circle of radius $r = \Lambda_1$). It knows nothing of the behaviour of the running of the coupling below Λ_1 and so is dominated only by the far-UV running — the logarithmic one-loop running. 96

4.3 Plots for the theory $N_c = 3$ and $N_f = 12$. [**a) top-left**] $\log c$ against $\log m_{\text{bare}}$ [**b) top-right**] numerical points for γ against $\log m_{\text{bare}}$ — γ is extracted by assuming the scaling relation $\langle\bar{q}q\rangle = m^{\frac{3-\gamma}{1+\gamma}}$ [**c) bottom**] the percentage difference between the extracted form of γ and the input form (solid line in b)). For all of these c is evaluated at ρ_{IR}. 98

4.4 $N_c = 3$: [**a) left**] γ versus m_{bare} from c for $N_f = 13$ [**b) right**] γ versus m_{bare} from c for $N_f = 15$ 99

4.5 $N_c = 3$, $N_f = 12$: [**a) top-left**] ρ-meson mass against quark mass [**b) top-right**] extracted value γ versus m_{bare} from ρ-meson mass spectrum. The solid line shows the holographic input of γ from the two-loop running [**c) bottom**] the percentage difference seen between the input γ running and the extracted γ running 102

4.6 $N_c = 3$, $N_f = 12$:[**a) left**] σ-meson mass against quark mass [**b) right**] Extracted value γ versus m_{bare} from σ-meson mass spectrum. The solid line shows the holographic input of γ from the two-loop running. 102

4.7 $N_c = 3$, $N_f = 12$:[**a) left**] π-meson mass against bare quark mass [**b) right**] Extracted value γ versus m_{bare} from π-meson mass spectrum. The solid line shows the holographic input of γ from the two-loop running. . 102

4.8 $N_c = 3$, $N_f = 12$: [**a) left**] ρ-mass versus π-mass [**b) right**] b versus M_π, where we've assumed $M_\rho \propto M_\pi^b$ 103

4.9 $N_c = 3$, $N_f = 12$:[**a) left**] f_ρ versus the bare quark mass [**b) right**] the extracted γ versus m_{bare} 103

4.10 $N_c = 3$, $N_f = 12$:[**a) left**] f_σ versus the bare quark mass [**b) right**] the extracted γ versus m_{bare} 104

4.11 The running of α_s for $N_f = 12$ switches drastically between the perturbative one-loop running in the UV to the fixed point behaviour in the IR around Λ_1. The profile for $N_f = 15$ is a lot smoother, pushing the conformal behaviour further out and blurring the two (IR and UV) regimes. 105

4.12 $N_c = 3$: [**a) left**] γ extracted from M_ρ against the bare quark mass at $N_f = 13$, $N_c = 3$ [**b) right**] The same for $N_f = 15$. 106

4.13 $N_c = 3$: [**a) top-left**] M_ρ versus M_π for $N_f = 13$ [**b) top-right**] extracted γ for $N_f = 13$ [**c) bottom-left**] M_ρ versus M_π for $N_f = 15$ [**d) bottom-right**] extracted γ for $N_f = 15$ 106

5.1 As the UV scale Λ_1 (associated to the one-loop running) gets pushed out as walking dominates, the condensate becomes enhanced and stretched the shape of the effective potential. For large walking regimes the potential radial direction flattens causing the sigma-mode to become light. This is in agreement with the walking region enlarging as N_f increases towards the point where chiral symmetry is regained and the sigma-mode becomes massless. 109

5.2 Plots of M_ρ against M_π^2 - in each case the points are normalized by M_ρ at $M_\pi = 0$ to set the non-perturbative scale Λ. As shown in the key, the plot shows the data for quenched lattice computations taken from [136] (and linearly fitted to find M_ρ at $M_\pi = 0$); the Constable Myers top down model; and the Dynamic AdS/QCD predictions. 110

5.3 A plot of the anomalous dimension γ in the top-down Constable-Myers model. It is compared to QCD by using the one-loop perturbative result for the running coupling in large N_c Yang-Mills theory ($\mu d\alpha/d\mu = -11N_c\alpha^2/6\pi$) as input for calculating the anomalous dimension γ ($\gamma = 3N_c\alpha(\mu)/4\pi$). We set the scale at which $\gamma = 1$ to be equal in each case. 115

5.4 A Log-Log plot of M_ρ versus M_π^2 - the plot displays the quenched lattice data from [136], the top-down Constable-Myers model of section 2 and the quenched results for varying N_c in Dynamic AdS/QCD from section 3. The solid line corresponds to $M_\rho = M_\pi$. 118

5.5 M_ρ versus M_π^2 in SU(N$_c$) theory with $N_F = 8$ fundamental quarks - the lower plot shows the same in Log Log format. The solid line corresponds to $M_\rho = M_\pi$. 120

5.6 SU(3) gauge theory with N_f fundamental quarks showing the approach to the conformal window at $N_f = 12$. The lower plot is a Log Log version of the top plot. The solid line corresponds to $M_\rho = M_\pi$. The plots also show lattice data for the quenched theory [136] and unquenched $N_f = 3$ theory [139–141]. 121

5.7 M_σ versus M_π^2 in SU(3) gauge theory with varying N_f fundamental quarks. The lower plot is a Log Log version of the top plot. The solid line corresponds to $M_\sigma = M_\pi$. 124

5.8 A Log-Log plot in the M_ρ-M_π^2 plane for SU(3) gauge theory. The plot shows the results in models with $N_f = 1$ but with the fermions in the fundamental, adjoint and 2-index symmetric representations. The middle figure shows the N_f dependence in the case with adjoint fermions and the bottom plot the same for the 2-index symmetric representation. The solid line corresponds to $M_\sigma = M_\pi$. 126

5.9 A Log-Log plot in the M_ρ-M_π^2 plane for SU(3) gauge theory. The top plot shows the N_f dependence in the case with adjoint fermions and the bottom plot the same for the 2-index symmetric representation. The solid line corresponds to $M_\sigma = M_\pi$. 127

5.10 A Log-Log plot in the M_ρ-M_π^2 plane for SU(N_c) gauge theory with $N_f = 2$ 2-index symmetric representation quarks. The solid line corresponds to $M_\sigma = M_\pi$. 128

5.11 A Log-Log plot in the M_ρ-M_π^2 plane for SU(N_c) gauge theory with $N_f = 3$ 2-index anti-symmetric representation quarks. The solid line corresponds to $M_\sigma = M_\pi$. 128

5.12 Log-Log plots in the M_σ-M_π^2 plane. The top plot shows the results in SU(3) gauge theory with adjoint quarks. The bottom plot is for SU(N_c) gauge theory with $N_f = 2$ 2-index symmetric representation quarks. The solid line corresponds to $M_\sigma = M_\pi$. 129

5.13 Log-Log plots in the M_σ-M_π^2 plane. Plot shows the spectra for SU(N_c) gauge theory with $N_f = 3$ 2-index anti-symmetric representation quarks. The solid line corresponds to $M_\sigma = M_\pi$. 130

5.14 The spectra of the $N_c = 3$ gauge theory with fundamental quarks - the top figure shows $N_f = 3$, the bottom $N_f = 11$. 132

6.1 First order phase transitions are discontinuous in the order parameter - for the chiral symmetry breaking transition this is the chiral condensate. Second order phase transitions are discontinuous in the first derivative of the order parameter. The crossover transition isn't strictly a phase transition but a smooth bridge between two regions of different phenomena. 134

6.2 Lattice results for the change in the quark condensate as a function of magnetic field strength over a range of temperatures - figure taken from [150]. 138

6.3 The holographic model's results for the change in the condensate of light quarks as a function of magnetic field strength over a range of temperatures for $N_c = N_f = 3$. T_{C0} is the thermal transition temperature at $B = 0$ which is used to set our holographic energy scale (and is approximately 160 MeV according to the lattice simulations). For this plot the model parameters are taken as $\kappa = 0.05$ and $b = 0.037$. 138

6.4 [**top**] At $T = 0$ there are two solutions to the embedding equation; the chirally symmetric solution $L = 0$ for which $\bar{q}q = 0$ (a), and the energetically more favourable chirally broken solution (b). A first order transition is signalled by the presence of a third unstable solution (c) for $T > 0$. At $T = T_c$, the chirally broken and chirally symmetric phases are degenerate (d). Above T_c, the chirally symmetric phases remains energetically favourable. [**bottom**] A second order phase transition occurs when the chirally broken phase (b) smoothly merges with the chirally symmetric phase (a) at $T = T_c$. 142

6.5 Thermal phase transitions in the holographic model with $N_c = N_f = 3$. For values of the parameter κ close to $\kappa = 1$, a first order chiral transition is present. As the value of κ is reduced and the black hole is deformed along the L-axis, the phase transition switches to becoming second order. The introduction of a background magnetic field can be seen to affect the value of the transition order parameter, σ. Here we show an example with magnetic catalysis at low temperature and inverse magnetic catalysis at higher temperatures, a phenomenon which reduces the critical temperature, $T_c(B) < T_c(0)$. 143

6.6 Plot showing the chiral embeddings (at $B = 0$) for a range of temperatures. Each embedding is coloured to match the black hole horizon pertaining to the relevant temperature. The second order nature of the transition is evident; the embedding smoothly transforms into the flat $L = 0$ embedding at the critical temperature, T_c. 143

6.7 The phase-structure of the holographic model in terms of the phenomenological parameters a and b. The $a - b$ plane can be dissected into four sectors wherein the condensate is affected differently with temperature and an external magnetic field. 145

6.8 Plots of the critical temperature against eB, $T_{C0} = 160$MeV. We show the best fit lattice data taken from [151] and the holographic model's best fit **(in the chiral limit)** to that data ($\kappa = 0.05, a = 0, b = 0.037$). We also show the holographic models prediction for another value of $b = 0.33$ - the model depends on the quantity bB^2 so the eB axis is simply rescaled by this change. 145

6.9 Plot showing the chiral embeddings at $T = 0.75T_{C0}$ for a range of magnetic field. Increasing B moves the embedding towards and on to the horizon but initially also increases the condensate value. 147

6.10 Plot showing the change in the chiral condensate as a function of B for different quark masses. The parameters are those used to make Fig 6.7. 148

7.1 Assuming a striped vev of the scalar ϕ from 7.5, a non-zero wavenumber k actively disfavours an instability in the potential. Here we show the profile of the potential for $0 = k_1 < k_2 < k_3 < k_4$. 153
7.2 Potential (normalized by that at $k = 0$) against $\ln[k/\Lambda_{QCD}]$ for varying values of the coefficient of the higher-dimension operator (which is a mix of $\tilde{\kappa}_2$ and $\tilde{\kappa}_3$. We set here $N_c = 3$ $N_f = 3$, the scale at which $\gamma = 1$ to be Λ_{QCD} and set $c = \Lambda^4_{QCD}$. 160

B.1 The $U(1)_A U(1)^2_{QED}$ triangle diagram calculation pinpoints to an anomalous $U(1)_A$ symmetry. 171
B.2 a) The $SU(N_f)_A SU(N_c)^2$ triangle diagram and b) the $U(1)_A SU(N_c)^2$ triangle diagram. 172
B.3 The $SU(N_f)_A U(1)^2_{EM}$ has direct consequences relating to the decay process $\pi^0 \to \gamma\gamma$. 173

List of Tables

2.1 Distinguishing quantities of representations of $SU(N_c)$ gauge theories with asymptotic freedom valid for any $N_c \geq 2$. $\dim(R)$ is the dimension of the representation, $C_2(R)$ is the quadratic Casimir of the representation and $N_f^{\max}$ is the maximum number of flavours allowed before asymptotic freedom is lost at fixed N_c. 31

2.2 Mode expansions for the left- and right-moving closed string solutions. . 42

2.3 The various forms of the AdS_5/CFT_4 correspondence appearing in different limits of the theories' parameters. 56

3.1 The D3-brane extends in the 0123-directions of 10d spacetime, whereas the D7-brane extends over the 01234567-directions. The branes thus overlap in the 0123-directions. Here 0 denotes the time direction. 64

3.2 The dictionary between the bulk AdS fields and the field theory operators on the boundary in a simple AdS/QCD model. The bulk fields masses are obtained via the relation $(\Delta - p)(\Delta + p - 4) = M^2$ (see section 2.5.7) 70

Declaration of Authorship

I, Marc Scott, declare that this thesis, entitled 'Dynamic AdS/QCD: A holographic approach to asymptotically free gauge theories' and the work presented in it are my own.

I confirm that

- This work was done wholly or mainly while in candidature for a research degree at this university.
- Where I have consulted the published work of others, this is always clearly attributed.
- Where I have quoted the work of others, the source is always given. With the exception of such quotations, this thesis is entirely my own work.
- I have acknowledged all main sources of help.
- Where the thesis is based on work done by myself jointly with others, I have made clear exactly what was done by others and what I have contributed myself.
- Work contained in this thesis has previously been published in references [1–4].

I have collaborated on the following paper, the contents of which are not outlined in this thesis:
Nick Evans, Peter Jones, and Marc Scott. Soft walls in dynamic AdS/QCD and the technidilaton. Phys. Rev., D92(10):106003, 2015, 1508.06540. [5]

Signed:

Date:

Acknowledgements

First and foremost, I would like to express my sincere gratitude towards my supervisor, Professor Nick Evans, for his tuition and guidance over the past four years and for always being available to answer any questions I had, no matter how basic. I would also like to thank him for giving me the opportunities to lecture on outreach days and to do illustrations for the SETI challenge. I would also like to thank the fellow members of the 4007 office for providing four years of downright bizarre, humorous and interesting conversations and antics. Of these, I would like to thank Matt 'Coffee Cup' Spraggs, Hamzaan 'Starcraft' Bridle, Anthony 'Cats' Preston, Tobi 'Diablo' Tsang, Andrew 'Lanny' Lawson and Thomas 'Something Controversial' Neder for providing much-needed coffee-break distractions. In particular, I must thank my house-mate, office companion and most importantly long-suffering friend of twenty years Andrew Meadowcroft for generally being an awesome person (and proof-reading most of this work!). I must also acknowledge Matthew Cobain and Greg Ashton for proof-reading parts of this work and sharing my fervent enthusiasm for a gin and tonic! Of the PhD cohort, I must also thank Peter Jones for pointing out issues in my work at the eleventh hour, but more seriously for also providing many laughs throughout my PhD. I would like to also thank my A-Level physics teachers Dr George White and Dr Teresa Ghoneim for encouraging the physicist in me; this thesis would not exist were it not for your enthusastic and captivating approach to the subject.

I would also like to thank all the members of Eagles Badminton Club (past and present) for making such a fantastic, friendly arena for playing competitive badminton and for being a much needed stress-relief throughout the writing of this work.

Last but certainly not least, it goes without saying that I am deeply indebted to my

parents and family for the long-term support they have given me despite not having a clue what I do.

Part I

Part One: Foundations

Chapter 1

AdS/QCD: A History

1.1 The road to 1974

Why has the path to understanding the strong nuclear force seemingly gone off-road, headed for the more mathematically abstract (and indeed abstruse) landscape of string theory and the arena of holography? This is a question that we address in this historical introduction, setting the scene for the relevance of the physics undertaken in the following work.

Quantum chromodynamics (QCD) is the fundamental theory of the strong interaction and its birth, and subsequent life, has been one of troubles, anguish and tribulations. Ever since the discovery of the neutron by Chadwick[1] in 1932 [6], it was known that the force that governs the interactions within the nuclei of atoms was different to the known electromagnetic force: like charges seemed to attract one another and the two nucleons appeared to be identical in all but their charge. The first major attempt at trying to postulate an underlying theory for the strong interaction was done in 1934 by Yukawa[2] [7]. In analogy to the quantisation of the electromagnetic interaction whereby a photon is exchanged between charged particles to mediate the force, Yukawa proposed the idea of the *meson*[3] as the 'carrier' of the strong interaction. Naturally, the theory had to be modified away from that of electromagnetism (EM). The strong inter-

[1] Sir James Chadwick, 1891-1974.
[2] Hideki Yukawa, 1907-1981.
[3] Originally, he called it the U-quantum.

action is only dominant at the scale of the nucleus ($\sim 10^{-15}$m) with its effects unseen at larger scales. Therefore the force carrier, the meson, had to be a massive particle ($\left(10^{-15}m\right)^{-1} \approx 200$MeV), unlike its massless EM twin, the photon, which mediates EM across an infinite range. A spin-1 mediator was forbidden since it generates a repulsive potential between like charges, so the meson had to be of either zero or even spin [8]. Since the force only affected one particle, the nucleon (in its two isospin forms), a scalar (spin-0) meson seemed the most plausible. Lastly, and somewhat most importantly, the interaction was 'strong', having to override the proton-proton EM interaction in the nucleus. This then implied that the coupling strength between this meson and each nucleon was big.

In 1936, Anderson[4] and Neddermeyer[5] discovered the muon from cosmic rays [9] and initially the particle was associated to the strong-interaction mediator, the meson[6], because of its mass ($\sim$ 105MeV) [10]. It just goes to show that some of the greatest minds in the field get it wrong occasionally. However, cosmic rays relinquished more particles in the form of a triplet of *pions* (π^+, π^-, π^0), detected in 1947, which seemed to fit the job. A Lagrangian formalism for this theory was constructed with the now-famous *Yukawa term* with coupling constant y:

$$i\bar{N}\gamma^\mu\partial_\mu N - m_N\bar{N}N + \frac{1}{2}\partial_\mu\pi^a\partial^\mu\pi^a - \frac{m_\pi^2}{2}\pi^a\pi^a - iy\bar{N}\gamma^5\tau^a N\pi^a, \tag{1.1}$$

where N is the nucleon doublet containing the neutron and proton, π^a is the pion triplet, γ^5 is the usual fifth Dirac matrix and τ^a are the Pauli matrices. Despite a Lagrangian formalism which seemed to describe the right physics witnessed by the strong interaction, there was still the omnipresent elephant in the room: the strength of the coupling. Because y had to be large, orders of magnitude stronger than the equivalent electromagnetic charge, there were no calculations that could be done with Lagrangian 1.1. Perturbation theory, as used for the quantum version of electromagnetism, Quantum Electrodynamics (QED), relies on a small coupling about which one can expand. Clearly

[4]Carl D. Anderson 1905-1991.

[5]Seth Henry Neddermeyer 1907-1988.

[6]The muon was initially called the *mesotron* and then the μ-meson. The meson was finally dropped when it became known that the muon was in fact a heavier version of the electron, an idea so uncontemplated that it lead Isador Rabi to exclaim the now famous "Who ordered that?!".

this isn't the case for Yukawa's meson theory. To add insult to injury, throughout the 1950's and into the 1960's, experiments unveiled an ever-expanding plethora of other particles [11–16] (on top of p, n and π) — the discoveries were so frenetically frequent that it become known as the 'particle zoo'. In 1961, in a (desperately needed) attempt to clean-up and categorise this 'zoo', Gell-Mann[7] found that the particles, collectively known as *hadrons*, could be grouped[8] into octets and decuplets (transforming in the **8** and **10**) of the group SU(3) [18, 19], see figure 1.1. This group became known as the *flavour symmetry* group. The question then arose as to what became of the seemingly non-existent fundamental representations, the triplets of this flavour group. The genius of Gell-Mann was to realise that, from a purely group theoretic perspective,

$$\mathbf{3} \otimes \bar{\mathbf{3}} = \mathbf{8} \oplus \mathbf{1} \tag{1.2}$$

and

$$\mathbf{3} \otimes \mathbf{3} \otimes \mathbf{3} = \mathbf{10} \oplus \mathbf{8} \oplus \mathbf{8} \oplus \mathbf{1}. \tag{1.3}$$

Gell-Mann named the fundamental field a *quark*[9] [20] and noticed that mesons, like the pion, were comprised of a quark-antiquark pair and *baryons* of three quarks. The nonet of light mesons comprised of the three quark flavours (up, down and strange) were the adjoint octet $(\pi^{\pm}, \pi^0, K^{\pm}, K^0, \bar{K}^0, \eta)$ plus the η' singlet. The baryon decuplet is comprised of the $(\Delta^{++}, \Delta^{\pm}, \Delta^0, \Sigma^{*\pm}, \Sigma^{*0}, \Xi^{*-}, \Xi^{*0}, \Omega^-)$, the octet is $(p, n, \Sigma^{\pm}, \Sigma^0, \Xi^-, \Xi^0, \Lambda)$ and the singlet is in fact forbidden to exist by the Fermi-Dirac statistics and thus is never seen. Particles like the discovered Δ^{++}, comprised of uuu all in the same spin state, seemingly violate the Pauli-Exclusion principle. In order to rectify this, Han[10] and Nambu[11] [21] (and independently by Greenberg[12] [22]) introduced another quantum number called *colour* from yet another SU(3) symmetry. The delta-baryon's quarks can

[7] Murray Gell-Mann 1929-.

[8] In fact, the Ω^- baryon, consisting of sss quark content, wasn't yet found when Gell-Mann devised this theory, yet he hypothesised its discovery to complete the decuplet. It was discovered in 1964 [17].

[9] Taken from James Joyce's *Finnegans Wake* — "Three quarks for Muster Mark!". George Zweig also must be credited with hypothesising the existence of these fundamental representations of SU(3)(-flavour), naming the particles *aces*.

[10] Moo-Young Han, 1934-2016.

[11] Yoichiro Nambu, 1921-2015.

[12] Oscar W. Greenberg, 1932-.

thus be differentiated by their colour quantum number and are therefore not all in the same quantum state.

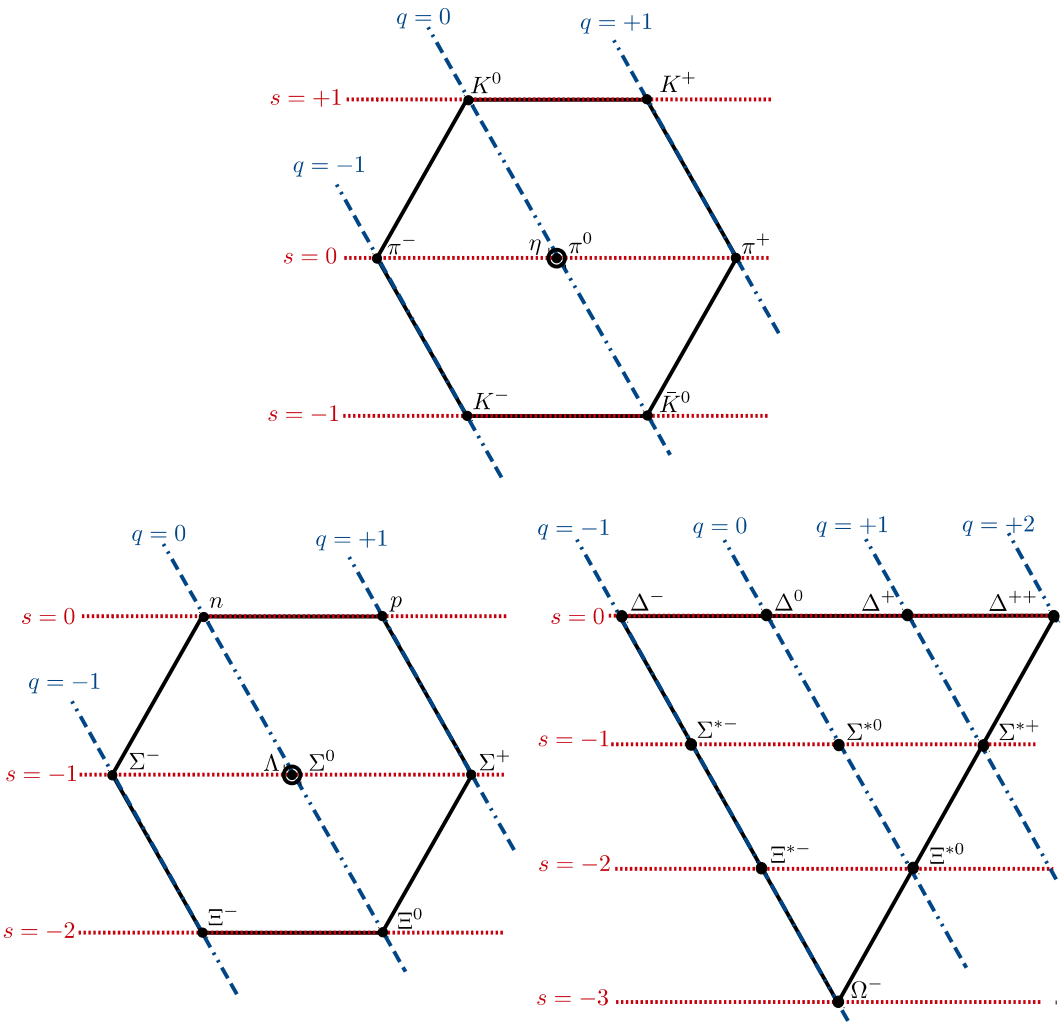

Figure 1.1: [**top**] Gell-Mann octet of mesons. They are grouped such that the horizontal layers each have the same strangeness quantum numbers, i.e. the same number of strange quarks inside, and the diagonal lines connect mesons of like charges. The singlet η' is missing from the diagram. [**bottom**] The same categorisation for the octet and decuplet of the baryons.

As soon as one question was answered, another seemed to pose itself. Why did we never observe these quarks as isolated particles? It was proposed that the quarks were somehow held prisoners of the hadrons they comprised, a theory so preposterous that many didn't believe in the existence of the quark at all, despite Gell-Mann's group theory arguments. It was not until the deep inelastic scattering experiments of the late 1960's

that the nucleons were indeed found to be comprised of point-like charges [23, 24], and were quickly associated with Gell-Mann's quarks — to quote Andrei Smilga '*interago ergo sum*' [25].

At last, things started falling into place. In 1973, it was proposed [26–28] that the theory that was being used to understand the weak interaction, a Yang[13]-Mills[14] formalism [29], could be employed to deal with its strong counterpart. The Yang-Mills theory of QCD described quark matter mediated by massless, vector particles in the adjoint of the non-Abelian, colour SU(3) group, the *gluons*. With the discovery of the running of the strong coupling by Gross[15], Wilczek[16] [30] and Politzer[17] [31], it was shown that at high energies the coupling asymptotically vanished and the quarks became free. In the IR the perturbative coupling is seen to rise and become strong at nuclear energy scales.

By the end of 1974, it is safe to say that QCD as we know it today had been born. Yet, there was still the small issue of the strong coupling at the interesting energy scales pertaining to subatomic physics. Perturbation theory remained defeated and confinement unproven (it still is).

1.2 To the present day

The strong interaction has a long and complicated past with string theory. Before the establishment of the theory we now know as QCD, at a time when questions about the strong interaction were plentiful but solutions scant, string theory was borne out of the need for a fundamental theory of the strong nuclear force. String theory described very well a phenomenological aspect of the strong interaction called Regge trajectories. Yet string theory, in its simplest format, is riddled with issues of tachyonic ground states, spin-2 particles (then and to some extent still) unobserved in nature and requiring more dimensions of space and time than anyone knew what to do with. One set of problems was replaced by another. QCD was soon formulated so the stringy nature of the strong

[13] Yang Zhenning 1922-.
[14] Robert Laurence Mills 1927-1999
[15] David Jonathan Gross 1941-.
[16] Frank Anthony Wilczek 1951-.
[17] Hugh David Politzer 1949-.

interaction was forgotten. In the framework of a gravity theory, string theory was redeveloped and its inconsistencies and foibles were eradicated. The field of string theory grew ever larger and in 1997, Maldacena[18] conjectured a mathematical duality (still as of yet formally unproven) that a particular branch of string theory (namely type IIB) on a specific geometry (that of a five dimensional Anti-de Sitter spacetime with compactified five-sphere — $AdS_5 \times S^5$) contained all the same information (i.e. degrees of freedom) of one particular type of gauge theory (an $\mathcal{N} = 4$ supersymmetric Yang-Mills theory in four dimensions). This is the AdS/CFT correspondence [32]. This duality has more treasures to bestow than initially meets the eye. Firstly, the duality is an example of the holographic principle, hypothesised by 't Hooft[19] and Susskind[20] [33] as a solution to a puzzle about entropy scaling in black hole thermodynamics. The holographic principle says that information contained in a volume, V, of a $d+1$-dimensional spacetime may be expressed in terms of the degrees of freedom on the volume's boundary ∂V. The AdS/CFT correspondence has the CFT living on the boundary of the higher-dimensional curved AdS_5 spacetime (or bulk). The second treasure, and this is one of particular importance to our story, is that in a particular form, the correspondence insists that when the gravity theory is weakly coupled, the gauge theory on its boundary is *strongly coupled*. If only there were such dualities between strongly-coupled QCD and a gravity dual, one could perform calculations on the gravity side and translate the results into QCD physics. Unfortunately, we are not so lucky. However, over the past decade or so, it has been the goal of many physicists to seek out such a duality by going back to Maldacena's conjecture and re-engineering the groundwork so that the gauge theory in the duality is more and more like QCD. To this end, research still continues to thrive in this field as the secrets of strongly coupled QCD slowly begin to be reveal themselves.

[18] Juan Maldacena 1968-.
[19] Gerardus 't Hooft 1946-.
[20] Leonard Susskind 1940-.

Chapter 2

Introduction

In the following sections, we will introduce the fundamental ideas that underpin the core of this body of work. We begin by looking at the phenomenon of chiral symmetry and how it is spontaneously broken in QCD-like gauge theories and then witness how QCD gauge theories 'run' with energy and the consequences thereof. We next embark on a brief guide to string theory, before uniting both the gauge theory and string aspects together as we discuss and outline the idea of the AdS/CFT correspondence. The aim (and the hope) of this section is to be a clear and pedagogical guide for all those interested in this field of research.

2.1 Chiral symmetry and its breaking

In this section, we introduce the concept of spontaneous symmetry breaking and its rôle in chiral Quantum Chromodynamics.

2.1.1 Spontaneous symmetry breaking

Consider the Lagrangian for a complex scalar field theory parameterised by the field ϕ,

$$\mathcal{L} = |\partial_\mu \phi|^2 + m^2 |\phi|^2 - \frac{\lambda}{4} |\phi|^4, \tag{2.1}$$

where m and λ are some real coupling constants and $\lambda > 0$. The Lagrangian has a global symmetry $\phi \to U\phi$, $\phi^* \to U^*\phi^*$, where U is the unitary[1] matrix (or operator) which induces the transformation leaving the Lagrangian invariant. For Lagrangian 2.1, $U \in U(1)$, i.e. $U = e^{i\alpha}$ for $\alpha \in \mathbb{R}$. For $m^2 < 0$, the global minimum of the potential is found at $\phi = 0$ (see figure 2.1A). If the sign of m^2 is, by some mechanism, driven to be $m^2 > 0$, then this theory becomes *unstable* around $\phi = 0$ and the potential minimum occurs at $|\phi|^2 = \frac{2m^2}{\lambda}$ (see figure 2.1B). The ground state is no longer invariant under the U(1) symmetry due to the existence of a non-zero vacuum expectation value of the field $\langle\phi\rangle \neq 0$ — this is spontaneous symmetry breaking (SSB).

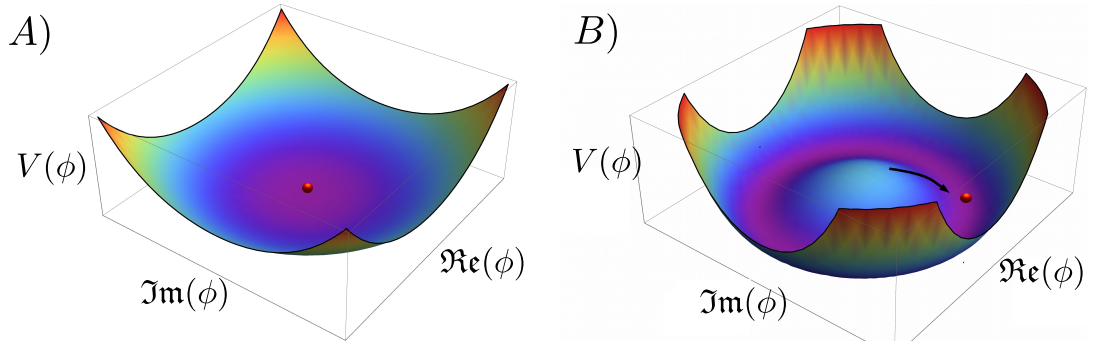

Figure 2.1: A) The potential with global minimum occurring at $|\phi| = 0$ exhibiting a global U(1) symmetry. B) The old minimum becomes an unstable extremum of the potential. The new global minimum is a set of solutions at fixed $|\phi| \neq 0$ – there is a non-zero vacuum expectation value of the field ϕ.

In the case of $m^2 > 0$, there is a ring of equivalent vacua henceforth parameterised as $\langle\Omega_\theta|\phi|\Omega_\theta\rangle = m\sqrt{\frac{2}{\lambda}}e^{i\theta}$ for $\theta \in \mathbb{R}$. The most convenient parameterisation is chosen to be, without loss of generality, $\theta = 0$, such that

$$\langle\Omega|\phi|\Omega\rangle = m\sqrt{\frac{2}{\lambda}} \equiv v, \tag{2.2}$$

and defines our new vacuum with the vacuum expectation value (vev) of the field ϕ given by v.

An expansion of ϕ about this vev may be expressed as

$$\phi(x) = \left[v + \frac{1}{\sqrt{2}}\sigma(x)\right] e^{i\frac{\pi(x)}{f_\pi}}, \tag{2.3}$$

[1]Unitarity implies $U^*U = \mathbb{I}$.

where $\sigma(x)$ parameterises the radial fluctuations in ϕ about v (in the complex plane of which ϕ is a vector), $\pi(x)$ parameterises the angular fluctuations in ϕ about the chosen $\theta = 0$, and $f_\pi \in \mathbb{R}$. Substituting 2.3 into the Lagrangian 2.1, we arrive at

$$\begin{aligned}\mathcal{L} =& \frac{1}{2}(\partial_\mu \sigma)^2 + \left(v + \frac{1}{\sqrt{2}}\sigma\right)^2 \frac{1}{f_\pi^2}(\partial_\mu \pi)^2 \\ &- \left\{m^2\sigma^2 + \frac{1}{2}\sqrt{\lambda} m \sigma^3 + \frac{1}{16}\lambda\sigma^4 - \frac{m^4}{\lambda}\right\}. \end{aligned} \tag{2.4}$$

Choosing $f_\pi = \sqrt{2}v$, we make the π-kinetic term canonically normalized. This Lagrangian is referred to as the *linear sigma model* [34]. The π-field is seen to be massless (a presupposition given it parameterises the equipotential angular fluctuations), whereas the σ-field has gained a mass.

Coleman's theorem & Goldstone's theorem

Consider a field theory Lagrangian that is invariant under a global SU(N_c) transformation parameterised by the special[2], unitary matrix U. The vacuum, $|\Omega\rangle$, being invariant under this transformation implies

$$U|\Omega\rangle = |\Omega\rangle. \tag{2.5}$$

From Noether's[3] theorem, we also recognise that a continuous SU(N_c) global symmetry implies conserved Noether currents $\partial^\mu J^a_\mu = 0$ with conserved charges $Q^a = \int d^3x J^a_0(x)$ [35], where a is an index running over the number of generators of the symmetry group. One may express the transformation matrix in the basis[4] $U = e^{i\alpha^a Q_a}$, where Q_a are the conserved charges, implying that the infinitesimal transformation is given by $U = 1 + i\alpha^a Q_a$. By using the infinitesimal transformation, equation 2.5 implies

$$Q_a|\Omega\rangle = 0. \tag{2.6}$$

[2] $\det(U) = 1$ and hence $\mathrm{tr}(U) = 0$.

[3] Amalie Emmy Noether, 1882-1935.

[4] Usually, one would write the transformation matrix as $U = e^{i\alpha^a t_a} \in$SU($N_c$), where t^a are the $N_c^2 - 1$ generators of the symmetry group. However, since the conserved charges, $Q^a = \int d^3x J^a_0$, satisfy the same Lie algebra, i.e. they satisfy the same commutation relations as t^a, then we can write the transformation matrix in a basis $\tilde{U} = e^{i\alpha^a Q_a}$.

This is the basis of *Coleman's*[5] *theorem*, which states that in order for the global symmetry of the Lagrangian to be spontaneously broken, the true vacuum or ground state of the theory must be charged under that symmetry, i.e. $Q|\Omega\rangle \neq 0$ [36].

The state $Q|\Omega\rangle$ is energetically degenerate with $|\Omega\rangle$ (see Appendix A). Momentum states constructed out of the vacuum from the symmetry current as,

$$|\pi(p)\rangle \sim J_0(p)|\Omega\rangle = \int d^3x e^{ip\cdot x} J_0(x)|\Omega\rangle, \tag{2.7}$$

have energies $E_\pi = E_\Omega + E(p)$, where E_Ω is the vacuum energy. In the limit as $p \to 0$, $|\pi(p)\rangle \to Q|\Omega\rangle$ and so $E_\pi \to E_\Omega$. From this we can conclude that the $|\pi\rangle$ states satisfy a massless dispersion relation and this is the crux of *Goldstone's*[6] *theorem*:

A spontaneous breaking of a continuous global symmetry implies massless particles in the spectrum - the (Nambu-)Goldstone bosons [37, 38].

The π-field from equation 2.4 then satisfies this criterion.

2.1.2 Chiral Quantum Chromodynamics

A more pertinent case of spontaneous symmetry breaking is the chiral symmetry breaking of SU(N_c) gauge theories.

The chiral Lagrangian

The Lagrangian of an SU(N_c) gauge theory (of N_c colours) with N_f fundamental, massless flavours can be expressed as[7]

$$\mathcal{L} = -\frac{1}{2}\mathrm{tr}\,(F^{\mu\nu}F_{\mu\nu}) + i\bar{q}\not{D}q, \tag{2.8}$$

with

$$F_{\mu\nu} = \frac{1}{g_s}[D_\mu, D_\nu], \qquad D_\mu = \partial_\mu + ig_s\lambda^a A^a_\mu \tag{2.9}$$

[5] Sidney Richard Coleman 1937-2007.
[6] Jeffrey Goldstone 1933-.
[7] The kinetic term may be recast as

$$\mathrm{tr}(F^{\mu\nu}F_{\mu\nu}) = \mathrm{tr}(F^{\mu\nu,a}t^a F^b_{\mu\nu}t^b) = F^{\mu\nu,a}F^b_{\mu\nu}\mathrm{tr}(t^a t^b) = \tfrac{1}{2}F^{\mu\nu,a}F^b_{\mu\nu}\delta^{ab} = \tfrac{1}{2}F^{\mu\nu,a}F^a_{\mu\nu},$$

where t^a are the generators of the SU(N_f) flavour symmetry.

and q is the *flavour N_f-component multiplet*

$$q = \begin{pmatrix} u \\ d \\ \vdots \end{pmatrix}. \tag{2.10}$$

Above, g_s denotes the strong coupling constant, λ^a are the $N_c^2 - 1$ generators of the $\mathrm{SU}(N_c)$ gauge group and the elements of q are each a four-component Dirac[8] spinor. Each Dirac spinor, e.g. u, can be expressed in terms of two, two-component Weyl[9] (or chiral) spinors $u = (u_L, u_R)^T$. We can then project out the left-handed and right-handed Weyl spinors[10]; e.g. $u_L = \frac{1}{2}(1 - \gamma^5)u$ and $u_R = \frac{1}{2}(1 + \gamma^5)u$. We can now see that the Lagrangian 2.8 exhibits two independent $\mathrm{U}(N_f)$ global symmetries (a $\mathrm{U}(N_f)_L \times \mathrm{U}(N_f)_R$ symmetry) since the left- and right-handed quarks are completely decoupled — this is the *chiral symmetry*. The chiral symmetry is easily re-expressed as $\mathrm{U}(N_f)_L \times \mathrm{U}(N_f)_R = \mathrm{SU}(N_f)_L \times \mathrm{SU}(N_f)_R \times \mathrm{U}(1)_L \times \mathrm{U}(1)_R$ and acts on the flavour multiplets as

$$q_L = \begin{pmatrix} u_L \\ d_L \\ \vdots \end{pmatrix} \to U_L \begin{pmatrix} u_L \\ d_L \\ \vdots \end{pmatrix} = e^{-i(l_a t^a + \theta_L)} \begin{pmatrix} u_L \\ d_L \\ \vdots \end{pmatrix}, \tag{2.11}$$

$$q_R = \begin{pmatrix} u_R \\ d_R \\ \vdots \end{pmatrix} \to U_R \begin{pmatrix} u_R \\ d_R \\ \vdots \end{pmatrix} = e^{-i(r_a t^a + \theta_R)} \begin{pmatrix} u_R \\ d_R \\ \vdots \end{pmatrix}, \tag{2.12}$$

where $U_{L,R} \in \mathrm{U}(N_f)_{L,R}$, t^a are the generators of the $\mathrm{SU}(N_f)$ subgroups with their group parameters labelled l^a and r^a for the left- and right-subgroups respectively and with the parameters θ_L and θ_R pertaining to the U(1) left- and right-subgroups. The associated

[8] Paul A. M. Dirac, 1902-1984.
[9] Hermann K. H. Weyl, 1885-1955.
[10] Naturally we have chosen the chiral basis for the gamma matrices, i.e.

$$\gamma^5 = \begin{pmatrix} -1 & 0 & 0 & 0 \\ 0 & -1 & 0 & 0 \\ 0 & 0 & 1 & 0 \\ 0 & 0 & 0 & 1 \end{pmatrix}$$

left- and right-handed SU(N_f) conserved currents are

$$L^{\mu,a} = \bar{q}_L \gamma^\mu t^a q_L, \qquad R^{\mu,a} = \bar{q}_R \gamma^\mu t^a q_R, \tag{2.13}$$

with the U(1) conserved singlet currents given by

$$L^\mu = \bar{q}_L \gamma^\mu q_L, \qquad R^\mu = \bar{q}_R \gamma^\mu q_R. \tag{2.14}$$

Recasting the global symmetry as a vector-axial symmetry, i.e.

$$\mathrm{SU}(N_f)_V \times \mathrm{SU}(N_f)_A \times \mathrm{U}(1)_V \times \mathrm{U}(1)_A,$$

we define our conserved *vector* and *axial* SU(N_f) currents as

$$V^{\mu,a} = R^{\mu,a} + L^{\mu,a} = \bar{q}\gamma^\mu t^a q, \qquad A^{\mu,a} = R^{\mu,a} - L^{\mu,a} = \bar{q}\gamma^\mu \gamma^5 t^a q, \tag{2.15}$$

and the *vector* and *axial* U(1) singlet currents as

$$V^\mu = R^\mu + L^\mu = \bar{q}\gamma^\mu q, \qquad A^\mu = R^\mu - L^\mu = \bar{q}\gamma^\mu \gamma^5 q. \tag{2.16}$$

The $\mathrm{U}(1)_A$ or axial singlet current, A^μ, is only conserved classically: at the quantum level, the ground state is charged under $U(1)_A$ — it is anomalous (see Appendix B).

Explicit symmetry breaking by mass

Adding in a mass term to the chiral Lagrangian 2.8 has the effect of destroying the chiral symmetry since it must mix the left- and right-handed quarks, in effect coupling

the two chiralities[11]. Taking a diagonal quark mass matrix of the form,

$$M = \begin{pmatrix} m_u & 0 & 0 \\ 0 & m_d & 0 \\ 0 & 0 & \ddots \end{pmatrix}, \tag{2.17}$$

i.e. adding a term $-\bar{q}Mq$ to the Lagrangian 2.8, the corresponding divergences of the vector and axial currents are found to be [39]

$$\partial_\mu V^{\mu,a} = i\bar{q}\left[M, \frac{t^a}{2}\right] q, \tag{2.18}$$

$$\partial_\mu A^{\mu,a} = i\bar{q}\gamma^5\left\{M, \frac{t^a}{2}\right\} q, \tag{2.19}$$

$$\partial_\mu V^\mu = 0, \tag{2.20}$$

$$\partial_\mu A^\mu = 2i\bar{q}\gamma^5 Mq - \frac{N_f T(R) g_s^2}{16\pi^2}\epsilon^{\alpha\nu\beta\lambda}F^b_{\alpha\nu}F^b_{\beta\lambda}, \tag{2.21}$$

where in 2.21, the second term is the aforementioned $\mathrm{U}(1)_A$ anomaly (see Appendix B). Now we can see directly that the singlet vector current is conserved even under the addition of an explicit mass term. The associated conserved charge,

$$Q_V = \int d^3x \bar{q}\gamma^0 q = \int d^3x q^\dagger q = N, \tag{2.22}$$

counts the number of quarks minus the number of antiquarks. If we break N up flavour-wise as $N = (N_u - N_{\bar{u}}) + (N_d - N_{\bar{d}}) + ...$, the eigenvalue of Q_V may also represent baryon number,

$$B \equiv \frac{Q_V}{N_f} = \frac{(N_u - N_{\bar{u}}) + (N_d - N_{\bar{d}}) + ...}{N_f}, \tag{2.23}$$

and hence the singlet vector symmetry is sometimes referred to as $\mathrm{U}(1)_B$.

From equation 2.18, it is evident that all of the $\mathrm{SU}(N_f)_V$ currents are once again

[11] Consider a diagonal mass matrix M with entries m. A term $\bar{q}Mq$ added to the Lagrangian can be expanded as

$$\begin{aligned} q^\dagger\gamma^0 Mq &= (q_L^\dagger, q_R^\dagger)\begin{pmatrix} 0 & 1 \\ 1 & 0 \end{pmatrix}\begin{pmatrix} m & 0 \\ 0 & m \end{pmatrix}\begin{pmatrix} q_L \\ q_R \end{pmatrix} \\ &= m\left(q_L^\dagger q_R + q_R^\dagger q_L\right). \end{aligned}$$

.

conserved *if* the mass matrix is a multiple of the identity, i.e. all quarks have the same mass. Even so, in the limit of non-equal masses, the diagonal SU(N_f) generators still commute with the mass matrix leaving some currents conserved and others not[12]. The fact that the currents pertaining to the diagonal generators are always conserved in this manner exposes the natural flavour conservation of these theories.

The corresponding SU$(N_f)_A$ currents do not, however, retain any symmetry under an explicit, non-vanishing mass term.

Chiral symmetry breaking and the chiral condensate

There is evidence from hadronic-scale QCD[13] (QCD), that the chiral symmetry is spontaneously broken. The first piece of evidence comes from the absence of parity doublets in the spectrum (see Appendix A). In $N_f = 2$ chiral QCD for example, the lowest-lying $J^\pi = 0^+$ and 1^+ candidate states, the sigma- and a_1-mesons, have masses of m_σ =500MeV and m_{a_1}=1260MeV respectively [40], whereas their axial counterparts, the pions and the rho-mesons, are, comparatively, a lot lighter at m_π=140MeV and m_ρ = 770MeV respectively [40]. This mass splitting is too large to be understood as the result of small explicit mass terms (for the up and down quarks) and so we must conclude that, at the hadronic scale at least, the chiral symmetry of QCD, SU$(N_f)_V \times$SU$(N_f)_A$, is not fully realised[14].

A second piece of evidence comes in the form of the interaction strength between a quark-antiquark pair increasing as the particles get further apart. It then becomes energetically more favourable for the ground state of QCD to consist of a condensate of quark-antiquark pairs. Since any change in the vacuum must have no net momentum or angular momentum, the quark-antiquark pair must consist of one left-handed quark field and the antiparticle of a right-handed quark field [41], see figure 2.2.

---

[12] In SU(2), $t^3 = \frac{1}{2}\begin{pmatrix} 1 & 0 \\ 0 & -1 \end{pmatrix}$ and thus $V^{\mu,3} = \bar{q}\gamma^\mu t^3 q = \bar{u}\gamma^\mu u - \bar{d}\gamma^\mu d$. The associated charge $Q_V^3 = \frac{1}{2}\int d^3(u^\dagger u - d^\dagger d)$ and reflects on isospin – its eigenvalue is generally written as I_3. In SU(3), both t^3 and t^8 are diagonal, the latter's respective charge eigenvalue being the strong hypercharge quantum number, $Y = \frac{2}{\sqrt{3}}Q_V^8$.

[13] An SU(3_c) gauge theory with SU(2_f)×SU(2_f) chiral symmetry. If the strange quarks are considered light then this becomes an SU(3_f)×SU(3_f) chiral symmetry.

[14] To reiterate the point, in the limit of chiral symmetry restoration, one would expect $M_\pi = M_\sigma$ and $M_{a_1} = M_\rho$.

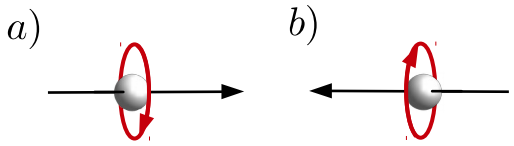

Figure 2.2: When quark-antiquark pairs are condensed out of the vacuum they must have zero net momentum and angular momentum. This leaves us with two quark fields; one right-handed quark field (a) and one antiparticle of a left-handed quark field (b) or *vice-versa*.

The ground state of QCD then has explicit interactions between left- and right-handed fields breaking the chiral symmetry.

À la Coleman's theorem, it can be shown [39] that the axial charge operators, Q_A^a, do not annihilate the vacuum, meaning the symmetry spontaneously breaks to

$$\mathrm{SU}(N_f)_V \times \mathrm{SU}(N_f)_A \to \mathrm{SU}(N_f)_V \tag{2.24}$$

when, by some mechanism (see section 2.2), the coupling strength g_s is driven to be greater than some critical value $g_s > g_s^\chi$. This is *spontaneous chiral symmetry breaking* (SχSB). In $N_f = 2$ chiral QCD, the corresponding axial Goldstone modes are the three massless[15] pions and in $N_f = 3$ chiral QCD, these also include the lightest, stranged, pseudoscalar mesons, the kaons and the η.

As alluded to in section 2.1.1, the dynamical generation of a non-zero vev of some field theory operator is responsible for the ground state becoming charged under a symmetry of the Lagrangian and thus defining SSB. In this light, the vev is an order parameter of the transition; a zero value implying that the Lagrangian shares the same symmetries as the ground state and a non-vanishing value indicating a spontaneous breaking of the symmetry. In the case of the SχSB of SU(N_c) theories, such an order parameter is found in [39]

$$\langle \bar{q}q \rangle \equiv \langle \Omega | \bar{q}q | \Omega \rangle. \tag{2.25}$$

This is the chiral- or quark-condensate, which can be interpreted as quark-antiquark pairs populating the vacuum, as described above. A non-zero value of the condensate

[15] Pions get a non-zero mass from an explicit $m_u = m_d \neq 0$ term in the QCD field Lagrangian.

can be seen to lead directly to $Q_A^a|\Omega\rangle \neq 0$ by using the relation[16]

$$[Q_A^a, \bar{q}\gamma^5 t^b q] = -\delta^{ab}\bar{q}q, \tag{2.26}$$

and taking the vacuum expectation value of both sides.

A 'massless' quark travelling through such a vacuum then obtains a dynamical mass of order $\langle\bar{q}q\rangle^{\frac{1}{3}}$; a broken chiral symmetry giving rise to dynamical Dirac mass terms mixing left- and right-handed fields. In $N_f = 2$ QCD, $\langle\bar{q}q\rangle \simeq (250\text{MeV})^3$, which explains why[17] the masses of hadrons, such as the proton, are so much heavier than the total mass of their constituent quarks.

Effective chiral Lagrangian

A low-energy, effective chiral Lagrangian can be written in terms of only the pion fields, $\pi^a(x)$. Here, we follow the work of [39]. We seek the simplest Lagrangian that exhibits an $\text{SU}(N_f)_L \times \text{SU}(N_f)_R$ global symmetry which is spontaneously broken to an $\text{SU}(N_f)_V$ symmetry. We invoke a linear-sigma model with the Lagrangian

$$\mathcal{L}_{\text{eff}} = |\partial_\mu \Phi|^2 + \mu^2|\Phi|^2 - \frac{\lambda}{4}|\Phi|^4, \tag{2.27}$$

that has such a behaviour. The transformation

$$\Phi \to L\Phi R^\dagger, \qquad L \in \text{SU}(N_f)_L \quad \text{and} \quad R \in \text{SU}(N_f)_R \tag{2.28}$$

leaves the Lagrangian invariant. The potential of the Lagrangian is arbitrarily chosen to be simple yet trigger the required SSB. An expansion about the vev $\langle\Phi\rangle \equiv v$ is carried

[16] This relationship can be derived using

$$Q_A^a = \int d^3x \bar{q}\gamma^0\gamma^5 t^a q$$

and the identity [39]

$$[\gamma^0\gamma^5 t^a, \gamma^5 t^a] = (t^a)^2\gamma^0.$$

[17] There is also a contribution from a non-zero gluonic condensate.

out, as performed in section 2.1.1,

$$\Phi(x) = (v + \frac{1}{\sqrt{2}}\sigma(x)) \exp(2i\pi^a(x)t^a/f_\pi). \tag{2.29}$$

We then write the group elements $L = \exp(i\theta_L^a t^a)$ and $R = \exp(i\theta_R^a t^a)$, with $\theta_{L/R}^a$ defined as the $\mathrm{SU}(N_f)_{L/R}$ group parameters with t^a as the group generators. Next, we apply the transformation 2.28 with these definitions to the Lagrangian 2.27 with Φ parameterised as in 2.29. In doing this, the σ-field remains invariant (expectedly since Φ was invariant) and so we can discard it altogether (since it is irrelevant to further predictions) but the π-fields transform as

$$\pi^a \to \pi^a + \frac{f_\pi}{2}(\theta_L^a - \theta_R^a) - \frac{1}{2}f^{abc}(\theta_L^b + \theta_R^b)\pi^c + ... \tag{2.30}$$

Since vector symmetries rotate the left- and right-handed fields by the same phase[18], i.e. $\theta_L^a = \theta_R^a$, the $\mathrm{SU}(N_f)_V$ vector symmetry, which remains unbroken after SχSB, leaves the pions transforming in an N_f-plet, i.e. the adjoint of $\mathrm{SU}(N_f)_V$,

$$\pi^a \to \pi^a - f^{abc}\theta^b\pi^c + ... \tag{2.31}$$

This agrees with $N_f = 2$ QCD of the Standard Model wherein the pions form a triplet under $\mathrm{SU}(N_f)_V$, $(\pi^\pm, \pi^0)$. The exponent in the angular fluctuations can be expanded as

$$\Theta(x) = e^{\frac{2i}{f_\pi}\pi^a t^a} = e^{\frac{2i}{f_\pi}\begin{pmatrix} \pi^0 & \sqrt{2}\pi^- \\ \sqrt{2}\pi^+ & -\pi^0 \end{pmatrix}}, \tag{2.32}$$

where we have set $\pi^0 \equiv \pi^{a=3}$ and $\pi^\pm = \frac{1}{\sqrt{2}}(\pi^1 \pm i\pi^2)$ [39]. We can thus write the field Φ as $\Phi = v\Theta(x)$. Since $\Theta(x)$ transforms under the $\mathrm{SU}(N_f)_L \times \mathrm{SU}(N_f)_R$ global symmetry, we may construct the most general Lagrangian out of $\Theta(x)$ and this will be a valid effective chiral theory describing low-energy QCD [39].

[18] Unlike the axial symmetries whereby the phase has a factor of γ^5, and so there is a sign difference between the phase rotating the left-handed fields and the right-handed counterparts.

2.2 Asymptotically free gauge theories

Let's return to the Lagrangian for an SU(N_c) gauge theory with massless quarks,

$$\mathcal{L} = -\frac{1}{2}\mathrm{tr}\left(F^{\mu\nu}F_{\mu\nu}\right) + i\bar{q}\not{D}q, \tag{2.33}$$

with

$$F_{\mu\nu} = \frac{1}{g_s}[D_\mu, D_\nu], \qquad D_\mu = \partial_\mu + ig_s\lambda^a A^a_\mu, \tag{2.34}$$

where λ^a are the generators of the SU(N_c) gauge group. Such a theory contains interaction vertices up to dimension four with a dimensionless coupling g_s and so is renormalizable in four dimensions.

2.2.1 Renormalization

The theory's parameters (masses, couplings etc.) will obtain radiative corrections to the bare values (those given in the Lagrangian) from higher order terms in the perturbative expansion [41]. Such corrections diverge as a result of unbounded loop-momenta. A *finite* number of counterterms subtracted from the bare Lagrangian are introduced in such a way as to cancel these divergences, leaving a finite, physical Lagrangian. This is done as follows. The bare parameters are recast as $X_{\text{bare}} = Z_X X_{\text{renorm}}$, where the new *finite* renormalized parameter is given by X_{renorm} and the renormalization constant Z_X soaks up the divergence of the bare parameters and is calculated perturbatively from the counterterms. Our Lagrangian containing the bare parameters can now be recast in two parts; a physical part containing only the finite renormalized parameters and a divergent counterterm Lagrangian,

$$\mathcal{L}_{(\text{bare})} = \mathcal{L}_{\text{phys}}(X_{\text{renorm}}) + \mathcal{L}_{\text{CT}}\left([Z_X - 1]X_{\text{renorm}}\right).$$

A renormalization scale, μ, is then defined in the process at which the new renormalized parameters are given. The fact that the bare parameters of the original Lagrangian are μ-independent but the finite renormalized parameters, to which they are related, aren't

(i.e. $X_{\text{bare}} = Z_X(\mu)X_{\text{renorm}}(\mu)$) leads to the first-order, differential Callan[19]-Symanzik[20] equation [42, 43],

$$\left(\mu\frac{\partial}{\partial\mu} + \beta(g_s)\frac{\partial}{\partial g_s} - \sum_i \gamma_i(\mu)\right) G^{(n)}(x_1, x_2, ..., x_n; \mu, g_s) = 0, \tag{2.35}$$

with

$$\beta(g_s) = \mu\frac{\partial g_s}{\partial\mu} \qquad \text{and} \qquad \gamma_i = \mu\frac{\partial}{\partial\mu}\left(\ln Z_i\right), \tag{2.36}$$

where Z_i is the renormalization constant for a coupling parameter or operator and $G^{(n)}$ is an n-point Green's function. g_s is now a renormalized parameter also. The so-called *beta-function*, $\beta(g_s)$, is a measure of how the renormalized, strong coupling varies with the renormalization scale μ. However, it is important to bear in mind that since the beta-function can only be calculated perturbatively, its prediction of physical behaviour outside of the regime where $g_s \ll 1$ should be taken *cum grano salis*.

2.2.2 The beta function & the running coupling

Given the form a general SU(N_c) Lagrangian (equation 2.33) with N_f massless flavours transforming in the representation R, the two-loop[21] beta-function of the theory can be expressed as follows[22] [41]

$$\beta(\alpha_s) = \frac{\partial\alpha_s}{\partial\ln\alpha_s} = -\beta_0\alpha_s^2 - \beta_1\alpha_s^3 + \mathcal{O}(\alpha_s^4), \tag{2.37}$$

with [44],

$$\beta_0 = \frac{1}{2\pi}\left(\frac{11}{3}C_2(G) - \frac{4}{3}N_f C_2(R)\frac{\dim(R)}{\dim(G)}\right) \tag{2.38}$$

and [44]

$$\beta_1 = \frac{1}{8\pi^2}\left(\frac{34}{3}\left[C_2(G)\right]^2 - \left[\frac{20}{3}C_2(G)C_2(R) + 4\left[C_2(R)\right]^2\right]N_f\frac{\dim(R)}{\dim(G)}\right), \tag{2.39}$$

[19] Curtis G. Callan, Jr., 1942-.
[20] Kurt Symanzik, 1923-1983.
[21] Beyond two-loop the beta-function becomes renormalization scheme dependent.
[22] The beta-function may be expressed directly in terms of g_s,

$$\beta(g_s) = -\beta_0\frac{g_s^3}{(4\pi)^2} - \beta_1\frac{g_s^5}{(4\pi)^4} + \mathcal{O}\left(g_s^7\right).$$

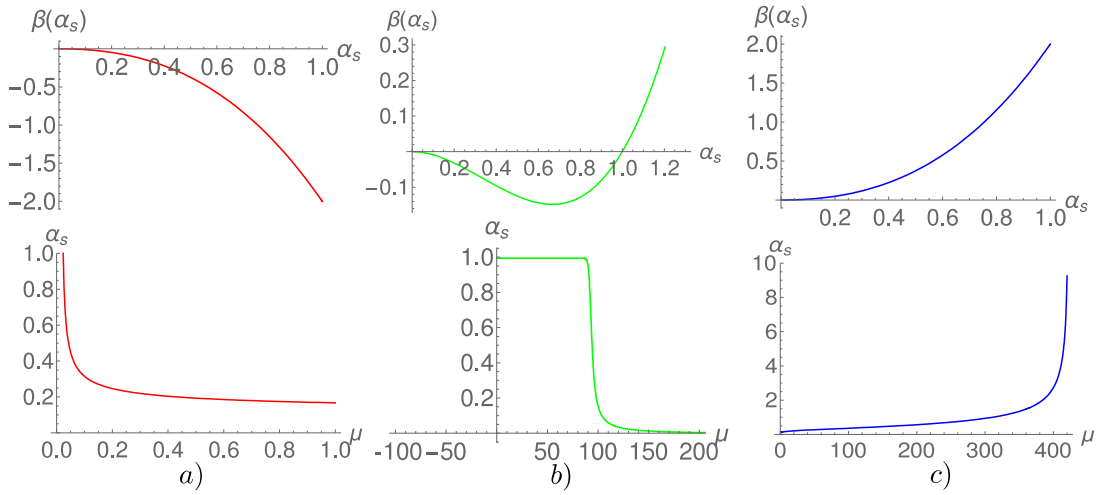

Figure 2.3: a) The beta function for $\beta_0 > 0$ and $\beta_1 > 0$ (top) with the running of the coupling (bottom). b) The beta function for $\beta_0 > 0$ and $\beta_1 < 0$ (top) with the running of the coupling (bottom) c) The beta function of $\beta_0 < 0$ and $\beta_1 < 0$ (top) with the running of the coupling (bottom).

where $\alpha_s \equiv \frac{g_s^2}{4\pi}$. Above, we denote the adjoint representation as G and its respective quadratic Casimir[23] as $C_2(G) \equiv N_c$. The form of β tells us directly about the running coupling. Figure 2.3 shows the three main profiles of β in SU(N_c) gauge theories and their respective running couplings. In 2.3 a), we see $\beta \leq 0\ \forall \alpha_s$, which occurs due to $\beta_0 > 0$ and $\beta_1 > 0$: it leads to profile of $\alpha_s(\mu)$ shared with the Standard Model QCD gauge theory with fundamental quarks. Values of α_s such that $\beta(\alpha_s) = 0$ indicate regions where the running has ceased and are therefore called *fixed-points*. In 2.3 a), this occurs at $\alpha_s = 0$ (a so-called *trivial*, and in this case *ultraviolet(UV)-trivial* fixed-point) and translates into the coupling strength asymptotically vanishing at large μ. This is the phenomenon of *asymptotic freedom* [30, 31], whereby the interaction strength between quarks asymptotically vanishes in the UV, yielding a free, non-interacting theory. The regime shown in figure 2.3 b) occurs when $\beta_0 > 0$ but $\beta_1 < 0$. This leads to there being two fixed points; the trivial one leading to asymptotic freedom and another *non-trivial* infrared (NTIR) fixed point at $\alpha_s = \alpha_s^*$. In the proximity of α_s^*, the running of the coupling's gradient is sufficiently small that it is referred to as *walking*, i.e. a slow run. As $\beta_0 \to 0^+$, the value of α_s^* is pushed closer to zero. Once the value of the coupling at

[23] Hendrik B. G. Casimir, 1909-2000.

the fixed point is small enough to be used as a valid perturbative parameter, $\alpha_s^* \ll 1$, we are said to be in the regime of a *(Caswell*[24]*-)Banks*[25]*-Zaks*[26] *fixed point* [45, 46]. If $\beta_0 < 0$, then asymptotic freedom is lost as the whole beta-function becomes positive, see figure 2.3 c). The remaining fixed-point is a trivial IR fixed-point, like that of QED.

The other key behaviour of the beta-functions displaying asymptotic freedom is the enhancement of the coupling in the IR, which in the case of figure 2.3 a) leads to an IR-pole. This can be interpreted as the interaction strength between quarks growing as their separation increases. Such a behaviour is known as *infrared slavery* and leads to the phenomenon of *confinement* [25,47], whereby fields charged under the SU(N_c) gauge group cannot be isolated but form only 'colour-neutral', bound states called hadrons. Of course, again, due to the perturbative nature of the beta-function, one cannot *a priori* trust β above $g_s \sim 1$, but experiment signifies that this type of behaviour is correct within the remit of QCD, see figure 2.4 [48].

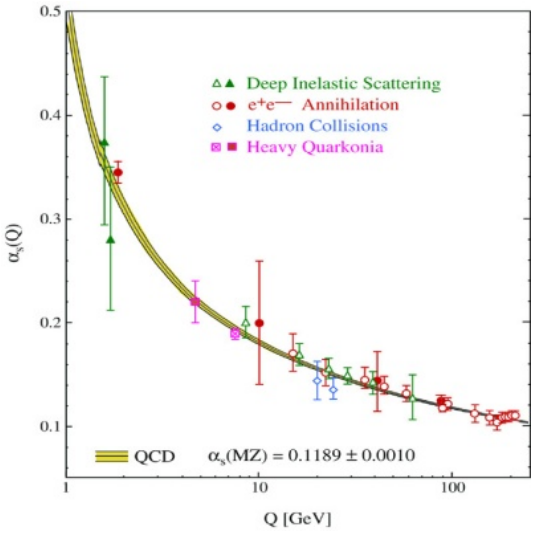

Figure 2.4: Experimental verification of the asymptotically free nature of the strong coupling parameter [48].

The scale at which these theories blow-up (i.e. the scale of the pole) is henceforth referred to as Λ_{QCD} and this sets the values of all non-perturbative parameters such as the chiral condensate, $\langle \bar{q}q \rangle$.

[24] William E. Caswell, 1947-2001.
[25] Tom Banks, 1949-.
[26] Alexander Zaks.

Walking & the conformal window

We can also define another scale Λ_χ, defined by[27] $\alpha_s^\chi = \alpha_s(\Lambda_\chi)$, at which SSB of the chiral symmetry occurs. It has been hypothesised that this scale of chiral symmetry breaking occurs when the anomalous dimension of the theory reaches unity; we discuss the rôle of the anomalous dimension below. If the running of the coupling $\alpha_s(\mu)$ passes through the critical value α_s^χ, chiral symmetry is spontaneously broken and the N_f massless quarks gain a dynamical mass $\sim \Lambda_\chi$. As such, at scales less energetic than Λ_χ, these degrees of freedom decouple leaving an '$N_f = 0$', or *pure glue*, running into the deep IR with a pole at a scale Λ_{glue}. This behaviour can give rise to profiles of $\alpha_s(\mu)$ which contain intermediate 'walking regimes'. In these walking scenarios, the running was destined for a fixed point at $\alpha_s^* > \alpha_s^\chi$ but trips the critical coupling value before reaching it, see figure 2.5. A third scale, Λ_1, may also be defined as the scale generated by the one-loop running, which roughly coincides with the transition between the UV-perturbative and the IR-walking behaviours. Theories with intermediate walking regimes are purely non-perturbative since in the framework of the perturbative beta-function, the NTIR fixed point is always reached even if the coupling passes the critical value.

If the values of β_0 and β_1 are such that α_s never reaches α_s^χ, and a fixed point is reached, $\alpha_s^* < \alpha_s^\chi$; this is the regime of the so-called *conformal window* [44, 49–56]. The running in the conformal window has such a shallow gradient that it effectively does not change over large aeons of the energy-scale, hence the name.

It is important to keep in mind that these walking and conformal window behaviours are merely hypothesised situations based on the perturbative beta-function to two-loops. Of course, we cannot know for sure that all these features do in fact appear in the full theory of any SU(N_c) model. It is purely a reasonable guess, given that there must (presumably) exist a smooth transition between the QCD-like runnings with an IR-pole and the (Caswell)-Banks-Zaks, fixed-point runnings as one changes either N_c or N_f whilst keeping the other fixed. A cartoon for SU(3) with N_f fundamental quarks is shown in figure 2.6 to show how we can move between these different hypothesised phases for this theory. A $N_f - N_c$ phase diagram for the same theory is shown in figure

[27] $\alpha_s^\chi = \frac{(g_s^\chi)^2}{4\pi}$.

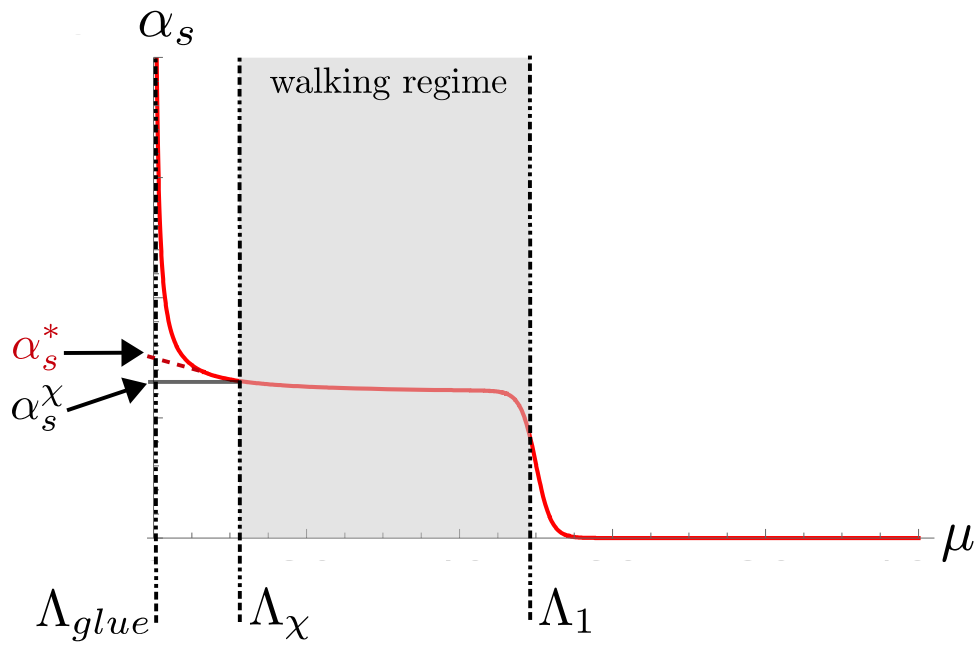

Figure 2.5: Plot of $\alpha_s(\mu)$ for the case $\alpha_s^* > \alpha_s^\chi$. The critical coupling is met at the scale, Λ_χ, triggering chiral symmetry breaking and generating a dynamic mass for the quarks of order this scale. Below Λ_χ, the quarks decouple and the theory then runs into the IR as '$N_f = 0$'. The scale Λ_1 can be seen as the UV boundary of the walking regime and it dictated by the scale generated by the one-loop running.

2.7.

2.2.3 Anomalous dimension

The Callan-Symanzik equation 2.35 also contains a second running function $\gamma_i(\mu)$ for each n-point operator of the action. In order to understand its origin, we must look at how those operators are affected by a rescaling of the coordinates $x^\mu \to \lambda x^\mu$, $\lambda \in \mathbb{R}$. Let's assume the operator $\mathcal{O}(x)$ has classical mass dimension Δ, then under such a rescaling we have

$$\mathcal{O}(x) \to \lambda^{-\Delta}\mathcal{O}(\lambda x). \tag{2.40}$$

In the renormalization process of quantum field theories, we have seen that the bare Lagrangian operators, $\mathcal{O}$, get recast as $\mathcal{O} = Z_{\mathcal{O}}(\mu)\mathcal{O}_{\text{renorm}}$, where $Z_{\mathcal{O}}(\mu)$ is the dimensionful

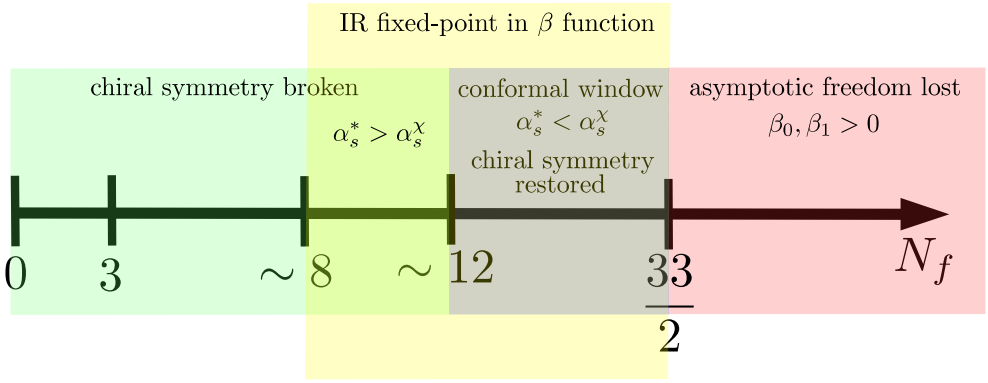

Figure 2.6: A cartoon showing the different phases of an SU(3) gauge theory with N_f fundamental flavours.

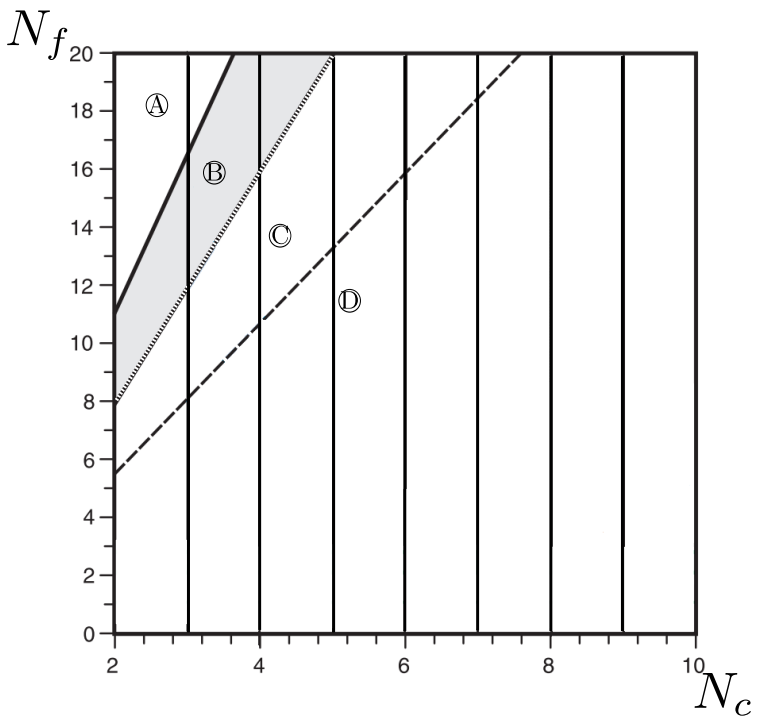

Figure 2.7: The $N_c - N_f$ phase space for the fundamental representation, adapted from [44]. Region A is where asymptotic freedom is lost. Region B is the conformal window. Region C is where walking regimes will occur since the beta function displays an NTIR fixed point but chiral symmetry is broken. Region D has only one trivial UV fixed point.

renormalization constant of the operator. Defining[28]

$$Z_{\mathcal{O}}(\mu) = \mu^{-\gamma_{\mathcal{O}}}, \tag{2.41}$$

and with the renormalized operator, $\mathcal{O}_{\text{renorm}}$, taking the same scaling dimension as the classical scaling dimension of $\mathcal{O}$, i.e. Δ, the bare Lagrangian operator $\mathcal{O}$ now has quantum scaling dimension $\Delta - \gamma_{\mathcal{O}}$. Consequently, $\gamma_{\mathcal{O}}$ is known as the *anomalous dimension*. If the renormalization constant of an operator vanishes then so does its anomalous scaling dimension.

Starting at equation 2.41 and taking the natural logarithm of both sides

$$\ln Z_{\mathcal{O}} = \gamma_{\mathcal{O}} \ln \mu, \tag{2.42}$$

we arrive at,

$$\gamma_{\mathcal{O}} = \frac{\partial}{\partial \ln \mu} \ln Z_{\mathcal{O}}, \tag{2.43}$$

in agreement with equation 2.36 defined as part of the Callan-Symanzik equation.

2.2.4 Representation of the matter fields

Up to this point, we have considered only matter fields transforming in the fundamental representation of the SU(N_c) gauge group. Changing the representation of the matter field affects the profile of the beta-function and hence the running of the coupling, see equations 2.38 and 2.39. Of course, any SU(N_c) group has an infinite number of higher dimensional representations which could be explored, however it has been shown that there are no asymptotically free theories satisfying $N_f \geq 2$ and $N_c \geq 10$ other than the fundamental, the adjoint and the two two-index (symmetric and antisymmetric) representations[29] [44]. In this light, for the purpose of this thesis, we shall only ever

[28] It is usual convention to have the mass dimension of the operator reduce in this fashion $\Delta \to \Delta - \gamma$ and its source to increase by the same value $(d-\Delta) \to (d-\Delta)+\gamma$ so that the source-operator combination in the Lagrangian is still of the correct dimension, d, of the field theory.

[29] The sign of the β_0 coefficient of the beta-function indicates whether the theory is asymptotically free or not — if $\beta_0 > 0$ then asymptotic freedom is a property of the running, if $\beta < 0$ it is not. From equation 2.38, we can see that as the dimension of the representation is increased, the matter contribution (i.e. the second term with the N_f coefficient) becomes more negative whereas the gauge term remains constant. From this, it is clear that a higher dimensional representation will lose asymptotic freedom earlier than a lower dimensional representation.

consider these four representations. In a similar vein to the fundamental $N_f - N_c$ phase space in figure 2.7, the $N_f - N_c$ phase space for all four of these representations can be seen in figure 2.8. An important property of the phase-space for the adjoint representation is that the transition values of N_f (in and out of the conformal window and with and without asymptotic freedom) are independent of N_c. This is clear from the structure of β_0 and β_1 whereby fixing $R = G$ leaves the value of N_f which solves $\beta_{0/1}(N_f) = 0$ independent of N_c. A table of the important, distinguishing parameters of the different representations can be seen in table 2.1.

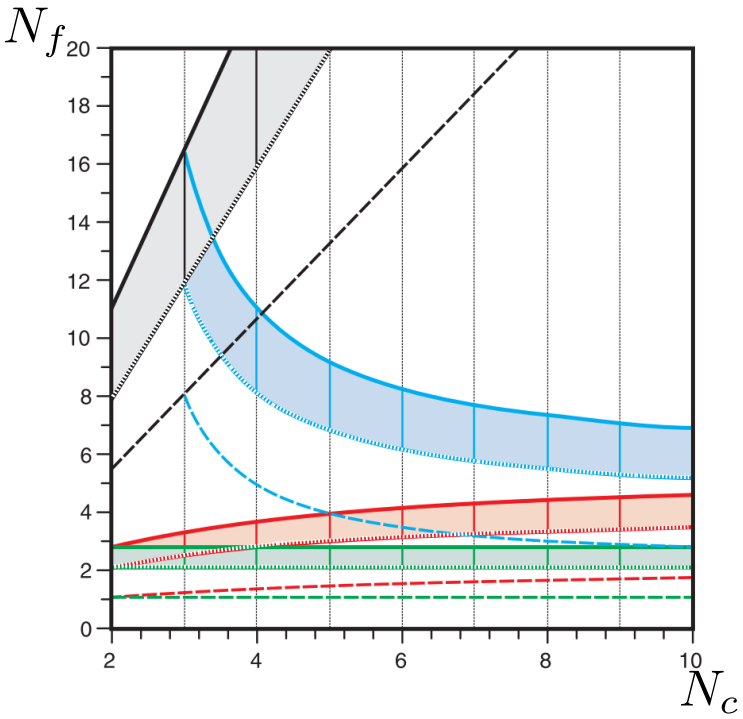

Figure 2.8: The $N_c - N_f$ phase space for the fundamental representation (black), the adjoint representation (green), the two-index symmetric representation (red) and the two-index antisymmetric representation (blue), adapted from [44].

2.2.5 Large-N_c expansion

In SU(N_c) gauge theories exhibiting a confining infrared, the coupling g_s is not a good expansion parameter at small μ. This prevents the use of the powerful perturbative tools, used to much success in the electroweak sector of the Standard Model, to try to understand hadronic scale QCD. It was suggested by 't Hooft [57], that a different expansion parameter, namely $1/N_c$ as $N_c \to \infty$, might be used in its place. In this

R	$\dim(R)$	$C_2(R)$	$N_f^{\max}$
Fundamental	N_c	$\frac{N_c^2-1}{2N_c}$	$\frac{11}{2}N_c$
Adjoint (G)	N_c^2-1	N_c	$2\frac{3}{4}$
2IS	$\frac{N_c(N_c+1)}{2}$	$\frac{(N_c-1)(N_c+2)}{N_c}$	$\frac{11}{2}\frac{N_c}{N_c+2}$
2IA	$\frac{N_c(N_c-1)}{2}$	$\frac{(N_c+1)(N_c-2)}{N_c}$	$\frac{11}{2}\frac{N_c}{N_c-2}$

Table 2.1: Distinguishing quantities of representations of $SU(N_c)$ gauge theories with asymptotic freedom valid for any $N_c \geq 2$. $\dim(R)$ is the dimension of the representation, $C_2(R)$ is the quadratic Casimir of the representation and $N_f^{\max}$ is the maximum number of flavours allowed before asymptotic freedom is lost at fixed N_c.

section, we follow [58].

Studying the one-loop beta function of such an SU(N_c) gauge theory with N_f fundamental flavours (see equation 2.38)

$$\beta(g_s) = \frac{\partial g_s}{\partial \ln \mu} = -\left(\frac{11}{3}N_c - \frac{2}{3}N_f\right)\frac{g_s^3}{(4\pi)^2}, \tag{2.44}$$

it is clear that the beta-function is ill-defined for large $N_c \to \infty$. In order to have a sensible expansion in N_c^{-1} for large N_c, a new coupling is defined as $\lambda \equiv g_s^2 N_c$, the so-called *'t Hooft coupling*. For λ to make sense as a coupling parameter as $N_c \to \infty$, one must also take the limit $g_s^2 \to 0$ such that λ is fixed — this is the *'t Hooft limit*. The beta-function can now be recast as

$$\frac{\partial \lambda}{\partial \ln \mu} = -\left(\frac{11}{3} - \frac{2}{3}\frac{N_f}{N_c}\right)\frac{\lambda^3}{(4\pi)^2}, \tag{2.45}$$

which is well-defined in the limit $N_c \to \infty$. Moreover, in the limit $N_c \to \infty$, the quark contribution is suppressed.

In order to appreciate the expansion in large N_c, we introduce a double line notation. In this notation, gauge fields no longer carry one adjoint index but rather one fundamental and one anti-fundamental index. The propagator of the gauge field is then represented by a double line; one fundamental propagator and one anti-fundamental propagator (examples of these diagrams can be see in figure 2.9). A schematic La-

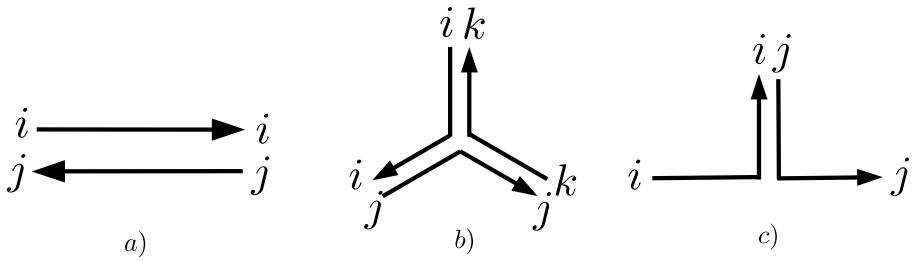

Figure 2.9: The double line notation for a) a gauge field propagator, b) a three point gauge field vertex and c) a matter field interacting with a gauge field.

grangian for the theory can then be crudely written as follows;

$$\mathcal{L} = \partial^\mu \Phi^i_j \partial_\mu \Phi^j_i + g_s \Phi^i_j \Phi^j_k \Phi^k_i + g_s^2 \Phi^i_j \Phi^j_k \Phi^k_l \Phi^l_i + i\bar{\Psi}^i \not{\partial} \Psi^i + g_s \bar{\Psi}^i \Phi^i_j \Psi^i, \tag{2.46}$$

where Φ^i_j represents a field transforming in the adjoint representation (representing the gauge field and now carrying one fundamental and one anti-fundamental index) and Ψ^i represents a fundamental degree of freedom (representing the matter fields).

The effective Lagrangian 2.46, under the three transformations, $\lambda = g_s^2 N_c$, $\tilde{\Phi}^i_j = \sqrt{\frac{\lambda}{N_c}} \Phi^i_j$ and $\tilde{\Psi}^i = \sqrt{\frac{\lambda}{N_c}} \Psi^i$ yields

$$\mathcal{L} = \frac{N_c}{\lambda} \left(\partial^\mu \tilde{\Phi}^i_j \partial_\mu \tilde{\Phi}^j_i + \tilde{\Phi}^i_j \tilde{\Phi}^j_k \tilde{\Phi}^k_i + \tilde{\Phi}^i_j \tilde{\Phi}^j_k \tilde{\Phi}^k_l \tilde{\Phi}^l_i + i\tilde{\bar{\Psi}}^i \not{\partial} \tilde{\Psi}^i + \tilde{\bar{\Psi}}^i \tilde{\Phi}^i_j \tilde{\Psi}^j \right). \tag{2.47}$$

From 2.47, it is easy to see that for a given diagram, every propagator contributes a factor of λ/N_c and each vertex yields a factor of N_c/λ. If every loop also contributes a factor of N_c to run over the different colours, each diagram has a coefficient

$$C \equiv \left(\frac{\lambda}{N_c}\right)^E \left(\frac{N_c}{\lambda}\right)^V N_c^L = N_c^{E-V+L} \lambda^{V-E}, \tag{2.48}$$

where E is the number of propagators (or edges), V the number of vertices and L the number of loops. The coefficient N_c^{E-V+L} is equivalent to N_c^{2-2g} where $2-2g$ is the Euler characteristic [59] of the diagram's topology having genus (i.e. number of handles) g. The coefficient, C, can be recast as

$$\frac{N_c^2 \lambda^{V-E}}{N_c^{2g}}, \tag{2.49}$$

which indicates that the *planar*, $g = 0$, diagrams dominate over higher genera in the $N_c \to \infty$ limit — see figure 2.10. In summary, to understand a QCD-like theory at large N_c, we need only to perform an expansion in the genus of the double-line diagram's topology; a calculation over all $g = 0$ diagrams yielding a first-order result and so on.

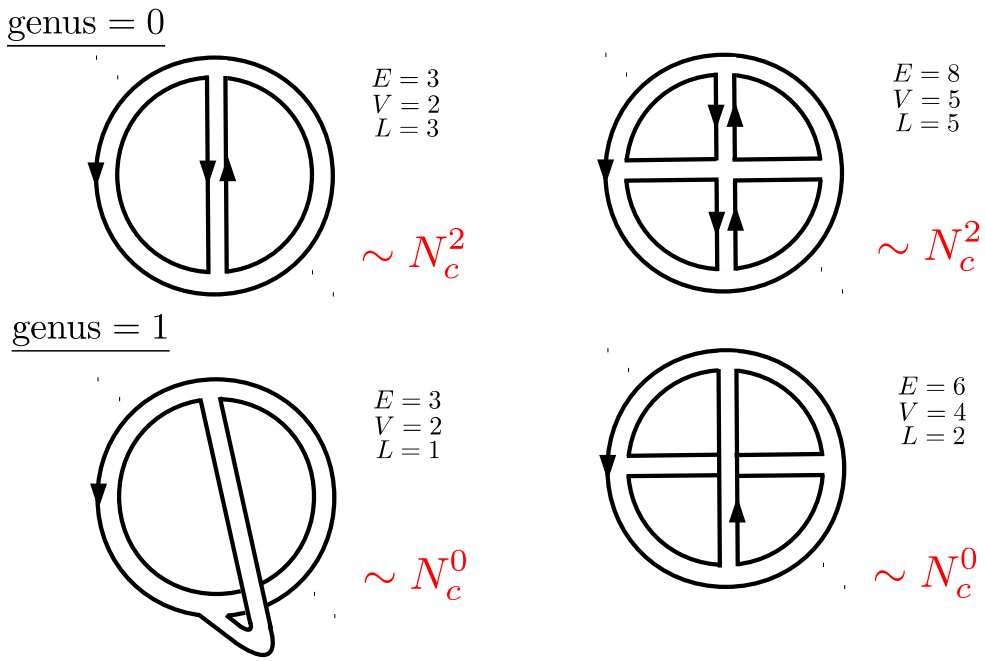

Figure 2.10: The lower genus diagrams in the double line notation dominate over higher genera. All diagrams of the same genus are proportional to the same power of N_c and so, to leading order, only the planar $g = 0$ diagrams, proportional to N_c^2 need be considered in the $N_c \to \infty$ limit.

2.3 String theory

Throughout the late 1950s and early 1960s, experimental evidence was surfacing that indicated a strong linear relationship between the rotational angular momentum of what we now know as hadrons and their squared masses; $L \sim m^2$. No matter what the hadron, the linear paths the excited states filled out on the (L, m^2)-plane were all, remarkably, parallel. Such paths are referred to as Regge trajectories[30] [60] and the gradient referred to as the Regge slope, α', giving $L = \alpha' m^2$. This linear behaviour is most unexpected from the viewpoint of particles as small 'billiard balls'. Spinning up a billiard ball to

[30] Named after Tullio Eugenio Regge (1931-2014) but first hypothesised by Geoffrey Chew (1924-) and Steven C. Frautschi (1933-).

greater and greater values of angular velocity will in turn increase its energy, up to a point[31], as $L \sim m$: this is true even on the atomic scale. It was known that these hadrons were necessarily composite, for one cannot spin up a point-particle[32], but the structure was still a mystery. One answer was that the bosonic hadron states (the mesons, as we now refer to them) were formed of a quark and an antiquark point particles connected by a string. A string is easily spun and, furthermore, a classical rotating string reproduces the $L \sim m^2$ behaviour of the experimental Regge trajectories.

The models proposed within the new field of string theory were plagued by systemic issues. The theories always seemed to predict a tachyon in the particle spectrum as well as a massless spin-2 particle that related to nothing seen in nature. Furthermore, these theories had to live in 26 dimensions and only accounted for the bosonic part of the spectrum. After the emergence of QCD in the 1970s, string theory began to lose favour as it became clear that QCD was able to satisfactorily explain the strong nuclear interaction at large energy scales.

Despite the loss of interest in string theories as a description for the strong nuclear interaction, they were later revived when it became apparent that the ineradicable spin-2 particle could be justified as a graviton. This 'discovery' of a graviton allowed the physics community to rationalise that such string theories might provide a candidate to reconciling the two pillars of modern physics, to wit: Quantum Field Theory (QFT) and General Relativity (GR). This section contains a brief introduction to string theory leading on to the following section on D-branes, higher dimensional string-like objects that are fundamental to the AdS/CFT correspondence and other related holographic models. For a more in depth discussion on the fundamentals of string theory (and the low energy supergravity limit), we recommend [61–66] whence the following brief introduction is adapted.

[31] Until the centrifugal forces on the ball become too large and it rips apart.
[32] The reasoning as to why no higher excited states of the electron are found, for example.

2.3.1 Bosonic string action

The underlying principle to string theory is to consider extended one-dimensional 'strings' of length[33] $l_s = \sqrt{\alpha'}$ as the fundamental objects rather than the point-like (zero-dimensional) 'particles' that are usually assumed. Just as a point-particle will sweep out a worldline as it moves, a one-dimensional string sweeps out a two-dimensional *world-sheet* that can be parameterised by two coordinates; τ, the proper time, and σ, the spatial range of the string, which, without loss of generality, we set to be $\sigma \in [0, \pi]$, for later convenience. The action of such a string is given by the area of the world-sheet (the worldsheet being denoted by Ω) swept out by the string, with the simplest parameterisation of such being the so-called Nambu-Goto action,

$$S_{NG} = -T \int_{\Omega} d\tau d\sigma \sqrt{-\det\left(G_{MN} \frac{\partial X^M}{\partial \sigma^a} \frac{\partial X^N}{\partial \sigma^b}\right)}, \tag{2.50}$$

where T is the string tension[34], X^M are the functions describing the embedding of the worldsheet, G_{MN} is metric of the d-dimensional target spacetime, the spacetime in which the worldsheet sits, and $\sigma^a = (\tau, \sigma)$. Instead of a two-dimensional worldsheet embedded in a higher-dimensional target space, one can just as easily interpret 2.50 as a two-dimensional field theory with d bosonic fields $X^M(\tau, \sigma)$. It is the excitations of these fields which are to be understood as the 'particle' spectrum of the string theory.

The Nambu-Goto action in its present, square-root form gives rise to a rather laborious undertaking to quantise the system. An alternative, equivalent action is the Polyakov[35] action,

$$S_P = -\frac{T}{2} \int_{\Omega} d\tau d\sigma \sqrt{\det h_{ab}} h^{ab} G_{MN} \frac{\partial X^M}{\partial \sigma^a} \frac{\partial X^N}{\partial \sigma^b}, \tag{2.51}$$

where we have now eliminated the uncooperative square root at the expense of an extra *auxiliary* field, h_{ab}. The equations of motion of h_{ab} obtained by variation of the action

[33] The string length is naturally proportional to the tension carried in the string. This tension can be cast in terms of the Regge slope parameter α', which pertains to how the angular momentum and mass of a meson are related as the particle is spun: the extension of the string between the quarks, in the string theory picture.

[34] The string tension (mass per unit length) is inversely proportional to the string length squared, given as $T^{-1} = 2\pi l_s^2$.

[35] Alexander M. Polyakov, 1945-.

2.51 acts as constraints[36] to recover the Nambu-Goto action — this can be seen explicitly by substituting the solutions to the equations of motion of h_{ab} into the Polyakov action to return to the form of the action in 2.50.

The Polyakov action 2.51 exhibits some important symmetries:

I) *Poincaré invariance* of the target spacetime covered by the metric G_{MN},

$$X^M \to X'^M = \Lambda^M_N X^N + c^M, \tag{2.52}$$

where Λ^M_N are the Lorentz transformations of the target spacetime and c^M are the translation transformations of the target spacetime.

II) *Diffeomorphism invariance.* The Polyakov action remains invariant under a reparameterisation of the worldsheet coordinates,

$$(\tau, \sigma) \to (\tau', \sigma') = (f(\tau), f(\sigma)). \tag{2.53}$$

III) *Weyl transformation invariance.* The Polyakov action is furthermore invariant under a local rescaling of the worldsheet metric,

$$h_{ab} \to h'_{ab} = e^{\omega(\tau,\sigma)} h_{ab}. \tag{2.54}$$

These symmetries allow us to choose a particular gauge in which the worldsheet metric h_{ab} is equivalent to the two-dimensional Minkowski metric, $\eta_{ab} = \text{diag}(-1, 1)$. As such, the Polyakov action can be recast as

$$\tilde{S}_P = -\frac{T}{2} \int_\Omega d\tau d\sigma \left(\dot{X}^M \dot{X}_M - X'^M X'_M \right), \tag{2.55}$$

where $\dot{X}$ refers to a derivative with respect to τ, and X' is likewise the derivative with respect to σ. It is evident from this form of the string action that the equation of motion

[36] These constraints are known as the Virasoro constraints and amount to the restrictions stemming from a vanishing stress-energy tensor $T_{ab} = 0$, an equivalence of requiring the variation of the action under h_{ab} to vanish.

for the fields $X^M(\tau,\sigma)$ is given by a relativistic wave equation,

$$\ddot{X}^M = X''^M, \tag{2.56}$$

with further constraint from a variational surface term yielding a supplementary boundary condition,

$$X'^M \Delta X_M\big|_0^\pi = 0. \tag{2.57}$$

This boundary condition leads to having one of two types of string; a *closed* string, whereby $X^M(\tau,0) = X^M(\tau,\pi)$ and $X'^M(\tau,0) = X'^M(\tau,\pi)$, or an *open* string with loose ends, which further imposes that either X'^M vanishes at $\sigma = 0,\pi$ (a *Neumann*[37] boundary condition), or that $\Delta X_M = 0$, equivalent to fixing the spacetime position of the string ends (a *Dirichlet*[38] boundary condition).

If the two ends of the open string satisfy Neumann boundary conditions, it can be shown that the total momentum of the string is conserved since the momentum at the ends of the string vanishes. Conversely, for a string with two Dirichlet-type ends, by fixing the location of the ends, we immediately break the translational invariance in the target-space dimensions along which the string end is fixed, resulting in no total momentum conservation in these directions. Therefore, we must postulate that the Dirichlet ends of strings must attach to hypersurfaces, known as Dirichlet- (or D-) *branes*, which carry the momentum away. As we shall see, these D-branes play an important rôle in holographic models.

Mode expansions

Classical solutions to the equation of motion, equation 2.56, are easily found to be a Fourier[39] series expansion. For the open string, we have the solution restricted by Neumann boundary conditions given by

$$X^M_{(N)}(\tau,\sigma) = x^M + l_s\tau p^M + i l_s^2 \sum_{n\neq 0} \frac{\alpha_n^M}{n} e^{in\tau}\cos(m\sigma), \quad \text{(N)} \tag{2.58}$$

[37] Carl Gottfried Neumann, 1832-1925.
[38] Johann P. G. L. Dirichlet, 1805-1859.
[39] Jean-Baptiste Joseph Fourier, 1768-1830.

where x^M is the centre-of-mass position of the string, p^M the total, enclosed momentum and α_n^M are the Fourier modes. The solution constrained by Dirichlet boundary conditions yields

$$X^M_{(D)}(\tau,\sigma) = X^M(\tau,0) + \frac{1}{\pi}\left(X^M(\tau,\pi) - X^M(\tau,0)\right)\sigma + l_s \sum_{n\neq 0} \frac{\alpha_n^M}{n} e^{-in\tau}\sin(n\sigma). \quad \text{(D)} \tag{2.59}$$

In the case of the closed string, there are two solutions corresponding to the left- and right-moving modes. In so-called light-cone coordinates, $\sigma_\pm = \tau \pm \sigma$, these are

$$X^M_{(L)}(\sigma_+) = \frac{1}{2}x^M + \frac{l_s^2}{2}p^M\sigma_+ + \frac{il_s}{2}\sum_{n\neq 0}\frac{\tilde{\alpha}_n^M}{n}e^{-in\sigma_+}, \quad \text{(L)} \tag{2.60}$$

and

$$X^M_{(R)}(\sigma_-) = \frac{1}{2}x^M + \frac{l_s^2}{2}p^M\sigma_- + \frac{il_s}{2}\sum_{n\neq 0}\frac{\alpha_n^M}{n}e^{-in\sigma_-}. \quad \text{(R)} \tag{2.61}$$

Here, p^M is the centre-of-mass momentum and we distinguish the Fourier modes of the left and right movers as $\tilde{\alpha}_n$ and α_n, respectively.

Quantisation

Quantisation leads us to promoting X^M to an operator in the corresponding Hilbert[40] space, equivalent to promoting x^M, p^M and α_n^M to operators. This gives the algebra

$$[x^M, p^N] = i\eta^{MN}, \tag{2.62}$$

$$[\alpha_m^M, \alpha_n^N] = [\tilde{\alpha}_m^M, \tilde{\alpha}_n^N] = m\delta_{m+n}\eta^{MN}, \tag{2.63}$$

$$[\alpha_m^M, \tilde{\alpha}_n^N] = 0. \tag{2.64}$$

The α-operators act like the raising and lowering operators of the quantised harmonic oscillator, moving between higher and lower excited states. For $n > 0$, $\left(\alpha_n^M\right)^\dagger/\sqrt{n} = \alpha_{-n}^M/\sqrt{n}$ acts as the raising operator and $\alpha_n^M/\sqrt{n}$ acts as the lowering operator. Negative

[40] David hilbert, 1862-1943.

norm states are removed by setting a normal ordering constant to be unity and ensuring that the number of spacetime dimensions is less than or equal to 26. The masses of the excited states can then be derived using light cone quantisation [61] as,

$$M^2 = \frac{1}{l_s^2}(N-1), \qquad \text{(open string)} \tag{2.65}$$

and

$$M^2 = \frac{2}{l_s^2}(N-1), \qquad \text{(closed string)} \tag{2.66}$$

where N is the eigenvalue of the operator $\hat{N} = \sum_{n=1}^{\infty} :\alpha^i_{-n}\tilde{\alpha}^i_n :$ (with $i = 0, 1, ..., d-2 = 24$), which acts like the number operator of the quantum harmonic oscillator, counting the number of modes[41].

From this, it is clear that the lowest lying state ($N = 0$), in either the open or closed sector, is tachyonic and therefore causing the vacuum, $|0\rangle$, to be unstable. In the open sector, the first excited state is a massless vector $\alpha^i_{-1}|0\rangle$ and this will be of importance when we discuss D-branes and the AdS/CFT correspondence.

The closed sector's first excitation, $\alpha^i_{-1}\tilde{\alpha}^j_{-1}|0\rangle$, is a set of $(d-2)^2 = 576$ states; a symmetric traceless part, the spin-2 graviton G^{MN}, a massless trace term, the dilaton $\varphi = \alpha^i_{-1}\tilde{\alpha}^i_{-1}|0\rangle$, and an anti-symmetric part $B^{MN} = -B^{NM}$.

Knowing the field content as described above, we can rewrite a general worldsheet action with at most two worldsheet derivatives (∂_a) as,

$$S = -\frac{T}{2}\int_\Omega d\tau d\sigma \sqrt{\det h_{ab}} \left\{ \left(h^{ab} G_{MN} + \epsilon^{ab} B_{MN} \right) \frac{\partial X^M}{\partial \sigma^a} \frac{\partial X^N}{\partial \sigma^b} - \alpha' R\varphi \right\}, \tag{2.67}$$

where ϵ^{ab} is the two-dimensional, totally antisymmetric tensor and R is the 2D Ricci scalar of the geometry. The Polyakov action is recovered under $B_{MN} = \varphi = 0$.

The final term,

$$\frac{1}{4\pi}\int d\tau d\sigma \sqrt{\det h_{ab}} R = \chi \tag{2.68}$$

is a topological invariant[42] in 2D for constant φ, measuring the Euler characteristic of

[41] Since there is no privileged position on the string, the number of left- and right-moving modes are imposed to be the same, $N = N_L = N_R$.

[42] cf. Gauss-Bonnet theorem.

the worldsheet.

2.3.2 Superstring theory

The bosonic string theory action has two major drawbacks; the lowest lying state is tachyonic (leaving the theory unstable) and it does not account for fermionic degrees of freedom, a necessity if string theory is to be a candidate for a UV-complete theory of nature. Tachyonic modes will be discussed later as they reoccur in the superstring formalism. Fermionic modes can be incorporated into the string framework by naturally extending the Polyakov action, gauged to set $h_{ab} = \eta_{ab}$ as before, by an extra term resemblant of a free Dirac action,

$$\mathcal{S} = -\frac{T}{2}\int d\tau d\sigma \eta^{ab}\left(\frac{\partial X^M}{\partial \sigma^a}\frac{\partial X_M}{\partial \sigma^b} + i\bar{\Psi}^M \rho_a \frac{\partial \Psi_M}{\partial \sigma^b}\right), \tag{2.69}$$

where now $M = 0, ..., 9$.

Here the fermionic fields, $\Psi^M(\tau, \sigma)$, are two-component spinors transforming as a vector under the Lorentz transformations of the target spacetime and ρ^a are the two-dimensional equivalents of the 4d gamma matrices of the Standard Model. Assuming the fermionic fields to be two component and Majorana (both components real), $\Psi = (\psi_+^M, \psi_-^M)^T$, we can transform the fermionic part of the action 2.69 with $\sigma_\pm = \tau \pm \sigma$ as

$$\mathcal{S}_f = -\frac{iT}{2}\int d\sigma_+ d\sigma_- \mathcal{J}\left(\psi_+^M \frac{\partial \psi_+^M}{\partial \sigma_+} + \psi_-^M \frac{\partial \psi_-^M}{\partial \sigma_-}\right), \tag{2.70}$$

with $\mathcal{J} \equiv \frac{1}{2}$ as the Jacobian of the transformation. As such, the equation of motion for the real components, $\psi_\pm$, are once again those describing relativistic wave equations, this time one left-moving wave and one right moving wave,

$$\frac{\partial \psi_-^M}{\partial \sigma_+} = \frac{\partial \psi_+^M}{\partial \sigma_-} = 0. \tag{2.71}$$

Once again, the variational methods used to derive 2.71 enforce boundary conditions required to set surface terms to zero,

$$\psi_-^M \Delta\psi_{-M}\big|_0^\pi = \psi_+^M \Delta\psi_{+M}\big|_0^\pi . \tag{2.72}$$

Open superstrings - Type I

If we are to have *open* superstrings, then we can make the surface term vanish by imposing

$$\psi_+^M = \pm\psi_-^M \tag{2.73}$$

at the string ends $\sigma = 0, \pi$. Fixing the $\sigma = 0$ end (without loss of generality) to take the positive sign leaves us with a choice of sign for the other end, $\sigma = \pi$.

The so-called *Ramond*[43]- (R-) sector chooses the *positive* sign,

$$\psi_+^M(\pi) = +\psi_-^M(\pi), \qquad \text{(R)} \tag{2.74}$$

giving the mode expansion of $\psi_\pm^M$ as,

$$\psi_\pm^M = \sum_{n\in\mathbb{Z}} d_n^M e^{-in\sigma_\pm}. \qquad \text{(R)} \tag{2.75}$$

Here, d_n^M are Fourier modes, which will become real, fermionic operators after quantisation, $\left(d_n^M\right)^\dagger = d_{-n}^M$. The masses of R open superstring states are then found to be

$$\alpha' M^2 = \sum_{n=1}^{\infty} \alpha_{-n}^i \alpha_n^i + \sum_{n=1}^{\infty} n d_{-r}^i d_r^i, \quad i = 1, .., 8. \tag{2.76}$$

The remaining Neveu[44]-Schwarz[45]- (NS-) sector chooses the *negative* sign,

$$\psi_+^M(\pi) = -\psi_-^M(\pi), \qquad \text{(NS)} \tag{2.77}$$

giving the mode expansion of $\psi_\pm^M$ as,

$$\psi_\pm^M = \sum_{r\in\mathbb{Z}+\frac{1}{2}} b_r^M e^{-ir\sigma_\pm}, \qquad \text{(NS)} \tag{2.78}$$

where b_r^M are Fourier modes, which will become real, fermionic operators after quanti-

[43] Pierre Ramond, 1943-.
[44] André Neveu, 1943-.
[45] John H. Schwarz, 1941-.

sation, but with a half-odd-integer index to satisfy the boundary condition. The masses of NS open superstring states are then found to be

$$\alpha' M^2 = \sum_{n=1}^{\infty} \alpha^i_{-n}\alpha^i_n + \sum_{r=\frac{1}{2}}^{\infty} r b^i_{-r} b^i_r - \frac{1}{2}, \quad i = 1, .., 8. \tag{2.79}$$

It is important to note that vacuum of the NS open superstring is tachyonic with $M^2 = -1/2\alpha'$. The seemingly innocuous choice of sign has a significant impact on the states after quantisation. The R-Sector (+ sign) leads to spacetime fermions (spinors) while the NS-Sector (- sign) leads to spacetime bosons.

Closed superstrings

The construction of *closed* superstrings is again possible. In this scenario, the surface term becomes a periodicity condition on the superstring,

$$\psi^M_{\pm}(\tau, \sigma) = \pm\psi^M_{\pm}(\tau, \sigma + \pi). \tag{2.80}$$

Choosing the positive sign describes periodic boundary conditions (again known as Ramond boundary conditions) and the negative sign describes an antiperiodic boundary condition (Neveu-Schwarz condition). Of course, we can impose either condition on the left- and right-moving wave solutions independently, generating four possible closed superstring states intuitively labelled (R, R), (NS, NS), (NS, R) and (R, NS) describing the boundary condition on the (left, right)-modes respectively, see table 2.2

Mode Expansion	**Sector**
Right-moving solutions:	$\psi^M_-(\sigma_-)$
$\sum_{n\in\mathbb{Z}} d^M_n e^{-in\sigma_-}$	R
$\sum_{r\in\mathbb{Z}+\frac{1}{2}} b^M_r e^{-ir\sigma_-}$	NS
Left-moving solutions:	$\psi^M_+(\sigma_+)$
$\sum_{n\in\mathbb{Z}} \tilde{d}^M_n e^{-in\sigma_+}$	R
$\sum_{r\in\mathbb{Z}+\frac{1}{2}} \tilde{b}^M_r e^{-ir\sigma_+}$	NS

Table 2.2: Mode expansions for the left- and right-moving closed string solutions.

After quantisation, the (NS, NS) and (R, R) states are bosonic string states whereas the mixed (NS, R) and (R, NS) states are fermionic.

Gliozzi-Scherk-Olive projection & type IIA/B

In order to remove the tachyonic degrees of freedom and ensure an equal number of bosonic and fermionic states (to satisfy having a manifest supersymmetry), we introduce a *G-Parity*[46] operator in the NS-sector,

$$G_{NS} = (-1)^{F+1}, \tag{2.81}$$

where $F = \sum_{r=\frac{1}{2}}^{\infty} b^i_{-r} b^j_r$ counts the number of b_r oscillators. The so-called Gliozzi[47]-Scherk[48]-Olive[49] (GSO) projection [67] removes the tachyonic mode by ensuring

$$G_{NS}|\text{state}\rangle = +|\text{state}\rangle.$$

Since the ground state has no b-oscillators, $F = 0$, leading to a negative G-parity state and is hence projected out of the spectrum. In the R-Sector, we define a similar operator,

$$G_R = \rho_{11}(-1)^F, \tag{2.82}$$

where F is now given by $\sum_{n=1}^{\infty} d^i_{-n} d^j_n$, counting the number of d-oscillators, and ρ_{11} is the 10-dimensional analogue of the γ_5 Dirac matrix. The massless string states in the R-sector can be said to have a definite chirality, if they satisfy

$$\rho_{11}|\text{state}\rangle = \pm|\text{state}\rangle. \tag{2.83}$$

Hence, by projecting out states of a certain G-parity in the R-sector, one imposes a chirality projection onto the spinors. The freedom in choice over the chirality of the R-sector fermionic modes leads to two different closed string theories; type IIA where

[46] The name is a remnant from when string theory was being proposed as a formalism for understanding hadronic physics.
[47] Ferdinando Gliozzi, 1940-.
[48] Joël Scherk, 1946-1980.
[49] David Ian Olive, 1937-2012.

the chiralities of the left- and right-movers are different and type IIB where they are the same.

Naturally, the (NS, NS)-type closed string is the same for types IIA and IIB; containing the graviton G^{MN}, dilaton φ and the antisymmetric *Kalb-Ramond* tensor field B^{MN}. The latter two-form is the string generalisation to the one-form electromagnetic potential A^{μ} and as such strings[50] can be seen as the source of B^{MN}, just as charged point-particles are the source of A^{μ} in electromagnetism. The (R, R)-sector differs between types IIA and IIB, as expected. In type IIB, we find[51] a scalar C, and two antisymmetric tensor fields C^{MN} and C^{MNPQ}, whereas in type IIA we get a vector C^{M} and an antisymmetric tensor field C^{MNP} at the massless level. The mixed (NS, R)- and (R, NS)-sectors contain the fermionic superpartners to the bosonic sectors.

2.3.3 Type IIB low-energy action

String coupling and the dilaton

In an *interacting* type II theory with coupling g_{σ}, one can calculate perturbatively the string scattering amplitudes via the formula [68]

$$\text{String Amplitude} = \sum_{\text{topologies}} g_{\sigma}^{-\chi} \int \mathcal{D}X^{M} \mathcal{D}h^{ab} e^{-S[X]} \prod_{i} V_{i}, \tag{2.84}$$

where $\chi = 2 - 2g$ is the Euler[52] characteristic [59] of the worldsheet and g the genus - a value counting the 'holes' in the worldsheet. V_i are the relevant vertex operators of the scattering.

Now assuming the dilaton field, φ, acquires a non-zero vacuum expectation value (vev), $\varphi \to \varphi + \langle\varphi\rangle$, then the string Boltzmann[53] factor e^{-S} changes by a constant factor of $e^{-\chi\langle\varphi\rangle}$ (see equation 2.68). It is then natural to associate the string coupling

[50] These fundamental strings are known as $F1$-strings in the literature [64].
[51] The notation for the type II fields is sometimes denoted by $C_{(r)}$ for an r-form; for example, the Kalb-Ramond tensor is often denoted as $B_{(2)}$.
[52] Leonhard Euler, 1707-1783.
[53] Ludwig Eduard Boltzmann, 1844-1906.

constant, g_σ, to the dilaton vev as

$$g_\sigma = e^{\langle\varphi\rangle}, \tag{2.85}$$

by direct comparison with equation 2.84. As such, the string coupling isn't an independent parameter of the theory; it is determined dynamically by the vev of the dilaton.

Supergravity limit

Up to this point, we have only considered the massless modes of the string spectrum. Since the masses of the higher excited modes are proportional to $(\alpha')^{-\frac{1}{2}}$, all but the massless modes are irrelevant in the low energy limit $\alpha' = l_s^2 \to 0$ — an effective zooming-out, seeing the strings as point-like. We are then able to do perturbative expansions about α', the leading order of this expansion is the limit of *supergravity* [65].

Type IIB supergravity action

We now turn our focus away from the worldsheet action and write down a target-space action, which encodes all of the same information and degrees of freedom contained in the above analysis. The *bosonic* part of the type IIB supergravity action can then be written as [65, 66]

$$\begin{aligned} S_{IIB} = \frac{1}{2^7\pi^7\alpha'^4}\Bigg[\int d^{10}X\sqrt{-\det G^{MN}}\Bigg\{e^{-2\varphi}\left(R + 4\partial_M\varphi\partial^M\varphi - \frac{1}{2}|H_{(3)}|^2\right) \\ -\frac{1}{2}|F_{(1)}|^2 - \frac{1}{2}|\tilde{F}_{(3)}|^2 - \frac{1}{4}|\tilde{F}_{(5)}|^2\Bigg\} - \frac{1}{2}\int C_{(4)}\wedge H_{(3)}\wedge F_{(3)},\Bigg] \end{aligned} \tag{2.86}$$

where we define

$$|F_{(r)}|^2 = \frac{1}{r!}G_{M_1N_1}...G_{M_rN_r}F^{M_1...M_r}\bar{F}^{N_1...N_r}$$

and $\bar{F}$ denoting the complex conjugate of F. We also define the field strength tensors of the RR-forms [65, 66]

$$\begin{aligned} F_{(p)} &= dC_{(p-1)} \qquad \tilde{F}_{(3)} = F_{(3)} - CH_{(3)} \\ \tilde{F}_{(5)} &= F_{(5)} - \frac{1}{2}C_{(2)} \wedge H_{(3)} + \frac{1}{2}B_{(2)} \wedge F_{(3)}, \end{aligned} \tag{2.87}$$

and we define $H_{(3)} = dB_{(2)}$ with d the exterior derivative.

2.4 D-branes

In this section, we briefly outline the importance of D-branes, the higher dimensional string-like objects that we earlier postulated to exist in the case of open strings with Dirichlet boundary conditions on their endpoints. For more discussion on D-branes we recommend [69].

T-duality and D-branes

As previously mentioned, D-branes play an important rôle in string theory. Such hypersurfaces are necessitated when open strings are chosen to have Dirichlet endpoints — see figure 2.11. One might argue, nonetheless, that if such Dirichlet endpoints in the open sector aren't compelled to exist then D-branes are nothing more than a hypothetical excrescence of the theory. This argument is however flawed when one looks at the so-called *T-dual* [70, 71] of a Neumann open string.

T-Duality[54] is a symmetry arising from the closed string sector under compactification of one spacetime dimension. For example, take a closed superstring theory compactified on a circle of radius R in the ninth spatial direction. Since the string points x^9 and $x^9 + 2\pi R$ should be identical, it follows that the translational operators should be identical $e^{-ip_9 x^9} = e^{-ip_9(x^9+2\pi R)}$ and as such the momentum is quantised in the compactified direction;

$$p^9 = \frac{K}{R}, \qquad K \in \mathbb{Z}. \tag{2.88}$$

[54] Or *target spacetime duality*.

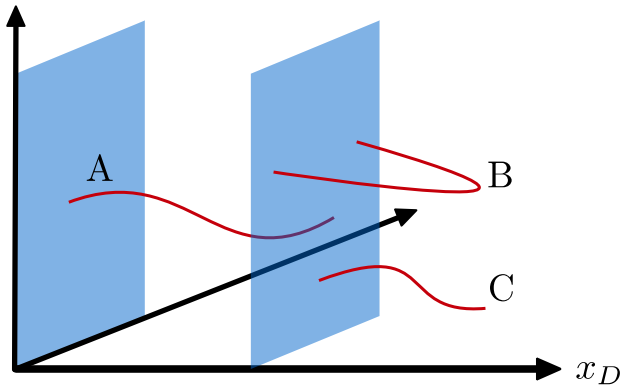

Figure 2.11: D-branes as hyperplanes over which Dirichlet strings can move freely, spanning the dimensions (or a subset thereof) of the target spacetime along which the string is Neumann. x_D are the dimensions in the target spacetime where the shown string ends are fixed. String A shows an open string with two Dirichlet ends stretched between two different D-branes, string B shows a string attached at both ends on the same brane and string C shows a string with one Dirichlet end (fixed to the D-brane) and one free-to-move Neumann end.

K is known as the Kaluza[55]-Klein[56] excitation quantum number. Since a closed string can also be wound around the compactified dimension[57], x^9 may not be single-valued, instead changing by $2\pi WR$, where $W \in \mathbb{Z}$ is the *winding number*. The masses of the string states are then amended to

$$\tilde{M}^2 = M^2 + \frac{K^2}{R^2} + W^2 \frac{R^2}{(\alpha')^2}. \tag{2.89}$$

T-Duality is the symmetry pertaining to the now-evident invariance under the simultaneous transformations

$$K \longleftrightarrow W \qquad \text{and} \qquad R \longleftrightarrow \frac{\alpha'}{R}, \tag{2.90}$$

i.e. the complete spectrum of the theory is unaware of a change in the radius of the compactified direction, $R \to \alpha'/R$, up to a relabelling of K and W. When $R^2 \gg \alpha'$, string effects are small and classical geometrical reasoning can be used, whereas in its

[55] Theodor F. E. Kaluza, 1885-1954.
[56] Oskar B. Klein, 1894-1977.
[57] Winding about a compact dimension is something which a point-particle cannot do and so it is a pure string effect unlike the Kaluza-Klein excitations.

T-dual, $\left(\frac{\alpha'}{R}\right)^2 \ll \alpha'$ and so string effects dominate. So T-dualising a theory can move one's system between two different regimes of validity; the classical and the stringy quantum.

Naturally, the idea of T-Duality related to the compactification $R^{1,9} \to R^{1,8} \times S^1$ can be extended to more complicated compactifications [72]. One consequence of T-Duality is that the chirality of the left-moving modes are flipped whereas the right-movers are unaffected: T-dualising a type II superstring theory then has the realisation of morphing type IIA theories into type IIB and vice-versa.

From equation 2.89 it can be seen that, as the radius of compactification becomes smaller and smaller, the Kaluza-Klein modes get heavier and become more costly to excite in opposition to the ever lighter winding modes. As $R \to 0$, we lose one dimension but it re-appears in the effective form of a continuum of winding modes (since they become ever easier to excite as R diminishes).

Considering a Neumann open string sector, no such winding number is present, since such a string can just unfurl. Therefore, as $R \to 0$, Neumann open strings really do only see $d-1$ dimensions — there is no continuum of winding modes to compensate. Since all interacting open string sectors contain closed strings[58] and closed strings *can* wind around the compactified dimension, we have a theory whereby open strings only see $d-1$ dimensions but the closed sector sees the full d dimensions. This threatens T-duality since the open strings 'know' if they are living in a theory with a large compactified circle or small, depending on the number of dimensions open to them. Such a quandary is solved when we recognise that only the *endpoints* of an open string are distinguishable from a point on a closed string. In this case, only the endpoints are restricted to move in $d-1$ dimensions allowing the rest of the string full knowledge of all d dimensions. This implies that the endpoints must have a Dirichlet boundary condition in the one dimension in which their movement is fixed. So an open string with Neumann boundary conditions in all directions at large-R compactification becomes an open string with Neumann boundary conditions in all but one direction in the T-Dual (the small circle $R \to 0$) and vice-versa. Thus we must postulate the existence of a D-brane to which

[58] An interacting open string can trivially become a closed string if its two endpoints interact and join!

the Dirichlet direction affixes. Thus T-Duality is an exact symmetry of the open sector too, equivalent of exchanging Neumann$\longleftrightarrow$Dirichlet endpoints along the T-dualised directions. D-branes are therefore necessary objects for a fully-realised string theory.

We classify D-branes by their spatial dimension: a Dp-brane extends in p spatial dimensions, making it a $p+1$ dimensional object. E.g. a D0-brane is therefore a point-particle, a D1-brane is itself a string, a D2-brane a *membrane* and so on.

2.4.1 The Dirac-Born-Infeld action

We wish now to construct an equivalent worldbrane action for a Dp-brane. In analogy to the Nambu-Goto worldsheet action of a string, we may write the bosonic part of the Dp-action as

$$S_{\mathrm{Dp}} = -\frac{1}{(2\pi\sqrt{\alpha'})^p\sqrt{\alpha'}}\int d^{p+1}\xi\, e^{-\varphi}\sqrt{-\det\left(\mathcal{G}_{ab}+\mathcal{B}_{ab}\right)}, \tag{2.91}$$

where

$$\mathcal{G}_{ab} = G_{MN}\frac{\partial X^M}{\partial\sigma^a}\frac{\partial X^N}{\partial\sigma^b} \quad \text{and} \quad \mathcal{B}_{ab} = B_{MN}\frac{\partial X^M}{\partial\sigma^a}\frac{\partial X^N}{\partial\sigma^b} \tag{2.92}$$

are the so-called *pullbacks* of the metric and the Kalb-Ramond antisymmetric tensor, and ξ^a are the $p+1$ coordinates of the worldvolume. Recall that in the open superstring NS-sector, after the removal of the tachyonic ground state by GSO projection, the lowest lying state is a massless vector $b^i_{-\frac{1}{2}}|0\rangle$. The components of this state longitudinal to a connected Dp-brane lie within the brane itself and so one can define a U(1) vector field A^I with $I = 1, ..., p-1$ that 'lives' in the brane. The remaining degrees of freedom transform as scalars on the D-brane world volume but naturally act as a vector field in the transverse directions. It is necessary to account for this vector field in the action of the D-brane. Appending this term, we arrive at the so-called Dirac-Born[59]-Infeld[60] (DBI) action,

$$S_{\mathrm{DBI}} = -\frac{1}{(2\pi\sqrt{\alpha'})^p\sqrt{\alpha'}}\int d^{p+1}\xi\, e^{-\varphi}\sqrt{-\det\left(\mathcal{G}_{ab}+\mathcal{B}_{ab}+2\pi\alpha' F_{ab}\right)}, \tag{2.93}$$

[59] Max Born, 1882-1970.
[60] Leopold Infeld, 1898-1968.

where F_{ab} is the associated field strength tensor of the additional U(1) gauge field. In the limit of a constant dilaton, $e^{-\varphi} = g_\sigma^{-1}$, we see that the D-branes are *non-perturbative* objects since their underlying Lagrangian is proportional to the inverse coupling. An expansion about small g_σ then is unavailable to us to probe the dynamics of these objects in string theory.

In flat space with $B_{MN} = 0$, we can expand the action as

$$S_{\text{DBI}} \sim \frac{1}{g_\sigma} \int d^{p+1}\xi \, F_{ab} F^{ab}, \tag{2.94}$$

where we have used $\det(X) = e^{\text{tr}\ln(1+X)} \sim 1 - \frac{1}{2}\text{tr}(X^2)$ for an antisymmetric matrix X. The DBI action now takes on a familiar form — that of a U(1) pure gauge (Yang-Mills) theory with $g_{\text{s}}^2 \propto g_\sigma$,

$$g_{\text{s}}^2 = \left(2\pi\alpha'\right)^{p-2} \left(\sqrt{\alpha'}\right)^{1-p} g_\sigma, \tag{2.95}$$

hinting towards the notion of a gauge/gravity duality.

Chan-Paton degrees of freedom

If we consider N D-branes stacked one on top of another, then there is no way to distinguish a particular brane on which an open string ends. To account for this, we introduce non-dynamical degrees of freedom called Chan-Paton factors λ_{ij}, which label a string stretched between brane i and brane j. The $N \times N$ matrix λ of elements of λ_{ij} turns out to be an element of the Lie algebra U(N). A string state (or wavefunction) can then be decomposed in a basis of the Chan-Paton factors,

$$|k\rangle = \sum_{i,j=1}^{N} |k, ij\rangle \lambda_{ij}. \tag{2.96}$$

2.5 Gauge/Gravity duality

In this section, we will introduce the Anti-de-Sitter/Conformal Field Theory (AdS/CFT) correspondence — a duality which relates a quantum field theory (QFT) on flat space-

time to a string theory[61], thus uniting the previous sections' discussions. This section is based on the texts [64, 73–78].

2.5.1 AdS/CFT correspondence: Motivation

The core of the AdS/CFT correspondence is the double interpretation of a stack of N_c coincident D3-branes in type IIB superstring theory. The interpretation, which is the most appropriate, depends upon the value of the string coupling constant, g_σ. Since both perspectives must describe the same theory, we conjecture that the interpretations in the different limiting cases should be equivalent.

A useful analogy

A useful analogy to have in mind when we discuss the two interpretations of the D3-brane stack is as follows. Consider the system of a heavy charged particle, a proton for example, being orbited by an electron. There are two ways we can look at the interaction between the proton and the electron:

1. By summing over all the appropriate Feynman[62] diagrams for the proton-electron interaction, or

2. By ignoring the presence of the proton altogether and just studying the motion of the electron in a non-trivial electric field background (one which would be generated by a proton).

We use similar reasoning below to obtain a dual-interpretation of the D3-brane stack.

Interpretation I

Consider D-branes as physical, dynamical entities sitting in the 10d-Minkowski spacetime and on which *open strings* may end.

We have seen that the low-energy ($\alpha' \to 0$) Dp-brane action 2.94 has a tension proportional to g_σ^{-1}. Therefore, for N_c D3-branes, the total tension, being just the

[61] Such a duality has been a great cause for excitement since it relates a string theory, a strong candidate for quantum gravity, to a QFT on *flat* spacetime, i.e. a theory with no gravitational degrees of freedom.

[62] Richard P. Feynman, 1918-1988.

sum of the individual tensions, implies the brane stress-energy tensor is proportional to $g_\sigma^{-1} N_c$. This additional contribution to the total stress-energy tensor has the effect of warping the original flat geometry into which the D3-branes were placed — the process of so-called *backreaction*. The associated geometry can then be found as a solution to the Einstein[63] equations,

$$R^{MN} - \frac{1}{2} g^{MN} R = 8\pi\kappa_{10} T^{MN}_{\text{brane}}, \tag{2.97}$$

where T^{MN}_{brane} is the stress-energy tensor taking into account the D-brane tension, and the ten-dimensional Newton's constant, κ_{10}, is proportional to g_σ^2 [73]. Overall, the right-hand side of equation 2.97 is proportional to $g_\sigma N_c \equiv \lambda$.

The first interpretation of the stack of D3-branes is described in the limit $\lambda \to 0$, whereby the stack has an infinitesimal backreaction. In this limit, we can subdivide the total action in this interpretation as follows;

$$\mathcal{S} = \mathcal{S}_{\text{brane}} + \mathcal{S}_{\text{bulk}} + \mathcal{S}_{\text{int}}, \tag{2.98}$$

where $\mathcal{S}_{\text{brane}}$ is the action pertaining to the D3-brane stack, $\mathcal{S}_{\text{bulk}}$ is the action of the closed strings in the 10d Minkowski spacetime or *bulk*, and $\mathcal{S}_{\text{int}}$ describes the interaction terms between the brane excitations and the closed strings in the bulk.

We have seen from equation 2.94 that the action of each D3-brane in the limit $\alpha' \to 0$ takes on the form of a U(1) Yang-Mills theory. It then follows that the action, $\mathcal{S}_{\text{brane}}$, of a stack of N_c coincident branes has the same form as an SU(N_c) Yang-Mills theory[64]. In fact, the action is equivalent to that of an $\mathcal{N} = 4$ supersymmetric Yang-Mills (SYM) theory with vector multiplet consisting of the SU(N_c) gauge fields A^I, four Weyl fermions, $\lambda^{1,\dots,4}$, and six scalars, $\Phi^{1,\dots,6}$, all in the adjoint of $SU(N_c)$. The six scalars can be seen to parameterise fluctuations in the D3-brane stack in the six transverse directions. The beta-function of $\mathcal{N} = 4$ SYM can be shown to vanish at

[63] Albert Einstein, 1879-1955.

[64] In fact, it directly follows that it takes the form of a U(N_c) Yang-Mills theory when examining the Chan-Paton degrees of freedom. However one U(1)$\subset$U(N_c) pertains to the symmetry associated to motion of the centre-of-mass of the stack and decouples, leaving us with an SU(N_c) symmetry on the brane itself.

all orders of perturbation theory and is thus *conformal*. The theory also has an SO(6), global *R-Symmetry*, an automorphism symmetry of the supersymmetry generators. The conformal symmetry of the SYM theory, SO(2,4), is identical to the isometry of AdS_5 spacetime.

$\mathcal{S}_{\text{bulk}}$ contains the closed string states and is given by the type IIB supergravity action 2.86. The interaction term $\mathcal{S}_{\text{int}}$ vanishes in the low energy limit [78], in effect decoupling the brane action from the bulk action and separating the system into two distinct parts:

$$(\text{SU}(N_c)\ \mathcal{N}=4 \text{ SYM Gauge Theory}) \ \oplus \ (\text{10d type IIB Supergravity}) \tag{2.99}$$

This interpretation is similar to the Feynman diagram approach to the electron-proton system of the aforementioned analogy. We are looking at open string excitations (fluctuations) of the D3-brane stack and summing over all string diagrams perturbatively, genus by genus, giving us the behaviour of an $\mathcal{N}=4$ SYM theory.

Interpretation II

The second, alternative interpretation is to be had in the $\lambda \to \infty$ limit. In this limit one cannot ignore the backreaction of the D3-brane stack. We thus have a non-trivial, deformed geometry given by the metric [73]

$$ds^2 = \frac{1}{\sqrt{\left(1+\frac{R^4}{r^4}\right)}}\eta_{ij}dx^i dx^j + \sqrt{\left(1+\frac{R^4}{r^4}\right)}\left[dr^2 + r^2 d\Omega_5^2\right], \tag{2.100}$$

where $i,j = 0,1,2,3$ are the directions parallel to the D3-branes and r, Ω_5 are the radial and angular coordinates describing the transverse plane, $r^2 = \sum_{i=4}^{9} x_i^2$. Importantly [73],

$$R^4 = 4\pi\lambda(\alpha')^2 \tag{2.101}$$

and sets the radius of curvature of the space: the supergravity limit is only valid when the curvature is large thus re-emphasising the $\lambda \to \infty$ limit we are in.

At large $r \gg R$, i.e. far from the D3-branes, the metric of 2.100 just returns the

10-dimensional Minkowski metric, η^{MN}. Close to the D3-branes at small $r \ll R$, called the *near-horizon limit*, $\sqrt{1+\frac{R^4}{r^4}} \to \frac{R^2}{r^2}$ and the metric reduces to

$$ds^2_{\text{horizon}} = \frac{r^2}{R^2}\eta_{ij}dx^i dx^j + \frac{R^2}{r^2}\left[dr^2 + r^2 d\Omega_5^2\right]. \tag{2.102}$$

This is nothing other than the metric for the geometry $AdS_5 \times S^5$, where the radius of curvature for each part is the same.

We now take the second perspective of the electron-proton system, whereby we just monitor how the electron moves in the non-trivial background. In this case we study how closed strings propagate in the background described by the metric 2.100.

Let's take the point-of-view of an observer located at $r = \infty$. Imagine a closed string sitting at a point $r = r_0$ with fixed energy $\tilde{E}$. The energy measured by the observer at infinity is red-shifted due to the gravitational potential well formed of the non-trivial spacetime geometry,

$$E_\infty = \sqrt{-G_{tt}}\tilde{E} = \frac{1}{\left(1+\frac{R^4}{r_0^4}\right)^{\frac{1}{4}}}\tilde{E}. \tag{2.103}$$

For a closed string state in the near-horizon limit ($r_0 \ll R$), no matter what the energy $\tilde{E}$, the observer at infinity sees a vanishing E_∞.

Therefore, close to the branes, in the near-horizon limit, one cannot simply ignore higher energy modes, since to an observer at $r = \infty$ they still appear to be low energy. This implies that, close to the horizon, one must reintroduce and utilise the full type IIB string theory rather than the supergravity limit. However, for closed string modes far from the horizon, one retains the supergravity limit. In fact, it can be shown that in the $\alpha' \to 0$ limit, the two scenarios decouple: the large-wavelength modes at infinity cannot 'see' the horizon and so the cross-section of interactions with near-horizon modes tends to zero. In summary, the theory from the closed string perspective decouples as

$$\left(\text{Type IIB superstring theory on } AdS_5 \times S^5\right) \;\oplus\; \left(\text{10D type IIB Supergravity.}\right) \tag{2.104}$$

2.5.2 AdS/CFT correspondence: A statement

Comparing the two different interpretations, we can see that both contain two decoupled theories one of which is 10d type IIB supergravity. The AdS/CFT correspondence, therefore, is conjectured on the basis that if both interpretations are equivalent descriptions of the same theory, then it must be true that 2.99 and 2.104 are equal. Therefore, we deduce that

$$\text{Type IIB superstring theory on } AdS_5 \times S^5 \equiv \text{SU}(N_c)\ \mathcal{N} = 4\ \text{SYM}. \tag{2.105}$$

This is *Maldacena's correspondence* [32], and forms the basis of the conjectured, more general AdS/CFT correspondence.

It is important to note that the stack of D3-branes that initiated this correspondence is now obsolete and doesn't feature on either side of the correspondence.

2.5.3 AdS/CFT correspondence: Parameter matching

In general, the $\text{AdS}_{d+1}/\text{CFT}_d$ correspondence postulates a relationship between $d+1$-dimensional gravity theories living on an asymptotically anti-de Sitter spacetime and conformal field theories in d dimensions. The most influential and celebrated of these dualities is the one relating type IIB superstring theory on $AdS_5 \times S^5$ with $\mathcal{N} = 4$ SYM theory in 3+1 dimensions — Maldacena's correspondence [32], equation 2.105. The free parameters on either side of the correspondence are related via equations 2.95 and 2.101. From equation 2.95, we can immediately see that the $\lambda = g_\sigma N_c$ parameter used to motivate the different D-brane interpretations in the previous section is nothing more than the 't Hooft coupling used for the large-N_c expansion of gauge fields. This shouldn't, retrospectively, be that surprising. The interacting string perturbation expansion, adding up worldsheet diagrams of ever increasing powers of the coupling g_σ, is identical to summing up worldsheet diagrams of ever increasing genus. This is also the case for the large-N_c perturbative expansion seen in section 2.2.5.

2.5.4 Forms of the correspondence

Depending on the limits to which the free parameters of the theories are taken, different 'forms' of the correspondence can be had. Since the gravitational side of the correspondence contains a string theory, the best method of obtaining tractable calculations is to be in the perturbative limit, $g_\sigma \ll 1$, keeping R and α' fixed. At leading order in g_σ, string perturbation theory considers only those interaction diagrams of null genus[65]. Equation 2.95 then implies that for $g_\sigma \ll 1$, the CFT side of the duality requires $g_s \ll 1$ with the other relationship, equation 2.101, imposing $g_s^2 N_c$ is fixed. This is nothing more than the 't Hooft limit described in section 2.2.5; $g_s \to 0$, $N_c \to \infty$ with $g_s^2 N_c$ fixed. In other words, a perturbative string expansion on the gravity side of the duality implies a large-N_c, planar limit of the conformal gauge theory. This is the so-called *'t Hooft* or *strong form* of the correspondence. A *weak form* of the correspondence is made when we impose $\lambda \to \infty$, whereby the field theory is strongly coupled. On the string side, such a limit imposes $R/\sqrt{\alpha'} \to \infty$ (see equation 2.101) whence it is deduced that the AdS curvature is much greater than the string length. This is the limit in which we can use type IIB supergravity on the AdS side of the correspondence. The weak form of the correspondence is also known as a *weak-strong duality* since the CFT is strongly coupled, yet its dual gravitational theory is weakly coupled. This is the foundation of why the AdS/CFT correspondence is such a powerful tool — one is able to look at non-perturbative gauge theories by calculating in a perturbative gravitational theory. It is the weak form of the correspondence that we will be exploiting for the remainder of this work. A table summarising the limits and forms of the correspondence is shown in 2.3.

Form	**Type IIB on $AdS_5 \times S^5$**	**$\mathcal{N} = 4$ SYM**
Strongest	Non-pert' string theory: any g_σ, R and α'	Any N_c and λ
't Hooft	Pert' string theory: $g_\sigma \to 0$, any R and α'	$N_c \to \infty$, λ fixed
Weak	Pert' supergravity: $g_\sigma \to 0$, $R/\alpha' \to \infty$	$N_c \to \infty$, $\lambda \to \infty$

Table 2.3: The various forms of the AdS_5/CFT_4 correspondence appearing in different limits of the theories' parameters.

[65] One can think of string Feynman diagrams where instead of interacting worldlines, one has interacting worldsheets. Therefore, higher order 'loop' diagrams are depicted as manifolds with greater numbers of 'holes' or of higher genus.

2.5.5 The conformal boundary of AdS space

Anti de-Sitter spacetime can be covered by a wide variety of coordinate patches, some emphasising certain properties of the geometry over others. In the derivation of the AdS/CFT correspondence, we stipulated that the near horizon D3-brane geometry took on the form of AdS_5 (crossed with the compactified S^5 which we drop here) with the metric

$$ds^2 = r^2 \eta_{ij} dx^i dx^j + \frac{1}{r^2} dr^2, \tag{2.106}$$

where we have set the radius of curvature to unity. Taking the transformation $r = \frac{1}{\zeta}$, we can convert to the so-called *Poincaré coordinates*

$$ds^2 = \frac{1}{\zeta^2} \left(-dt^2 + dx^2 + dy^2 + dz^2 - d\zeta^2 \right), \tag{2.107}$$

where we have explicitly expanded $\eta_{ij} dx^i dx^j$ of equation 2.106. We can see that this is nothing more that the Minkowski space, $\mathbb{R}^{3,1}$, foliated over an extra coordinate ζ. For each slice of the AdS space at constant ζ we recover a 4d Minkowski spacetime warped by a factor ζ^{-2}. We define the *boundary* of the spacetime as the ζ-constant slice for which the metric diverges; for the metric given in 2.107, this happens as $\zeta \to 0$ ($r \to \infty$). In order to analytically continue the metric onto the boundary in a sensible fashion, we can make use of a *conformal rescaling* of the metric $g_{MN} \to \Omega(\mathbf{x}, \zeta) g_{MN}$, for some function Ω, which leaves all distances and angles on the original metric invariant under the change. For example, if we allow $\Omega = \zeta^2 f(\mathbf{x}, \zeta)$, where $f(\mathbf{x}, \zeta)$ is a well-defined, smooth, positive-definite function in $\mathbf{x}$ and ζ, then the boundary is simply defined as,

$$ds^2_{\partial \mathrm{AdS}_5} = f(\mathbf{x}, \zeta) \left(-dt^2 + dx^2 + dy^2 + dz^2 \right). \tag{2.108}$$

The ability to choose the function $f(\mathbf{x}, \zeta)$ leaves a whole class of equivalent boundaries, Minkowskian in nature, related by conformal transformations.

2.5.6 The holographic principle

The holographic principle [33, 79] is an idea inspired from black hole thermodynamics, wherein the (Bekenstein[66]-Hawking[67]) entropy of the black hole scales as the surface area, A, of its horizon [80]. This is in stark contradiction to the expectations of quantum field theory, which states that the entropy should scale as the volume[68]. In an attempt to reconcile this, the holographic principle prescribes that information contained within a $d+1$-dimensional volume of spacetime V can be equally understood from the viewpoint of degrees of freedom living on the d-dimensional boundary $\partial V = A$.

Working in the weak form of the AdS/CFT correspondence whereby $\lambda \to \infty$, we have a duality between type IIB supergravity on $AdS_5 \times S^5$ and a large N_c, $\mathcal{N} = 4$ SYM gauge theory in 4 dimensions. In a Kaluza-Klein reduced form of $AdS_5 \times S^5$, whereby we can 'ignore' the compactified 5-sphere, we are left with an AdS_5 spacetime which we have shown in section 2.5.5 to have a conformal boundary. The isometries of this spacetime, namely SO(4,2), are the conformal symmetries associated to the $\mathcal{N} = 4$ SYM theory to which the spacetime is dual [73]. One may argue that the boundary of the AdS-spacetime encodes all of the same degrees of freedom as the SYM theory and thus the gauge theory can be postulated to 'live' on the boundary. This is a realisation of the holographic principle at play.

2.5.7 Field-operator map

Having set up the nature of the correspondence, we now need to put it into a form which we can utilise. In order to do this, one needs to set up a *dictionary* of rules that allows us to interpret results calculated on one side of the duality into corresponding results on the other. From [81], a mathematical formulation of the duality was set out which allows one to initiate such a dictionary. The partition function of the 4d interacting field theory can be expressed as

$$\mathcal{Z}[\bar{\phi}] = \left\langle \exp\left(\int d^4x \sum_i \bar{\phi}_i(x) \mathcal{O}_{\bar{\phi}_i}(x) \right) \right\rangle , \tag{2.109}$$

[66] Jacob David Bekenstein, 1947-2015.
[67] Stephen W. Hawking, 1942-.
[68] The entropy of a system is an extensive property and thus should scale up with the system.

where the fields $\bar{\phi}_i$ are sources of the operators $\mathcal{O}_{\bar{\phi}_i}$. The gravitational side of the duality is governed by a supergravity action over[69] AdS_5 containing fields $\phi(x,r)$. The partition function of the supergravity dual, $\mathcal{Z}_{\text{sugra}}$, is then related to $\mathcal{Z}$ via,

$$\mathcal{Z} \equiv \mathcal{Z}_{\text{sugra}}\big|_{\phi(x,r\to\infty)}\,. \tag{2.110}$$

The crux of equation 2.110 is that

boundary values of the supergravity fields $\phi(x, r \to \infty)$ are equivalent to the sources, $\bar{\phi}$, of operators in the field theory.

An example of this statement can be seen as follows. Let us consider a scalar field $\phi = \phi(x,r)$ and with mass M_ϕ living in AdS_5. The action is simply given by

$$S = \int d^4x dr \sqrt{-g}\left(g^{MN}\partial_M\phi\partial_N\phi - M_\phi^2\phi^2\right), \tag{2.111}$$

where $g = \det(g_{MN})$ and the AdS_5 metric is given by

$$g_{MN} = \begin{pmatrix} -r^2 & 0 & 0 & 0 & 0 \\ 0 & r^2 & 0 & 0 & 0 \\ 0 & 0 & r^2 & 0 & 0 \\ 0 & 0 & 0 & r^2 & 0 \\ 0 & 0 & 0 & 0 & r^{-2} \end{pmatrix}, \tag{2.112}$$

where we have set the radius of curvature to unity. The equations of motion for the radial dependent part of ϕ, $\phi(r)$, take the form,

$$\partial_r\left(r^5\partial_r\phi(r)\right) - r^3M_\phi^2 = 0, \tag{2.113}$$

which has solution

$$\phi(r) = \frac{A}{r^\Delta} + \frac{B}{r^{4-\Delta}}, \tag{2.114}$$

[69] The type IIB supergravity action over $AdS_5\times S^5$ is Kaluza-Klein reduced to five dimensional AdS_5.

where[70]

$$\Delta(\Delta - 4) = M_{\phi}^2. \tag{2.116}$$

The supergravity scalar field $\phi(r)$ has no mass-dimension, therefore the coefficients A and B are dimensionful with respective mass-dimensions Δ and $4 - \Delta$. In the limit $r \to \infty$, the B-coefficient term dominates[71], so we have

$$\lim_{r\to\infty} \phi(x, r) = \frac{B(x)}{r^{4-\Delta}}, \tag{2.117}$$

which by equation 2.110 means that $B(x) = \bar{\phi}_i(x)$. It subsequently transpires that we can identify the coefficient A as the vev of the operator $\mathcal{O}_{\bar{\phi}_i}$ [82]. The solution to the equation of motion of the bulk field $\phi(r)$ can then be reformulated as,

$$\phi(r) = \frac{\langle \mathcal{O}_{\bar{\phi}} \rangle}{r^{\Delta}} + \frac{\bar{\phi}(x)}{r^{4-\Delta}}. \tag{2.118}$$

The results of equations 2.116 and 2.118 make the correspondence quite explicit: Fields in the bulk can be expressed in terms of field theory operators and sources and the bulk field's mass pertains to the mass-dimension of those sources.

[70] The following constraint can also be recast as $\Delta = 2 + \sqrt{4 + M_{\phi}^2}$. More generally than adding a scalar to the spacetime, a p-form can be added with the same solutions but with the more generalised mass constraint,

$$(\Delta - p)(\Delta + p - 4) = M_{\text{p-form}}^2. \tag{2.115}$$

[71] The B-coefficient term is often referred to as the *non-normalizable* term, in the respect that its contribution to the action 2.111 diverges. This is unlike the A-coefficient term, which is elsewise referred to as the *normalizable* term and whose contribution to the action remains finite.

Chapter 3

Holographic QCD

We now motivate the ideas behind using the AdS/CFT correspondence as a tool to probe strongly coupled gauge theories like QCD.

3.1 Towards holographic QCD

The AdS/CFT correspondence in its weak form of a duality between type IIB supergravity on $AdS_5 \times S^5$ and a large N_c, large $\lambda = g_s^2 N_c$, $\mathcal{N} = 4$ SYM theory is well understood [32, 83, 84]. However, the gauge theory is far removed from the non-supersymmetric, asymptotically free, SU(N_c) gauge theories that are of interest in the wider particle physics community, such as $SU(3)_c$ QCD or Technicolor models. Such models do not share large N_c values, are not supersymmetric and contain fundamental rather than adjoint matter fields, i.e. quarks. The hope of future physicists is to construct a gravity dual of confining SU(N_c) gauge theories. It is quite beyond the current standing of particle physics to obtain a full correspondence between theories like QCD and a gravity dual on the grounds that the perturbative regime of the gauge theory will be dual to a non-perturbative quantum string theory on a non-trivial background — analysis of which is outside the realms of our current capabilities. However, as we shall show in the rest of this work, it is possible to incorporate quarks and running couplings into holographic theories and slowly begin to edge towards constructing holographic methods to understand asymptotically free gauge theories.

3.1.1 Top-down *versus* bottom-up approaches

Holographic models for QCD-like theories can be roughly split into two differing sectors; top-down and bottom-up approaches. Top-down models start directly from a pure string theory perspective such as the D3-brane scenario from which the Maldacena correspondence [32] (between $\mathcal{N} = 4$ SYM and type IIB supergravity on $AdS_5 \times S^5$) was conjectured. In order to adapt the correspondence to accommodate different boundary field theories, the bulk is re-engineered, by the addition of new brane and string structures. Some of the most successful top-down models to describe QCD-like gauge theories, including the Sakai-Sugimoto model [85,86] and probe-brane constructions [87], introduce new D-branes into the bulk which allow the description of phenomena such as fundamental matter and confinement. The major drawback of working in a top-down framework is the innate mathematical complexity of the base string theory and the veritable smörgåsbord of gravity fields which must be kept track of in order to fully understand the dual field theory.

In bottom-up models, usually referred to as *AdS/QCD models* [82,88–90], inspiration is taken from top-down approaches[1] but with the bulk geometry and fields chosen to ensure the required phenomenological properties of the gauge theory. In this regard, the mathematical rigour of the top-down models is lost but to the advantage of a cleaner, more tractable model. Below, we will outline some key, basic top-down extensions and use these as a springboard into the simpler bottom-up approach.

3.2 Top-down models

Two of the most important features of QCD-like gauge theories, for which $\mathcal{N} =$ SYM is lacking, are fundamental matter fields, i.e. quarks, and a running coupling which may or may not trigger chiral symmetry breaking. The following sections begin to address these problems from a top-down approach.

[1] Usually bottom-up models bear close relationship to truncated top-down models whereby undesired fields have been omitted .

3.2.1 Introducing flavour

The dual field theory of the Maldacena correspondence, $\mathcal{N} = 4$ SU(N_c) SYM, only has adjoint degrees of freedom. This stems from all open string states starting and ending on one of the N_c D3-branes in the coincident stack. To understand this, recall that a stack of N_c D3-branes has a $U(N_c)$ gauge group living on it. A string wavefunction can then be in a superposition of N_c^2 different pure-states (a string from brane A to brane B, from brane A to brane C and so on - see figure 3.1) and is therefore described by the adjoint of the U(N_c) gauge group on the stack which has N_c^2 generators. For an SU(N_c) gauge theory on the stack (where we have lost one U(1)$\subset$U(N_c) since it decouples in the AdS/CFT correspondence as it associates to the degree of freedom pertaining to the centre-of-mass of the stack), we have $N_c^2 - 1$ generators or independent pure states.

In order to add fundamental degrees of freedom, all that is required is to apply the restriction that only one end of the string states may finish on the D3-brane stack. This way, we only generate N_c possible string configurations, rather than N_c configurations *per brane* [87]. The remaining string end must attach to another brane. In principle, we can consider either another D3 brane, a D5 brane, a D7-brane or a D9-brane within the remit of type IIB string theory. The D9-brane is ruled out immediately since it fills the whole spacetime and thus cannot be separated from the D3-brane stack. This is severely limiting when one wishes to describe massive fundamental degrees of freedom. The D3- and D5-brane solutions lead to defect theories [91] [92–95] and so we are left with the D7-brane. Multiple D7-branes can be introduced to mimic the number of flavours of quarks, N_f.

Defining a p-q string as a string stretched between a Dp-brane and a Dq-brane, we have in summary, 3-3 strings responsible for an $\mathcal{N} = 4$ adjoint multiplet, 3-7 strings realising fundamental[2] fields ($\mathcal{N} = 2$ hypermultiplet) and 7-7 strings which represent mesonic operators again in the *adjoint* of SU(N_f) (as both strings end on a D7-brane in the D7-brane coincident stack). Figure 3.1 demonstrates the different possible string configurations. The corresponding dual field theory with this form of brane construction

[2]The 3-7 string is in fact bifundamental in both the SU(N_c) gauge field on the D3-brane stack and the SU(N_f) gauge field on the D7-brane stack. This implies that the quark can be seen to be in the fundamental representation of colour and flavour, just like QCD.

is then an $\mathcal{N} = 4$ SYM gauge theory coupled to $\mathcal{N} = 2$ matter.

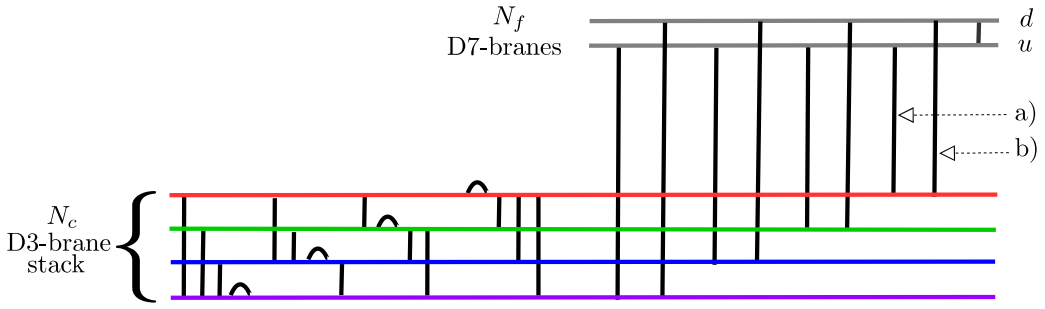

Figure 3.1: The D3/D7-brane set-up allows for fundamental fields e.g. quarks. Multiple D7-branes allows for different flavours of quarks. E.g. string a) pertains to a red up-type quark and string b) pertains to a red down-type quark. 3-3 strings generate the $\mathcal{N} = 4$ SYM theory, 3-7 strings realise quark-like fields and 7-7 strings represent mesons.

The number of D7-branes must be small compared to the number of D3-branes, $N_f \ll N_c$, to avoid backreaction warping the $AdS_5 \times S^5$ geometry and destroying the Maldacena correspondence. This is referred to as the *quenched approximation* on the field theory side or the *probe brane limit* in the supergravity bulk. Since we're in the 't Hooft limit whereby $N_c \to \infty$, the quark contributions are suppressed unless $N_f \to \infty$ also.

D7-brane metric

dim	0	1	2	3	4	5	6	7	8	9
D3	X	X	X	X	·	·	·	·	·	·
D7	X	X	X	X	X	X	X	X	·	·

Table 3.1: The D3-brane extends in the 0123-directions of 10d spacetime, whereas the D7-brane extends over the 01234567-directions. The branes thus overlap in the 0123-directions. Here 0 denotes the time direction.

Let's imagine that the N_f coincident D7-branes lie along the 01234567-directions of the 10d spacetime, overlapping in coordinates with the D3-brane stack occupying the 0123-directions, see table 3.1. Let the $AdS_5 \times S^5$ metric be recast as

$$ds^2 = r^2 \eta_{ij} dx^i dx^j + \frac{1}{r^2} \left(d\rho^2 + \rho^2 d\Omega_3^2 + dL^2 + L^2 d\phi^2 \right), \tag{3.1}$$

where $r^2 = \rho^2 + L^2$. From this, we can see that the D7-branes fill out the AdS-space as

well as an $S^3 \subset S^5$ of radius ρ. The induced metric on the D7-worldvolume is therefore given by

$$ds^2_{D7} = (\rho^2 + L^2)\eta_{ij}dx^i dx^j + \frac{1}{\rho^2 + L^2}d\rho^2 + \frac{\rho^2}{\rho^2 + L^2}d\Omega_3^2, \tag{3.2}$$

since it is sitting in the $AdS_5 \times S^5$ geometry generated by the D3-brane stack.

When the probe D7-branes are coincident with the D3-brane stack, the 3-7 strings are naturally massless and the conformal nature of the dual field theory is still explicit. However, if the D7-branes are separated from the D3-branes (in the L-direction), the SO(2,4) isometry of the AdS_5 spacetime, equivalent to the conformal symmetry on the boundary, is naturally broken by the presence of the brane obstruction. The broken conformality goes hand in hand with the 3-7 strings now having a finite length and thus becoming massive. Returning to the induced D7-metric 3.2, the limit $L \to 0$ whereby the separation of the D3 and D7 brane vanishes, we see the D7-metric reduces to an $AdS_5 \times S^3$ geometry returning the conformal structure. We show below the explicit introduction of a mass scale, the quark mass, by the D7-brane embedding.

D7-brane embedding

Figure 3.2 shows the 10d spacetime set-up of the D3/D7 system.

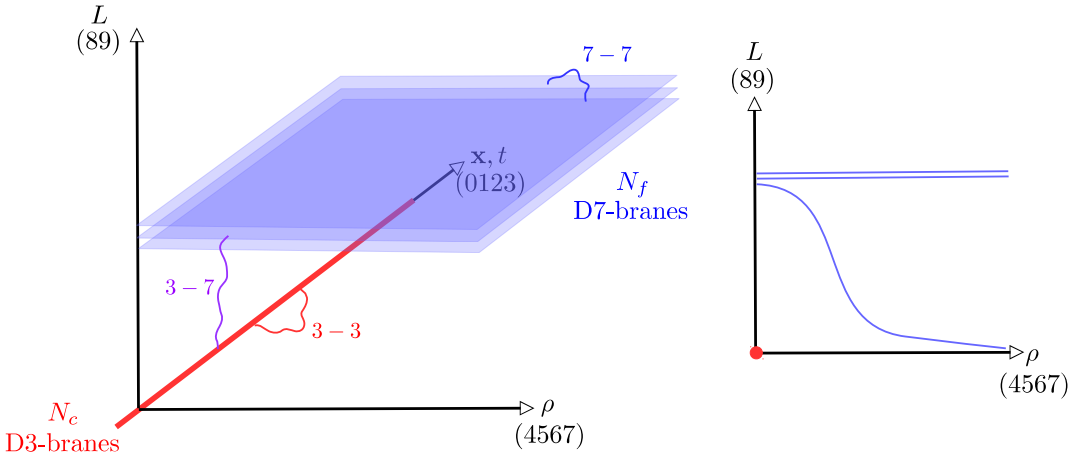

Figure 3.2: 10d spacetime set-up of the D3/D7 system. The most stable configuration of the D7 brane might have a non-trivial relation between L and ρ (as seen on the left plot).

The action governing the worldvolume of the D7-brane is given by the appropriate DBI action (see section 2.4.1), which at constant dilaton (or fixed string coupling) is given by

$$S_{\rm D7} = -\frac{1}{(2\pi)^2(\alpha')^4 g_\sigma}\int d^8\xi\sqrt{-\det(\mathcal{G}_{ab}+2\pi\alpha' F_{ab})}, \tag{3.3}$$

where $\mathcal{G}_{ab}$ is the pullback of the metric on the D7-worldvolume, equation 3.2. Taking into account that L could be a function of ρ, see figure 3.2, $\mathcal{G}_{ab}$ is explicitly given by

$$\mathcal{G}_{ab} = \begin{pmatrix} -r^2 & 0 & 0 & 0 & 0 & 0 & 0 & 0 \\ 0 & r^2 & 0 & 0 & 0 & 0 & 0 & 0 \\ 0 & 0 & r^2 & 0 & 0 & 0 & 0 & 0 \\ 0 & 0 & 0 & r^2 & 0 & 0 & 0 & 0 \\ 0 & 0 & 0 & 0 & \frac{1}{r^2}\left(1+(\partial_\rho L)^2\right) & 0 & 0 & 0 \\ 0 & 0 & 0 & 0 & 0 & \frac{\rho^2}{r^2} & 0 & 0 \\ 0 & 0 & 0 & 0 & 0 & 0 & \frac{\rho^2}{r^2} & 0 \\ 0 & 0 & 0 & 0 & 0 & 0 & 0 & \frac{\rho^2}{r^2} \end{pmatrix}, \tag{3.4}$$

where $r^2 = \rho^2 + L(\rho)^2$. The action can now be simply expressed as[3]

$$S_{\rm D7} \sim \int d^4x d\rho\ \rho^3\sqrt{1+(\partial_\rho L(\rho))^2}. \tag{3.5}$$

The equation of motion of $L(\rho)$ is given by

$$\frac{\partial}{\partial\rho}\left(\rho^3\frac{\partial_\rho L}{\sqrt{1+(\partial_\rho L)^2}}\right) = 0, \tag{3.6}$$

which is known as the *embedding equation* since the solution $L(\rho)$ describes the profile of the D7-brane in the 10d spacetime. Equation 3.6 can be satisfied by the solution $L(\rho) = m$, for some constant m. This is a *flat* D7-brane embedding. For $m = L = 0$, the D7-branes are sitting on top of the D3-branes and we retain the conformal invariance of the dual field theory. However, if $m \neq 0$, the 3-7 strings, identifying as quarks, now have a fixed, non-zero length, and thus a mass proportional to m. Such a mass breaks

[3]Setting $F_{ab} = 0$. Integration over the angular coordinates yielding a non-important constant factor.

the conformal invariance of the boundary field theory as expected for $L \neq 0$. The radial direction ρ has dimensions of energy and is interpreted as the renormalization scale[4] , μ. The flat embedding therefore implies a non-renormalization of the quark mass, an effect of supersymmetric gauge theories.

In the limit $\rho \to \infty$, the general solution to equation 3.6 is given by

$$L(\rho) = m + \frac{c}{\rho^2} + ... \tag{3.7}$$

where m and c are constants to be interpreted (see Appendix C).

Equation 3.7 agrees well with $L(\rho)$ taking the rôle of a supergravity scalar of mass-squared -3. For small $\partial_\rho L \to 0$, the action of 3.5 can be linearised to,

$$S \sim \int d\rho\rho^3 \left(\partial_\rho L\right)^2 = \int d\rho\rho^3 \left(\rho^2 \left(\partial_\rho \phi\right)^2 + \phi^2 + 2\rho\phi\partial_\rho\phi\right), \tag{3.8}$$

where $\phi = \frac{L(\rho)}{\rho}$. Integration by parts on the final term of the right-hand side of equation 3.8 yields

$$2\int d\rho\rho^4\phi\partial_\rho\phi = -4\int d\rho\rho^3\phi^2, \tag{3.9}$$

implying the action can be recast as

$$S \sim \int d\rho\rho^3 \left(\rho^2 \left(\partial_\rho \phi\right)^2 - 3\phi^2\right), \tag{3.10}$$

which is the Klein-Gordon[5] action of a scalar in AdS_5 of mass-squared -3. This is shown as follows. From 2.116, ϕ corresponds to a field-theory operator vev and source combination of respective mass-dimensions $\Delta = 3$ and $4 - \Delta = 1$ such as the $\bar{q}q$ operator and the quark mass. Hence we can write ϕ as

$$\phi(\rho) = \frac{m}{\rho} + \frac{\langle\bar{q}q\rangle}{\rho^3}. \tag{3.11}$$

[4]This is not quite accurate; the RG scale directly corresponds to the AdS_5 radial coordinate r and therefore the true relation between the RG scale and ρ is given by $r^2 = \rho^2 + L(\rho)^2$. This will become of importance in the following chapters.

[5]Walter Gordon, 1893-1939.

Recalling $L(\rho) = \rho\phi$, equation 3.11 implies that $L(\rho)$ can be identified as such

$$L(\rho) = m + \frac{\langle \bar{q}q \rangle}{\rho^2}, \tag{3.12}$$

agreeing with equation 3.7, where $c \equiv \langle \bar{q}q \rangle$.

3.2.2 Constable-Myers and dilaton flows

The next step towards a holographic dual of asymptotically free gauge theories is to incorporate a running coupling. This can be enabled by having a radially dependent dilaton field or *dilaton flow*, which can be obtained by a deformation of the AdS-geometry. Since the dilaton is related to the string coupling and the string coupling is dual, in some manner, to the field theory coupling, a dilaton flow is dual to a running of the field theory coupling.

One such a solution is the *Constable-Myers* flow [96]. The metric of the bulk spacetime in this scenario is given by

$$\begin{aligned} ds^2 =& \frac{1}{\sqrt{H(r)}} \left(\frac{r^4 + b^4}{r^4 - b^4} \right)^{\frac{\delta}{4}} \eta_{ij} dx^i dx^j + \\ & \sqrt{H(r)} \left(\frac{r^4 + b^4}{r^4 - b^4} \right)^{\frac{2-\delta}{4}} \frac{r^4 - b^4}{r^4} \left(d\rho^2 + \rho^2 d\Omega_3^2 + dL^2 + L^2 d\phi^2 \right), \end{aligned} \tag{3.13}$$

with

$$H(r) = \left(\frac{r^4 + b^4}{r^4 - b^4} \right)^{\delta} - 1, \tag{3.14}$$

where again $r^2 = \rho^2 + L^2$, b is a measure of the deformation and $\delta = 1/2b^4$ [97]. The geometry approaches $AdS_5 \times S^5$ of unit radius of curvature in the large-r limit, such that the field theory returns to $\mathcal{N} = 4$ SYM in the UV. The dilaton is given by

$$e^{\phi} = e^{\phi_0} \left(\frac{r^4 + b^4}{r^4 - b^4} \right)^{\frac{\Delta}{2}}, \tag{3.15}$$

where $e^{\phi_0} = g_\sigma$ and $\Delta^2 + \delta^2 = 10$ [97]. At the scale $r = b$, the dilaton (and the geometry) diverge. Such a scale then mimics the rôle of Λ_{QCD} on the field theory side of the dual.

Combining both the Constable-Myers dilaton flow with additional probe D7-branes allows for a dual field theory with quarks and a running coupling. The action of the D7-brane with the appropriate Constable-Myers metric is given by

$$S_{\mathrm{D7}} \sim e^{\phi_0} \int d\rho\, \lambda(r) \rho^3 \sqrt{1 + (\partial_\rho L)^2}, \tag{3.16}$$

with

$$\lambda(r) = \frac{r^8 - b^8}{r^8} \left(\frac{r^4 + b^4}{r^4 - b^4} \right)^{\frac{\Delta}{2}}. \tag{3.17}$$

Evidently the action looks the same as equation 3.5 with the addition of a ρ-dependent prefactor $\lambda(r)$ controlling the dilaton flow.

Let us now consider the action 3.16 in the limit $L(\rho), \partial_\rho L \to 0$, i.e. a perturbation away from the $L = 0$ chiral embedding. We can perform a series expansion on $\lambda(r)$ as follows,

$$\begin{aligned} \lambda(r) = \lambda(r)|_{L=0} + L \left(\frac{\partial \lambda}{\partial r} \frac{\partial r}{\partial L} \right) \Big|_{L=0} + \frac{1}{2} L^2 \left(\left(\frac{\partial r}{\partial L} \right)^2 \frac{\partial^2 \lambda}{\partial r^2} \right) \Big|_{L=0} \\ + \frac{1}{2} L^2 \left(\frac{\partial^2 r}{\partial L^2} \frac{\partial \lambda}{\partial r} \right) \Big|_{L=0} + \mathcal{O}(L^3). \end{aligned} \tag{3.18}$$

Recalling $r^2 = \rho^2 + L^2$, $\partial_L r = L r^{-1}$, which vanishes in the limit $L \to 0$, and so we can simplify $\lambda(r)$ to

$$\lim_{L \to 0} \lambda(r) = \lambda(r)|_{L=0} + \frac{1}{2} \frac{L^2}{r} \frac{\partial \lambda}{\partial r} \Big|_{L=0}. \tag{3.19}$$

Substituting back into the action and expanding the square-root to first order we have,

$$S \sim \int d\rho \rho^3 \left(\lambda(r)|_{L=0} + \frac{1}{2} \frac{L^2}{r} \frac{\partial \lambda}{\partial r} \Big|_{L=0} \right) \left(1 + \frac{1}{2} (\partial_\rho L)^2 \right). \tag{3.20}$$

Again expanding to leading order we arrive at the action

$$S \sim \int d\rho \rho^3 \left(\frac{1}{2} \lambda|_{L=0} (\partial_\rho L)^2 + \frac{\partial \lambda}{\partial (L^2)} \Big|_{L=0} L^2 \right), \tag{3.21}$$

where we have used $\partial_{L^2} \lambda = (2r)^{-1} \partial_r \lambda$. It is now evident that adding a non-trivial dilaton to these models allows for the masses of the bulk fields, such as L, to change

with radial coordinate r. Since the masses of the bulk fields relate (see section 2.5.7) to the mass-dimensions of the corresponding field theory operators, then a dilaton flow can be seen directly as a running anomalous dimension in the field theory. We shall capitalise on this when we turn to Dynamic AdS/QCD.

3.3 Bottom-up models

We now turn to the bottom-up approach, building-on and extending the ideas formed from top-down models with the goal of trying to best mimic the phenomenology of QCD-like gauge theories in a holographic arena.

Known as AdS/QCD, the starting point of these models is a much simpler AdS_5 spacetime, on the boundary of which we seek a QCD-like gauge theory. The AdS_5 metric of unit radius is given by

$$ds^2 = r^2 \eta_{ij} dx^i dx^j + \frac{1}{r^2} dr^2. \tag{3.22}$$

The bulk must contain fields which correspond to necessary source-operator combinations in the field theory. Therefore, we require one scalar field of mass-squared -3 to encode the quark mass and condensate as well as two massless gauge fields corresponding to the $SU(N_f)_L$ and $SU(N_f)_R$ current operators. A summary of the dictionary can be seen in table 3.2

Bulk Field	**Mass**	$\leftrightarrow$	**QFT Operator**	$\Delta =$ **dim**	p**-form**
$X(\mathbf{x}, \rho)$	$M^2 = -3$	$\leftrightarrow$	$\bar{q}q$	3	p=0
$L^{M,a}(\mathbf{x}, \rho)$	$M^2 = 0$	$\leftrightarrow$	$L^{\mu,a} = \bar{q}_L \gamma^\mu t^a q_L$	3	p=1
$R^{M,a}(\mathbf{x}, \rho)$	$M^2 = 0$	$\leftrightarrow$	$R^{\mu,a} = \bar{q}_R \gamma^\mu t^a q_R$	3	p=1

Table 3.2: The dictionary between the bulk AdS fields and the field theory operators on the boundary in a simple AdS/QCD model. The bulk fields masses are obtained via the relation $(\Delta - p)(\Delta + p - 4) = M^2$ (see section 2.5.7)

Collecting all the relevant pieces together, we can construct a bulk action which

encodes the very basics of a QCD-like theory:

$$S = \int d^4x dr \sqrt{-\det g_{MN}} \mathrm{Tr} \left\{ (D_M X)^\dagger (D^M X) + 3X^\dagger X - \frac{1}{4g_5^2} \left[F_{L,MN} F_L^{MN} + F_{R,MN} F_R^{MN} \right] \right\}, \tag{3.23}$$

where

$$D_M X = \partial_M - iL_M^a X + iX R_M \tag{3.24}$$

and

$$F_{L,MN} = \partial_M L_N - \partial_N L_M - i[L_M, L_N] \tag{3.25}$$

with $L^M = L^{a,M} t^a$ and likewise for $F_{R,MN}$. We choose the scalar X to have the form

$$X(\mathbf{x}, r) = L(r) e^{2i\pi^a(\mathbf{x}) t^a}, \tag{3.26}$$

taken from the effective chiral approach in section 2.1.2, such that fluctuations in the $\mathbf{x}$-dependence of the scalar can describe the pion fields. The radial coordinate r acts as an energy scale and so is matched to the renormalisation scale μ of the field theory.

Hard-wall *versus* soft-wall

There is still however one small issue; the AdS_5 spacetime implies a conformal symmetry in the field theory, which is not the case for QCD-like theories. One way to overcome this obstacle is to impose a boundary or *hard wall* into the spacetime at fixed $r = r_0$ (see [82, 88]). By doing so, we break the SO(2,4) isometry of the spacetime and in turn break the conformal invariance of the field theory. The bulk theory is then only valid in the region $r_0 < r < \infty$, cutting out the deep infrared. The energy scale r_0 then acts like Λ_{QCD} in the same way that it is the only scale in the system available to set dimensionful parameters. The major drawback to the hard-wall method is that the corresponding field theory has unnatural Regge trajectories of excited states of mesons $M_n^2 \sim n^2$.

One alternative approach is to introduce a so-called *soft-wall* in place of the hard boundary (see [98]). This means having a non-trivial dilaton $\phi(r)$, amending the action

to

$$S = \int d^4x dr \sqrt{-\det g_{MN}} e^{\phi(r)} \mathrm{Tr} \left\{ (D_M X)^\dagger (D^M X) + 3X^\dagger X - \frac{1}{4g_5^2} \left[F_{L,MN} F_L^{MN} + F_{R,MN} F_R^{MN} \right] \right\}. \tag{3.27}$$

Choosing a dilaton with profile $\phi(r) \sim r^{-2}$ as $r \to 0$ ensures the correct Regge trajectories, $M_n^2 \sim n$, whilst retaining the broken conformal symmetry of the field theory dual [73, 98].

3.3.1 Dynamic AdS/QCD

We now turn to the model with which the rest of this work was undertaken. Based on the bottom-up AdS/QCD approach with influence from the D3/probe-D7 top-down models, the model referred to as *Dynamic AdS/QCD* [1–3, 89] is set up as follows.

We work with the action

$$S = \int d^4x d\rho \rho^3 \mathrm{Tr} \left[\frac{1}{\rho^2 + L^2} (D^M X)^\dagger (D_M X) + \frac{\Delta m^2}{\rho^2} |X|^2 + \frac{1}{2g_5^2} (F_{L,MN} F_L^{MN} + F_{R,MN} F_R^{MN}) \right], \tag{3.28}$$

where

$$X = L(\rho) e^{2i\pi^a t^a}. \tag{3.29}$$

Having outlined the standardised bottom-up approach in the previous section, such an action might, at first sight, seem unexceptional. However, there are a few key differences. Firstly we are working with the 5-dimensional metric inspired from the D3/probe-D7 models,

$$ds^2 = (\rho^2 + L^2) \eta_{ij} dx^i dx^j + \frac{1}{\rho^2 + L^2} d\rho^2, \tag{3.30}$$

where, exactly like the top-down models, the scalar field $L(\rho)$ enters into the metric, defining a dummy radial coordinate $r^2 = \rho^2 + L^2$. The scale r will then be associated to the renormalisation scale, μ, of the field theory — again like the D3/D7 model. This metric is used for spacetime contractions. We have also chosen the $\sqrt{-g} = \rho^3$ factor

directly from the D3/D7 model rather than the would-be factor of $(\rho^2 + L^2)^{\frac{3}{2}}$ using metric 3.30. This is to ensure a soft-IR wall behaviour: when L is non-zero, the dummy radial coordinate r cannot access the deep infrared, i.e. $r < L$, no matter how small the holographic coordinate ρ becomes. As $L \to 0$, the deep IR is once again available, metric 3.30 becomes that of AdS_5 and the boundary field theory returns to being conformal. Thirdly, the action contains a term proportional to $|X|^2 = L^2$, which is inherited directly from the L^2 term of the action for top-down models with a dilaton flow, 3.21. It allows the model's scalar field to have a radially dependent mass corresponding to an energy-dependent mass-dimension of the field theory operator $\bar{q}q$. For $\Delta m^2 = 0$, the scalar returns to $M^2 = -3$.

The action can be expanded out fully (see Appendix D) giving

$$\begin{aligned} S = \int d^4x d\rho \rho^3 \mathrm{Tr} \Bigg(& (\partial_\rho L)^2 + \frac{\Delta m^2}{\rho^2} L^2 + 4L^2 A_\rho^2 + \frac{4L^2}{(\rho^2 + L^2)^2} (\partial_\mu \pi - A_\mu)^2 \\ & + \frac{1}{2g_5^2} (\partial_M V_N^a - \partial_N V_M^a) \left(\partial^M V^{a,N} - \partial^N V^{a,M}\right) \\ & + \frac{1}{2g_5^2} (\partial_M A_N^a - \partial_N A_M^a) \left(\partial^M A^{a,N} - \partial^N A^{a,M}\right) \Bigg). \end{aligned} \tag{3.31}$$

Understanding g_5

We now turn to calculating the vector two-point function in the Dynamic AdS/QCD model and match it to perturbative QCD results in the UV, i.e. on the boundary. This will fix the coupling g_5. We follow [73] and [82].

Firstly, we find the solution to the equation of motion of the vector gauge field to be

$$V^a(\rho) = 1 + \frac{q^2}{4\rho^2} \ln\left(\frac{q^2}{\rho^2}\right) + ..., \tag{3.32}$$

where $V_M^a = \varepsilon_M V^a(\rho) e^{-iq\cdot x}$ and $V^a(\rho \to \infty) \to 1$ (see Appendix E). Evaluating the action 3.31 on the solution 3.32 then allows us to yield the vector-vector correlator from the theory [73],

$$\Pi_{\mathrm{VV}}(q^2) = \frac{1}{g_5^2} \ln(q^2). \tag{3.33}$$

Comparing this to the perturbative QCD results [99]

$$\Pi_{\rm VV}(q^2) = \frac{N_f N_c}{24\pi^2}\ln(q^2), \tag{3.34}$$

one can see that we may match

$$g_5^2 = \frac{24\pi^2}{N_c N_f}. \tag{3.35}$$

The vacuum structure

In order to ascertain the vacuum structure of the theory, all fields except the scalar $L(\rho)$ are switched off. The action for L is given by

$$S = \int d^4x d\rho\ \rho^3 \left((\partial_\rho L)^2 + \Delta m^2 \frac{L^2}{\rho^2} \right). \tag{3.36}$$

For $\Delta m^2 = 0$, the UV solution to the equation of motion is given by $L = m + \langle \bar{q}q \rangle / \rho^2$ with m and $\langle \bar{q}q \rangle$ pertaining to the quark mass and condensate respectively. A non-zero $\Delta m^2(\rho)$ allows the scalar to have a radially dependent mass relating to a energy-dependent mass-dimension of the operator vev $\langle \bar{q}q \rangle$ — the equivalent of introducing a running anomalous dimension, $\gamma(\mu)$.

If the mass-dimension of a field theory operator changes from Δ to $\Delta - \gamma$ as the corresponding AdS-scalar's mass grows from M^2 to $M^2 + \Delta m^2$, then equation 2.116 becomes

$$(\Delta - \gamma)(\Delta - \gamma - 4) = M^2 + \Delta m^2, \tag{3.37}$$

implying

$$\Delta m^2 = \gamma^2 - 2\gamma(\Delta - 2). \tag{3.38}$$

So for the operator vev $\langle \bar{q}q \rangle$, for which $\Delta = 3$, we have $\Delta m^2 = \gamma^2 - 2\gamma$. The profile of $\Delta m^2(\rho)$ can then be imposed by using the *one-loop* result for the perturbative anomalous dimension for the gauge theory [41],

$$\gamma_1(\mu; R) = \frac{3C_2(R)}{2\pi}\alpha_s(\mu; R), \tag{3.39}$$

where α_s is the two-loop perturbative running coupling and R denotes the representation of the N_f quarks. Assuming γ is small, the leading order result gives us ($\Delta m^2 = -2\gamma$),

$$\Delta m^2(r) = -3\frac{C_2(R)}{\pi}\alpha_s(\mu; R), \tag{3.40}$$

where we re-emphasise $r = \sqrt{\rho^2 + L^2}$ corresponds to μ. Of course, beyond the regime where the coupling is weak, the perturbative form of $\gamma_1(\mu)$ must be used with caution and is no sense rigorous. However, methods used with such a parameterisation of the running might uncover the broad behaviours exhibited by the gauge theories with similar running profiles. The modified equation of motion becomes

$$\partial_\rho \left(\rho^3 \partial_\rho L\right) - \rho \Delta m^2 L = 0. \tag{3.41}$$

Assuming Δm^2 to be constant and non-zero, i.e. the regime of a fixed point whereby $\gamma \neq 0$, the solution takes the form

$$L(\rho) = \frac{m_{FP}}{\rho^\gamma} + \frac{c_{FP}}{\rho^{2-\gamma}}, \tag{3.42}$$

such that $\gamma(\gamma - 2) = \Delta m^2$. In other scenarios, where Δm^2 takes on the non-trivial running profile of γ_1, the solution to the equation of motion 3.41 must be found numerically. To do so, one must impose boundary conditions. We choose the conditions

$$L(\rho_{\text{IR}}) = \rho_{\text{IR}} \quad \text{and} \quad \partial_\rho L(\rho)|_{\rho=\rho_{\text{IR}}} = 0. \tag{3.43}$$

These are very similar to those conditions imposed on the D3/D7, top down models ($L(0) =$ constant and $\partial_\rho L(0) = 0$) but imposed at the renormalization scale where the theory becomes 'on mass-shell'. We assume $L(\rho)$ behaves like a constituent quark mass at the RG scale pertaining to ρ and therefore the imposed boundary conditions force the constituent masses to always be less than the energy scale.

An example of the $L(\rho)$ profile, of SU(3) with 3 flavours of fundamental quarks, shown in figure 3.3, displays chiral behaviour since the constituent mass of the quark vanishes as one approaches the boundary $\rho \to \infty$. However the chiral symmetry breaking

is self-evident as the constituent quark mass renormalizes to non-zero values as you push towards the IR.

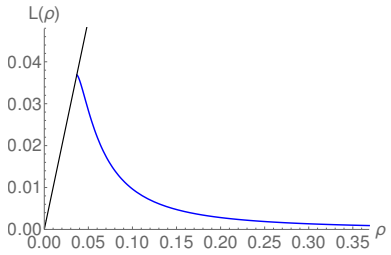

Figure 3.3: Plot of $L(\rho)$ for SU(3) with $N_f = 3$ in the fundamental representation. The plot shows the chiral embedding, i.e. the profile asymptotes as $\langle\bar{q}q\rangle/\rho^2$ as $\rho \to \infty$ ($\gamma \to 0$ in the field theory). Here the boundary condition on the beta function is imposed as $\alpha(0) = 0.14$.

Breitenlohner-Freedman bound

An important feature of the beta functions of QCD-like theories is whether the running coupling passes through a critical value triggering chiral symmetry breaking. How does this feature get brought into the Dynamic AdS/QCD model? As we have seen, chiral symmetry breaking is tripped when the coupling constant passes through a critical value causing the chirally symmetric ground state to become unstable. We must then look for a method of triggering such an instability in the bulk.

In flat space, fields with negative mass-squared have a potential which is globally unbounded from below and thus unstable. A similar feature occurs in AdS backgrounds. Scalar fields in AdS_{d+1} of unit curvature which have the asymptotic solution[6]

$$\phi(r) = \frac{A}{r^{\Delta}} + \frac{B}{r^{d-\Delta}}, \tag{3.44}$$

where $\Delta = \frac{d}{2} + \sqrt{\frac{d^2}{4} + M_\phi^2}$, become tachyonic, i.e. have an unstable potential, when

$$M_\phi^2 < -\frac{d^2}{4}. \tag{3.45}$$

This is known as the Breitenlohner[7]-Freedman[8] (BF) bound [100].

[6] This is the generalised version of equation 2.114 for $d+1$ dimensional AdS-spacetime.
[7] Peter Breitenlohner, 1940-2015.
[8] Daniel Z. Freedman, 1939-.

When the mass of the scalar field representing the field theory operator $\bar{q}q$ drops below the BF bound, the theory becomes unstable around the 'old' global minimum, just like chiral symmetry breaking. In Dynamic AdS/QCD in the AdS_5 background, this instability occurs when the mass of the scalar $L(\rho)$ drops below $M_L^2 = -4$. This pertains to a value of $\Delta m^2 = -1$. Using equation 3.38 (recalling in this case $\Delta = 3$), we arrive at $\gamma = 1$ being the critical value of chiral symmetry breaking in the gauge theory.

The soft-wall behaviour of the Dynamic AdS/QCD model is now important. Were the BF-bound to be violated and the L-field to become unstable, then equating the RG scale, μ, directly to the AdS radial coordinate ρ would lead to a theory whereby the L-field potential becomes unbounded from below in the IR. However, by setting, as we have done, $\mu = \sqrt{\rho^2 + L(\rho)^2}$, when L is finite, the deep IR cannot be accessed and so we keep stable AdS solutions but at a different vacuum pertaining to a non-zero $\langle \bar{q}q \rangle$. In terms of the $L - \rho$ plane and the profile $L(\rho)$ for the scalar, this amounts to a circular region $\rho^2 + L^2 \leq \mu_\gamma^2$ (where μ_γ is the scale for which $\gamma = 1$) which cannot be accessed by the field. The least-energetic, i.e. vacuum solution, of the L-embedding then takes on a profile which rises off of the ρ-axis in the IR to meet the BF-bound scale, μ_γ, near the on-mass shell condition $L = \rho$. This is expected since at μ_γ (identical to the scale Λ_χ) the quarks get their dynamical mass $\propto \mu_\gamma$. Below this scale however, there is not enough energy to excite these masses and so are decoupled. Off course in the Dynamic AdS/QCD model, this is only approximate since the Lagrangian contains only the lowest order terms in L following from a top-down DBI expansion. In the limit where all the higher order terms are put back, the profile of $L(\rho)$ should match exactly to $L = \rho$ at μ_γ.

Meson spectra

Recall from the D3/probe-D7, top-down models that the 7-7 strings, which can be perceived as fluctuations of the D7-branes, pertained to mesonic operators. Bottom-up models, such as Dynamic AdS/QCD, build on this idea with the scalar, vector and axial mesons being described as perturbative fluctuations of the scalar L and the gauge fields V_M^a and A_M^a respectively.

The isoscalar (σ) mesons are described by linearised, perturbative fluctuations, $\delta(\rho)$, about the vacuum configuration, $L_0(\rho)$ (the solution to equation of motion of the Lagrangian given in the action 3.36). Writing the scalar field *plus fluctuation* as

$$L(\rho) = L_0(\rho) + \delta(\rho)e^{iq_\mu x^\mu}, \tag{3.46}$$

with $q^2 = -M_\sigma^2$ defining the meson's mass, we can write the equation of motion of $\delta(\rho)$ as

$$\partial_\rho\left(\rho^3\partial_\rho\delta\right) - \Delta m^2\rho\delta - \rho L_0\delta\left.\frac{\partial\Delta m^2}{\partial L}\right|_{L=L_0} + M_\sigma^2\frac{\rho^3\delta}{(L_0^2+\rho^2)^2} = 0. \tag{3.47}$$

Just as for $L_0(\rho)$, solutions with the UV asymptotics of $\delta \sim \rho^{-2}$ are sought with the IR boundary condition $\partial_r\delta|_{\rho_{IR}} = 0$.

The isovector (ρ) meson spectrum can be determined similarly from the normalizable solution of the equation of motion of the vector gauge field (derived in Appendix E)

$$\partial_\rho\left(\rho^3\partial_\rho V\right) + \frac{\rho^3 M_\rho^2}{(L_0^2+\rho^2)^2}V = 0. \tag{3.48}$$

The axial meson spectrum is determined from the equation of motion of the axial gauge field,

$$\partial_\rho\left(\rho^3\partial_\rho A\right) - g_5^2\frac{L_0^2\rho^3}{(L_0^2+\rho^2)^2}A + \frac{\rho^3 M_a^2}{(L_0^2+\rho^2)^2}A = 0. \tag{3.49}$$

Finally, the pion mass spectrum is identified from the equation of motion of the spacetime-dependent phase field $\pi^a(x)$ of the scalar X; $X = L(\rho)\exp\left(2i\pi^a(x)t^a\right)$,

$$\partial_\rho\left(\rho^3 L_0^2\partial_\rho\pi^a\right) + M_\pi^2\frac{\rho^3 L_0^2}{(L_0^2+\rho^2)^2}\pi^a = 0. \tag{3.50}$$

Adding temperature and magnetic field

Understanding the gauge theories in question at finite temperature and within a finite constant magnetic field is important to ensure a full comprehension of their phase diagrams. A temperature is added into the model by augmenting the AdS_5-like Dynamic AdS/QCD metric to AdS-Schwarzschild[9]-like metric, which at constant unit curvature

[9]Karl Schwarzschild, 1873-1916.

is given by [73]

$$ds^2 = -\rho^2 f(\rho) dt^2 + \rho^2 d\mathbf{x}^2 + \frac{1}{f(\rho)\rho^2} d\rho^2, \tag{3.51}$$

where

$$f(\rho) = 1 - \frac{r_H}{(L(\rho)^2 + \rho^2)^2}, \tag{3.52}$$

with black hole horizon radius r_H. The thermal description of the gauge theory is then introduced [73] (at constant unit AdS curvature) via

$$r_H = \pi T, \tag{3.53}$$

i.e. the Hawking temperature is defined as the hadronic temperature of the gauge field. The black hole, in effect, reduces the available AdS-space, preventing access to values of r below r_H, i.e. energy scales below the corresponding renormalization scale. If the temperature of the black hole exceeds the energy scale pertaining to the BF-bound, μ_γ, then the BF-bound violating region of the $L - \rho$ plane is swallowed by the black hole thus cutting it out of the accessible plane. Since the existence of this region pertained to a chiral symmetry breaking, if $\pi T > \mu_\gamma$ the chiral symmetry is restored.

Introducing a constant, finite magnetic field strength into the fray requires us to withdraw a couple of steps back to the top-down probe-brane models. In the D7-brane DBI action 2.93, by switching on a single magnetic component in the brane gauge field-strength tensor, F_{MN} (keeping $B_{MN} = 0$), we can modify our metric to include a source of a magnetic field in the gauge theory. Choosing all components of F, except $F_{12} = B$,

to vanish, the total pullback on the D7 brane (with spacetime metric 3.1) becomes

$$\mathcal{G}_{ab} = \begin{pmatrix} -f(r)r^2 & 0 & 0 & 0 & 0 & 0 & 0 & 0 \\ 0 & r^2 & B & 0 & 0 & 0 & 0 & 0 \\ 0 & -B & r^2 & 0 & 0 & 0 & 0 & 0 \\ 0 & 0 & 0 & r^2 & 0 & 0 & 0 & 0 \\ 0 & 0 & 0 & 0 & \frac{1}{f(r)r^2}\left(1+(\partial_\rho L)^2\right) & 0 & 0 & 0 \\ 0 & 0 & 0 & 0 & 0 & \frac{\rho^2}{r^2} & 0 & 0 \\ 0 & 0 & 0 & 0 & 0 & 0 & \frac{\rho^2}{r^2} & 0 \\ 0 & 0 & 0 & 0 & 0 & 0 & 0 & \frac{\rho^2}{r^2} \end{pmatrix}, \tag{3.54}$$

where we've also added the Schwarzschild factors $f(r)$ governing the thermal effects of the model. Using 3.54, we can write down the D7-brane Lagrangian as

$$\mathcal{L} \sim \rho^3 \sqrt{1+f(r)\left(\partial_\rho L\right)^2}\sqrt{1+\frac{B^2}{r^4}}. \tag{3.55}$$

Linearising about small $\partial_\rho L$ and B/r^2, we simplify the Lagrangian to

$$\mathcal{L} - \rho^3\left(f(r)\left(\partial_\rho L\right)^2 + \frac{B^2}{(\rho^2+L^2)^2}\left[1+\frac{1}{2}f(r)\left(\partial_\rho L\right)^2\right]\right). \tag{3.56}$$

Under the assumption L is small, we can use

$$(\rho^2+L^2)^{-2}\big|_{L=0} = \rho^{-4} - 2L^2\rho^{-6} + ... \tag{3.57}$$

to simplify the Lagrangian further to

$$\mathcal{L} = \rho^3\left(f(r)\left(\partial_\rho L\right)^2 + \frac{B^2}{\rho^4}\left[1+\frac{1}{2}f(r)\left(\partial_\rho L\right)^2 - \frac{2L^2}{\rho^2} + \mathcal{O}\left(L^4\right)\right]\right). \tag{3.58}$$

Returning to our bottom-up Dynamic AdS/QCD model, we allow for finite magnetic field effects by the inclusion of the lowest order magnetic terms as derived above (equation 3.58) but with undetermined coefficients which can be tuned to give different phenomenological behaviour in the gauge theory.

3.4 A few questions

At this point, I think it is useful to answer some of the questions that may (or may not) be puzzling the astute reader.

Why have we been matching to QCD in the UV, where QCD is perturbative and thus weakly coupled?

The premise of the AdS/CFT correspondence in its weak form is that it is a duality between a weakly coupled string theory and a strongly coupled gauge theory. In the discussions above, we have often matched the boundary to perturbative QCD. For example, the mass dimension of the $\bar{q}q$ operator represented by the scalar L is $\Delta = 3$ on the boundary, its value in the weakly-coupled, perturbative limit. Also g_5 is determined by matching the vector-vector correlator at the boundary to that of perturbative QCD. So in what sense is it at all rigorous to use a weakly coupled string theory and match to a boundary gauge theory with perturbative coupling? The simple answer is that is not! In fact, early AdS/QCD models were trialled on the basis that such a duality should not work but what was the harm in trying. In fact, by some odd quirk of mathematics (or nature), a weakly coupled QCD theory is remarkably well described by an $\mathcal{N} = 4$ strongly coupled supersymmetric theory as is still present on the boundary of most AdS/QCD models, including Dynamic AdS/QCD [101–105]. This is in part due to the anomalous dimensions of $\bar{q}q$ and m (and other source-operator combinations) being the same in both the weakly-coupled limit of QCD and in the infinitely strongly coupled $\mathcal{N} = 4$ SYM theories. The fact that in the AdS/QCD models the running causes γ to increase into the IR is, from the point of the view of the quark content on the boundary, irrelevant.

Do we still have supersymmetries left over on in our 'QCD' theory?

Yes. The metric used in the Dynamic AdS/QCD model and other bottom-up approaches returns to that of AdS_5 in the limit of approaching the boundary. In this regard, the boundary retains the supersymmetries of the conformal theories from the probe-D7 top-down models from which they derive. As addressed in the previous question, it is a remarkable coincidence that weakly coupled QCD is somehow similar to these

supersymmetric theories in the respect that the bottom-up models match experimental data very well and in the far-UV QCD is itself conformal with coupling approximately zero.

We showed that D3-brane stack had a supergravity action akin to that of $\mathcal{N} = 4$ SYM ergo the D3-branes are sat at the boundary of my holographic model, correct? It is a common misconception that, because the D3-branes share a supergravity YM action with $\mathcal{N} = 4$ SYM, the D3-branes are still there in the AdS/CFT correspondence. We showed in section 2.5.2 that, when we take the decoupling limit to arrive at the AdS/CFT correspondence, the D3-brane stack is irrelevant to the descriptions on either side of the duality.

Part II

Part Two: Research

Chapter 4

HyperScaling Relations in the Conformal Window

In this chapter and in those that follow, we utilise the Dynamic AdS/QCD model, outlined in brief in the previous section, to probe the behaviours of asymptotically free gauge theories akin to QCD.

This chapter focuses on using the model to describe the conformal window [44, 45, 49–55] of SU(N_c) gauge theories with N_f fundamental flavours. Again, it is important to stipulate that the boundary theory in our holographic approach still retains supersymmetry and is strongly coupled but its preservation of the perturbative SU(N_c) anomalous dimensions allow us to have a perturbative SU(N_c) gauge theory on the boundary. For a theory with quarks in the fundamental representation, asymptotic freedom sets in when $N_f < 11N_c/2$. Immediately below that point, at least at large N_c, the two loop beta function enforces a perturbative infra-red (IR) fixed point [45, 46]. The fixed point behaviour is expected to persist into the non-perturbative regime as N_f is further reduced. This behaviour is seen in the two-loop perturbative computation of the running of the coupling of α and hence γ. We will use that ansatz here to model these theories. Of course as the fixed point leaves the perturbative regime this becomes just a sensible 'parametrization' of the non-perturbative physics.

Below some critical value of the number of flavours, N_f^c, the coupling is expected to be strong enough to trigger spontaneous symmetry breaking by the formation of a quark

anti-quark condensate (so-called walking theories live just on the symmetry breaking side of that transition). Above that critical value, chiral symmetry is restored and only broken explicitly by the introduction of a non-zero quark mass - this is the regime of the conformal window, see figure 4.1. Holographic models describe the quark condensate by a scalar in AdS whose mass is related to the mass dimension, Δ, of the field theory operator via [32, 83, 84] $m^2 = \Delta(\Delta - 4)$. As Δ falls below 2 (or equivalently $\gamma \geq 1$), a clear instability sets in as the mass violates the Breitenlohner-Freedman (BF) bound in AdS_5 [100]. Remarkably, the $\gamma = 1$ criterion precisely matches that deduced from gap equation analysis of the same problem [106, 107]. By using the two loop running for γ, the BF bound violation occurs for $N_f \gtrsim 4N_c$.

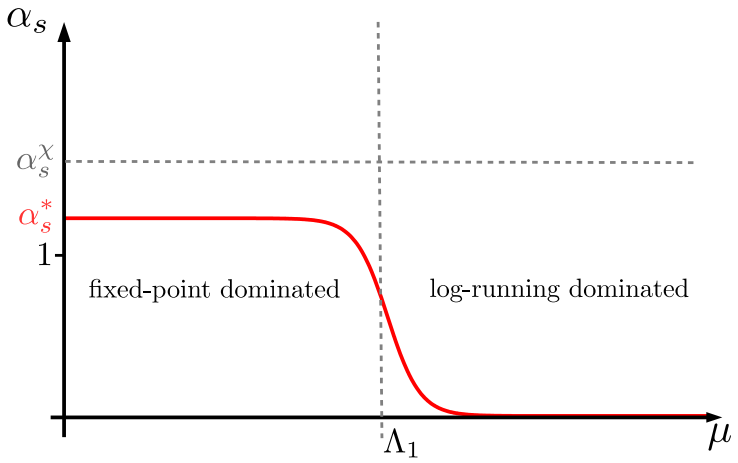

Figure 4.1: An example of the running in the conformal window. The value of the coupling at the IR fixed-point is below the critical coupling to trigger SχSB. The scale Λ_1, set by the perturbative *one-loop* log-running of α_s roughly separates the fixed-point regime from the perturbative regime. Quarks with masses $m > \Lambda_1$ don't see the IR fixed point behaviour whereas as much lighter quarks will be affected by its presence.

We use as our main example an $N_c = 3$ theory with fundamental quarks ($N_f^c \simeq 11.9$) and look at a few discrete values of N_f (12, 13 and 15) which span the conformal window regime. These examples suffice to explore the qualitative behaviour of observables on the different running profiles with IR fixed points and are easily extendible to different N_c. In the massless quark limit, theories like these inside the conformal window flow to a non-trivial and strongly coupled IR conformal theory. The existence of such theories is of great theoretical interest and a sizeable lattice community [108–120] is seeking evidence

for them in numerical simulations. On a lattice, the massless limit can only be obtained as a fine tuned point in parameter space. Simulations are therefore performed with finite mass and signals of the presence of, and approach to, the conformal phase are sought. For this reason a simple model such as Dynamic AdS/QCD, that makes predictions for this limit, should be helpful in identifying expected behaviours in physical, measurable quantities as one approaches the fixed point. We will therefore concentrate on studying the dependence of the quark condensate, meson masses and decay constants as a function of the quark mass, m.

The condensate $\langle \bar{q}q \rangle$ has a leading divergence in the UV of the form $m\Lambda_{UV}^2$, where Λ_{UV} is a UV cutoff scale, as one would expect on dimensional grounds[1]. In the IR conformal regime γ is a non-vanishing constant. Here, therefore, the divergence grows as $m\Lambda_{UV}^{2-2\gamma}$. This again matches the naïve dimensional analysis — the mass has scaling dimension $1+\gamma$ and the condensate scaling dimension $3-\gamma$, therefore we expect this dependence on the UV cutoff scale. There is also a sub-leading term in the condensate which grows as $m^3 \ln \Lambda_{UV}$ in the UV but changes to $m^{\frac{3-\gamma}{1+\gamma}} \ln \Lambda_{UV}$ in the IR, due to the fixed point regime with non-vanishing, constant γ. This is again consistent with dimensional analysis in the IR. These are the hyperscalings relations found in [121]. One of the powers the Dynamic AdS/QCD model is that it reproduces this scaling behaviour when the condensate is measured.

Changing the precise IR boundary condition on the AdS scalar leaves these power relations invariant but changes the constant of proportionality between $\langle \bar{q}q \rangle$ and $m^{\frac{3-\gamma}{1+\gamma}}$. Once this constant is chosen the model allows one to follow the renormalization group flow of the mass and the condensate. Numerical work lets us look at intermediate regimes where the quark mass is of order the scale Λ_1 (the scale generated by the one-loop beta function) where the coupling transitions from the perturbative regime (dominated by the one-loop logarithmic running) in the UV to the non-perturbative fixed point in the IR[2] (see figure 4.1). To analyze the impact of Λ_1, we fit to a simple scaling relation of the

[1] The only scale in the theory is the quark mass, m, and so the remaining dimensions are made up from the imposed UV cutoff scale Λ_{UV}.

[2] We take only the one-loop beta-function here because it is this which is concerned about the behaviour in the UV. The sign of β_0 dictates whether or not we see asymptotic freedom. The two-loop beta function modifies the behaviour in the IR.

form $\langle \bar{q}q \rangle \sim m^b$. The exponent b can then be mapped, using the hyperscaling relation, to an extracted value for γ which we compare to the functional form of γ that we have input into the model (through the running of α_s). In the running regime around Λ_1, we find significant deviations from the input γ, showing that the one-scale m^b functional form breaks down in this regime where the running is fast. Of course, here the second scale Λ_1 will also enter into the scaling relations and so this is as expected. Our analysis allows us to quantify the deviations.

Most importantly, for comparison to lattice simulations, are computations of physical observables. We compute the meson spectrum including M_ρ, M_π and M_σ and their decay constants and display their scalings with m and against each other. When we compute these dimension 1 quantities, we expect a hyperscaling behaviour for dimension one objects of the form $m^{\frac{1}{1+\gamma}}$. We again extract γ from each variable and display variations from the input γ function in the different regimes. The hyperscaling relations are matched in the deep UV and IR fixed point regimes but there are significant deviations in the running regime where Λ_1 again enters the physics. These are the main results of our analysis.

4.1 Dynamic AdS/QCD

Dynamic AdS/QCD [89], as introduced in detail in section 3.3.1, will be briefly recapped here for convenience. The model maps onto the action of a probe D7 brane in an AdS geometry expanded to quadratic order [122, 123]. The anomalous dimension of the quark mass/condensate is encoded through a mass term that depends on the radial AdS coordinate ρ.

The five dimensional action of our effective holographic theory is

$$\begin{aligned} S &= \int d^4x\, d\rho\, \mathrm{Tr}\, \rho^3 \left[\frac{1}{\rho^2 + |X|^2} |DX|^2 \right. \\ &\left. + \frac{\Delta m^2}{\rho^2} |X|^2 + \frac{1}{2} F_V^2 \right]. \end{aligned} \tag{4.1}$$

The field X describes the quark condensate degree of freedom. Fluctuations in $|X|$

around its vacuum configurations will describe the scalar meson. The π fields are the phase of X,

$$X = L(\rho)\ e^{2i\pi^a T^a}. \tag{4.2}$$

f_V are vector fields that will describe the vector (V) mesons. It is possible to include additional mesonic states through extra holographic fields that describe further QCD operators. For example, the a-mesons can be described through an axial gauge field F_A. In this chapter, we take a simpler model which suffices to contain enough physical observables to display the scaling behaviours we are interested in.

We work with the five dimensional metric

$$ds^2 = \frac{d\rho^2}{(\rho^2 + |X|^2)} + (\rho^2 + |X|^2)dx^2, \tag{4.3}$$

which will be used for contractions of the space-time indices. ρ is the holographic coordinate ($\rho = 0$ is the IR, $\rho \to \infty$ the UV) and $|X| = L$ enters into the effective radial coordinate in the space, i.e. there is an effective radial coordinate $r^2 = \rho^2 + |X|^2$. This is how the quark condensate generates a soft IR wall for the linearized fluctuations that describe the mesonic states: when L is nonzero, the theory will exclude the deep IR at $r = 0$.

The normalizations of X and F_V are determined by matching to the gauge theory in the UV. External currents are associated with the non-normalizable modes of the fields in AdS. In the UV, we expect $|X| \sim 0$ and we can solve the equations of motion for the scalar, $L = K_S(\rho)e^{-iq.x}$, and vector field, $V^\mu = \epsilon^\mu K_V(\rho)e^{-iq.x}$. Each satisfies the same equation,

$$\partial_\rho[\rho^2\partial_\rho K] - \frac{q^2}{\rho}K = 0\,, \tag{4.4}$$

with the UV solution ($\rho \to \infty$) being

$$K_i = N_i\left(1 + \frac{q^2}{4\rho^2}\ln(q^2/\rho^2)\right), \quad (i = S, V), \tag{4.5}$$

where N_i are normalization constants that are not fixed by the linearized equation of motion. Substituting these solutions back into the action gives the scalar correlator Π_{SS}

and the vector correlator Π_{VV}. Performing the usual matching to the UV gauge theory requires us to set

$$N_S^2 = N_V^2 = \frac{N_c N_f}{24\pi^2}. \tag{4.6}$$

The vacuum structure of the theory can be determined by setting all fields except $|X| = L$ to zero. We assume that L will have no dependence on the x coordinates. The action for L is given by

$$S = \int d^4x \; d\rho \; \rho^3 \left[(\partial_\rho L)^2 + \Delta m^2 \frac{L^2}{\rho^2} \right]. \tag{4.7}$$

If $\Delta m^2 = 0$ then the scalar, L, describes a dimension 3 operator and a dimension 1 source as is required for it to represent $\bar{q}q$ and the quark mass m. That is, in the UV the solution for the L equation of motion is $L = m + \langle \bar{q}q \rangle / \rho^2$. A non-zero Δm^2 allows us to introduce an anomalous dimension for this operator. If the mass squared of the scalar violates the BF bound of -4 ($\Delta m^2 = -1$, $\gamma = 1$) then the scalar field L becomes unstable and the theory enters a chiral symmetry breaking phase.

We will fix the form of Δm^2 using the two loop running of the gauge coupling in QCD (with fundamental matter) which is given by

$$\mu \frac{d\alpha}{d\mu} = -b_0 \alpha^2 - b_1 \alpha^3, \tag{4.8}$$

where

$$b_0 = \frac{1}{6\pi}(11 N_c - 2 N_f), \tag{4.9}$$

and

$$b_1 = \frac{1}{24\pi^2} \left(34 N_c^2 - 10 N_c N_f - 3 \frac{N_c^2 - 1}{N_c} N_f \right). \tag{4.10}$$

Asymptotic freedom is present provided $N_f < 11 N_c / 2$. There is an IR fixed point with value

$$\alpha^* = -b_0 / b_1 \,, \tag{4.11}$$

which rises to infinity at $N_f \sim 2.6 N_c$.

The one loop result for the anomalous dimension of the quark mass is

$$\gamma_1 = \frac{3C_2}{2\pi}\alpha, \qquad C_2 = \frac{(N_c^2-1)}{2N_c}\,. \tag{4.12}$$

Using the fixed point value α^*, the condition $\gamma = 1$ occurs at $N_f^c \sim 4N_c$ (precisely $N_f^c = N_c\left(\frac{100N_c^2-66}{25N_c^2-15}\right)$).

We will identify the RG scale μ with the AdS radial parameter $r = \sqrt{\rho^2+L^2}$ in our model. Note it is important that L enters here. If it did not and the scalar mass was only a function of ρ then, were the mass to violate the BF bound at some ρ, it would leave the theory unstable however large L grew. Including L means that the creation of a non-zero but finite L can remove the BF bound violation leading to a stable solution.

Working perturbatively from the AdS result $m^2 = \Delta(\Delta-4)$ we have

$$\Delta m^2 = -2\gamma_1 = -\frac{3(N_c^2-1)}{2N_c\pi}\alpha\,, \tag{4.13}$$

where γ_1 is the one-loop perturbative gamma-function. This will then fix the r dependence of the scalar mass through Δm^2 as a function of N_c and N_f.

Again, it is important to stress that using the perturbative result outside the perturbative regime is in no sense rigorous but simply a phenomenological parametrization of the running as a function of μ, N_c, N_f that shows fixed point behaviour. Similarly the relation between Δm^2 and γ_1 is a guess outside of the perturbation regime.

4.2 Scaling behaviour of the quark condensate

We are now ready to study the scaling behaviours of the parameters of the gauge theory. Firstly, we will study the vacuum structure of an SU(3) gauge theory with N_f fundamental quarks in the conformal window range $12 \leq N_f \leq 15$. These theories are conformal when the quarks are massless[3] so we will study the theories with a quark mass which breaks conformality. We will show that the model correctly encodes the running

[3]In the AdS space this pertains to the vacuum embedding of the scalar L to have the profile $L = 0$ and so $m = \langle\bar{q}q\rangle = 0$. This is expected since the chiral symmetry is not spontaneously broken in the conformal window of the gauge theory.

dimensions of the quark mass and condensate.

The Euler-Lagrange equation for the determination of L, in the case of a constant Δm^2, is

$$\partial_\rho[\rho^3\partial_\rho L] - \rho\Delta m^2 L = 0\,. \tag{4.14}$$

If Δm^2 depends on L then there is an additional term $-\rho L^2\partial_L\Delta m^2$ in the above equation of motion. At the level of the equation of motion this is an effective contribution to the running of the anomalous dimension γ that depends on the gradient of the rate of running in the gauge theory. At one-loop in the gauge theory there is no such term depending on the gradient of the rate of running and as such we elect to drop it. We are then effectively imposing the RG running of Δm^2 only at the level of the equations of motion, i.e. after the equations of motion have been derived at constant Δm^2. Since we are interested in theories that run from a trivial UV fixed point to an IR fixed point the dropped term would only influence the intermediate regime and then only for the smaller values of N_f where the running is fast. We have checked there is no qualitative change in the theory in the conformal window by including it.

To find solutions for $L(\rho)$ and express the quark condensate in terms of the bare mass, one needs to impose a regularity condition in the IR. The top-down D3-D7 system [86,87,91] has the IR condition $\partial_\rho L(0) = 0$ as that condition. However, this issue is more subtle in this model as we will show. The IR solutions do not satisfy $\partial_\rho L(0) = 0$ except in the conformal massless limit. We believe the reason for this is that the model does not include the backreaction to the quark flavour's mass (and condensate). Were the mass' backreaction to be included, it would generate a small shift in the value of the dilaton at the scale of the mass as the flavours decouple from the QCD running. We would expect that variation in the geometry to accommodate a solution with $\partial_\rho L(0) = 0$. Rather than attempt the backreaction, we shall simply use an on-mass shell condition in the IR to terminate the RG flow. We discuss this issue in detail in the IR and UV.

In the full running theory at large energy scales, the running of the anomalous dimension γ is determined by the one loop QCD results. There is then a regime, around a scale we will call Λ_1, where the coupling is sufficiently strong that the two loop contribution to the running of the coupling will become important and at scales somewhat

below this, the theory will approach an IR fixed point — see figure 4.1. A quark with large bare mass ($\gg \Lambda_1$) will only experience the high energy regime since it will be integrated from the theory at its mass scale which will be well above Λ_1. For quarks with very small bare mass ($\ll \Lambda_1$) their IR physics will be determined by the fixed point behaviour. It is therefore useful to study these two extreme regimes before looking at the full theory.

4.2.1 Infrared fixed point behaviour

In the IR of the conformal window $\alpha \to -b_0/b_1$, γ_1 becomes constant and hence Δm^2 is a non-zero constant. Δm^2 must lie in the regime $-1 < \Delta m^2 < 0$ for the theory to be stable and remain conformal in the IR without a dynamical chiral condensate forming. Let us first, for simplicity, consider the theory that lives at the fixed point at all scales and so has no running of the coupling (or therefore running of γ).

The solutions of the RG flow equation (7.20) at the fixed point (with $\Delta m^2 = \gamma^*(\gamma^* - 2)$, γ^* being the fixed point value of the anomalous dimension) are of the form

$$L = \frac{m^*}{\rho^{\gamma^*}} + \frac{c^*}{\rho^{2-\gamma^*}}. \tag{4.15}$$

Here m^* and c^* are interpreted as being the operator-source combination for the operator $\bar{q}q$ but, of course in this theory, they have dimensions $1+\gamma^*$ and $3-\gamma^*$.

To extract the chiral condensate, we substitute the solution back into the action (7.14), integrate over ρ upto a cut off Λ_{UV}, and compute $\frac{1}{Z}\frac{dZ}{dm^*}\big|_{m^*}$. We find (see Appendix F)

$$\begin{aligned} \langle \bar{q}q \rangle^* &= \tfrac{(\Delta m^2 + (\gamma^*)^2)}{(1-\gamma^*)} m^* \Lambda_{UV}^{2-2\gamma^*} \\ &+ 2(\Delta m^2 + \gamma^*(2-\gamma^*)) c^* \ln \Lambda_{UV} \end{aligned} \tag{4.16}$$

The first term is the expected UV divergence in the condensate in the presence of a mass - the mass and condensate share the same symmetry properties and the dimension is then made up with the UV cutoff scale. Since the condensate has dimension $3-\gamma^*$ and m^* dimension $1+\gamma^*$, the power of Λ_{UV} is the correct one to match this dimensional analysis. This is already a sign that the model correctly describes scaling dimensions.

The second term is, upto log renormalization, a constant times the parameter c^*. Therefore this term, in the $m^* = 0$ limit, implies c^* is directly proportional to the condensate $\langle \bar{q}q \rangle^*$. We will study c^*'s scaling behaviour shortly.

To find solutions for $L(\rho)$ and express c^* in terms of m^* one needs to impose a regularity condition in the IR. The solutions in (4.15) clearly do not satisfy $\partial_\rho L(0) = 0$ except in the conformal $m^* = c^* = 0$ limit. As we discussed in the introduction to this chapter, this is most likely a failure of the model to include the backreaction of the quark decoupling on the background metric. We will rectify this by choosing a suitable boundary condition. A sensible first guess for the IR boundary condition is

$$L(\rho = \rho_{IR}) = \rho_{IR}, \qquad L'(\rho = \rho_{IR}) = 0. \tag{4.17}$$

This IR condition is similar to that from top down models but imposed at the renormalization scale where the flow becomes 'on-mass-shell'. Here we are treating $L(\rho)$ as a constituent quark mass at each scale ρ. We then find (see Appendix G)

$$m^* = \left(\frac{\gamma^* - 2}{2\gamma^* - 2} \right) \rho_{IR}^{1+\gamma^*} \tag{4.18}$$

and

$$c^* = \frac{\gamma^*}{2\gamma^* - 2} \left(\frac{2\gamma^* - 2}{\gamma^* - 2} \right)^{\frac{3-\gamma^*}{1+\gamma^*}} (m^*)^{\frac{3-\gamma^*}{1+\gamma^*}}. \tag{4.19}$$

This shows analytically that the model obeys the 'hyperscaling' relation one would expect at the conformal fixed point. The condensate has dimension $3 - \gamma^*$ and the mass dimension $1 + \gamma^*$. Since m^* is the only intrinsic scale, $c^* \sim (m^*)^{\frac{3-\gamma^*}{1+\gamma^*}}$ is ensured. In the full theory with a running coupling, relations of this form will hold in any regime where γ^* is running slowly and with the c and m parameters those appropriate to that energy regime.

The boundary condition $L'(\rho = \rho_{IR}) = 0$ is not crucial to obtain the hyperscaling relations since the relative dimensions of m^* and $\langle \bar{q}q \rangle^*$ are fixed in the holographic model. Instead, the choice of this boundary condition fixes the proportionality constant between $\langle \bar{q}q \rangle^*$ and $(m^*)^{\frac{3-\gamma^*}{1+\gamma^*}}$. Given that there is some freedom in this choice of boundary condition, we will not be predicting this value - for this reason in our numerics we will

choose a boundary condition to set the proportionality constant to unity in all cases. That is, we will assume at the IR boundary the solution is of the form

$$L = \frac{m^*}{\rho^{\gamma^*}} + \frac{(m^*)^{\frac{3-\gamma^*}{1+\gamma^*}}}{\rho^{2-\gamma^*}}, \tag{4.20}$$

i.e. $\langle \bar{q}q \rangle^* = (m^*)^{\frac{3-\gamma^*}{1+\gamma^*}}$, and hence use the boundary conditions

$$\begin{aligned} L(\rho)|_{\rho_{IR}} &= \rho_{IR}, \\ L'(\rho)|_{\rho_{IR}} &= -\frac{\gamma^* m^*}{\rho_{IR}^{\gamma^*+1}} + \frac{\gamma^*-2}{\rho_{IR}^{3-\gamma^*}}(m^*)^{\frac{3-\gamma^*}{1+\gamma^*}}. \end{aligned} \tag{4.21}$$

Note here that the value of γ^* used in the initial condition is that determined by (7.19) (and the discussion below) evaluated at the scale

$$\begin{aligned} \mu &= \sqrt{\rho^2 + L^2}\Big|_{L=\rho=\rho_{IR}} \\ &= \sqrt{2}\rho_{IR}. \end{aligned} \tag{4.22}$$

4.2.2 The large quark mass limit

If we now consider asymptotically free theories that lie at $\alpha < \alpha^*$ in the UV, then the far-UV running of Δm^2 is controlled by the one-loop perturbative running coupling. Holographic theories where the L profile lives only at large values of $r = \sqrt{L^2 + \rho^2}$ will see only this behaviour, i.e. we can extract the large quark mass behaviour from this limit. See figure 4.2.

Using $\Delta m^2 = -2\gamma$, and with the one-loop logarithmic running of α_s given by $\alpha_s = \frac{1}{\beta_0 \ln(\rho/\Lambda_1)}$, the embedding equation (7.20) becomes

$$\partial_\rho[\rho^3 \partial_\rho L] + \frac{2k\rho}{\ln\left(\frac{\rho}{\Lambda_1}\right)} L = 0, \tag{4.23}$$

where Λ_1 is the one-loop running scale and k is a constant which, at the one loop level, can be shown to take the form $k = 3\frac{N_c^2-1}{N_c \pi b_0}$ (see Appendix H). The solution to 4.23 has

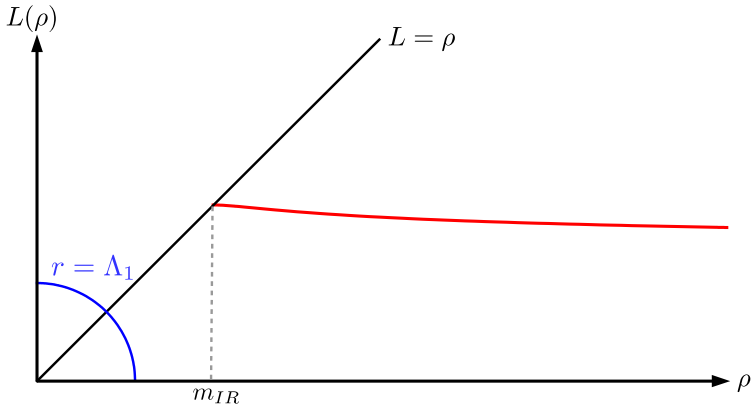

Figure 4.2: Profile for $L(\rho)$ living only at scales above Λ_1 (i.e. outside the circle of radius $r = \Lambda_1$). It knows nothing of the behaviour of the running of the coupling below Λ_1 and so is dominated only by the far-UV running — the logarithmic one-loop running.

the behaviour

$$\begin{aligned} L &= \frac{m_{UV}}{\left(\ln\left(\frac{\rho}{\Lambda_1}\right)\right)^k} + \frac{c_{UV}}{\rho^2}\left(\ln\left(\frac{\rho}{\Lambda_1}\right)\right)^k, \\ &\equiv m(\rho) + \frac{c(\rho)}{\rho^2}. \end{aligned} \tag{4.24}$$

To obtain the bare quark mass one simply extracts the non-normalizable term of the solution at some fixed far-UV scale (we choose $\rho = e^{500}$ for the numerical work below[4]) — this is what we will refer to as m_{bare} in plots that follow.

Applying the simple boundary conditions

$$L(\rho = \rho_{IR}) = \rho_{IR}, \qquad L'(\rho = \rho_{IR}) = 0, \tag{4.25}$$

gives

$$m_{UV} = -\frac{2c_{UV}}{k\rho_{IR}^2}\left(\ln\frac{\rho_{IR}}{\Lambda_1}\right)^{2k+1}, \tag{4.26}$$

and

$$c_{UV} = -\frac{k}{2\left(\ln\frac{\rho_{IR}}{\Lambda_1}\right)^{4k+1}} m_{UV}^3. \tag{4.27}$$

This shows that $c_{UV} \sim m_{UV}^3$ in the UV upto a logarithmic renormalization. The model is again correctly determining the scaling relations between the mass and condensate.

[4]To approximate the far-UV in the conformal window, a large value of ρ is necessary because the running is so slow. Ideally we wish to run out to values of ρ whereby $\gamma \ll \gamma^*$ and for the conformal window this pushes the cutoff up to high values $\rho \sim e^{500}$. In theories where the running is fast, the far-UV can be approximated with values of $\rho \sim 100$ or less.

We assumed that $L'(\rho_{IR}) = 0$ here so that we could display the scaling behaviours analytically. In our numerical work, we will use the boundary condition in (4.21) which sets $c_{UV} = m_{UV}^3$ in the IR for large quark masses also.

4.2.3 Numerical solutions for the full running theory

We have seen that the model correctly describes scaling dimensions in the IR and UV fixed point regimes. The transition between these fixed points is more model dependent but also of more interest for lattice simulations where one would be interested in an estimate of how quickly the IR scaling behaviour is likely to set in. We can see what results this model gives by numerically solving for the mass and condensate as a function of RG scale with the full two-loop running implemented.

We first discuss results for $N_c = 3$ and $N_f = 12$ as an example. This model lies close to the lower edge of the conformal window ($N_f^c < N_f < 11N_c/2$). Specifically, it displays an IR fixed point value for γ of γ^*=0.8 (a value calculated from the one and two loop QCD beta-functions). We proceed by solving (7.20) subject to the IR boundary condition (4.21). Then for intermediate values of ρ (between the IR and UV), we fit L, L' and L'' to the functional form

$$L = \frac{m}{\rho^\gamma} + \frac{c}{\rho^{2-\gamma}} \tag{4.28}$$

to extract an estimate of the running mass, m, condensate, c, and γ. Note here m is a parameter that in the UV has dimension 3 and displays logarithmic running consistent with the discussion of (4.24) whilst in the IR it runs to be a source of scaling dimension $1 + \gamma$. This ansatz (equation 4.28) for the fitting is sound in the UV and IR fixed point regimes and will likely be good locally in slowly running regimes but is necessarily approximate.

Let us first evaluate the condensate at the deepest IR point (i.e. ρ_{IR}) for each value of quark mass for each flow. We have fixed L' at this point, assuming that the solution takes the form in 4.20, therefore in the IR and UV fixed point regimes (i.e. at low and high quark mass), we expect the numerical solution to match that form precisely. In the intermediate regime where γ is running, the form in (4.20) is only approximate. The

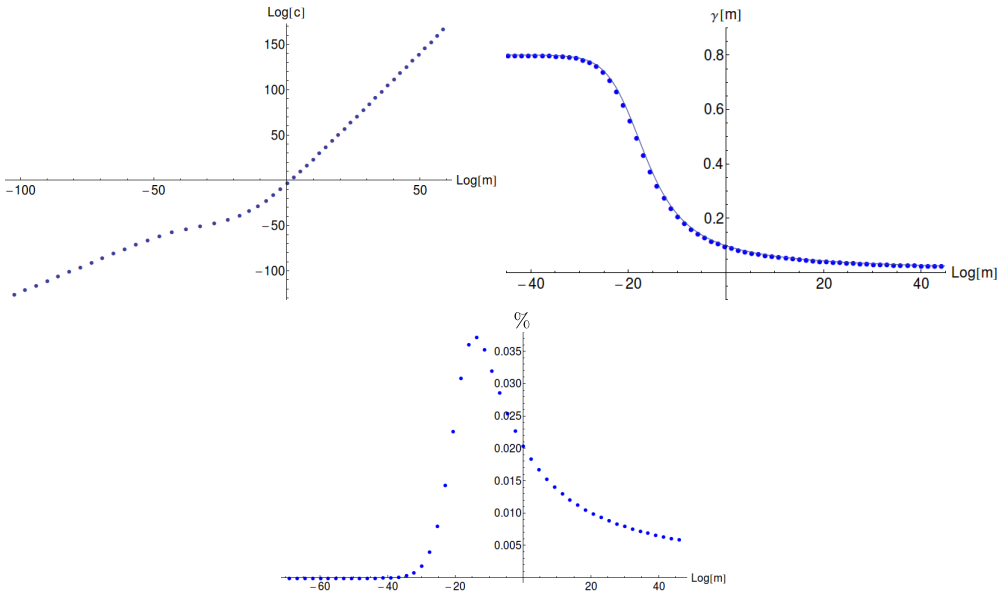

Figure 4.3: Plots for the theory $N_c = 3$ and $N_f = 12$. [**a) top-left**] $\log c$ against $\log m_{\text{bare}}$ [**b) top-right**] numerical points for γ against $\log m_{\text{bare}}$ — γ is extracted by assuming the scaling relation $\langle \bar{q}q \rangle = m^{\frac{3-\gamma}{1+\gamma}}$ [**c) bottom**] the percentage difference between the extracted form of γ and the input form (solid line in b)). For all of these c is evaluated at ρ_{IR}.

numerical solutions for the quark condensate parameter c against the quark mass are displayed in figure 4.3a). The plot shows clear UV and IR scaling regimes where $c \sim m^b$ with a transition period between. Remember that a large bare mass ($m_{\text{bare}} > \Lambda_1$) comes from a theory that doesn't see the IR fixed point behaviour. As the bare mass is decreased, it is able to 'see' more and more of the IR-running behaviour such that a mass $m_{\text{bare}} \ll \Lambda_1$ is dominated by the fixed-point behaviour.

In figure 4.3b), the value of γ extracted from b is plotted over the input form of γ as discussed below Eq (7.19). If one assumes that b takes the form $b = \frac{3-\gamma}{1+\gamma}$, one should expect to return the input value of γ, since the IR regularity condition is deliberately chosen so that $c = m^{\frac{3-\gamma}{1+\gamma}}$ and we are evaluating c at the IR boundary. It is clear from figure 4.3b) that the extracted γ does indeed agree very well with the input form bar marginal discrepancies in the regime of steepest running. The extent of the deviation in this intermediate regime can be seen more clearly in figure 4.3c) as a percentage difference from the input form. Clearly the ansatz (4.15) works well at all scales. The slight deviation between the input and output γ, which reflects the additional scale Λ_1

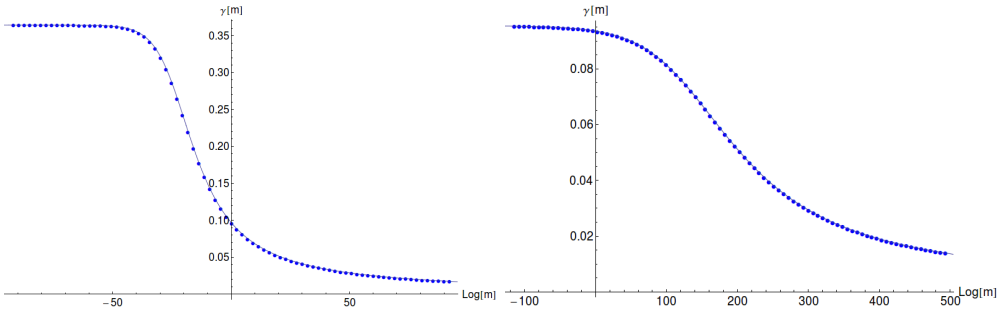

Figure 4.4: $N_c = 3$: [**a) left**] γ versus m_{bare} from c for $N_f = 13$ [**b) right**] γ versus m_{bare} from c for $N_f = 15$

from the running, seems to persist for several decades of energy on either side of the strongest running regime in this model. Such behaviour, if true of the full theory, would further complicate lattice studies of such theories by requiring a very large box size to include both the UV and IR fixed point behaviours.

The behaviour for other values of N_f in the conformal window are very similar in spirit to the $N_f = 12$ case we have looked at in detail. To summarize the other cases, we simply produce the plot of γ extracted from the fit of the form $c \sim m^{(3-\gamma)/(1+\gamma)}$ against quark mass overlaid on the input γ function from the two loop running. We show results for the cases $N_f = 13$ and $N_f = 15$ in figure 4.4. These plots indicate that the aforementioned discrepancy in the regime of strongest running becomes increasingly less dominant at higher values of N_f. This trait encapsulates the idea that as the number of flavours increases, the fixed point value of γ drops and the rate of running slows causing the IR fixed point behaviour to extend further away from $\mu = 0$.

4.3 Bound state masses

So far our analysis has consisted of checking that the vacuum configuration of the model is consistent with naïve scaling arguments. One of the powers of holographic models is that these relations are inbuilt. We now turn to computing the physical parameters, the masses of the bound states and their decay constants. These parameters are true predictions of the model now that the dynamics has been included through the running scalar mass and the condensate fixed by the IR boundary condition.

4.3.1 Linearized fluctuations

The scalar $\bar{q}q$ (σ) mesons are described by linearized fluctuations of L about its vacuum configuration, L_0. We look for space-time dependent excitations, ie $|X| = L_0 + \delta(\rho)e^{-iq.x}$, $q^2 = -M_\sigma^2$. The equation of motion for δ is, linearizing (7.20),

$$\partial_\rho(\rho^3\delta') - \Delta m^2\rho\delta - \rho L_0\delta \left.\frac{\partial\Delta m^2}{\partial L}\right|_{L_0} + M_\sigma^2 R^4 \frac{\rho^3}{(L_0^2+\rho^2)^2}\delta = 0\,. \tag{4.29}$$

We seek solutions with, in the UV, asymptotics of $\delta = \rho^{-2}$ and with $\partial_\rho\delta|_{\rho_{IR}} = 0$ in the IR, giving a discrete meson spectrum. Note that the distinction between this IR boundary condition and that of the normalizable mode in (4.21) is negligible in the spectrum obtained (of order 1 part in 10^5). Recalling previous discussion of the $\partial_L\Delta m^2$ term, we elect to ignore it since it has negligible effects on the spectrum.

We must normalize δ so that the kinetic term of the σ meson is canonical, i.e.

$$\int d\rho \frac{\rho^3}{(\rho^2 + L_0^2)^2}\delta^2 = 1\,. \tag{4.30}$$

The scalar meson decay constant can be found using the solutions for the normalizable and non-normalizable wave functions. We concentrate on the action term (after integration by parts)

$$S = \int d^4x\; d\rho\;\; \partial_\rho(-\rho^3\partial_\rho L)L\,. \tag{4.31}$$

We substitute in the normalized solution δ and the external non-normalizable scalar function K_S at $q^2 = 0$ with normalization N_S to obtain the dimension one decay constant f_σ as

$$f_\sigma^2 = \int d\rho\partial_\rho(-\rho^3\partial_\rho\delta)K_S(q^2 = 0)\,. \tag{4.32}$$

The vector (ρ) meson spectrum is determined from the normalizable solution of the equation of motion for the spatial pieces of the vector gauge field $V_{\mu\perp} = \epsilon^\mu V(\rho)e^{-iq.x}$

with $q^2 = -M^2$. The appropriate equation is

$$\partial_\rho \left[\rho^3 \partial_\rho V\right] + \frac{\rho^3 M^2}{(L_0^2+\rho^2)^2} V = 0\,. \tag{4.33}$$

We again impose $\partial_\rho V|_{\rho_{IR}} = 0$ in the IR and require in the UV that $V \sim c/\rho^2$. To fix c we normalize the wave functions such that the vector meson kinetic term is canonical

$$\int d\rho \frac{\rho^3}{(\rho^2+L_0^2)^2} V^2 = 1\,. \tag{4.34}$$

The vector meson decay constant is given by substituting the solution back into the action and determining the coupling to an external $q^2 = 0$ vector current with wave function K_V. We have for the dimension one f_V

$$f_V^2 = \int d\rho \partial_\rho \left[-\rho^3 \partial_\rho V\right] K_V(q^2=0)\,. \tag{4.35}$$

The pion mass spectrum is identified by assuming a space-time dependent phase $\pi^a(x)$ of the AdS-scalar X describing the $\bar{q}q$ degree of freedom, i.e.

$$X = L(\rho)\exp(2i\pi^a(x)T^a). \tag{4.36}$$

The equation of motion of the pion field is then,

$$\partial_\rho\left(\rho^3 L_0^2 \partial_\rho \pi^a\right) + M_\pi^2 \frac{\rho^3 L_0^2}{(\rho^2+L_0^2)^2}\pi^a = 0. \tag{4.37}$$

Again, we impose at the IR boundary that $\partial_\rho \pi^a|_{\rho_{IR}} = 0$.

4.3.2 Bound states of the $N_c = 3, N_f = 12$ theory

Focusing in detail once more on the $N_c = 3, N_f = 12$ theory with $\gamma^* \simeq 0.8$, we use the formalism outlined above to compute the ρ, π and σ meson masses as a function of quark mass. Hyperscaling arguments lead to the expectation that in a fixed point theory the meson mass will scale as $m_{\rm bare}^{1/1+\gamma}$ (in the UV $\gamma = 0$ whilst in the IR $\gamma = 0.8$). In figures 4.5a), 4.6a) and 4.7a), we plot the dependence on the ρ-mass, σ-mass and the

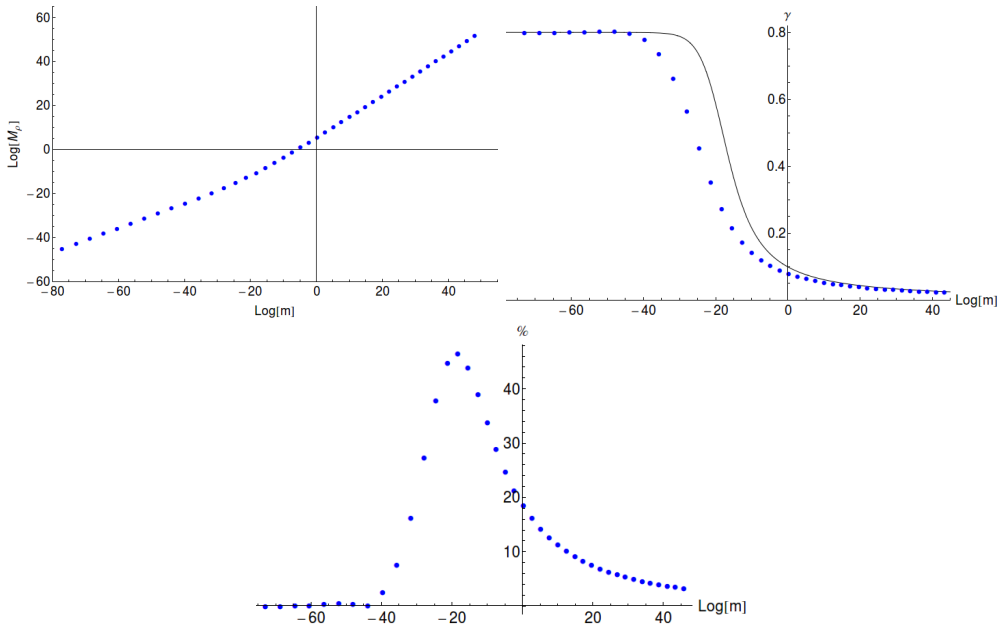

Figure 4.5: $N_c = 3$, $N_f = 12$: [**a) top-left**] ρ-meson mass against quark mass [**b) top-right**] extracted value γ versus m_{bare} from ρ-meson mass spectrum. The solid line shows the holographic input of γ from the two-loop running [**c) bottom**] the percentage difference seen between the input γ running and the extracted γ running

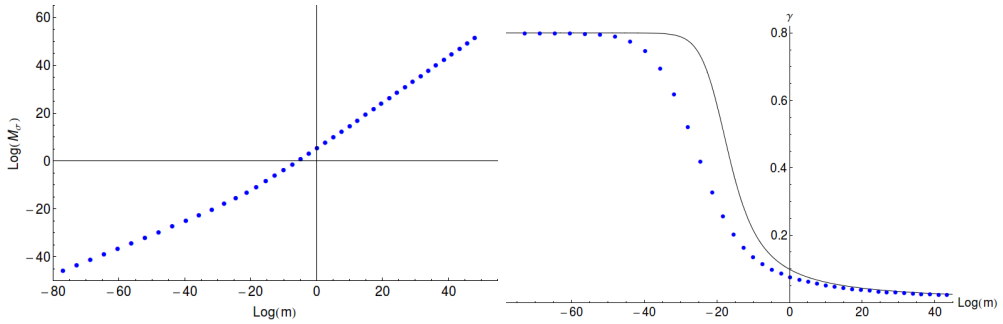

Figure 4.6: $N_c = 3$, $N_f = 12$:[**a) left**] σ-meson mass against quark mass [**b) right**] Extracted value γ versus m_{bare} from σ-meson mass spectrum. The solid line shows the holographic input of γ from the two-loop running.

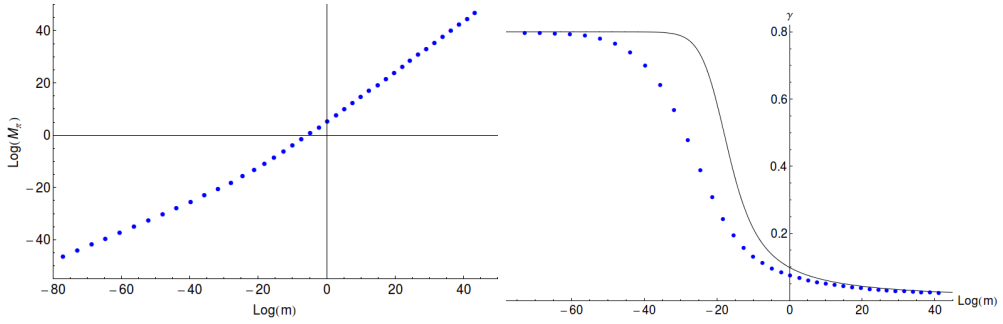

Figure 4.7: $N_c = 3$, $N_f = 12$:[**a) left**] π-meson mass against bare quark mass [**b) right**] Extracted value γ versus m_{bare} from π-meson mass spectrum. The solid line shows the holographic input of γ from the two-loop running.

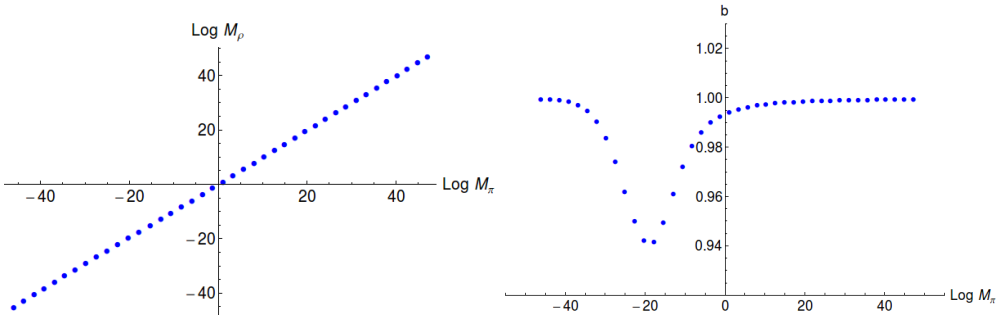

Figure 4.8: $N_c = 3$, $N_f = 12$: [**a) left**] ρ-mass versus π-mass [**b) right**] b versus M_π, where we've assumed $M_\rho \propto M_\pi^b$

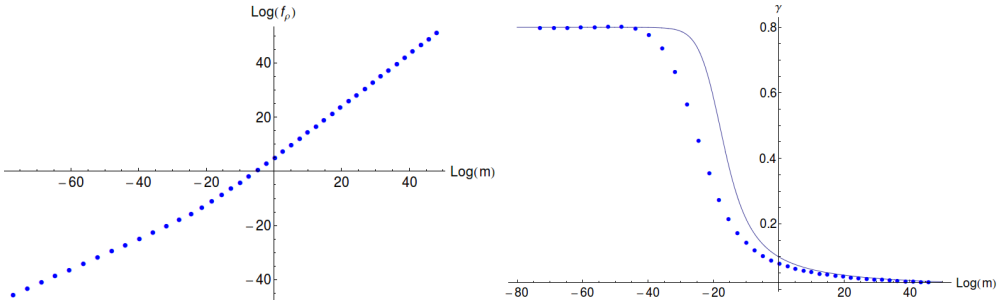

Figure 4.9: $N_c = 3$, $N_f = 12$:[**a) left**] f_ρ versus the bare quark mass [**b) right**] the extracted γ versus m_{bare}

π-mass respectively, against the bare quark mass m_{bare}. Note here we define the bare quark mass as the running quark mass evaluated at a very high UV scale of $\rho = e^{500}$. In figures 4.5b), 4.6b) and 4.7b), we plot γ extracted from the hyperscaling relation, again as a function of the quark mass, and show the comparison to the input running of γ. In a similar vein to the quark condensate scaling, we see excellent agreement with the hyperscaling relations in the UV and IR regimes but a discrepancy in the intermediate running region. In the central region, the discrepancy again reflects the presence of the second scale Λ_1 in the running coupling. The deviations from the naïve IR and UV fixed point values seem to persist in the meson masses over a slightly wider running period than in the input γ. The percentage deviation in γ extracted from the ρ mass and the initial two-loop γ input is shown in figure 4.5c). In the regime of strongest running, the disagreement is found to be as much as 47%.

Another interesting plot is to remove the unphysical quark mass and directly plot M_ρ versus M_π. Here, we naturally expect at a fixed point that $M_\rho \propto M_\pi^b$ with $b = 1$. In figure 4.8 we plot these masses against each other and the extracted value of b against

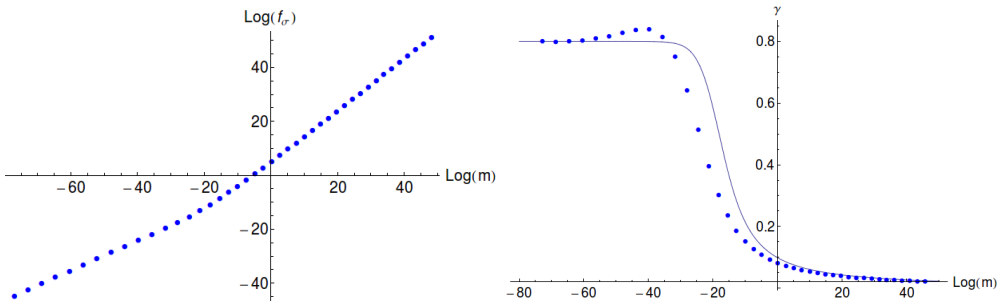

Figure 4.10: $N_c = 3$, $N_f = 12$:[**a) left**] f_σ versus the bare quark mass [**b) right**] the extracted γ versus m_{bare}

M_π. We indeed see the expected proportionality between the masses in the fixed point regimes as well as the deviation in the running regime between these, a telltale sign of the running scale Λ_1 entering the relation. Here the deviations from the fixed point scaling is only of order 5%.

Finally, we can compute the decay constants f_ρ and f_σ and plot them against the quark mass, see figures 4.9a) and 4.10a). Once again, we extract γ, assuming a power law relationship $f_{\rho,\sigma} \propto m_{\text{bare}}^{\frac{1}{1+\gamma}}$ and plot the results in figures 4.9b) and 4.10b). They show similar behaviour to the meson masses.

4.3.3 $N_c = 3$, $N_f = 13, 15$ mesons

For completion, we have also computed the mesonic variables for $N_f = 13$ and $N_f = 15$ in the $N_c = 3$ theory, so that we can test this model across a large span of the conformal window. We begin, as before, by computing the mass spectra of the ρ- and σ-mesons as a function of the quark mass and extract the corresponding γ, which can be seen in figure 4.12a) for $N_f = 13$ and figure 4.12b) for $N_f = 15$. A similar behaviour to that at $N_f = 12$ is observed with the clear IR and UV scaling regimes of $M_\rho \propto m_{\text{bare}}^{\frac{1}{1+\gamma^*}}$ and $M_\rho \propto m_{\text{bare}}$ respectively. We see the deviation from the input γ running in the central region where the running is strongest. However, as N_f is increased away from N_f^c, the IR fixed point value, γ^*, decreases thus reducing the rate of the running with RG scale so the deviation in γ becomes less and less. It is most evident for the case $N_f = 15$ in figure 4.12b), that not only does the discrepancy between the input γ and the extracted γ become less pronounced with increased N_f (at most only $\sim 4.8\%$ difference compared

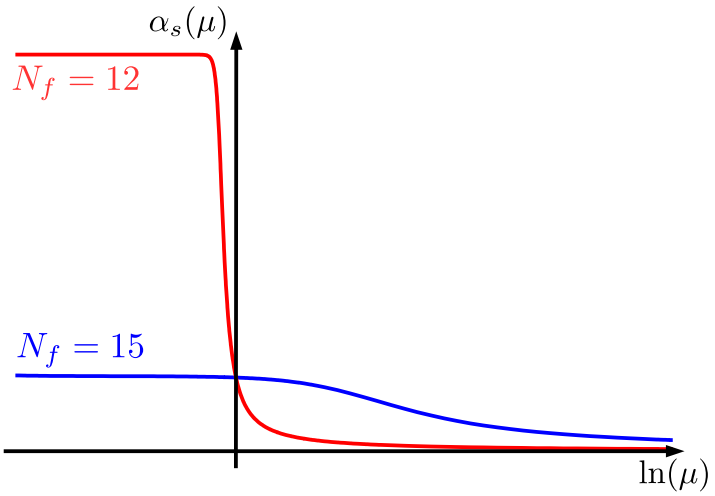

Figure 4.11: The running of α_s for $N_f = 12$ switches drastically between the perturbative one-loop running in the UV to the fixed point behaviour in the IR around Λ_1. The profile for $N_f = 15$ is a lot smoother, pushing the conformal behaviour further out and blurring the two (IR and UV) regimes.

to 47% for $N_f = 12$), but that the conformal IR fixed point behaviour gets 'pushed' further out, slowly (over many aeons of energy scale) blurring the drastic change between fixed point and perturbative one-loop behaviours. As such, the importance of the UV scale Λ_1 is masked and suppressed. To illustrate this, figure 4.11 shows the difference in runnings for $N_f = 12$ and $N_f = 15$.

Next we turn again to plots of M_ρ versus M_π which remove the unphysical mass parameter m_{bare}, see figures 4.13a) and 4.13c). In each of the cases, $N_f = 13$ and $N_f = 15$, the linear relationship $M_\rho \propto M_\pi$, expected in the IR and UV regions, is clearly observed and only by examining the exponent, b, of an assumed $M_\rho \propto M_\pi^b$ relationship do we notice the discrepancy attributed to the additional running scale Λ_1; see figures 4.13b) and 4.13d). Once more we observe that an increase in the number of flavours leads to an extended IR fixed point region and a reduction in the rate of running of the anomalous dimension with RG scale. Figure 4.13d), showing b versus M_π at $N_f = 15$, provides a prime example of such an observation - the greatest difference between the extracted value of b and the linear behaviour ($b = 1$) is only of the order of 0.03%.

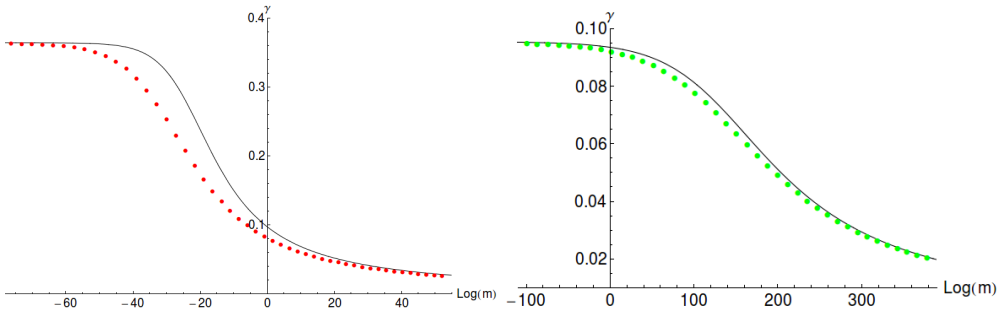

Figure 4.12: $N_c = 3$: [**a) left**] γ extracted from M_ρ against the bare quark mass at $N_f = 13$, $N_c = 3$ [**b) right**] The same for $N_f = 15$.

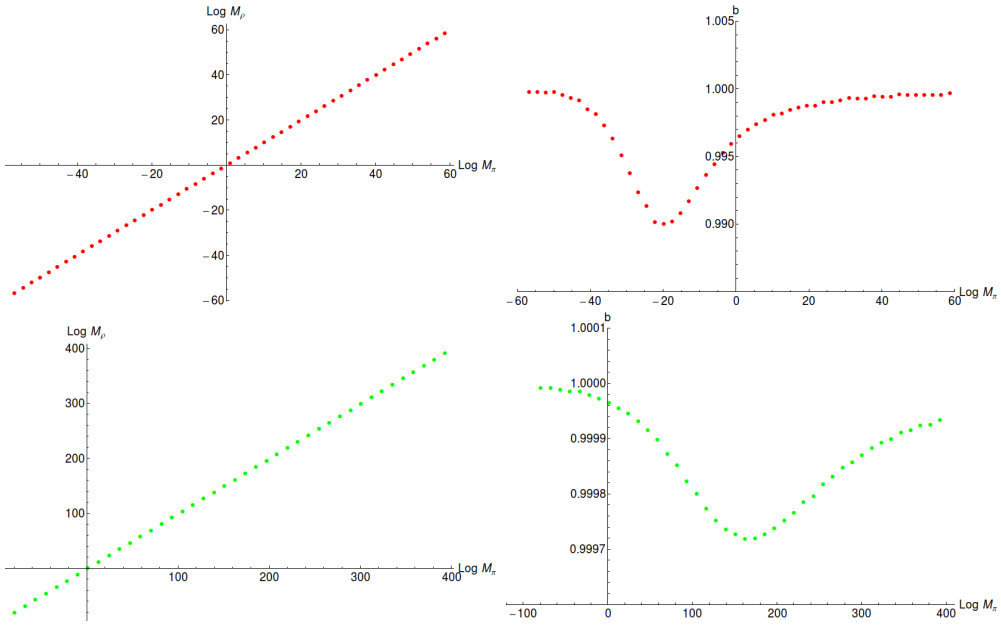

Figure 4.13: $N_c = 3$: [**a) top-left**] M_ρ versus M_π for $N_f = 13$ [**b) top-right**] extracted γ for $N_f = 13$ [**c) bottom-left**] M_ρ versus M_π for $N_f = 15$ [**d) bottom-right**] extracted γ for $N_f = 15$

Chapter 5

Meson Spectra of Asymptotically Free Gauge Theories

Asymptotically free gauge theories are notoriously difficult to study since they run to strong coupling in the infrared. Computing the bound state spectrum of theories such as QCD is therefore very hard. First-principle lattice calculations are possible but very numerically expensive and are typically guided by the answers observed in nature. It is hard to easily explore the range of behaviour across the full space of asymptotically free theories. As we have seen throughout this work, the holographic description of large N_c $\mathcal{N}$=4 gauge theory [32, 83, 84] has raised the prospect of a dual gravitational picture for these theories in which the spectrum might be computed in a purely classical theory. Top-down attempts [86, 87, 91, 97, 124] to rigorously find a gravity dual originating from ten-dimensional string theory are complicated by the need to find a brane construction that decouples all unwanted super-partners, and also by the challenge of finding the appropriate gravitational background for embedding those branes. In any case, when the gauge theory is weakly coupled, such as in the ultraviolet, the gravitational theory will itself become strongly coupled. Bottom-up approaches to holographic modelling [82, 88, 89] have taken broad brushstroke ideas from the AdS/CFT correspondence and attempted to model the mesonic and glueball degrees of freedom. Basic AdS/QCD models appear to work reasonably well, even at the quantitative 10% level or better. In this section, we will firstly provide further support for the success of an existing top-

down model and secondly, we present the bottom-up Dynamic AdS/QCD analysis for a large range of different gauge theories.

The focus of this chapter will be the how the meson spectra varies with N_c, N_f and the matter representation, R. We will explore all representations which have asymptotically free solutions for $N_c, N_f \geq 2$, i.e. fundamental, adjoint and the two-index representations. Of particular interest will be how the meson spectrum alters as one approaches walking theories. Walking theories are expected to have a quark condensate which is enhanced in the UV. In these theories, there are two scales which dominate the running; the scale Λ_1 which characterises the transition between the perturbative logarithmic running in the UV and the slow walking regime in the IR (roughly the scale generated by the one-loop beta function), and the scale Λ_χ where the running trips the critical value to break chiral symmetry (where $\gamma = \gamma^\chi$). The UV condensate is then given by the dimension $3 - \gamma^\chi$ IR condensate $\propto \Lambda_\chi^{3-\gamma^\chi}$ with the dimensions made up from the remaining UV scale,

$$\langle \bar{q}q \rangle_{UV} \propto \Lambda_\chi^{3-\gamma^\chi} \Lambda_1^{\gamma^\chi}.$$

Since $\gamma^\chi \sim 1$, it follows that $\langle \bar{q}q \rangle_{UV} = \Lambda_\chi^2 \Lambda_1$. As the walking theory becomes more dominant (i.e. as N_f increases at fixed N_c and representation) the scale Λ_1 gets pushed further into the UV and so the condensate becomes enhanced. This enhancement of the condensate is responsible for the subsequent enhancement of the ρ mass and the π mass to a lesser degree. A secondary effect of the enhancement of the condensate is the suppression of the σ mass [121, 125–135]. As the condensate (i.e. the vev of $\bar{q}q$) is pushed out to high scales, the effective $\bar{q}q$-potential flattens in the radial direction characterised by the σ-mass, see figure 5.1. As such, the σ-mass becomes light. Of course, this coincides with the transition that the $\sigma-$meson becomes massless when the chiral symmetry is restored in the conformal window. We observe all of these phenomena in our model.

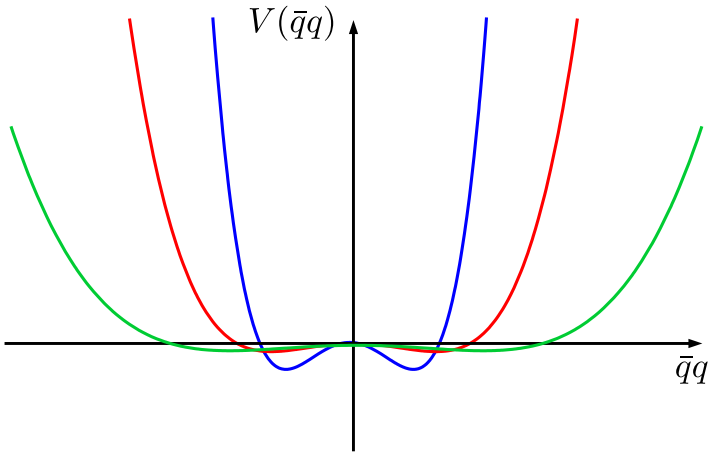

Figure 5.1: As the UV scale Λ_1 (associated to the one-loop running) gets pushed out as walking dominates, the condensate becomes enhanced and stretched the shape of the effective potential. For large walking regimes the potential radial direction flattens causing the sigma-mode to become light. This is in agreement with the walking region enlarging as N_f increases towards the point where chiral symmetry is regained and the sigma-mode becomes massless.

5.1 A top-down model

An early holographic description of QCD [97] was provided by placing D7-brane probes in the dilaton flow geometry of Constable and Myers [96]. D3-D7 strings introduce quenched quark degrees of freedom. The Constable-Myers deformation of $AdS_5 \times S^5$ is a very simple description of a gauge theory with a running coupling that breaks the $\mathcal{N} = 4$ supersymmetry completely. The non-trivial dilaton profile is dual to that running coupling and has an IR pole which is ill-understood. In practice, the geometry describes a gravity dual of a soft-wall since the singularity is repulsive to probe branes. The D7 probes bend away from the singularity and asymptotically the embedding describes a dynamically generated quark condensate at zero quark mass. In [91], the light meson spectrum was computed and moreover, the M_ρ versus M_π^2 plot was compared to quenched lattice data [136]. We update these computations in figure 5.2. The fit is remarkably good. This had seemed very surprising since the gauge theory apparently lies close to infinitely strongly coupled $\mathcal{N} = 4$ gauge theory with all the associated super-partners and has no asymptotic freedom. In this section, we return to this model and analyse it in the spirit of [122] to shed some light on the success at describing the

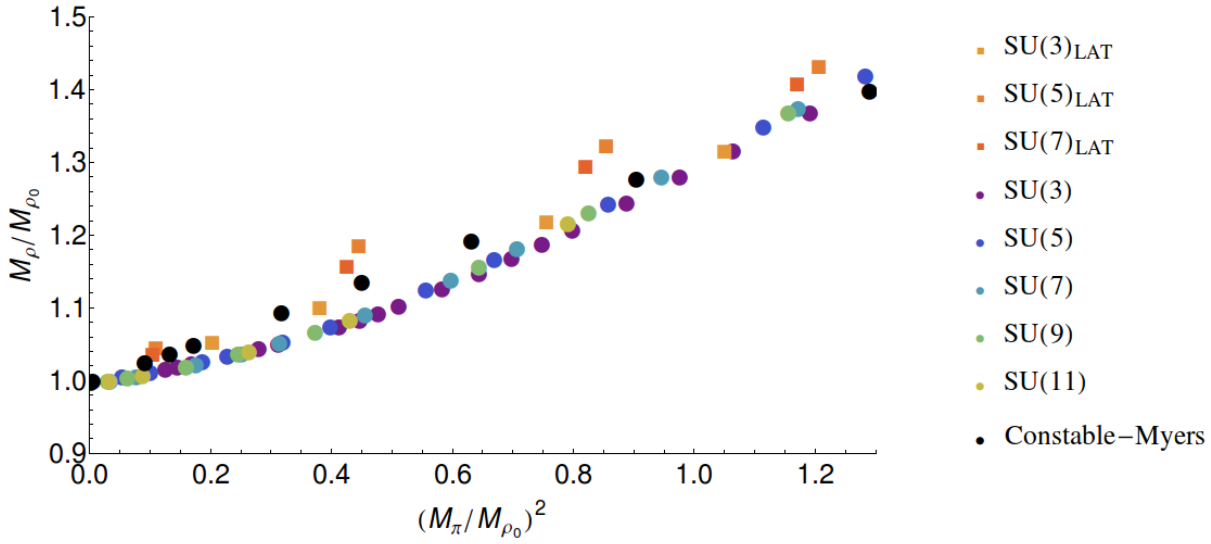

Figure 5.2: Plots of M_ρ against M_π^2 - in each case the points are normalized by M_ρ at $M_\pi = 0$ to set the non-perturbative scale Λ. As shown in the key, the plot shows the data for quenched lattice computations taken from [136] (and linearly fitted to find M_ρ at $M_\pi = 0$); the Constable Myers top down model; and the Dynamic AdS/QCD predictions.

QCD spectrum.

5.1.1 Constable-Myers geometry: A recapitulation

Here we recap the Constable-Myers dilaton flow as described fully in section 5.1. The gravity background of Constable and Myers [96] has the geometry

$$ds^2 = H^{-1/2}\left(\frac{w^4+b^4}{w^4-b^4}\right)^{\delta/4}\sum_{j=0}^{3}dx_j^2 + H^{1/2}\left(\frac{w^4+b^4}{w^4-b^4}\right)^{(2-\delta)/4}\frac{w^4-b^4}{w^4}\sum_{i=1}^{6}dw_i^2\,, \quad (5.1)$$

where b is the scale of the geometry that determines the size of the deformation ($\delta = R^4/(2b^4)$ with R the AdS radius) and

$$H = \left(\frac{w^4+b^4}{w^4-b^4}\right)^{\delta} - 1\,, \qquad w^2 = \sum_{i=1}^{6} {w_i}^2\,. \quad (5.2)$$

In this coordinate system, the dilaton and four-form are, with $\Delta^2 + \delta^2 = 10$,

$$e^{2\Phi} = e^{2\Phi_0}\left(\frac{w^4+b^4}{w^4-b^4}\right)^{\Delta}, \quad C_{(4)} = -\frac{1}{4}H^{-1}dt\wedge dx\wedge dy\wedge dz\,. \quad (5.3)$$

This geometry returns to $AdS_5 \times S^5$ in the UV as may be seen by explicitly expanding at large radial coordinate w.

To add quarks [97] we will use an embedded probe D7-brane. The D7-brane will be embedded with world-volume coordinates identified with $x_{0,1,2,3}$ and $w_{1,2,3,4}$. Transverse fluctuations will be parameterized by w_5 and w_6 (or L and ϕ in polar coordinates) - it is convenient to define a coordinate ρ such that $\sum_{i=1}^{4} dw_i^2 = d\rho^2 + \rho^2 d\Omega_3^2$ and the radial coordinate is given by $w^2 = \rho^2 + {w_5}^2 + {w_6}^2 = \rho^2 + L^2$.

The Dirac-Born-Infeld action of the D7-brane probe in the Constable-Myers background takes the form

$$S_{D7} = -T_7 R^4 \int d^8\xi \; \epsilon_3 \; e^{\phi} \mathcal{G}(\rho, L) \Big(1 + g^{ab} g_{LL} \partial_a L \partial_b L + g^{ab} g_{\phi\phi} \partial_a \phi \partial_b \phi + 2\pi\alpha' F^{ab}\Big)^{1/2}, \tag{5.4}$$

where

$$\mathcal{G} = \rho^3 \frac{((\rho^2 + L^2)^2 + b^4)((\rho^2 + L^2)^2 - b^4)}{(\rho^2 + L^2)^4}.$$

Here we have rescaled w and b in units of R, so that factors of R only occur as an overall factor on the embedding Lagrangian.

5.1.2 Analysis

From this action, we derive the corresponding equation of motion. We look for classical solutions of the form $L(\rho)$, $\phi = 0$. Numerically, we shoot from a regular boundary condition in the IR ($L' = 0$) and find solutions with the asymptotic behaviour $L \sim m + c/\rho^2$. These coefficients are then identified with the quark mass and condensate $\langle\bar{\psi}\psi\rangle$ respectively (formally c is only the unique contribution to the condensate in zero mass limit [137]), in agreement with the usual AdS/CFT dictionary obtained from the asymptotic boundary behaviour.

Mesonic states are identified by looking at linearized fluctuations about the background embedding. Fluctuations in ϕ correspond to the pion (since it parameterises the angular fluctuations) and fluctuations in the worldvolume gauge field correspond to the ρ meson. In each case, one seeks solutions of the form $f(\rho)e^{ik.x}, k^2 = -M^2$ with the

mass states being picked out by the condition that $f(\rho)$ is regular.

figure5.2 shows the first example of the plots we will be producing in this chapter: it shows the ρ meson mass as a function of the pion mass squared. Note that in any given theory, we must fix the strong coupling scale Λ. Here and throughout this chapter, we choose to do this by setting the ρ mass at $M_\pi = 0$ (ie when the quark mass is zero) to be the same in all theories, and we express all physical quantities in units of that fixed mass. The figure shows the results from the Constable-Myers model. We also display quenched lattice results for the plot in theories with gauge group SU(3), SU(5) and SU(7) (data taken from [136]). It is important to note that in order to place the lattice data on the plot we have taken the two data points at lowest M_π and linearly extrapolated (to $M_\pi = 0$) to find the value of M_ρ at $M_\pi = 0$. This is somewhat naïve and we will argue later that this maybe puts the points a little high in the plane. Conservatively, we will use the spread of the lattice data across the different SU(N_c) theories as reflective of the systematic errors in the lattice simulations. The remarkable thing is the lack of dependence on N_c in the lattice data and the match of the holographic model to this data. The aim of this section is to identify why there is such a close match given the large deviations in the holographic dual that includes different adjoint particle content and UV behaviour.

Following [122], we argue that the key element for the quark physics in the top-down model is the running of the anomalous dimension γ with the renormalization scale. We show that this running is very similar to that in QCD, especially in the regime where $\gamma \simeq 1$, the point at which the BF bound-violating instability sets in causing chiral symmetry breaking. To study this instability, we look for when the flat chirally symmetric $L = 0$ embedding becomes unstable. We simply take our DBI action, which up to a multiplicative constant, we may write as

$$S_{D7} = \int d\rho \lambda(\rho, L)\rho^3 \sqrt{1 + (\partial_\rho L)^2}, \tag{5.5}$$

where $\lambda(\rho, L) = \rho^{-3} e^{\phi} \mathcal{G}(\rho, L)$ and $r = \sqrt{\rho^2 + L^2}$, and expand around $L = L' = 0$ to

quadratic order

$$\begin{aligned} S_{D7} &= \int d\rho\ \rho^3 \left(\lambda|_{L=0} + \tfrac{\partial\lambda}{\partial L^2}\big|_{L=0}\, L^2 \right) \left(1 + \tfrac{1}{2}\,(\partial_\rho L)^2 \right) , \\ &= \int d\rho\ \rho^3 \left(\tfrac{1}{2}\ \lambda|_{L=0}\,(\partial_\rho L)^2 + \partial_{L^2}\lambda|_{L=0}\, L^2 \right) . \end{aligned} \tag{5.6}$$

In order to ensure that the kinetic term in our Lagrangian is canonical, we perform a coordinate transformation on ρ,

$$\lambda(\rho)\rho^3 \frac{\partial}{\partial\rho} \equiv \tilde{\rho}^3 \frac{\partial}{\partial\tilde{\rho}}, \tag{5.7}$$

that is,

$$\tilde{\rho} = \sqrt{\frac{1}{2} \frac{1}{\int_\rho^\infty \frac{1}{\lambda\rho^3} d\rho}}. \tag{5.8}$$

We may rewrite our action in terms of the $\tilde{\rho}$-variable. Along with writing $L(\rho) = \tilde{\rho}\,\phi(\tilde{\rho})$, we obtain

$$S_{D7} = \int d\tilde{\rho}\ \frac{1}{2}\tilde{\rho}^3 \left(\tilde{\rho}^2(\partial_{\tilde{\rho}}\phi)^2 + 3\phi^2 + \lambda \frac{\partial\lambda}{\partial\rho}\bigg|_{L=0} \frac{\rho^5}{\tilde{\rho}^4}\phi^2 \right) . \tag{5.9}$$

The first two terms in the action describe a canonical $m^2 = -3$ scalar in AdS_5, whereas the remaining term gives a ρ-dependent mass to the scalar field in AdS_5. We find an overall mass squared

$$m^2 = -3 - \delta m^2, \qquad \delta m^2 \equiv -\lambda \frac{\partial\lambda}{\partial\rho}\bigg|_{L=0} \frac{\rho^5}{\tilde{\rho}^4}. \tag{5.10}$$

Using the standard scalar mass/operator dimension relation of the AdS/CFT dictionary, $m^2 = \Delta(\Delta - 4)$, but now assuming the mass dimension of the $q\bar{q}$-operator to be $3 - \gamma$, where γ is the running anomalous dimension of the gauge theory quark mass, we obtain the relation

$$m^2 = -3 - 2\gamma + \gamma^2. \tag{5.11}$$

Thus we associate $\delta m^2 = -2\gamma + \gamma^2$, and are thus able to extract a running anomalous dimension in the Constable-Myers background.

The key point to note is that the only way that the background geometry and running dilaton enters into the equation for the embedding is through the running of γ. The background D7 embedding is then the key ingredient for the computation of linearized fluctuations that determine the mesonic masses. Effectively, the origin of the running of γ is lost and so questions about whether the background has too many superpartners of the gauge fields, or whether the running coupling is correctly that of QCD in the UV, and so forth become subsumed into simply asking whether γ is close to that of QCD.

In figure 5.3, we plot the RG scale dependence of the anomalous dimension γ extracted from the Constable-Myers model and the one loop running of large N_c quenched QCD theory. We have matched the strong-coupling scale of the two theories by assuming that they each take the value $\gamma = 1$ at the same scale. Setting the AdS radius R to one, we identify the RG scale and the radial coordinate by $\mu = \ln \rho$ (i.e. we are arbitrarily choosing to set this relation by matching to the calculation of the physical RG scale in the quenched QCD theory). This is the scale where chiral symmetry breaking is triggered, in the holographic model by the BF bound violation. From the figure it is immediately obvious that the scale dependence of the anomalous dimension γ is similar in both cases, and the gradient of γ is almost the same near $\gamma = 1$. Deviations in the UV are present but are mild. They occur in the regime where the BF bound is not violated in the holographic model.

This close matching of the scale dependence of the anomalous dimension is, we believe, the reason for the success of the holographic model. It is worth pointing out that the reason that the holographic description and QCD match in the UV is somewhat artificial. The UV of the Constable-Myers theory is infinitely strongly coupled $\mathcal{N} = 4$ super Yang-Mills theory, yet the theory's large amount of supersymmetry preserves the perturbative dimension of the quark operator, i.e. $\gamma = 0$. In QCD, the UV result $\gamma = 0$ simply follows from weak coupling. This coincidence has long been behind the successes of AdS/QCD models.

Given that the key ingredient to describe the mesonic spectrum is simply the running of γ, it seems an obvious step to do away with the background construction of a geometry that mimics QCD, since there is no top-down holographic construction of real QCD, and

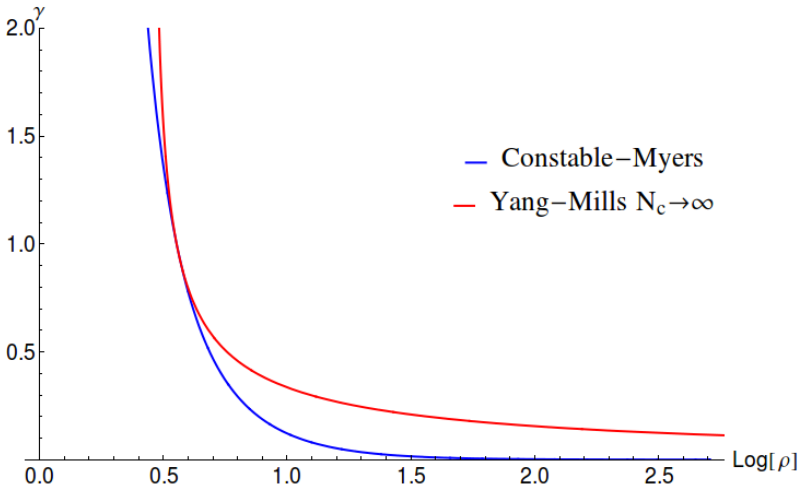

Figure 5.3: A plot of the anomalous dimension γ in the top-down Constable-Myers model. It is compared to QCD by using the one-loop perturbative result for the running coupling in large N_c Yang-Mills theory ($\mu d\alpha/d\mu = -11N_c\alpha^2/6\pi$) as input for calculating the anomalous dimension γ ($\gamma = 3N_c\alpha(\mu)/4\pi$). We set the scale at which $\gamma = 1$ to be equal in each case.

to simply use the assumed form of γ as an input in the DBI action. This is essentially the starting point for the bottom-up model Dynamic AdS/QCD [89], which we will now move to using.

5.2 Dynamic AdS/QCD

We now turn to the bottom-up Dynamic AdS/QCD model. As we have encountered, the model is just the linearized DBI action of the D3/probe-D7 system, but with an arbitrary running for γ. Using the standard AdS relations, the running can be translated into a radially dependent mass squared for the scalar describing the condensate. The model then makes predictions for the spectrum of the theory. The Dynamic AdS/QCD model allows us to explore the space of gauge theories as a function of N_c, N_f and the representation of the quarks through the input running of the gauge theory γ-function. In this chapter, we will again concentrate on calculating and analysing the spectrum of masses pertaining to the ρ meson and the pions, as well as the σ meson (i.e. the singlet $\bar{q}q$ bound state with vanishing quantum numbers, also identified with the f_0) and the lightest glueball. For the glueball, only qualitative statements are possible since the Dynamic AdS/QCD model concentrates on the quark sector.

5.2.1 The running of γ

For the analysis that follows, we use the two loop running of the gauge coupling in QCD with N_f flavours transforming under a representation R. This takes the form

$$\mu\frac{d\alpha}{d\mu} = -b_0\alpha^2 - b_1\alpha^3,$$

where

$$b_0 = \frac{1}{6\pi}\left(11C_2(G) - 4N_f C_2(R)\frac{\dim(R)}{\dim(G)}\right),$$

and

$$b_1 = \frac{1}{8\pi^2}\left(\frac{34}{3}\left[C_2(G)\right]^2 - \left[\frac{20}{3}C_2(G)C_2(R) + 4\left[C_2(R)\right]^2\right]N_f\frac{\dim(R)}{\dim(G)}\right).$$

Again, denoting the adjoint representation as G, its respective Casimir is given by $C_2(G) = N_c$. Table 2.1 in section 2.2.4 shows all the distinguishing quantities associated to each of the representations we consider: the dimension of the representation, $C_2(R)$, and the minimum number of flavours required for loss of asymptotic freedom, $N_f^{\max}$.

The one loop result for the anomalous dimension of the quark mass is

$$\gamma_1(\mu; R) = \frac{3C_2(R)}{2\pi}\alpha(\mu; R). \tag{5.12}$$

Working perturbatively from the AdS result $m^2 = \Delta(\Delta - 4)$ we have

$$\Delta m^2 = -2\gamma_1(\mu; R) = -\frac{3C_2(R)}{\pi}\alpha(\mu; R). \tag{5.13}$$

This will then fix the r dependence of the scalar mass through Δm^2 as a function of N_c and N_f for each R. Note that if one were to attempt such a matching beyond two loop order the perturbative result would become gauge dependent. We hope that the lower order gauge independent results provide sensible insight into the running in the theory.

5.2.2 Linearized fluctuations

We now turn to computing the physical parameters, the masses of the (ρ, σ, π)-mesons and the scalar glueball, for each viable representation. These parameters are true pre-

dictions of the model which, just as in the gauge theories, depend only on the choice of the quark mass, N_c, N_f and the scale Λ.

The isoscalar $\bar{q}q$ (σ) mesons are described by linearized fluctuations of L about its vacuum configuration, L_0. We look for space-time dependent excitations, ie $|X| = L_0 + \delta(\rho)e^{iq.x}$, $q^2 = -M_\sigma^2$. The equation of motion for δ is, linearizing (7.20),

$$\partial_\rho(\rho^3\delta') - \Delta m^2\rho\delta - \rho L_0\delta \left.\frac{\partial\Delta m^2}{\partial L}\right|_{L_0} + M_\sigma^2 R^4 \frac{\rho^3}{(L_0^2+\rho^2)^2}\delta = 0\,. \tag{5.14}$$

We seek solutions with, in the UV, asymptotics of $\delta = \rho^{-2}$ and with $\partial_\rho\delta|_{L_0} = 0$ in the IR, giving a discrete meson spectrum.

The isovector (ρ) meson spectrum is determined from the normalizable solution of the equation of motion for the spatial pieces of the vector gauge field $V_{\mu\perp} = \epsilon^\mu V(\rho)e^{iq.x}$ with $q^2 = -M^2$. The appropriate equation is

$$\partial_\rho\left[\rho^3\partial_\rho V\right] + \frac{\rho^3 M^2}{(L_0^2+\rho^2)^2}V = 0\,. \tag{5.15}$$

We again impose $\partial_\rho V|_{L_0} = 0$ in the IR and require in the UV that $V \sim c/\rho^2$.

The pion mass spectrum is identified by assuming a space-time dependent phase $\pi^a(x)$ of the AdS-scalar X describing the $\bar{q}q$ degree of freedom, i.e $X = L(\rho)\exp(2i\pi^a(x)T^a)$. The equation of motion of the pion field is then,

$$\partial_\rho\left(\rho^3 L_0^2\partial_\rho\pi^a\right) + M_\pi^2\frac{\rho^3 L_0^2}{(\rho^2+L_0^2)^2}\pi^a = 0. \tag{5.16}$$

Again, we impose at the IR boundary that $\partial_\rho\pi^a|_{L_0} = 0$.

5.2.3 Meson spectra results

The results presented in this section will be in the style of 'Edinburgh' plots [138] used by lattice gauge theorists. These plots display only physical observables, such as the mass of the ρ as a function of the pion mass, in order to remove scheme-dependent quantities such as the bare quark mass. Firstly, we have again fixed the strong coupling scale Λ by ensuring that the ρ mass at $M_\pi = 0$ is the same for each choice of representation, N_f

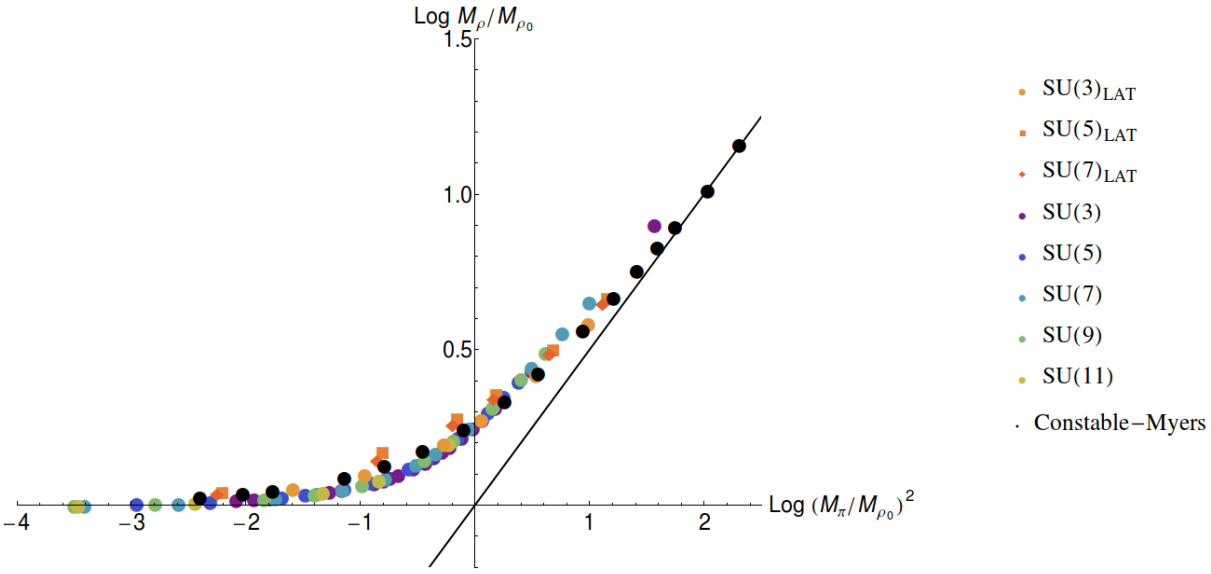

Figure 5.4: A Log-Log plot of M_ρ versus M_π^2 - the plot displays the quenched lattice data from [136], the top-down Constable-Myers model of section 2 and the quenched results for varying N_c in Dynamic AdS/QCD from section 3. The solid line corresponds to $M_\rho = M_\pi$.

and N_c. We express all quantities in units of that scale. It follows therefore that within our plots, the only input parameters are the quark mass, N_f and N_c. We will explore a range of gauge theories with different quark matter.

Quenched fundamental representation

To test the model, we first compute M_ρ and M_π in the model with quenched fundamental quarks. This means that we do not include the quark contribution in the running of the gauge coupling — effectively a pure YM theory. We compute the meson masses as functions of N_c to compare with the previously discussed quenched lattice data of Fig 5.2. The results are shown alongside the lattice data in Fig 5.2. We note that all choices of SU(N_c) give essentially the same curve in this plot. This curve lies below, but within 5% of the prediction of the Constable-Myers top-down model. The results from the Dynamic AdS/QCD model in this plot display some curvature over the range of the lattice data, suggesting that the linear extrapolation used to place the lattice data on the plot could be incorrect. Moreover, the expected lattice data point for M_{ρ_0} (i.e. M_ρ at $M_\pi = 0$) should be greater than that predicted by the linear fit, meaning the lattice points should be reduced by up to 5%. Indeed in [136], evidence is presented for

a non-linear fit already in the lattice data. Given the expectation of some systematic error on the lattice data (see [136]) the match between all these models is remarkable and lends considerable support to further predictions of the Dynamic AdS/QCD model.

To emphasise how well the results match, we also plot the same Dynamic AdS/QCD and lattice data on a Log-Log plot in Fig 5.4. The figure also displays the line $M_\rho = M_\pi$, which would be the one appropriate to a very weakly coupled (i.e. perturbative) theory. In such a theory, the bare and constituent quark masses are approximate and the mesons masses become just twice the bare quark mass. This line is expected to be approached at large M_π, i.e. in the limit of large quark mass since a heavy quark decouples in the IR and knows only of the UV perturbative running. Clearly, the very different computations for these theories agree rather well. Whilst both the holographic model's curves are compatible with the lattice data at the level of the errors due to the coarse lattice spacing taken in [136], the top-down Constable Myers model does fit the data mildly better (the M_ρ points are raised by upto 2% or so), including in the large M_π limit. This may be reasoned by the profile of γ in the Constable-Myers model falling to zero more quickly than in the quenched-QCD, and so the holographic description of the UV is probably closer to perturbative QCD where $\gamma = 0$.

Fundamental representation

The quenched results display very little dependence on N_c. The reason is that the running of γ at the point $\gamma = 1$ is very fast in all these cases so the dynamics comes out very similar. To see some N_c dependence we should unquench the theory and include a sufficient number of quarks to affect the running. For example, in Fig 5.5, we show the N_c variation in the $M_\rho - M_\pi^2$ plane of a theory with $N_f = 8$. The dependence on N_c is again not large but there is a clear distinction between theories at low N_c and those at larger values which are effectively quenched. This further emphasises the success of the holographic model in lying so close to the quenched lattice data. The fact that the Dynamic AdS/QCD spectra of the quenched SU(N_c) theories of the previous subsection were all similar could have easily been misinterpreted as being ignorant of N_c and N_f. However, here we see that is clearly not the case.

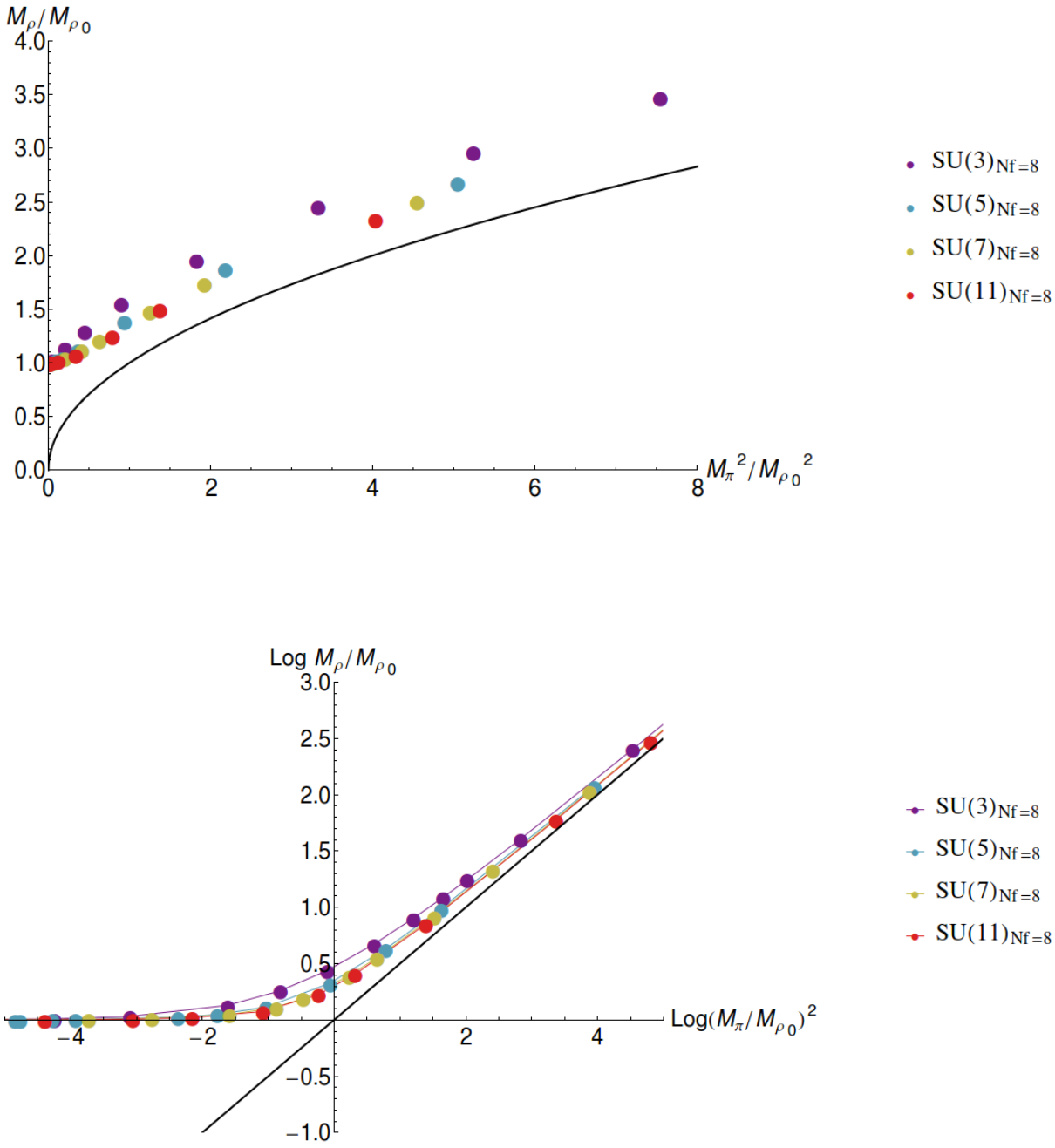

Figure 5.5: M_ρ versus M_π^2 in SU(N_c) theory with $N_F = 8$ fundamental quarks - the lower plot shows the same in Log Log format. The solid line corresponds to $M_\rho = M_\pi$.

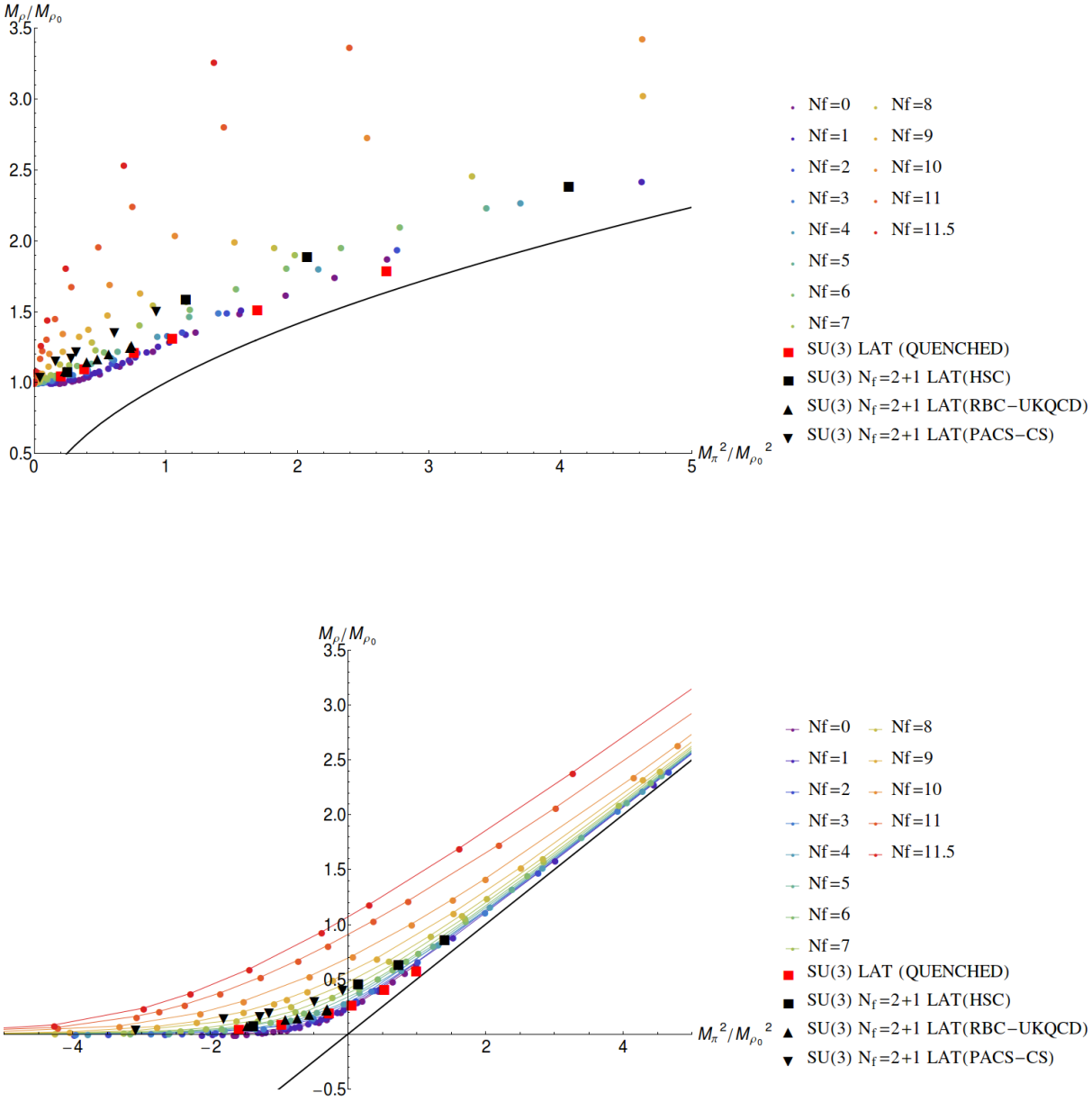

Figure 5.6: SU(3) gauge theory with N_f fundamental quarks showing the approach to the conformal window at $N_f = 12$. The lower plot is a Log Log version of the top plot. The solid line corresponds to $M_\rho = M_\pi$. The plots also show lattice data for the quenched theory [136] and unquenched $N_f = 3$ theory [139–141].

We can now turn to study the question of whether there are choices of N_f and N_c that provide spectra very different from QCD-like theories. As is well known, the theories that are most unlike QCD are those on the edge of the conformal window exhibiting walking behaviours. To demonstrate the impact of this on the spectrum, we plot the N_f dependence of the SU(3) theory in the M_ρ - M_π^2 plane in figure 5.6. The ρ mass is substantially enhanced relative to the π mass at larger N_f. The usual expectation is that the ρ mass will be proportional to $\langle\bar{q}q\rangle^{1/3}$ whilst the π mass will scale as $m_q^{1/2}\langle\bar{q}q\rangle^{1/6}$. An enhancement of the condensate, as occurs in these walking theories, would therefore raise M_ρ at any fixed M_π as is seen in figure 5.6. Generically for different N_c we observe the same behaviour as $N_f/N_c \to 4$.

This is a good point to compare our Dynamic AdS/QCD theory to unquenched lattice data [139–141]. We have seen that the effect of including more flavours within our model is that the value of M_ρ rises at fixed M_π. This suggests that the effect of quark loops is to raise M_ρ. We display lattice data in the top plot of figure 5.6 — we show both the quenched results previously discussed for SU(3) gauge theory, but now also unquenched data for the same theory with $N_f = 3$, taken from [139–141]. The three sets of lattice data show some spread in the low M_π region, but we indeed observe a shift upwards in M_ρ by 20% or so. In fact, the fit to the Dynamic AdS/QCD model for $N_f = 3$ is a little poorer than the fit to the quenched lattice data. The lattice points here are more similar to the $N_f = 5$ version of Dynamic AdS/QCD (ignoring the uncertainty provided in the spread of lattice results). This is most plausibly explained as a failure of the very naïve perturbative based running ansatz we have used as an input into the model. The key measure is the gradient of γ at the scale where $\gamma = 1$ (the scale of chiral symmetry breaking/BF-bound violation). For $N_f = 3$, $\gamma' = -4.25$, whereas at $N_f = 5$ the value of γ is $\gamma' = -3.70$. This implies that the shift in the spectrum is caused by a 15% shift in this gradient. Clearly, the perturbative ansatz cannot be trusted at this level of accuracy. It is not surprising that the precise features of the spectrum are dependent on the choice of assumed running for γ. It is encouraging that the Dynamic AdS/QCD model correctly gets the gross features correct, such as the rise in M_ρ in theories with more quark loops. This gives us confidence that the holographic model

can be useful in understanding broad trends in the spectrum as quark content of the theory is changed.

As we have discussed, an additional expectation in a walking theory is that the σ mode $\bar{q}q$ bound state should become light as one approaches the edge of the conformal window from below. To observe this, let us now turn to computing the σ meson mass. We will again pick $N_c = 3$ as an example and show the N_f dependence of M_σ against M_π^2 in figure 5.7. The $N_f = 7$ curve is perhaps what one would have predicted for QCD - at large quark mass the σ and π masses become degenerate. Heavy quarks only see the perturbative UV running and aren't witness to the chiral symmetry breaking scale in the IR. As such, they see an effective restoration of the chiral symmetry and the π and σ mesons become degenerate parity doublets. On the other hand, at low quark mass, as the π mass tends to zero, the σ mass saturates to a non-zero value. If the sigma-mass saturates to a value less than that of the ρ mass, one might then identify this state with the $f_0(500)$, lighter than the 770MeV ρ, as observed in experiment. However, for $N_f = 3$ the holographic model predicts that the lightest σ is *heavier* than the ρ and it looks more sensible to match it to the $f_0(980)$ which it matches at the 10% level. An explanation of the origin of the lighter f_0 would then be needed. In fact, the literature has considerable speculation about this state which might be a molecule or some other exotic state (see for example [142]). We can not resolve this issue here. However, the main use of our model is to look at significant trends in the behaviour of the spectra as we adjust the running of γ. Here our plot very strongly supports the speculation that this σ mode becomes light as one approaches the walking regime and the edge of the conformal window at $N_f = 12$.

Other representations

As we have stressed above, Dynamic AdS/QCD can accommodate a description of any arbitrary quark representation. The flavour representation enters through the running of the anomalous dimension γ (for which we continue to use the two loop perturbative result). In this section, we provide some plots showing some exploration of the larger space of theories.

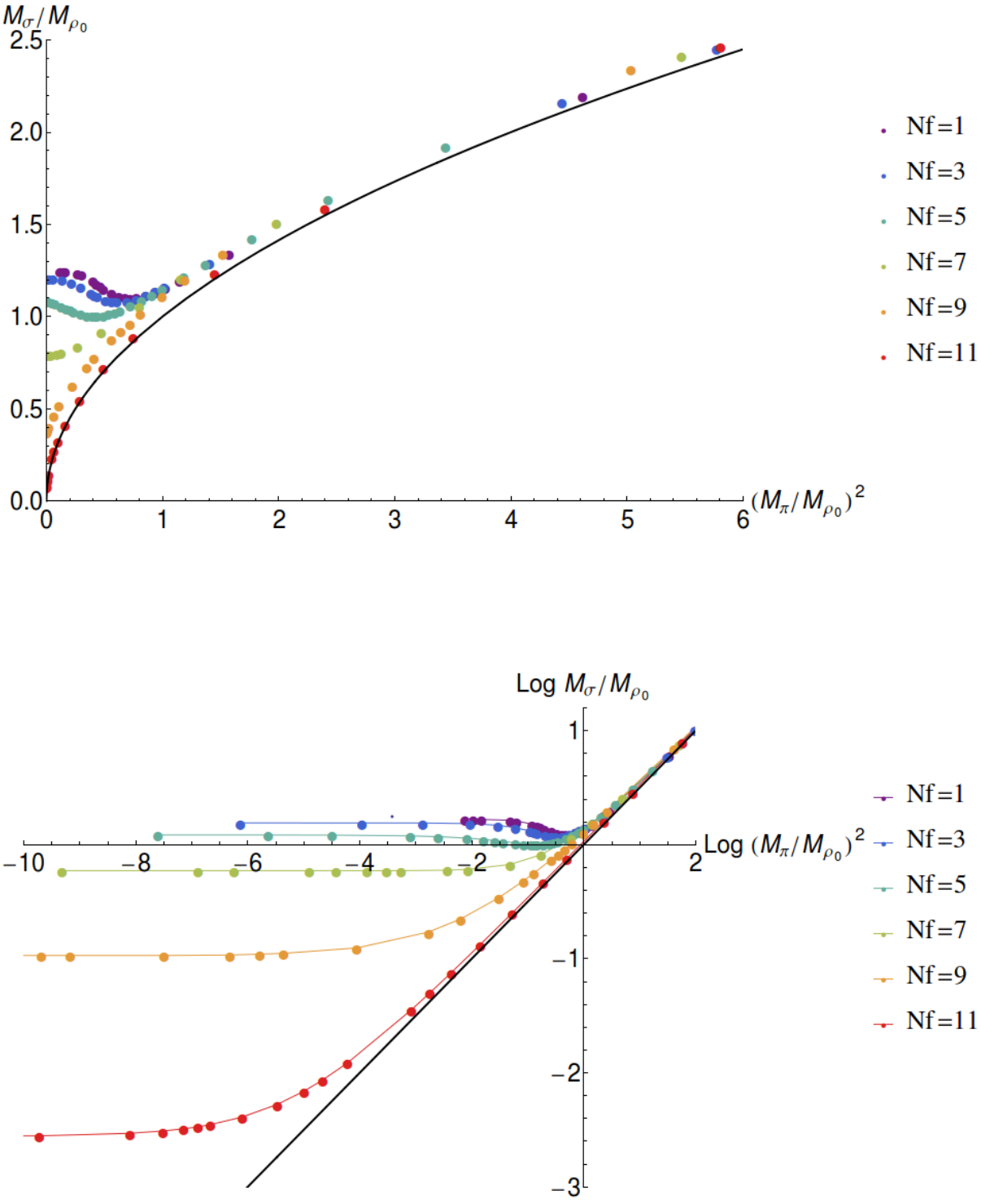

Figure 5.7: M_σ versus M_π^2 in SU(3) gauge theory with varying N_f fundamental quarks. The lower plot is a Log Log version of the top plot. The solid line corresponds to $M_\sigma = M_\pi$.

As a first example, in figures 5.8 and 5.9 we show results for different representations for $N_c = 3$. The top plot shows the results in the $M_\rho - M_\pi^2$ plane for the theory with a single quark in the fundamental representation (here the same as the two-index anti-symmetric representation), the adjoint representation, and the two-index symmetric representation. Increasing the size of the representation makes a bigger impact on the running of the coupling and moves the curve away from QCD-like towards the walking regime. In the lower two plots we show the N_f dependence for the adjoint and two-index symmetric representation (here we allow $N_f = 1.5$ since by $N_f = 2$ chiral symmetry breaking is lost). Adding flavours makes the theory more walking in behaviour.

We can also explore the N_c dependence of these theories at fixed N_f. For example, in figure 5.10 we vary N_c with two, two-index symmetric representation quarks. Increasing N_c moves the theory closer to the quenched limit and a more QCD-like spectrum. Within this space of theories, we do not find any additional structure beyond the dependence on the rate of running at the point $\gamma = 1$.

One final interesting case is that of two-index anti-symmetric representation quarks. As one moves to higher N_c at fixed N_f the two-loop IR fixed point value of the coupling actually decreases due to the nature of the beta function's dependence on N_c. For these theories increasing N_c moves one towards the walking regime. We show this in figure 5.11.

The walking regimes of these theories also display a light σ meson. We show this trend for a variety of sequences of theories moving towards the walking regime in figures 5.12 and 5.13. The trends in the spectrum as one approaches the walking regime across a wide range of theories are very similar.

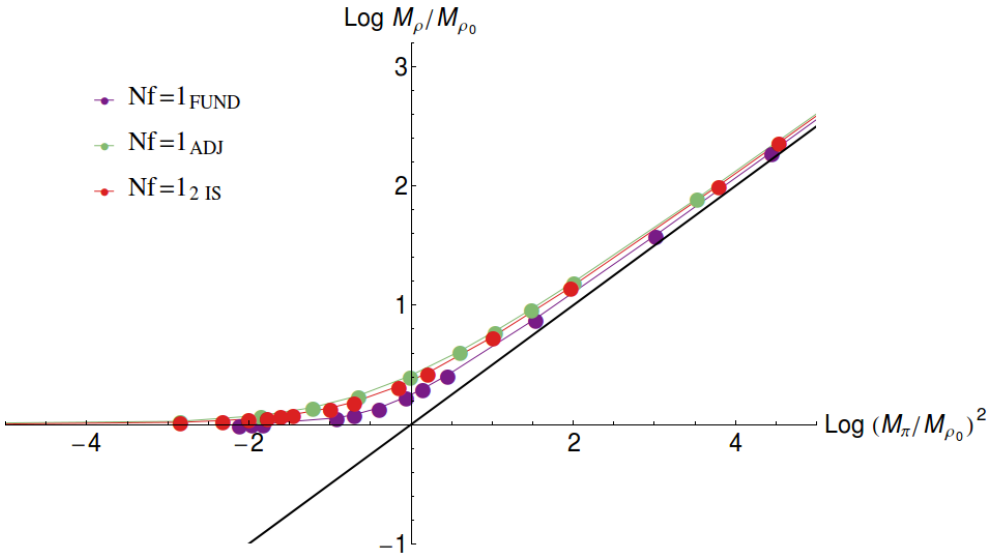

Figure 5.8: A Log-Log plot in the M_ρ-M_π^2 plane for SU(3) gauge theory. The plot shows the results in models with $N_f = 1$ but with the fermions in the fundamental, adjoint and 2-index symmetric representations. The middle figure shows the N_f dependence in the case with adjoint fermions and the bottom plot the same for the 2-index symmetric representation. The solid line corresponds to $M_\sigma = M_\pi$.

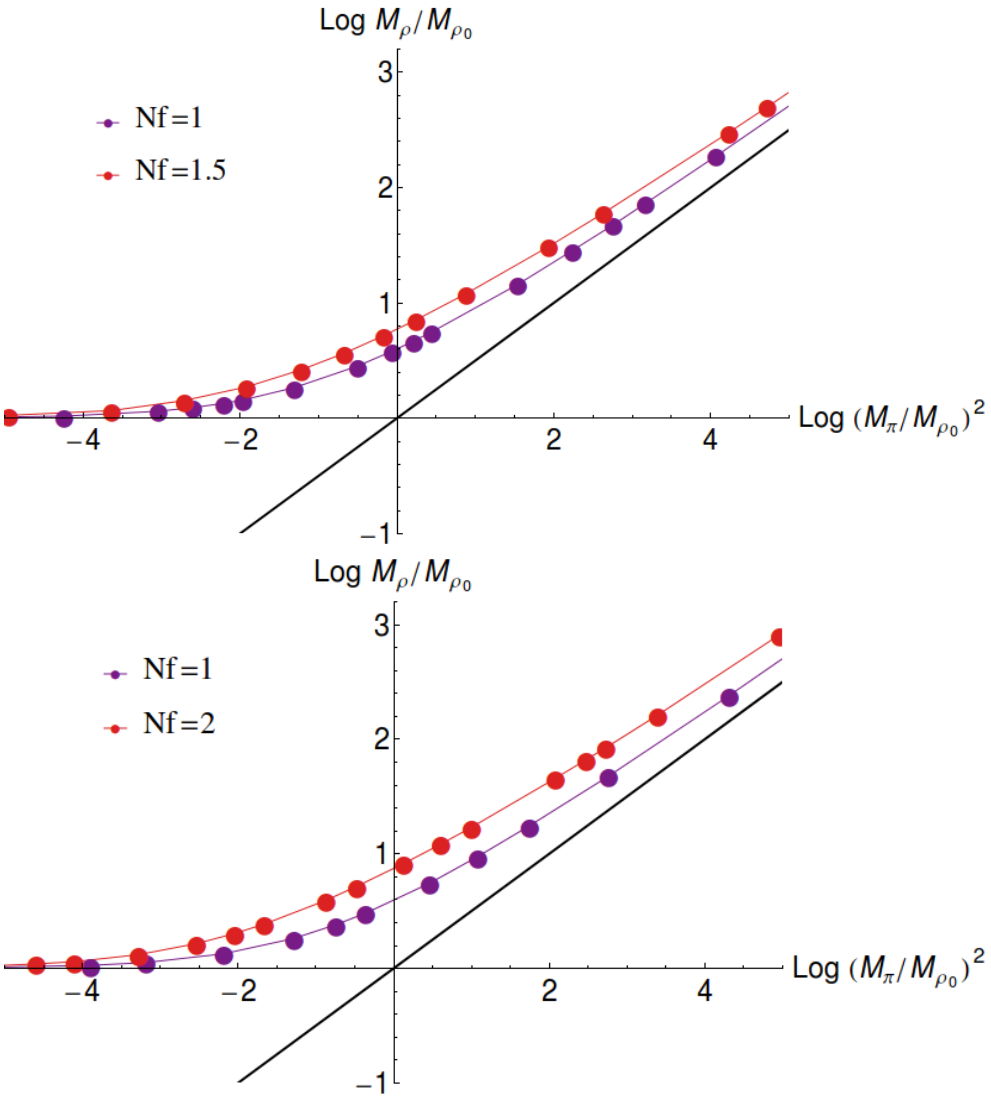

Figure 5.9: A Log-Log plot in the M_ρ-M_π^2 plane for SU(3) gauge theory. The top plot shows the N_f dependence in the case with adjoint fermions and the bottom plot the same for the 2-index symmetric representation. The solid line corresponds to $M_\sigma = M_\pi$.

5.2.4 The scalar glueball

Another state that one might be interested in studying as part of the lightest spectra of these theories is the lightest glueball state (see [56, 121, 132–135] for some discussions in preliminary lattice simulations). AdS/QCD is not suited to study this state since the model is fundamentally a description of the quark sector. The glueball could be included as a separate scalar in AdS but one would then need to correctly encode its dynamics to describe the gauge theory's vacuum ($\mathrm{Tr}F^2$) condensate and make a guess

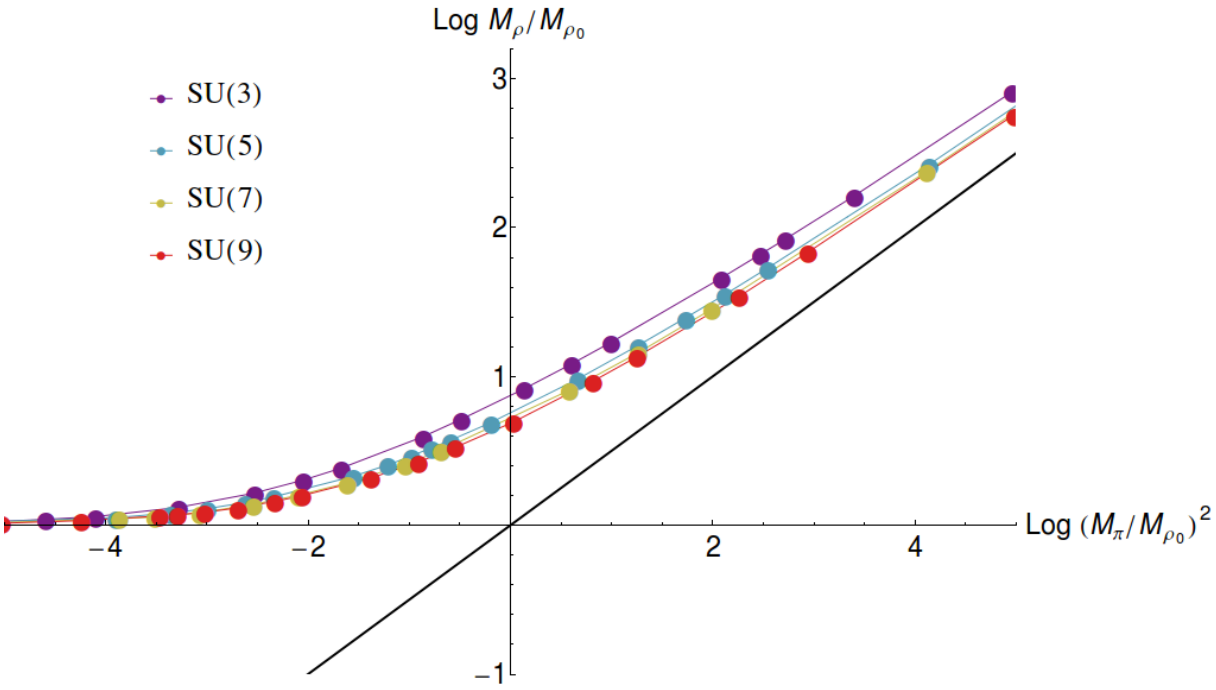

Figure 5.10: A Log-Log plot in the M_ρ-M_π^2 plane for SU(N_c) gauge theory with $N_f = 2$ 2-index symmetric representation quarks. The solid line corresponds to $M_\sigma = M_\pi$.

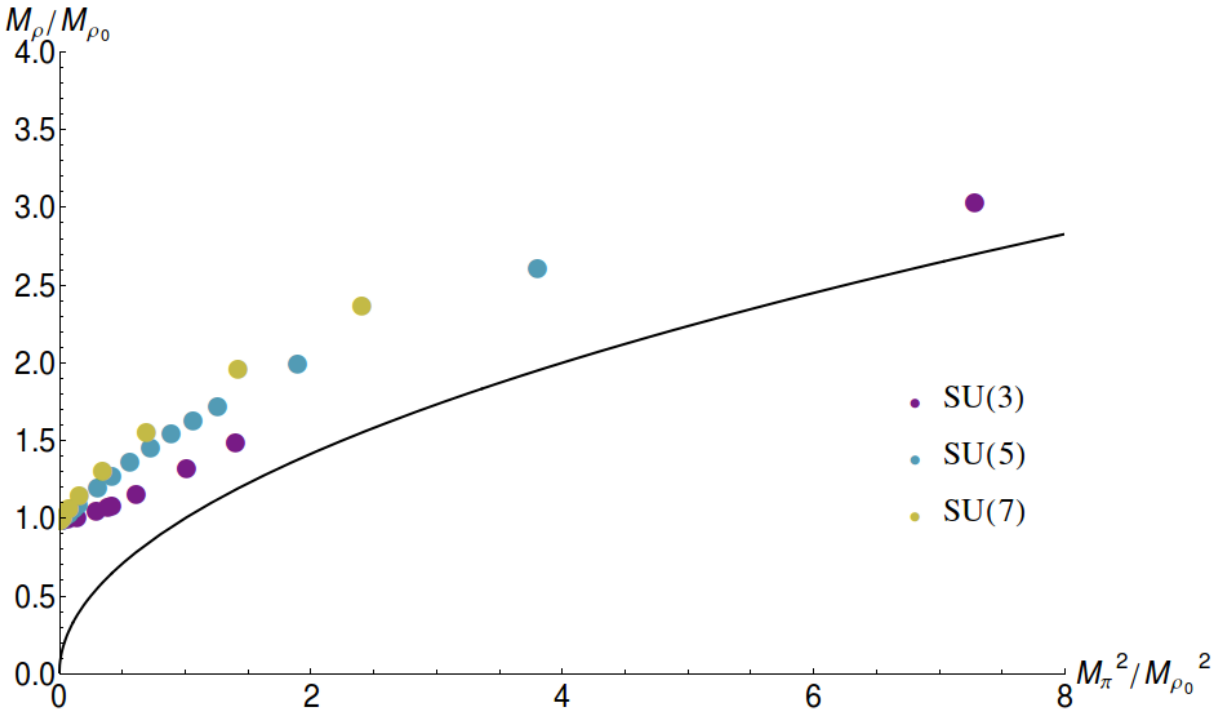

Figure 5.11: A Log-Log plot in the M_ρ-M_π^2 plane for SU(N_c) gauge theory with $N_f = 3$ 2-index anti-symmetric representation quarks. The solid line corresponds to $M_\sigma = M_\pi$.

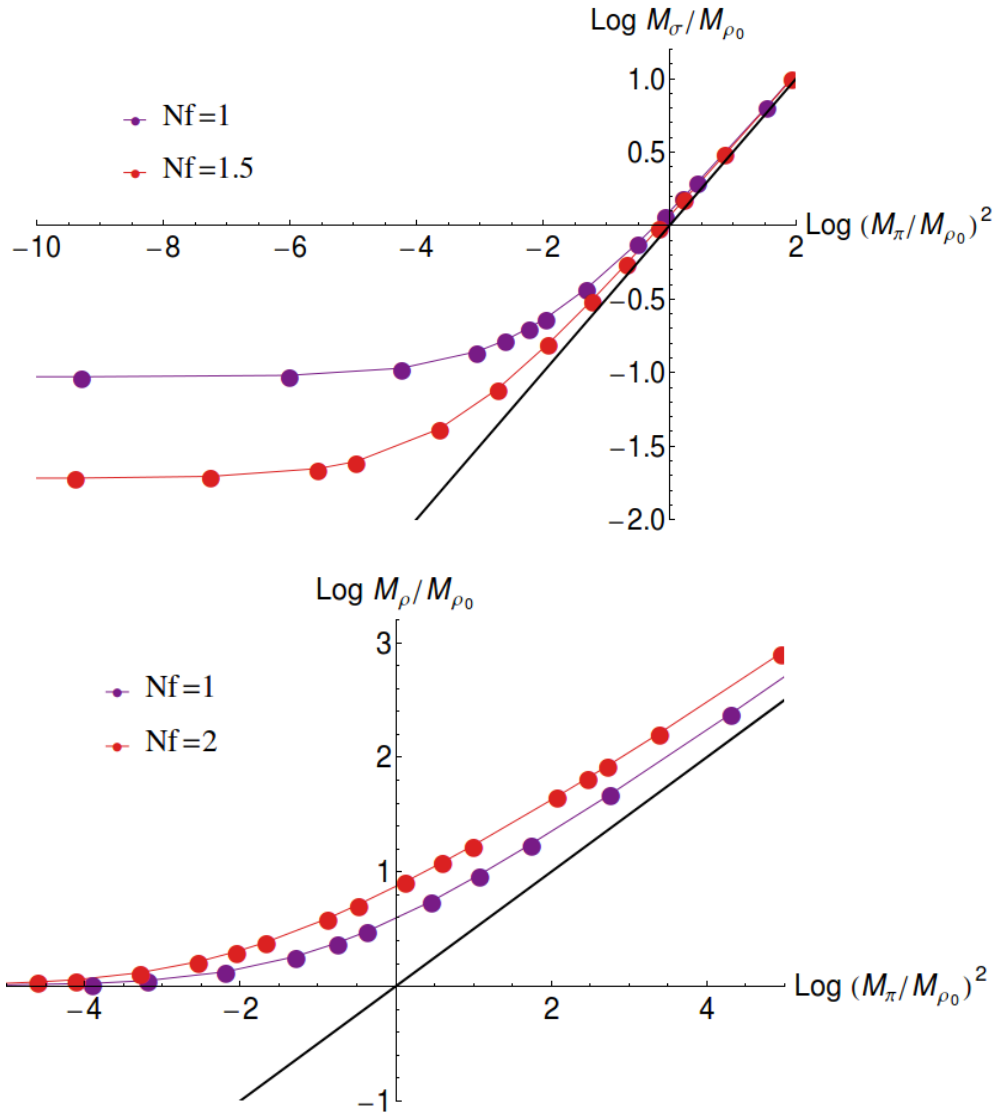

Figure 5.12: Log-Log plots in the M_σ-M_π^2 plane. The top plot shows the results in SU(3) gauge theory with adjoint quarks. The bottom plot is for SU(N_c) gauge theory with $N_f = 2$ 2-index symmetric representation quarks. The solid line corresponds to $M_\sigma = M_\pi$.

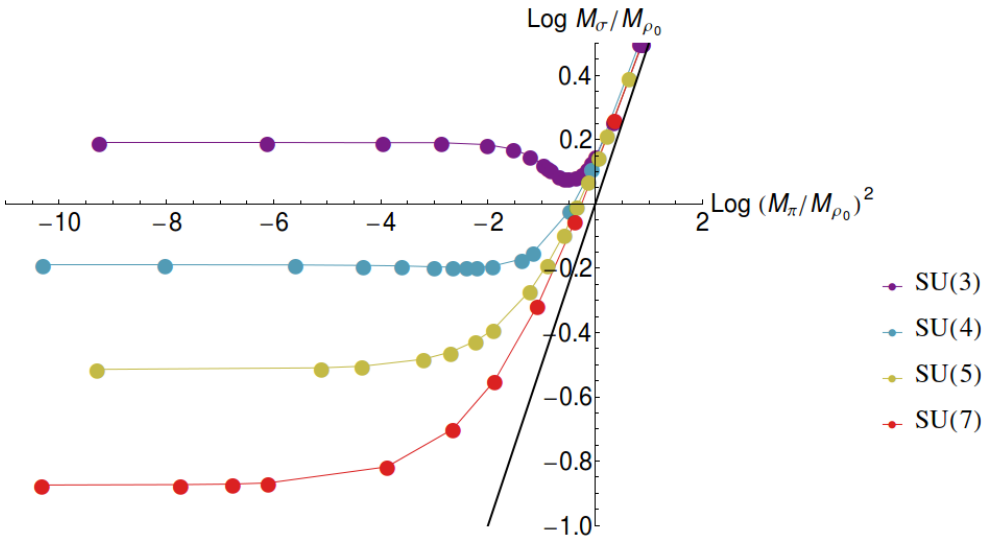

Figure 5.13: Log-Log plots in the M_σ-M_π^2 plane. Plot shows the spectra for SU(N_c) gauge theory with $N_f = 3$ 2-index anti-symmetric representation quarks. The solid line corresponds to $M_\sigma = M_\pi$.

as to how it couples, in the scalar potential, to the quark condensate field X. There are a lot of unknown parameters that describe the mixing of the σ and glueball state. Rather than attempt this here, we will instead make a back of the envelope computation for the glueball state.

In pure Yang Mills, the glueball is expected to be between 5 and 10 times the one loop strong coupling scale, figures originating from lattice data [143]. In the Dynamic AdS/QCD model, we have assumed the two-loop running for the gauge coupling to obtain γ and then the IR quark mass gap, the value of L at the on-mass shell condition, is computed. A simple thing to do is to decouple the quarks at that scale $L_{\text{on-mass}}$ and use the one loop pure Yang Mills coupling into the IR. We compute the position of the IR pole and multiply by 8 to estimate the glueball mass. This will at least give a ball-park behaviour although mixing is explicitly not addressed.

In figure 5.14, we display the spectra of the $N_c = 3$ theory for $N_f = 3$ (QCD-like) and $N_f = 11$ (close to walking) *including* the glueball. As we have seen before, the σ becomes light and interchanges ordering with the ρ as one approaches the walking regime. For large quark masses, the glueball is the lightest state in both N_f theories. The heavy quarks again decouple at their mass scale, where the glue is still weakly coupled, and the pure glue theory then runs logarithmically to strong coupling at a

much lower scale, Λ_{glue}, which sets the glueball mass. Since $8\Lambda_{glue} < 2m_q$, the glueball appears light. For a very small quark mass, the glueball becomes the heaviest state in both cases. At the light quark mass scale, the gauge coupling is sufficiently strong that the BF-bound has been violated and the quarks acquire a dynamical mass. The pure-glue running between the quark mass scale and the IR pole is very fast since we are already at strong coupling when the quarks decouple. Here, Λ_{glue} is set by essentially the quark decoupling scale and the glueball mass $\sim 8\Lambda_{glue}$ is much heavier than the meson masses set by the condensate $\langle \bar{q}q \rangle \sim \Lambda_{glue}^3$ ($m \sim \Lambda_{glue}$).

The interesting difference between the two cases with different N_f is in the intermediate regime. The crossover between these two cases is fast for the $N_f = 3$ theory but much slower for the walking $N_f = 11$ theory. The reason is that, for a range of intermediate quark mass scales, the walking theory has run to a strong regime but with a coupling insufficient to trip the critical value triggering chiral symmetry breaking. Since it is walking, the quark mass scale, at which the quarks decouple, and the pure-glue, IR pole are pushed apart and so the cross-over occurs over a wider range of quark mass. This is a signal in the spectra of walking theories. Such a signal is important because it does not depend on gauge dependent objects such as the coupling itself.

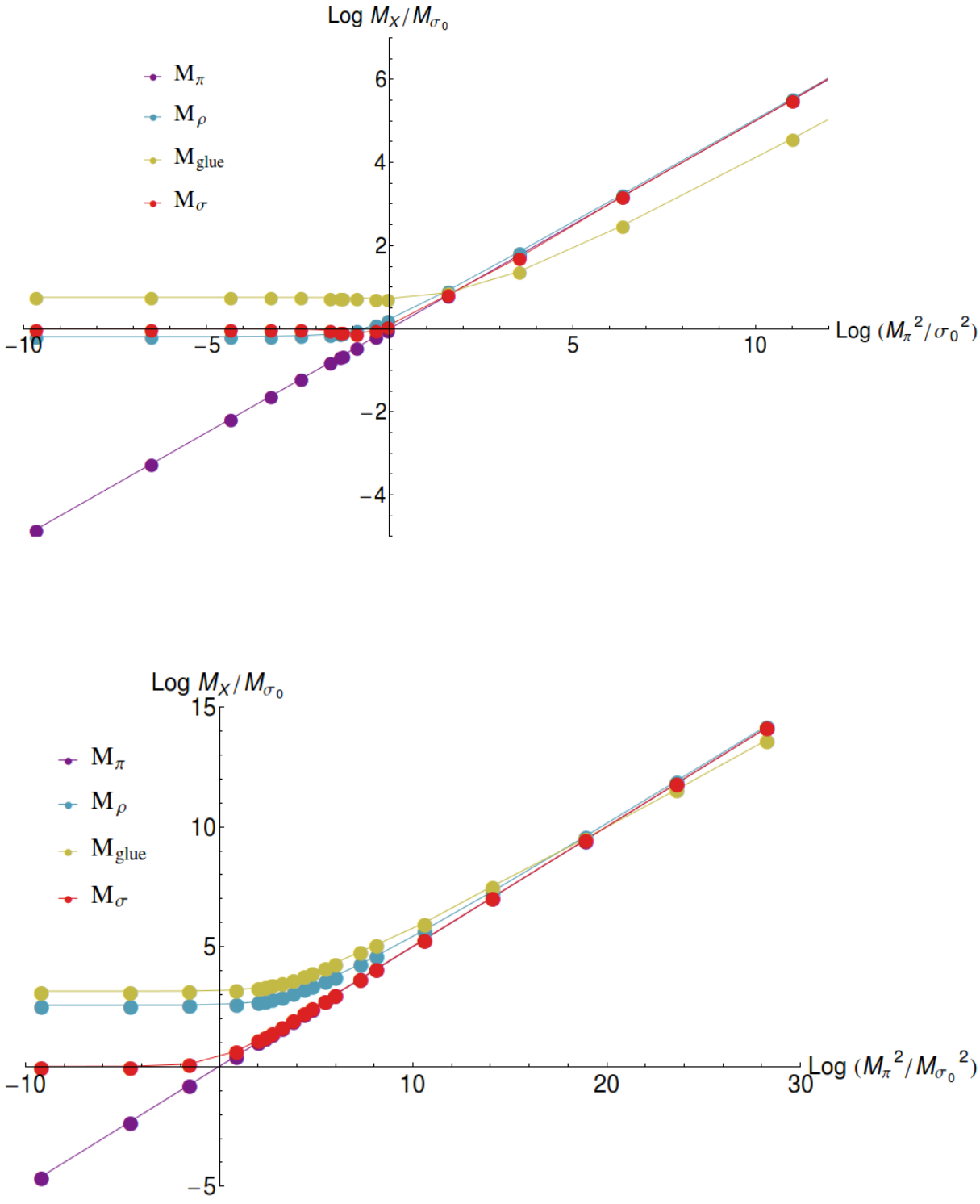

Figure 5.14: The spectra of the $N_c = 3$ gauge theory with fundamental quarks - the top figure shows $N_f = 3$, the bottom $N_f = 11$.

Chapter 6

Inverse Magnetic Catalysis

The study of strongly coupled theories at finite temperature in the presence of an external magnetic field is a topic of great interest for QCD. Cosmologically, large magnetic fields may have been present at phase transitions [144, 145] and such conditions are also being produced in collisions at the Large Hadron Collider (LHC) and Relativistic Heavy Ion Collider (RHIC) [146]. A key question is how they impact on the thermal, chiral restoration transition. As we have seen, at zero temperature the strong dynamics of QCD forms a non-zero chiral condensate that breaks the global chiral flavour symmetries to the vector subgroup. At high temperatures, where asymptotic freedom sets in and renders the coupling small (less than the critical value for SχSB), the condensate vanishes. The two phases are separated by a second order transition at zero temperature; i.e. the order parameter (the chiral condensate) becomes discontinuous in its first derivative at the critical temperature T_c. At small quark mass, this becomes a crossover transition [147, 148] such that there is no discontinuity in the order parameter or any of its derivatives (i.e. it's not strictly a phase transition); see figure 6.1 for an illustrative guide.

Recent lattice studies of QCD with light quarks and an applied magnetic field [149–151] have revealed some surprisingly complex behaviour. At zero temperature, the presence of an external magnetic field enhances the chiral condensate $\sigma \equiv \langle \bar{q}q \rangle$, a process known as *magnetic catalysis*, which is a generally predicted effect in many models [152–158]. However, at temperatures approaching the critical temperature of

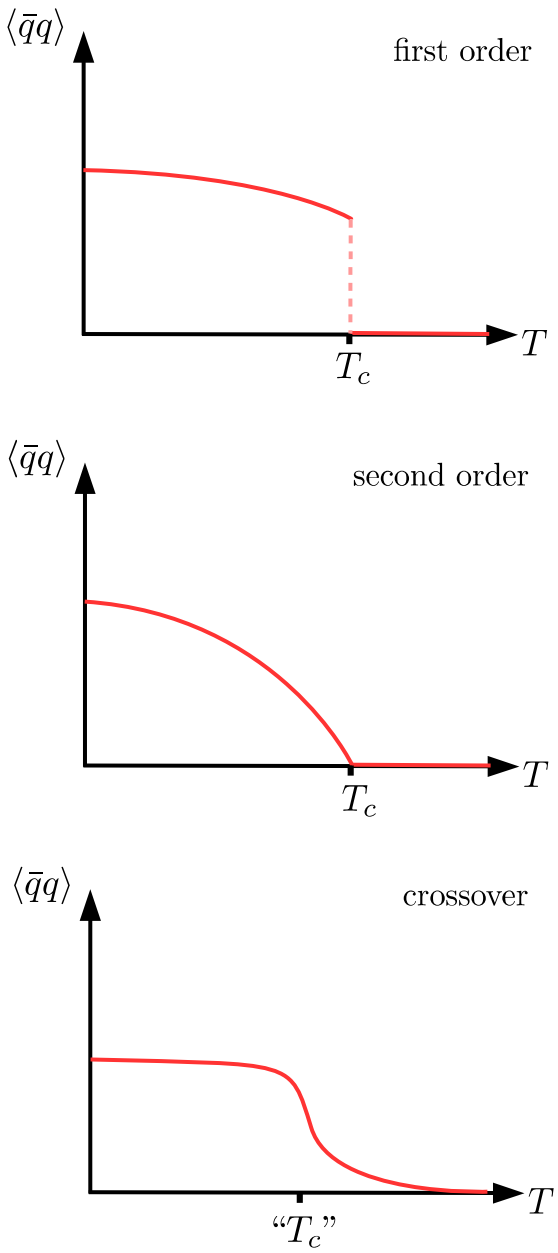

Figure 6.1: First order phase transitions are discontinuous in the order parameter - for the chiral symmetry breaking transition this is the chiral condensate. Second order phase transitions are discontinuous in the first derivative of the order parameter. The crossover transition isn't strictly a phase transition but a smooth bridge between two regions of different phenomena.

the transition for no external field, the magnetic field has been shown to reduce the chiral condensate thus lowering the critical temperature of the transition; so-called *inverse* magnetic catalysis. At intermediate temperatures there appears a non-monotonic

behaviour with small magnetic field, B, favouring chiral condensation but larger B disfavouring it. These results are summarized in Fig 6.2 taken from [150].

There has been considerable work in a number of approaches to explain these results [159–180]. One such approach is holography [32,58,81,84,91], which we continue to pursue here within the remit of the Dynamic AdS/QCD model. The effects of magnetic field in gauge theories with known duals from a top-down perspective have been studied in [124,181–184]. Bottom up holographic approaches have also considered external magnetic fields within gauge theories [183,185,186], and the work in the following chapters using Dynamic AdS/QCD naturally adds to this latter literature.

6.1 Dynamic AdS/QCD in the context of finite temperature & magnetic field strength

The main assumption of Dynamic AdS/QCD is that the chiral phase transition is the most important behaviour in QCD. At that transition the quarks acquire a constituent mass and integrate from the running of the IR, pure glue theory. Since the glue is already at very strong coupling it will essentially instantaneously run into the regime of confinement. In [122] it was shown that the instability for chiral condensation is governed by the DBI action expanded to quadratic order in the fields, since one is expanding about the zero solution. Any dilaton profile or warp factor of the background metric in this expansion simply shows as the running mass of an AdS scalar describing the chiral condensate. One can therefore discard the details of the background, replacing them with a sensible ansatz for the running mass, and concentrate on the quark physics. Naïvely, the probe approximation is a quenched approximation, $N_f \ll N_c$, but one should view it as looking at the dynamics of a single quark in an unquenched background including backreaction of the remaining quarks. N_f-dependent factors enter through the running of the AdS scalar mass and potentially other parameters of the AdS theory. This N_f-dependent physics is put in by hand in the model, which, given the absence of a true dual, is inevitable.

The background space of the model then is AdS_5 so that there is a clear identification

of the RG scale with the AdS radius, ρ. The chiral condensate $\sigma \equiv \langle \bar{q}q \rangle$ is identified with a scalar field in the bulk, which from the top-down intuition can be thought of as a brane embedding. The QCD dynamics at $T = B = 0$ is introduced by hand by giving the AdS scalar a radially dependent mass term so that the anomalous dimension, γ, of σ matches that in QCD perturbation theory (naïvely extrapolated to the strongly coupled regime near Λ_{QCD}). When the mass of the AdS scalar runs down through the Breitenlohner-Freedman (BF) bound [100] (at which point $\gamma = 1$) the scalar becomes unstable and chiral condensation occurs [90, 122, 123]. Finite temperature can be introduced by replacing the AdS space with an AdS Schwarzschild black hole of the appropriate radius [81]. Here, a single phenomenological parameter [187] can be dialled to switch the order of the phase transition (between first and second order and vice versa). We select a value of this parameter to give an appropriate second order transition to match QCD [147, 148].

To introduce the magnetic field, we revert back to the top-down approach. Since the lowest lying mode of the open-string sector is a vector field, its components transverse to the D7-branes manifest themselves as a U(1) gauge-field on the field theory dual. This must then be accounted for in the pullback metric of the D7-branes. As the Dynamic AdS/QCD model inherits a lot from these D3/D7 top-down models, the lowest-order interactions between the D7-brane embedding, parameterised as the scalar field L, and the magnetic field component of the gauge field, B, are then added to the bottom-up dynamic model. See section 3.3.1 Here, we take the *two* lowest-order terms that link the chiral condensate field to a background magnetic field and study their impact. The coefficients of these terms are not *a priori* fixed (unlike in the top-down scenarios) and it is not surprising that by picking suitable signs they can be made to favour or disfavour chiral condensation. The two terms have different temperature dependence so one can also play them off against each other to find regions of parameter space in which there is magnetic catalysis at low T but inverse magnetic catalysis at high T. This confirms that the Dynamic AdS/QCD model allows the behaviour seen in the lattice QCD simulations, which is a positive sign for the approach but perhaps not surprising given the freedom of the model's parameters.

The model can however offer some more interesting insights. It turns out that it is possible to reproduce the QCD behaviour with just a single one of the two lowest-order terms. The reason is down to this term producing magnetic catalysis in the low T phase where the brane embedding lies off the black hole but inverse catalysis for the phase where the brane lies on the black hole. In the intermediate regime of the model, $\sigma(B,T)$ exhibits non-monotonicity, enhancing the condensate for small B but suppressing it at larger values. A summary of the typical behaviour we find is shown in Fig 6.3 for comparison with the lattice results in Fig 6.2. The similarity in the generic behaviour is quite striking although the extremum in the holographic model is a point of discontinuity since it is associated with the second order meson-melting phase transition, i.e. the point where the embedding brane touches the black hole from a top-down perspective (see Section 6.1.1 below).

Adjustment of the UV boundary conditions on the bulk field describing σ allows the study of heavier quarks also. Generically, these are associated with embeddings that typically do not touch the black hole horizon (unless T becomes comparable to m) and we see magnetic catalysis for such configurations persist to larger B. One should be careful though not to extrapolate the results to too large m or B since the holographic framework is presumably unreliable when the key physics is happening in the asymptotically free, weakly coupled regime (the duality is of course built on the premise that a weakly coupling string description implies that the gauge theory is strongly coupled).

6.1.1 Meson melting

From a top-down perspective, the transition from embeddings that avoid the black hole to those that end on its horizon is associated with the mesons developing a thermal width [97, 188–190]. Those branes avoiding the black hole have fluctuations that are completely supported by the brane, i.e. the meson's wavefunction cannot fall into the black hole — the meson has a zero-width and so is a perfectly stable particle ($\Gamma \sim \tau^{-1}$). However, for the branes which end on the black hole, the fluctuations can be lost and so the meson develops a non-zero, *thermal width* implying a non-infinite decay time. As T increases, the black hole eats more and more of the spacetime and so the width will rise

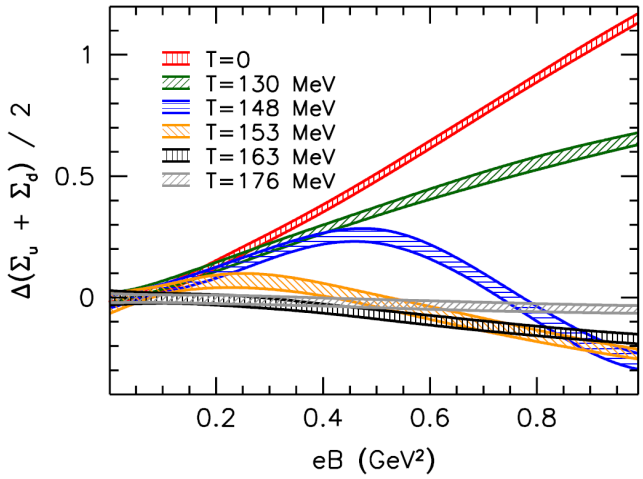

Figure 6.2: Lattice results for the change in the quark condensate as a function of magnetic field strength over a range of temperatures - figure taken from [150].

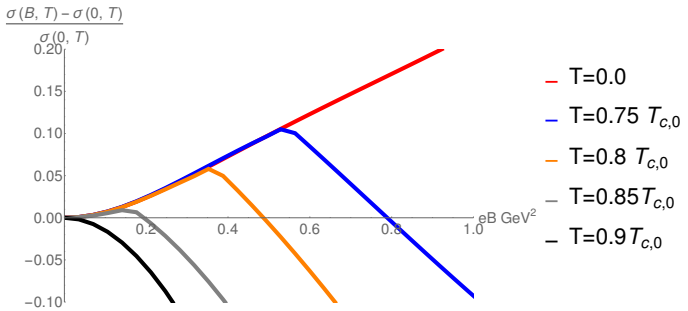

Figure 6.3: The holographic model's results for the change in the condensate of light quarks as a function of magnetic field strength over a range of temperatures for $N_c = N_f = 3$. T_{C0} is the thermal transition temperature at $B = 0$ which is used to set our holographic energy scale (and is approximately 160 MeV according to the lattice simulations). For this plot the model parameters are taken as $\kappa = 0.05$ and $b = 0.037$.

sufficiently until one considers the meson melted. We do not perform the full analysis of this phenomenology in this work. As pointed out in [187], such models naturally predict that the transition where the thermal width develops, i.e. the smallest value of T such that there occurs an embedding ending on the black hole horizon, happens *ahead of* the chiral transition. For a second order phase transition, the flavour brane of the model smoothly encounters (the point at which a thermal width develops) and then moves along the black hole horizon to reach the chirally symmetric phase. To this point, the model has been tuned to match expectations in QCD. This is illustrated in figure 6.6.

6.2 The Dynamic AdS/QCD model at finite temperature

Finite temperature can be included in Dynamic AdS/QCD by replacing the background metric with an AdS-Schwarzschild metric with the black hole horizon at $r = r_H$ [81],

$$ds^2 = \rho^2(-f dt^2 + dx_3^2) + \frac{d\rho^2}{f\rho^2}, \qquad f = 1 - \frac{r_H^4}{r^4}, \tag{6.1}$$

where r_H is proportional to the temperature ($T = r_H/\pi$). The action for the scalar L, again describing the mass and quark condensate, becomes instead

$$S = \int d^4x d\rho \ \left(\rho^3 f(\partial_\rho L)^2 + \rho \Delta m^2(\rho) L^2\right). \tag{6.2}$$

One then again seeks numerical solutions of the Euler-Lagrange equations subject to $L \to 0$ as $\rho \to \infty$ to describe massless quarks. In the IR, one chooses either $\partial_\rho L = 0$ at the on-mass shell condition or for the end point of the flow to lie perpendicular to the black hole horizon.

Again, we choose to relate the RG scale μ to the effective radial coordinate r (inspired from the top-down D3/D7-model),

$$r = \sqrt{\rho^2 + \kappa L^2}, \tag{6.3}$$

where we have introduced a new parameter $\kappa \in \mathbb{R}$, which in all previous calculations was set to unity. As shown in Fig 6.5, the phase transition for $\kappa = 1$ is first order. The main signal of the first order transition is that of a third embedding solution which emerges from the chirally symmetric $L = 0$ embedding and then moves up the black hole horizon to join the off-black hole solution at a higher temperature. This extra solution corresponds to the local maximum of the effective potential between the chiral symmetry breaking and the chirally symmetric solutions; see figure 6.4. The first-order transition occurs when the black hole eats enough of the $L = 0$ embedding such that its action is reduced to that of the off-black hole embedding. At temperatures above this value the action of the $L = 0$ embedding is always less than that of the second solution no matter how large the black hole becomes. In the limit of large temperature, the two

solutions become identical.

As pointed out in [187], lower values of κ turn the transition second order. Here, we are distorting the surface of the black hole so that it is not a circle in the $\rho - L$ plane. In particular, if the energy scale μ is stretched along the L-axis, as the temperature of the black hole increases the horizon moves up the L-axis quicker than along the ρ-axis. This in turn means that the horizon will consume less of the $L = 0$ embedding (and its action) and makes a transition to the chirally symmetric phase less likely, favouring a second order transition. In the second order transition case, the solution for L transforms smoothly from the off-black hole chiral symmetry breaking solution to a solution ending on the black hole horizon. The solution then slides down the black hole horizon to merge with the $L = 0$ embedding at the critical temperature. In Fig 6.5, we plot the chiral condensate, σ, against T for $\kappa = 0.05$; a value which is close to the largest κ that generates a second order transition. Making κ smaller, squashes the black hole further towards and along the L-axis and has little effect qualitatively on the physics: the L-profile in the bulk away from small ρ is indifferent to this. Larger values of κ revert back to first order transitions. In Fig 6.6, we show the explicit second-order behaviour at $\kappa = 0.05$ by plotting the embeddings of the scalar L in the chiral limit (i.e. $L(\rho \to \infty) = 0$) as the temperature is increased towards the critical value. At $\rho = 1$ it is already evident that the value of the condensate, which is proportional to the gradient of the embedding $\partial_\rho L|_{\rho\to\infty}$, decreases with increasing temperature. Moreover, as we approach the critical temperature, the angle subtended by the arc of the black-hole horizon between $L(\rho)$ and $L = 0$ decreases smoothly to zero at $T = T_c$. Above this value only the flat, chirally symmetric $L = 0$ embedding exists.

It's important to stress the physics of the two continuous transitions shown in Fig 6.6. At low temperatures, the embedding lies off the black hole horizon and small fluctuations about the embedding are associated with mesonic modes [86]. They are stable in this phase. When the embedding moves on to the black hole the mesonic fluctuations become replaced by quasi-normal modes that describe unstable plasma fluctuations [190]. The configuration then continues to evolve with T until a flat embedding is reached and chiral symmetry is restored. Clearly in a second order transition these two transitions

must be separate and the development of a thermal width for the mesons must occur earlier.

In the effective description of the model, we view κ as a parameter one must adjust to correctly reproduce the expected phase structure at a given N_c, N_f. To represent QCD, we will choose the second order behaviour and $\kappa = 0.05$. We will use the value of r_H at which the phase transition occurs (at $B = 0$) to set the scale of the radial energy direction, ρ, in the holographic model. We set $T_{C0} = 160$MeV as is generally predicted from empirical data.

6.3 Magnetic fields in Dynamic AdS/QCD: Introduction and analysis

Background U(1) electromagnetic fields are introduced into AdS/CFT via sources for the operator $\bar{q}\gamma^\mu q$ [181–184]. These operators are described by a bulk, massless U(1) gauge field. The quark condensate has no baryon number charge so interactions will be products between the field L plus its derivative $\partial_\rho L$ and F^2. The leading two terms in an expansion in L and F are

$$\Delta S = \int d^4x d\rho \ \left(a\rho F^2 L^2 + b\rho^3 f F^2 (\partial_\rho L)^2\right). \tag{6.4}$$

In the case of a fixed external magnetic field, including the metric factors, $F^2 = B^2/\rho^4$ and we will treat a and b as phenomenological parameters.

The expansion in fields is valid at small B and for studying the instability of the $L = 0$ embedding, but generically in the chirally broken phase, or at larger B, terms with higher orders of L may play an equal role. We will however just study these two terms as the lowest-order example to try to provide insight into the response of the theory to an applied B field. We hope to provide some qualitative insight more than explicit, quantitative results.

Returning to the action with the extra terms of equation 6.4, the a-term is then a direct B-dependent contribution to the running of the L mass or anomalous dimension of the quark condensate. Clearly, choice of the sign of a can favour or disfavour chiral

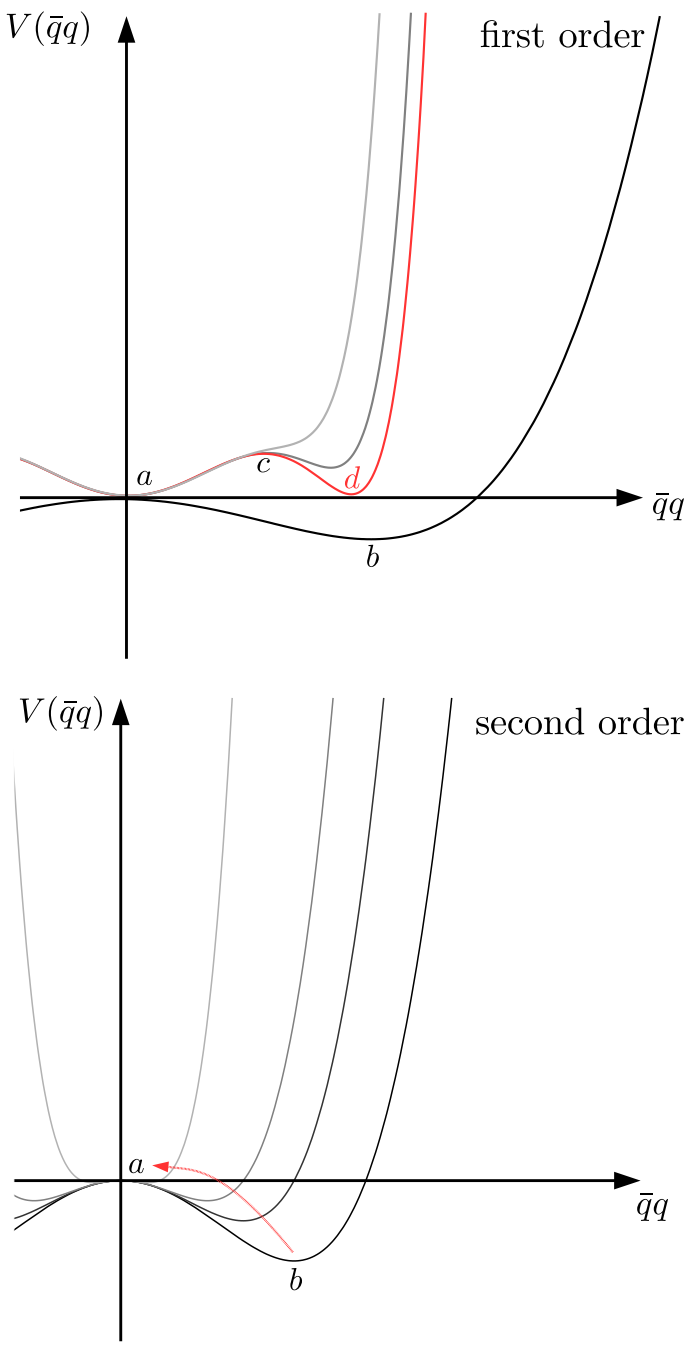

Figure 6.4: [**top**] At $T = 0$ there are two solutions to the embedding equation; the chirally symmetric solution $L = 0$ for which $\bar{q}q = 0$ (a), and the energetically more favourable chirally broken solution (b). A first order transition is signalled by the presence of a third unstable solution (c) for $T > 0$. At $T = T_c$, the chirally broken and chirally symmetric phases are degenerate (d). Above T_c, the chirally symmetric phases remains energetically favourable. [**bottom**] A second order phase transition occurs when the chirally broken phase (b) smoothly merges with the chirally symmetric phase (a) at $T = T_c$.

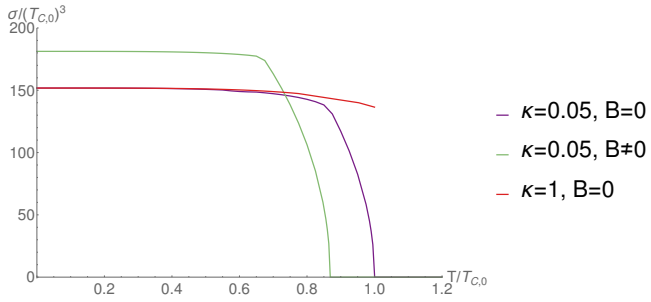

Figure 6.5: Thermal phase transitions in the holographic model with $N_c = N_f = 3$. For values of the parameter κ close to $\kappa = 1$, a first order chiral transition is present. As the value of κ is reduced and the black hole is deformed along the L-axis, the phase transition switches to becoming second order. The introduction of a background magnetic field can be seen to affect the value of the transition order parameter, σ. Here we show an example with magnetic catalysis at low temperature and inverse magnetic catalysis at higher temperatures, a phenomenon which reduces the critical temperature, $T_c(B) < T_c(0)$.

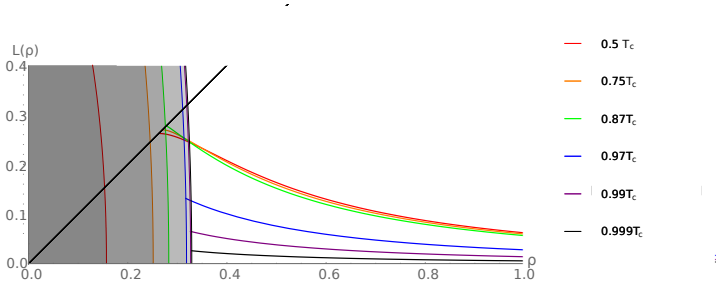

Figure 6.6: Plot showing the chiral embeddings (at $B = 0$) for a range of temperatures. Each embedding is coloured to match the black hole horizon pertaining to the relevant temperature. The second order nature of the transition is evident; the embedding smoothly transforms into the flat $L = 0$ embedding at the critical temperature, T_c.

condensation by affecting where the BF-bound is violated. The b-term, again depending on the sign, either favours or disfavours curvature in the L-profile which again encourages or discourages L to take up a profile away from $L = 0$ (the chirally symmetric state). Note that the magnetic field now enters into the action in the combinations aB^2 and bB^2 so it is possible by choice of the magnitude of a and b to move the scale of effects in B.

Interestingly, only the second $b-$term has temperature dependence when one naïvely inserts the metric factors (from the ρ index contraction in $(\partial_\rho L)^2$). This term decreases as one approaches the black hole horizon. One can hope to play these $a-$ and $b-$ terms off against each other. At zero temperature the $b-$term might dominate and favour chiral condensation. At finite temperature though, it will be less favoured and the $a-$term might take over suppressing chiral condensation. This is our initial strategy to realize the observed pattern of catalysis and inverse catalysis with temperature.

The numerical analysis is again to find the solutions for L at each value of T and B for our chosen values of a, b and κ at N_f=N_c=3. For κ of order one, the thermal transition is first order as discussed: The embedding profile for L jumps from a solution off the black hole to the flat embedding ending on the horizon. The transition is driven by the black hole eating the $L = 0$ configuration until its action is less than the chiral symmetry breaking embedding. For this reason, the chirally symmetric, low-T phase is fairly insensitive to the actual temperature and it is very hard to engineer T dependent behaviour. The only shifts from magnetic catalysis to inverse catalysis that we can find occur when the a and b terms are so finely tuned that they have negligible net effect at $T = 0$. The catalysis effect is well below a percent. We conclude that the QCD behaviour with B, T is a result of the second order transition behaviour.

Hence we turn to $\kappa = 0.05$ as an example of a model with a second order transition. For each point in the (a, b)-plane, we can plot the condensate against T at non-zero B. In all cases, the transitions are second order. An example curve is shown in Fig 6.5 for a case where the condensate is enhanced at small T but suppressed at $T \simeq T_{C,0}$, where $T_{C,0}$ is the critical temperature at zero magnetic field.

In Fig 6.7, we show the phase structure of the model in terms of the phenomenological

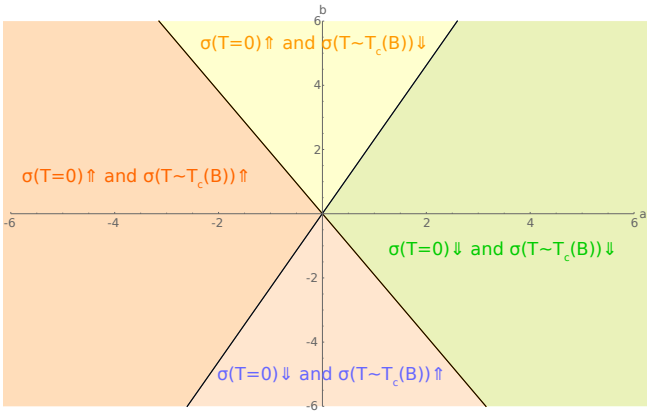

Figure 6.7: The phase-structure of the holographic model in terms of the phenomenological parameters a and b. The $a-b$ plane can be dissected into four sectors wherein the condensate is affected differently with temperature and an external magnetic field.

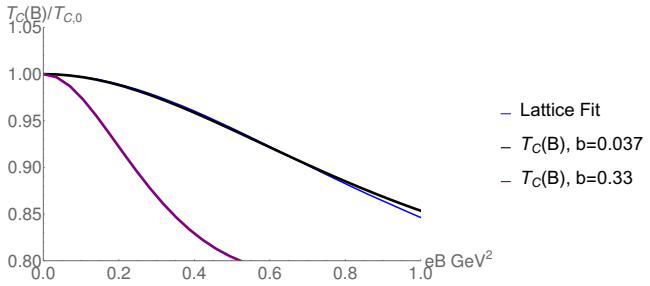

Figure 6.8: Plots of the critical temperature against eB, $T_{C0} = 160$MeV. We show the best fit lattice data taken from [151] and the holographic model's best fit **(in the chiral limit)** to that data ($\kappa = 0.05, a = 0, b = 0.037$). We also show the holographic models prediction for another value of $b = 0.33$ - the model depends on the quantity bB^2 so the eB axis is simply rescaled by this change.

parameters a and b. This $a-b$ phase space comprises four different sectors; a region in which the chiral condensate, σ, is *always* enhanced relative to no external magnetic field, a region in which σ is *always* suppressed relative to no external magnetic field and two regions where it is either enhanced at low temperatures and suppressed at high temperatures or vice versa.

The value of the critical temperature of the chiral phase transition is dependent on how the external magnetic field affects the value of the condensate. If at high temperatures the value of the condensate is suppressed due to inverse magnetic catalysis, the value of the critical temperature is reduced, see an example in Fig 6.8, or if enhanced at high temperatures the critical temperature is increased.

The Lattice QCD data from [150], shown in Fig 6.2, indicates a non-trivial relationship between the chiral condensate and the strength of the external magnetic field. At low temperatures, magnetic catalysis of the condensate is apparent and at temperatures approaching the $B = 0$ critical value, there is a suppression of the condensate (inverse magnetic catalysis). This, first of all, points us to working in the top centre quadrant of the $a - b$ plane seen in Fig 6.7. It is encouraging that the holographic model can incorporate the QCD behaviour although we must stress again that the freedom of the $a - b$ parameter space suggested it should be possible.

A further interesting feature of the lattice plot is that for a narrow range of temperatures approaching the critical value, $\sigma(B)$ behaves non-monotonically, indicating magnetic catalysis for small values of the magnetic field but as the strength of the external B-field is increased, the field catalyses a suppression - we will refer to this intermediate behaviour as the 'cross-over' regime. One question we could ask of our model is whether or not this cross-over behaviour can be obtained if one were to select values of the phenomenological parameters a and b to be inside the appropriate sector of the $a - b$ plane.

The key observation that allows us to achieve this cross-over behaviour in the holographic model is to notice that the appropriate quadrant in Fig 6.7 contains the b-axis along which $a = 0$. Intriguingly, the b-term alone can generate magnetic catalysis at low temperatures but inverse catalysis at higher temperatures. Further exploration shows that it is because the b-term acts differently on black hole embeddings to off-black hole embeddings. In Fig 6.9, we show the effect of B on the embeddings at an intermediate temperature $T = 0.75T_c$. For $B = 0$, we are still in the phase before the mesons have melted. As B rises in the theory with just the b-dependent interaction term, derivatives are encouraged in the UV but not close to the horizon where the b-term is killed off due to its T-dependence. The result is that, in the IR, the B-field moves the embedding towards a melted phase whilst the UV condensate grows. Once the embedding is brought onto the black hole, further increasing B moves the embedding down the horizon pulling the UV behaviour and the UV condensate down. We did not deliberately engineer this behaviour but it does match the observed lattice results.

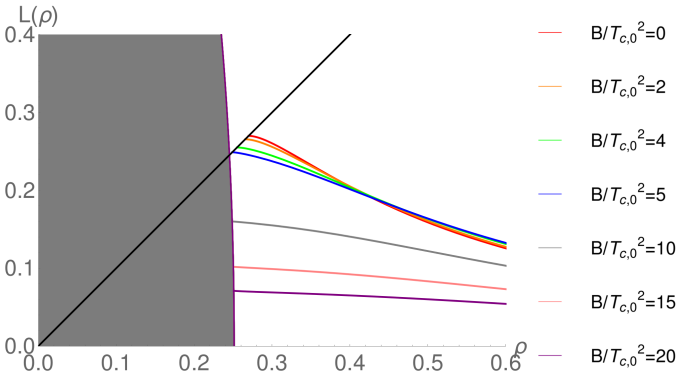

Figure 6.9: Plot showing the chiral embeddings at $T = 0.75T_{C0}$ for a range of magnetic field. Increasing B moves the embedding towards and on to the horizon but initially also increases the condensate value.

One can now survey the (a, b, κ)-space for the best fit to the QCD behaviour. Here we work in the chiral limit of the holographic model. Although the lattice data lies away from that limit, we will see shortly that small quark masses do not change the holographic model's numerical predictions greatly We have found a decent fit to the QCD behaviour when we take $\kappa = 0.05$ and $a = 0$. To fit b we have used the lattice fit in [151] for the B-dependence of the critical temperature in the theory. There, they fit to the form

$$\frac{T_C(eB)}{T_{C0}} = \frac{1 + \alpha(eB)^2}{1 + \beta(eB)^2}, \tag{6.5}$$

where $e^2/4\pi = 1/137$. The lattice results find central values, from fitting to the light quark condensate, of $\alpha = 0.54$ and $\beta = 0.82$. In Fig 6.8, we show our fit to this data for $b = 0.037$ — the lattice and holographic models can be made to lie very close to each other when $b = 0.037$. Here, the holographic model best fits the functional form with $\alpha = 0.78$ and $\beta = 1.08$.

Now, with all parameters fixed, we can plot the fractional change in the condensate against eB at different T as shown in Fig 6.3. We see the enhancement of the condensate at zero temperature but a suppression near the critical value. Of course, it should be reiterated that without the lattice data already in place displaying the behaviour it does, we do not know *a priori* which values of a and b should be chosen to best fit QCD. Having chosen these appropriate values for the parameters a and b, it is no surprise that we reproduce the expected enhancement and suppression of σ at low and high

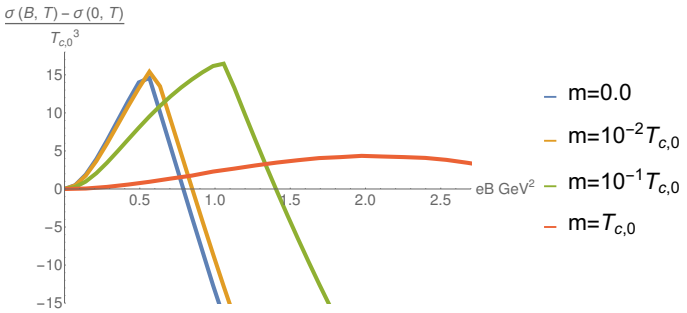

Figure 6.10: Plot showing the change in the chiral condensate as a function of B for different quark masses. The parameters are those used to make Fig 6.7.

temperatures respectively. More remarkable however, as we have discussed, is that we also find the cross-over regime needed by Fig 6.2. For intermediate temperatures, a transition occurs at some value of B at which the condensate switches from increasing to decreasing with an increasing magnetic field strength. The turn over point of this transition can be identified in the holographic model as the value of the magnetic field at which the chiral embedding switches from being off the black hole to being a solution ending on the black hole, i.e. the meson-melting phase transition. The match between Fig 6.2 and Fig 6.3 is not perfect: the holographic model has less catalysis at low T and too much inverse catalysis at higher T but the general structure is similar. The Dynamic AdS/QCD model teaches us that the meson melting behaviour is key to the structure of the transitions seen with B.

6.4 Non-zero quark masses

It is straightforward to include quark mass into the analysis. The asymptotic value of the field L is simply the UV quark mass and we can set it to some finite value at a large-ρ scale. We show the variation in the quark condensate with B in Fig 6.10. Raising the mass increases the B-value at which inverse catalysis takes over from catalysis. Since the effective theory does not apply at B-field values that begin to probe the asymptotically free regime, and since perturbative analysis suggests only magnetic catalysis, this hints at our results possibly moving smoothly to an absence of catalysis at large m. It is indeed found on the lattice that inverse catalysis is present only for small quark masses.

Chapter 7

Translational Symmetry Breaking & Striped Condensation

Translational invariance is known to be spontaneously broken in a number of superconducting cuprate systems [191]. They display phases where the condensate varies spatially as $\sin(kx)$ manifesting as visible stripes in some measurements. The existence of such translationally non-invariant phases have also been speculated to exist in finite density gauge theory [192–194]. There has been some work recently on modelling such phases in holographic descriptions of superconductors and finite density QCD [195–199]. More complex, two-dimensional chequer-board patterns are also possible [200]. The chemical potential in these systems already breaks Lorentz invariance[1] and provides a natural Lorentz frame for stripes to form. In this section however, we wish to ask whether spontaneous breaking of Lorentz invariance, in this pattern, can occur in scalar or gauge theories at *zero* chemical potential (see [201] for a well known related discussion of Lorentz violation in string theory).

A preference for spatially dependent vacuum expectation values for operators essentially requires that the relevant operators have negative kinetic terms in the unbroken vacuum which manifest in the effective potential as a negative k^2 dependent contribution to the mass term. Normally, this is associated with ghost like behaviour and seems

[1] The addition of chemical potential to a field theory implies the existence of an additional term in the action $\sim \mu N$, counting the number of particles N in the system. In QFT, we can associate the number operator as $\psi^\dagger \pi$ giving us and extra term in the Lagrangian equivalent to $\mu \bar{\psi} \gamma^0 \psi$. However, $\psi^\dagger \psi$ is not a Lorentz invariant quantity and so the Lagrangian no-long contains this symmetry explicitly.

forbidden at weak coupling. We will argue though that it can happen in a theory where many higher-dimension operators are present and are sufficiently large that, when symmetry breaking occurs, they generate effective terms that mimic negative kinetic terms. The true vacuum will then be characterized by Lorentz breaking vevs and fluctuations will then be ghost free in the true vacuum. Again, in principle, higher-dimension operators evaluated in the striped vacuum can correct the signs and leave a stable theory. One could therefore imagine a Higgs-like theory with condensation occurring close to its UV-cutoff scale displaying dynamical Lorentz invariance breaking. A natural environment for such an effective theory is the strong coupling regime of a gauge theory. At the scale of strong coupling, many higher-dimension operators become important and simultaneously, chiral condensation and the gluonic condensation of $\mathrm{Tr}F^2$ occur. It at least seems possible that within the space of gauge theories, Lorentz symmetry breaking dynamics might exist. Our effective field theory discussions will not prove that any particular theory will behave in this way but it is a novel possibility that should be borne in mind in lattice simulations of models beyond the Standard Model. Alternatively, in gauge theories without translational symmetry breaking, one can reinterpret our results as bounds on the sizes of certain higher-dimension operators in the effective theory.

We present our results in the remit of the Dynamic AdS/QCD holographic model [89, 90]. We describe the operators $\mathrm{Tr}F^2$, $\bar{q}q$ and $\bar{q}F^2q$ and represent their running anomalous dimensions as running mass-squareds for the appropriate scalars in AdS space. The UV of the theory is stable and has vanishing operator vevs. As the Breitenlohner Freedman (BF) bound [100] is violated in the IR, condensation occurs and, if suitable (k^2 dependent) potentials are chosen, an instability for Lorentz violating vevs can emerge.

Whilst the possibility of Lorentz violation is intriguing in itself, we also present a more explicit phenomenological motivation. It has recently been shown [202, 203] that in R^2 gravity, short distance fluctuations in the metric can be converted by the non-linearities of the Einstein's equations into an effective long distance cosmological constant. Our interest in Lorentz violating vacua is partially motivated by thinking about how to generate such short distance fluctuations with sufficient power. Intriguingly, if one considers this mechanism in Starobinsky early-universe inflation models,

where the R^2 term is set by the scalaron[2] scale of $M \sim 10^{13}$ GeV, then stripes at the electroweak scale generate the observed cosmological constant!

Could gauge theories close to the Standard Model involve Lorentz violation? The answer is fairly strongly *no*. Limits on Lorentz violation [204, 205] in the electron-photon system are extremely stringent and constrain any coupling of such a system to be associated with very high scales. Therefore, if stripes are the source of the observed cosmological constant then they must be well hidden in a dark sector.

One might also presume that the spontaneous breaking of Lorentz symmetry would generate Goldstone poles in the non-relativistic propagators of the theory but clearly no such massless modes exist in the visible Universe. In fact, the number of long range propagating Goldstone modes depends on the pattern of symmetry breaking as has been discussed in [206]. There are massless modes associated to each broken direction of translation but they only propagate along unbroken directions transverse to the breaking[3]. Thus there will be long-range propagating Goldstones for striped (one broken dimension) or chequer-board (two broken dimensions) configurations where there still exist unbroken directions. However, this will not be the case for cuboid or general crystal-like configurations (where three dimensions have broken Lorentz invariance). We will not exhibit these Goldstone structures here since we concentrate on the instability for the formation of stripes rather than a full model of the final ground state. Since phenomenologically the Lorentz breaking sector must be extremely weakly coupled to

[2] A general $f(R)$ Lagrangian,

$$f(R) = R + \frac{R^2}{6M^2} + \mathcal{O}(R^3), \tag{7.1}$$

can be recast as a scalar-tensor theory (in the *Jordan frame*)

$$f(R) = \phi R - V(\phi), \tag{7.2}$$

under the Legendre transformation,

$$f'(R) = \phi \quad \text{and} \quad V'(\phi) = R. \tag{7.3}$$

The dimensionless scalar, ϕ, is then a parameterisation of the theory's scalar mode, the *scalaron*. Truncating $f(R)$ at R^2, leaving the only the *Starobinsky* Lagrangian, yields a potential of the form

$$V(\phi) = \frac{3M^2}{2}(\phi - 1)^2. \tag{7.4}$$

[3] This is identical to the case of massless modes resulting from D-brane fluctuations. The open string gauge field components transverse to the brane are seen in the bulk as massless scalar modes. E.g. we have seen the six massless scalar modes transverse to the D3-brane stack when building up the idea of the AdS/CFT correspondence.

the visible sector, the presence of Goldstones in anycase is probably not an issue.

Finally we note that we have considered whether striped ground states are ruled out in QCD-like gauge theories by the theorems of Vafa and Witten [207, 208]. For example, one theorem [207] (see Appendix J for a derivation) asserts that any state associated with the $\bar{q}q$ operator must be heavier than the pion; given the pion may be made massive by a small explicit quark mass, breaking of vector symmetries is, for example, forbidden. This may indeed forbid the appearance of striped and chequer board phases in vector-like gauge theories where there will be Goldstone modes able to propagate in some directions but does not clearly prevent cuboid phases where the Goldstones can not propagate.

7.1 Effective Higgs theories

Let us begin by writing down the simplest possible Higgs theory with one scalar and to quadratic order to demonstrate the usual instability

$$\mathcal{L} = \partial^\mu \phi^* \partial_\mu \phi - V(|\phi|), \qquad V = -m^2 |\phi|^2 \,. \tag{7.5}$$

Now, if we consider a ground state where the vev of the scalar is striped in one direction, $\langle \phi \rangle = v \sin kx$, then there is an effective potential

$$V = -(m^2 - k^2)|\phi|^2, \tag{7.6}$$

with the additional term arising from the kinetic term after condensation in ϕ; i.e. $|\partial \langle \phi \rangle|^2$.

Non-zero k reduces the strength of the potential instability and is therefore disfavoured in this set-up; see figure 7.1. We can see that for there to be an instability that favours stripes (i.e. favouring a non-zero k), we need to reverse the sign of the scalar kinetic term. However, we can not simply flip the sign on the kinetic term since the theory would become ill-behaved with ghosts.

Scalar theories like this are known to suffer from a hierarchy problem and the naï

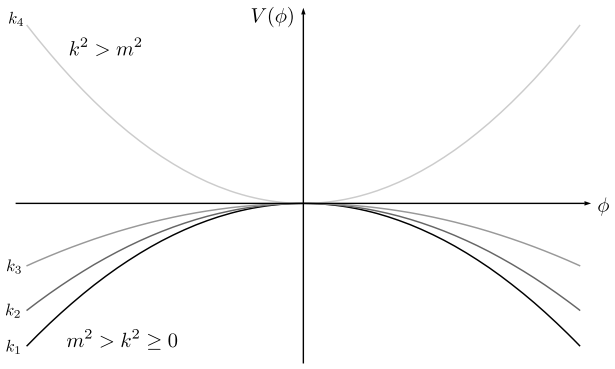

Figure 7.1: Assuming a striped vev of the scalar ϕ from 7.5, a non-zero wavenumber k actively disfavours an instability in the potential. Here we show the profile of the potential for $0 = k_1 < k_2 < k_3 < k_4$.

ve expectation is that new physics will enter at a scale reasonably close to the scalar's mass; we will call this somewhat higher scale Λ_{UV}. The expectation is that at the scale Λ_{UV}, higher-dimension operators will generically be present (having been suppressed at perturbative values of the coupling). Such higher-dimension operators can, once symmetry breaking is triggered, lead to *effective kinetic terms* that have the right sign to favour translational symmetry breaking. For example, let us consider including an additional scalar f. We can imagine an additional Lagrangian term containing f to be

$$\Delta\mathcal{L} = -\frac{\kappa_0}{\Lambda_{UV}^2}|f|^2\partial^\mu\phi^*\partial_\mu\phi, \tag{7.7}$$

for some generic coefficient κ_0. Were f to condense at some scale and κ_0 be large enough then the reversal of the kinetic term's sign can be achieved.

Once a striped phase has condensed, other higher-dimension operators can step in to secure the ghost inducing negative $(\partial_t\phi)^2$ term is not present in the true vacuum. For example, consider the term

$$\Delta\mathcal{L} = \frac{\kappa_1}{\Lambda_{UV}^4}|\partial^\mu\phi|^2|\partial^\nu\phi|^2 \tag{7.8}$$

evaluated on the symmetry breaking solution (a Lorentz invariant term results if the vev occurs twice in one derivative term but a spatially preferring term occurs if the two vevs occur in the different derivative terms). This term will distinguish the spatial

directions in which there are stripes from the temporal direction and the coefficient could be concocted to cure the ghost problem once the stripy vev had formed.

Of course, in this discussion many other terms might be present that oppose the effect, or indeed κ_0 might be small or negative. We simply wish to identify terms that could trigger translational symmetry breaking. Another possible mechanism is to introduce yet another new scalar, χ, with the same symmetry properties as the original ϕ. In doing so, we consider the Lagrangian containing the terms

$$\Delta\mathcal{L} = |\partial^\mu\phi|^2 + |\partial^\mu\chi|^2 + m^2|\phi|^2 - M^2|\chi|^2 + \frac{\kappa_2}{\Lambda_{UV}^2}|f|^2\partial^\mu\phi^*\partial_\mu\chi. \tag{7.9}$$

Were f to get a vev then an off-diagonal kinetic mixing is induced for the ϕ, χ pair. The effective k dependent quadratic potential is then given by

$$(\phi,\chi)\begin{pmatrix} -m^2+k^2 & \frac{\kappa_2}{\Lambda_{UV}^2}\langle f\rangle^2 k^2 \\ \frac{\kappa_2}{\Lambda_{UV}^2}\langle f\rangle^2 k^2 & M^2+k^2 \end{pmatrix}\begin{pmatrix}\phi\\ \chi\end{pmatrix}. \tag{7.10}$$

For small k, the negative mass-squared eigenvalue becomes

$$m_1^2 = -m^2 + k^2 - \frac{1}{2}\frac{\left(\frac{\kappa_2}{\Lambda_{UV}^2}\langle f\rangle^2 k^2\right)^2}{M^2-m^2}. \tag{7.11}$$

Again for not unreasonable choices of parameters this term could be made to favour translational symmetry breaking. Of course, this is an argument for an instability rather than a full model of the final vacuum. The potential at large k^2 would need to be stabilized by terms with higher powers and the dynamically determined value of k may lie close to Λ_{UV}. The precise form of the vacuum is also dynamically determined — one could envisage 1D stripes, 2D chequer board patterns or 3D cuboid patterns.

Such Lorentz violation would have to dynamically pick a frame of reference in our Universe, however, it seems likely that the innate frame of the matter in the Universe that sets the frame of the 3K cosmic microwave background radiation would be chosen. As the gauge theory cooled and condensed the small chemical potential of the Universe would be the only parameter biasing a specific frame.

Such scalar models with ϕ, χ and f may at first glance appear baroque and overwrought. To argue that this is a sensible arena for discussion, we should recast this analysis as the effective description of a QCD-like gauge theory. Consider an SU(N_c) gauge theory and consider a single, quenched quark ($N_f \ll N_c$) in that theory. We know that the vacuum has a non-zero value of the quark condensate $\langle \bar{q}q \rangle$ which carries a U(1)$_A$ charge of +2 (neglecting the U(1)$_A$ anomaly). This operator should be mapped to ϕ. We also know that the operator TrF^2 is non-zero in the vacuum and a singlet under flavour symmetries. It is the scalar f above. Finally, χ could represent the higher-dimension operator of the form $\bar{q}F^2q$ (or possibly those with higher powers of F): this operator has the same symmetry properties as $\bar{q}q$ but in the quantum theory is a distinct operator whose vev should be determined by the effective theory. In fact, above we assumed that the χ field does not condense but simply mixes with ϕ.

In asymptotically free theories, the running coupling enters a regime of strong coupling at some scale which should be associated with the cutoff Λ_{UV} of the scalar theory. At this scale the strong coupling is expected to generate higher-dimension operators including of the form we have discussed above. The chiral condensate will then form in QCD quite quickly in RG running.

These arguments map the dynamics of strongly coupled gauge theories to the scalar models discussed above and suggest that translational symmetry breaking is at least possible in the vacuum. Of course, we have in no way proved the phenomena occurs or, indeed, is even likely. However, given the wide range of asymptotically free gauge theories that can be constructed, it is possible that amongst them there exists some that do concoct their higher-dimension operator couplings to conspire to this end.

In the main bulk of this chapter, we will construct a holographic model of a gauge theory's dynamics that reproduces this line of argument and moreover carefully takes into account the scaling dimensions and RG flow in such a theory.

7.2 A holographic model

To demonstrate the effective field theory arguments above a little more robustly, we will utilise our Dynamic AdS/QCD model to inspect gauge theories with such phenomena. It

will show the possible translational symmetry breaking instability of a QCD-like gauge theory we discussed above. We assume there is some SU(N_c) gauge theory with a small number of quenched quarks. As usual, we place the effective theory in AdS_5

$$ds^2 = \frac{dr^2}{r^2} + r^2 dx^2_{3+1}\,, \tag{7.12}$$

with $r^2 = \sqrt{\rho^2 + |X|^2}$ as usual. We will identify the RG scale μ with the AdS radial parameter r in our model. We assume the underlying Yang-Mills theory generates a vev for the four-dimensional operator $\mathrm{Tr}F^2$. Using the relation $(\Delta - p)(\Delta + p - 4) = M^2$ with $\Delta = 4$ and $p = 0$, we represent the $\mathrm{Tr}F^2$ operator as a *massless* scalar of in the AdS_5 background. Following the rules of the correspondence (see equation 2.118), the scalar will take the asymptotic ($r \to \infty$) form

$$f = \frac{c}{r^4}\,. \tag{7.13}$$

Our model will concentrate on the quenched quark sector rather than the generation of this vev.

Although we will allow the AdS space to extend to $r = \infty$, such a gravity description should really only extend to the UV cutoff where the asymptotically free theory crosses over to strong coupling (as r is decreased). Experience teaches us that the models still work well without a UV cutoff because the dynamics is determined around the scale of the BF-bound violation.

The behaviour of the $\bar{q}q$ operator in the theory is as before. The Dynamic AdS/QCD model represents $\bar{q}q$ by a field X with action

$$S = \int d^4x\; d\rho\, \rho^3 \left[\frac{1}{r^2}|DX|^2 + \frac{\Delta m^2}{\rho^2}|X|^2\right]. \tag{7.14}$$

If $\Delta m^2 = 0$ then the scalar, X, describes a dimension 3 operator and dimension 1 source as is required for it to represent $\bar{q}q$ and the quark mass m. That is, in the UV the solution for the X equation of motion is $|X| \sim m + \bar{q}q/\rho^2$. We will work in the chiral limit with the quark mass zero henceforth. A non-zero Δm^2 allows us to introduce an

anomalous dimension for this operator, γ. If the mass squared of the scalar violates the BF bound of -4 ($\Delta m^2 = -1$, $\gamma = 1$) then the scalar field X becomes unstable and the theory enters a chiral symmetry breaking phase. We will fix the form of Δm^2 using the two loop perturbative running of the gauge coupling in QCD with N_f flavours transforming under a representation R. Of course, it is important to reiterate that this is but a crude approximation to the running of the anomalous dimension γ, yet it serves as a reasonable guess. This then takes the form

$$\mu \frac{d\alpha}{d\mu} = -b_0 \alpha^2 - b_1 \alpha^3, \tag{7.15}$$

where

$$b_0 = \frac{1}{6\pi}\left(11 C_2(G) - 4 N_f C_2(R) \frac{\dim(R)}{\dim(G)}\right), \tag{7.16}$$

and

$$\begin{aligned} b_1 \quad = \quad & \tfrac{1}{8\pi^2}\left(\tfrac{34}{3}\left[C_2(G)\right]^2\right. \\ & \left. - \left[\tfrac{20}{3} C_2(G) C_2(R) + 4\left[C_2(R)\right]^2\right] N_f \tfrac{\dim(R)}{\dim(G)}\right) \end{aligned} \quad . \tag{7.17}$$

The one loop result for the anomalous dimension of the quark mass is

$$\gamma_1(\mu; R) = \frac{3 C_2(R)}{2\pi} \alpha(\mu; R). \tag{7.18}$$

Working perturbatively from the AdS result $m^2 = \Delta(\Delta - 4)$ we have

$$\Delta m^2 = -2\gamma_1(\mu; R) = -\frac{3 C_2(R)}{\pi} \alpha(\mu; R). \tag{7.19}$$

This will then fix the r dependence of the scalar mass through Δm^2 as a function of N_c and N_f for each R. The Euler-Lagrange equation for the vacuum embedding X is given at fixed Δm^2 by the solution of

$$\frac{\partial}{\partial \rho}\left(\rho^3 \partial_\rho X\right) - \rho \Delta m^2 X = 0. \tag{7.20}$$

Again, to find $X(\rho)$ we solve the equation of motion numerically with shooting techniques

with an input IR initial condition. We have once more the IR boundary condition set to be

$$X(\rho = X_0) = X_0, \qquad X'(\rho = X_0) = 0. \tag{7.21}$$

Now we can introduce the scalar field Y that describes the operator $\bar{q}F^2q$. It will have an intrinsic action

$$S = \int d^4x \; d\rho \, \rho^{11} \left[\frac{1}{r^2}|DY|^2 + \frac{\Delta m_Y^2}{\rho^2}|Y|^2 \right], \tag{7.22}$$

where we must now accommodate for Y in the RG scale by setting

$$r^2 = \rho^2 + |X|^2 + \rho^8|Y|^2. \tag{7.23}$$

Here, Y has energy dimension of -3 and when $\Delta m_Y^2 = 0$ has the solution

$$Y = \alpha + \frac{\beta}{\rho^{10}} \, . \tag{7.24}$$

α is the dimension -3 source for the $\bar{q}F^2q$ term in the action and β has the dimension of the vev. If we include an r-dependent Δm_Y^2, as we have done for the field X, then the dimension of $\bar{q}F^2q$ will run away from the UV value of 7. For this toy model, we will assume the dimension is $7 - \gamma_1$ so its dimension falls but the BF-bound for this scalar will not be violated at the scale where $\gamma_1 = 1$ where X condenses.

We can now include higher order terms in the action, mixing the fields that favour translational symmetry breaking. For example we might include

$$\Delta\mathcal{L} = \tilde{\kappa}_3 \frac{\rho^7}{r^2}|f|^2 \partial_M X^\dagger \partial^M Y \, , \tag{7.25}$$

where $\tilde{\kappa}_3$ is dimensionless. As the vev of f grows this will introduce a kinetic mixing term that will drive the lowest mass eigenstate more negative by a k-dependent factor. As written, this term tends to drive the kinetic term in the holographic ρ direction negative also. However, there are terms that break the $\rho - x$ symmetry after the f field

acquires a vev. For example, we might consider the term

$$\Delta\mathcal{L} = \tilde{\kappa}_4 \frac{\rho^9}{r^4} (\partial_M f \partial^M X^\dagger)(\partial_N f \partial^N Y)\,. \tag{7.26}$$

$\tilde{\kappa}_4$ is again dimensionless. Since f is only dependent on the holographic coordinate ρ, upon substitution of its profile in equation 7.13, we simply get a correction to the ρ-derivative mixing of the X and Y scalars. By picking $\tilde{\kappa}_4$ appropriately ($\tilde{\kappa}_3 = -16\tilde{\kappa}_4$) one can remove the mixing term in the ρ derivative but leave a mixing term behind in the x^μ coordinates,

$$\Delta\mathcal{L} = \tilde{\kappa}_2 \frac{c^2}{\rho r^4} \partial_\mu X^\dagger \partial^\mu Y\,. \tag{7.27}$$

For our computation below we will assume that the correction to the ρ kinetic term is zero and that $\tilde{\kappa}_2$ is our free parameter.

In such a model, one can numerically solve the coupled ODEs for the profiles of X and Y and then evaluate the action on those solutions to determine the effective potential of a solution. Performing this computation for a solution of the form $Q \sim f_Q(\rho) \sin kx$, for $Q \in \{X, Y\}$, allows one to plot the potential against k. For example, to set the runnings, we can study $N_c = 3$ $N_f = 3$ (of course QCD with these values does not generate stripes but these choices are indicative of the behaviour), with the scale at which $\gamma = 1$ to be Λ_{QCD} and further set $c = \Lambda_{QCD}^4$. In Figure 1, we plot the potential as a function of k^2 for different choices of the higher-dimension operator's coefficient, $\tilde{\kappa}_2$. We see that for $\mathcal{O}(1)$ negative values, an instability for stripes is indeed present. Strictly for the case of QCD, which we know respects Lorentz invariance, we have placed limits on $\tilde{\kappa}_2$ by this argument. The instability mechanism may be present in other gauge theories however.

At this point we will cease speculating about such unknown gauge dynamics and simply assume that field theories with translational symmetry broken in the vacuum exist. We will explore whether they are phenomenologically interesting and viable as part of Beyond the Standard Model physics.

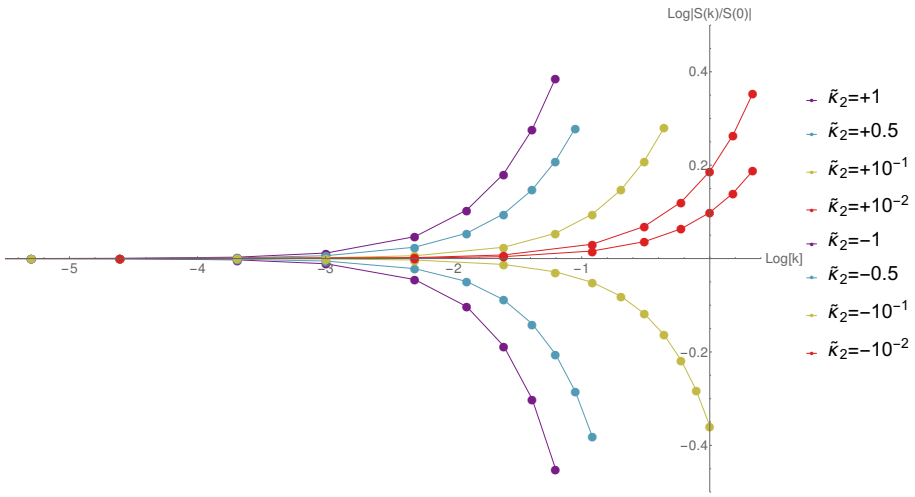

Figure 7.2: Potential (normalized by that at $k = 0$) against $\ln[k/\Lambda_{QCD}]$ for varying values of the coefficient of the higher-dimension operator (which is a mix of $\tilde{\kappa}_2$ and $\tilde{\kappa}_3$. We set here $N_c = 3$ $N_f = 3$, the scale at which $\gamma = 1$ to be Λ_{QCD} and set $c = \Lambda^4_{QCD}$.

7.3 Striped phases and the cosmological constant in R^2-gravity

Our interest in such striped, chequer-board-like or cuboid phases is that they could have a dramatic cosmological consequence. The basic observation is that the response of the metric to such an inhomogeneity in the mass-energy distribution will be replaced by some average effect on scales much larger than $1/\Lambda_{\rm stripe}$, the scale that sets the wavelength of the Lorentz symmetry breaking stripe. Since the dynamical equations for the metric are non-linear, this averaging does not lead to the same dynamical equations for some 'average' metric but rather results in corrections to the equations themselves.

The fact that inhomogeneity can in general result in a "cosmological back-reaction" has been widely investigated, see *e.g.* [209–216]. These papers were inspired by the possibility that cosmological inhomogeneity (the fact that matter is not uniformly distributed at scales smaller than about 100 Mpc, but instead concentrated in walls and clusters of galaxies, containing stars and planets *etc.*) leads to corrections to the average expansion rate which could explain the observations that indicate that the universe is currently undergoing accelerated expansion, such as [217]. However to date the results of these studies have been either negative or inconclusive.

One particularly elegant and clean approach to inhomogeneity in a cosmological context, was put forward by Green and Wald [218,219]. A brief summary of the analysis is as follows: one splits the metric as

$$g_{ab} = g^{(0)}_{\alpha\beta} + h_{\alpha\beta}\,, \tag{7.28}$$

where $g^{(0)}_{\alpha\beta}$ is the Freedman-Robertson-Walker metric of standard cosmology and $h_{\alpha\beta}$ is the piece sensitive to the matter distribution which here we imagine is the stripy phase of the gauge theory with structure on scale Λ_{stripe}. The $R_{\alpha\beta} - \frac{1}{2}g_{\alpha\beta}R$ terms in the equation of motion split into the standard ones for $g^{(0)}_{\alpha\beta}$ plus extra pieces dependent on $h_{\alpha\beta}$. The philosophy is to take the spatial average of the pieces dependent on $h_{\alpha\beta}$ and then treat the resulting terms as an effective addition to the stress energy tensor of the matter content of the Universe. Assuming that a certain *weak limit* exists, they perform a rigorous diffeomorphism-invariant averaging process of the gravitational response to mass density fluctuations through the application of this weak limit. Assuming that the matter stress-energy tensor $T_{\alpha\beta}$ satisfies the weak energy condition ($T_{\alpha\beta}t^\alpha t^\beta \geq 0$ for every time-like vector field t^α), Green and Wald prove that the averaged effect of the coupled matter plus gravitational fluctuations is then encoded in this limit in an additive correction $t^{(0)}_{\alpha\beta}$ to the stress-energy which is traceless and also satisfies the weak energy condition. They therefore identify it with gravitational radiation. In particular in a FLRW background metric, $t^{(0)}_{\alpha\beta}$ is diagonal, corresponding to an effective fluid with pressure $p = \rho/3 \geq 0$, leading to the conclusion that such a backreaction cannot mimic dark energy.

The situation changes dramatically however, if we now entertain the possibility that Einstein's General Relativity equations themselves already have gravitational corrections. In the Starobinsky model of 'R^2 inflation' [220,221], a theory that remains highly favoured observationally [222], one can show that such a backreaction can mimic Dark Energy. In this model, the Lagrangian density is given by

$$\mathcal{L} = \frac{1}{2\kappa}\left(R + \frac{R^2}{6M^2}\right) + \mathcal{L}_{Matter} \tag{7.29}$$

(where $\kappa = 8\pi G$, and $\sqrt{-g}$ is included in the integration measure of the action). The new parameter is the so-called scalaron mass, which must be $M \approx 3\times 10^{13}$ GeV, in order to agree with cosmological observations. Following the above philosophy, we continue to assume that the underlying (quantum field theoretic) net vacuum energy effectively vanishes (hence the absence of a cosmological constant term above). Back-reaction is again encoded in a diffeomorphism-invariant, effective additive correction, $t^{(0)}_{\alpha\beta}$, to the matter stress energy tensor, however it is now not traceless. Instead [202]

$$\kappa\, t^{(0)} \underset{weak}{=} -\frac{{R^{(1)}}^2}{6M^2}\,, \tag{7.30}$$

where $R^{(1)}$ is the linearised Ricci scalar of the gravitational fluctuations $h_{\alpha\beta}$, $t^{(0)}$ is the trace of $t^{(0)}_{\alpha\beta}$ with respect to the full background metric and the equality holds rigorously in a certain weak limit. Encouragingly, $t^{(0)}$ thus must be negative, in agreement with the current acceleration of the universe. Furthermore it behaves parametrically in the right way, in the sense that if we assume that the fluctuations are generated independently of the scalaron scale, then we recover the tracelessness of the additive correction [218, 219] in the limit $M \to \infty$. Therefore, it seems reasonable to apply order of magnitude estimates to 7.30 in order to obtain a rough estimate of the effective cosmological constant generated by gravitational back-reaction from a striped phase. Setting $R^{(1)} \sim \partial^2 h \sim \kappa\rho$ where ρ is the local mass over-density, we have from 7.30 that the effective vacuum energy $t^{(0)} \sim -\kappa\langle\rho^2\rangle/(6M^2)$. Now we recognise that $\kappa = 1/M^2_{\rm Planck}$, where the reduced Planck mass is $M_{\rm Planck} = 2.44\times 10^{18}$ GeV, that $t^{(0)} = -E^4_{\rm vac}$ where the current effective vacuum energy is $E_{\rm vac} = 10^{-12}$ GeV in order to agree with observations, and finally that the RMS value $\sqrt{\langle\rho^2\rangle} \sim \Lambda^4_{\rm stripe}$, where $\Lambda_{\rm stripe}$ is the energy scale that sets both the amplitude and wavelength of the striped phase. Combining these, we therefore find that

$$E_{\rm vac} \sim \frac{\Lambda^2_{\rm stripe}}{\sqrt{6MM_{\rm Planck}}}\,, \tag{7.31}$$

from which we deduce that $\Lambda_{\rm stripe} \sim 140$ GeV, intriguingly close to the Higgs' mass and the EW (electroweak) scale. Of course, if $t^{(0)}$ is to mimic a cosmological constant and thus drive the present day acceleration of the universe, it must also be (at least

approximately) constant. This is guaranteed by the present mechanism since, as the universe expands, the stripes are not diluted (unlike the matter content and the more rapidly diluted radiation content of the Universe) but instead rearrange and get created to fill the 'gaps', since the wavelength is set at Λ_{stripe} by the microscopic dynamics described in the previous section.

We note again that we have *not* suggested a mechanism that naturally suppresses large contributions to the cosmological constant, in other words we are not attempting to solve the infamous cosmological constant problem. Nevertheless, we have still shown how to generate a new type of contribution that can be significant, indeed can be sufficiently large to explain on its own the value deduced from the present day cosmological acceleration.

Chapter 8

Concluding Remarks

The last few pages in a complete, fundamental theory of QCD are far from being written. The strongly-coupled, non-perturbative aspects such as confinement, walking theories, phase transitions, meson and baryon spectra *et cetera* are still providing many puzzles to answer. Whether on the lattice, using holographic approaches or by other means, research into this field will likely continue for a long time.

In the first chapter, we saw an overview of the history of the field and introductory material on the fundamental topics of chiral symmetry, asymptotically free gauge theories, string theory and D-branes. We then turned to motivating the AdS/CFT correspondence which allows us to equate the partition functions of a CFT to that of a type IIB string theory in $AdS_5 \times S^5$. This correspondence supports all of the following chapters' work. In chapter 3, we turned our focus on re-engineering the famous Maldacena conjecture to work in the arena of gauge theories with flavour and a running coupling like that of QCD and associated asymptotically free theories. We examined both top-down and bottom-up approaches, in particular the theory of Dynamic AdS/QCD. Sticking with latter, part two of this work looked into using the Dynamic AdS/QCD theory to examine various aspects of asymptotically free gauge theories. In chapter 4, we studied the so-called hyperscaling relations of the quark mass and condensate (as well as meson states) with RG scale in theories with an IR fixed point. Chapter 5 dealt with calculating the spectra of mesons, including the pions, the rho and sigma mesons, as well as the scalar glueball for a range of asymptotically free theory of varying numbers of

flavours and colours, and in multiple representations. In Chapter 6, we examined the effect of temperature and magnetic field on QCD-like theories, finding a non-monotonic relationship between the condensate and the magnetic field strength also found in lattice calculations. The final chapter uses the Dynamic AdS/QCD theory to probe whether or not it is possible to obtain striped condensate phases in QCD-like theories and the ramifications of such a phenomenon in the physical world.

One question remains. What is left for the future of this field? Of course, the bottom-up approaches to QCD such as Dynamic AdS/QCD are still relatively young, and although they are reproducing lattice results within 5-10% error, there is still much that can be done to improve upon the theories and still many more phenomena to explore regarding them. Future directions of the Dynamic AdS/QCD model are to look at asymptotically *safe* theories and the physical phenomena that they provide as well as investigating the renowned Banks-Casher result from a holographic perspective. At the moment of writing this thesis, I am currently working on using this theory in collaboration with particle phenomenologists to look at the current standing of technicolor and whether such theories remain a viable candidate for extending the Standard Model of Particle Physics.

Appendices

Appendix A

Parity doublets of chiral symmetry

The full chiral symmetry necessitates parity doublets in the following way. Consider a state $|\alpha,+\rangle$ which has energy E_α, $H|\alpha,+\rangle = E_\alpha|\alpha,+\rangle$, and has a positive parity, $P|\alpha,+\rangle = +|\alpha,+\rangle$. We now define a new state $|\psi^a\rangle = Q_A^a|\alpha,+\rangle$. $|\psi^a\rangle$ is degenerate in energy with $|\psi^a\rangle$,

$$H|\psi^a\rangle = HQ_A^a|\alpha,+\rangle = ([H,Q] + Q_A^a H)|\alpha,+\rangle = Q_A^a H|\alpha,+\rangle = E_\alpha|\psi^a\rangle,$$

but has opposite parity,

$$P|\psi^a\rangle = PQ_A^a P^{-1}P|\alpha,+\rangle = PQ_A^a P^{-1}|\alpha,+\rangle = -Q_A^a|\alpha,+\rangle = -|\psi^a\rangle.$$

Hence for every state $|\alpha,+\rangle$ there is a state $|\psi^a\rangle$ which is degenerate but of opposite parity eigenvalue.

Appendix B

$\mathrm{U}(1)_A$ anomaly

This Appendix follows [41]. In order to investigate the anomalous behaviour of axial currents we begin by examination of the anomaly associated with the $\mathrm{U}(1)_A\mathrm{U}(1)^2_{QED}$ triangle diagram — referred to as the Adler-Bell-Jackiw (ABJ) anomaly, see figure B.1.

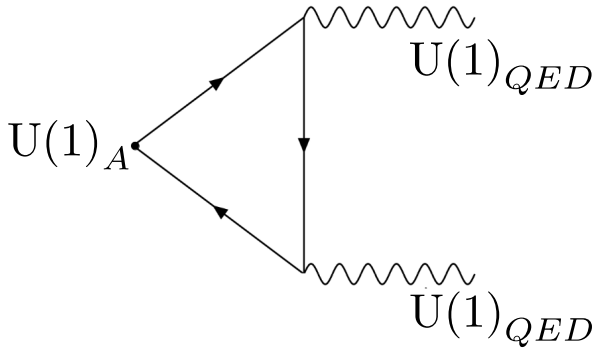

Figure B.1: The $\mathrm{U}(1)_A\mathrm{U}(1)^2_{QED}$ triangle diagram calculation pinpoints to an anomalous $\mathrm{U}(1)_A$ symmetry.

Such a diagram is the leading order contribution to the matrix element

$$\langle p, k|A^\mu(x)|\Omega\rangle,$$

where A^μ is the associated $\mathrm{U}(1)_A$ current[1] and the momenta p and k pertain to the two

[1]The $\mathrm{U}(1)_A$ comes from the global chiral symmetry $\mathrm{U}(1)_L\times\mathrm{U}(1)_R = \mathrm{U}(1)_V\times\mathrm{U}(1)_A$ of the massless

external $\mathrm{U}(1)_{QED}$ fields. Following [41], one can show, with strict implementation of some regulator (e.g. dimensional regularisation), that $\langle p,k|\partial_\mu A^\mu(x)|\Omega\rangle$ is non-zero,

$$\langle p,k|\partial_\mu A^\mu(0)|\Omega\rangle = -\frac{e^2}{16\pi^2}\langle p,k|\epsilon^{\alpha\nu\beta\lambda}F_{\alpha\nu}F_{\beta\lambda}|\Omega\rangle. \tag{B.1}$$

Hence $\partial_\mu A^\mu \neq 0$ and the symmetry is thus anomalous.

In theories such as QCD, we are also interested the fate of the axial currents in triangle diagrams such as $\mathrm{SU(N}_f\mathrm{)}_A\mathrm{SU(N}_c\mathrm{)}^2$ and $\mathrm{U(1)}_A\mathrm{SU(N}_c\mathrm{)}^2$, as shown in figure B.2, the axial currents again stemming from the global, flavour symmetry of the chiral Lagrangian.

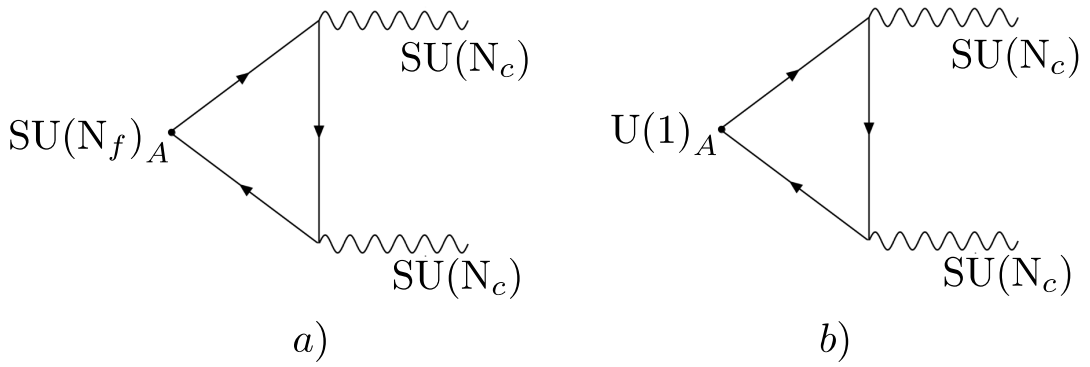

Figure B.2: a) The $\mathrm{SU(N}_f\mathrm{)}_A\mathrm{SU(N}_c\mathrm{)}^2$ triangle diagram and b) the $\mathrm{U(1)}_A\mathrm{SU(N}_c\mathrm{)}^2$ triangle diagram.

The equivalent versions of equation B.1 can be adapted by reading off the additional group theory factors arising at the vertices. For the $\mathrm{SU(N}_f\mathrm{)}_A\mathrm{SU(N}_c\mathrm{)}^2$ diagram we have

$$\langle p,k|\partial_\mu A^{\mu,a}(0)|\Omega\rangle = -\frac{g_s^2}{16\pi^2}\mathrm{tr}(t^a\lambda^b\lambda^c)\langle p,k|\epsilon^{\alpha\nu\beta\lambda}F^b_{\alpha\nu}F^c_{\beta\lambda}|\Omega\rangle, \tag{B.2}$$

where t^a are the generators of $\mathrm{SU(N}_f\mathrm{)}$ and λ^b are the generators of $\mathrm{SU(N}_c\mathrm{)}$. We can factorise the trace over flavours and colours as $\mathrm{tr}(t^a\lambda^b\lambda^c) = \mathrm{tr}(t^a)\mathrm{tr}(\lambda^b\lambda^c)$, which vanishes as a result of the tracelessness of all SU(N) generators. Hence such a diagram doesn't suffer an ABJ-type chiral anomaly.

The second diagram of figure B.2 *is* afflicted by an ABJ-anomaly since $\mathrm{tr}(t^a)$ is

Dirac Lagrangian and is different from the QED U(1) gauge symmetry.

replaced by $\mathrm{tr}(\mathbb{I}_{N_f \times N_f}) = N_f$. Hence

$$\partial_\mu A^\mu = -\frac{N_f T(r) g_s^2}{16\pi^2} \epsilon^{\alpha\nu\beta\lambda} F^b_{\alpha\nu} F^b_{\beta\lambda}, \tag{B.3}$$

using the relation $\mathrm{tr}(\lambda^a \lambda^b) = T(r)\delta^{ab}$, where $T(r)$ is the Dynkin index of the representation r of the $\mathrm{SU(N_c)}$ group — e.g. in the fundamental representation, $T(\mathrm{F}) = \frac{1}{2}$, $\forall$ N_c and in the adjoint representation $T(\mathrm{G}) = \mathrm{N}_c$, $\forall$ N_c. This is the root of the axial singlet current being non-zero. Thus the true chiral symmetry of a chiral Dirac Lagrangian of the form in equation 2.8 is

$$\mathrm{SU(N}_f)_V \times \mathrm{SU(N}_f)_A \times \mathrm{U(1)}_V.$$

We might be convinced that the non-Abelian $\mathrm{SU}(N_f)_A$ group is anomaly-free, yet

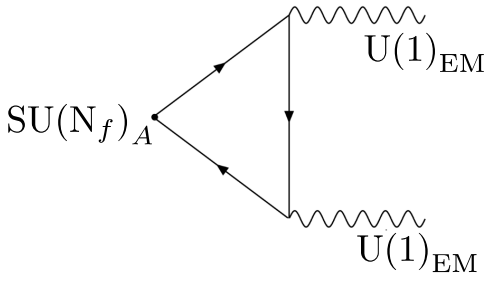

Figure B.3: The $\mathrm{SU}(N_f)_A\mathrm{U}(1)^2_{EM}$ has direct consequences relating to the decay process $\pi^0 \to \gamma\gamma$.

we're missing part of the whole picture. Quarks, being charged particles, couple under the electromagnetic interaction to photons and thus one needs to consider the triangle diagram $\mathrm{SU}(N_f)_A\mathrm{U}(1)^2_{EM}$, see figure B.3, which yields a matrix-element,

$$\langle p, k|\partial_\mu A^{\mu,a}(0)|\Omega\rangle = -\frac{1}{16\pi^2}\mathrm{tr}(t^a N_c Q^2)\langle p, k|\epsilon^{\alpha\nu\beta\lambda} F^b_{\alpha\nu} F^c_{\beta\lambda}|\Omega\rangle, \tag{B.4}$$

where Q is the quark charge matrix,

$$Q = \begin{pmatrix} q_u = +\frac{2}{3}e & 0 & 0 \\ 0 & q_d = -\frac{1}{3}e & 0 \\ 0 & 0 & \ddots \end{pmatrix}. \tag{B.5}$$

The right-hand side of B.4 vanishes identically for all off-diagonal generators. However the diagonal generators (t^3 for SU(2), t^3, t^8 for SU(3), t^3, t^8, t^{15} for SU(4) etc.) leave an anomalous term thanks to a non-vanishing $\mathrm{tr}(t^a N_c Q^2)$. In SU(2) the diagonal generator is related to the neutral pion, π^0, (see section 2.1.2) and so it is the anomalous $A^{\mu,3}$ current which leads to the decay channel, $\pi^0 \to \gamma\gamma$.

Appendix C

UV expansion of $L(\rho)$

Let's start with the metric of $AdS_5 \times S^5$ in *global coordinates* with unit radius of curvature,

$$\begin{aligned} ds^2 = &- r^2 \left(1 + \frac{1}{4r^2}\right)^2 dt^2 + r^2 \left(1 - \frac{1}{4r^2}\right)^2 d\Omega_3^2 \\ &+ \frac{1}{r^2}\left(d\rho^2 + \rho^2 d\Omega_3^2 + dL^2 + L^2 d\phi^2\right), \end{aligned} \tag{C.1}$$

where $r^2 = \rho^2 + L^2$. The metric on the D7-worldvolume is thus simply

$$\begin{aligned} ds^2_{\mathrm{D7}} = &- r^2 \left(1 + \frac{1}{4r^2}\right)^2 dt^2 + r^2 \left(1 - \frac{1}{4r^2}\right)^2 d\Omega_3^2 \\ &+ \frac{1}{r^2}\left(d\rho^2 + \rho^2 d\Omega_3^2\right). \end{aligned} \tag{C.2}$$

The D7 DBI-action is given by equation 3.3 with $F_{ab} = 0$ and $\mathcal{G}_{ab}$ given by,

$$\mathcal{G}_{ab} = \begin{pmatrix} -r^2X^2 & 0 & 0 & 0 & 0 & 0 & 0 & 0 \\ 0 & r^2Y^2 & 0 & 0 & 0 & 0 & 0 & 0 \\ 0 & 0 & r^2Y^2 & 0 & 0 & 0 & 0 & 0 \\ 0 & 0 & 0 & r^2Y^2 & 0 & 0 & 0 & 0 \\ 0 & 0 & 0 & 0 & \frac{1}{r^2}\left(1+(\partial_\rho L)^2\right) & 0 & 0 & 0 \\ 0 & 0 & 0 & 0 & 0 & \frac{\rho^2}{r^2} & 0 & 0 \\ 0 & 0 & 0 & 0 & 0 & 0 & \frac{\rho^2}{r^2} & 0 \\ 0 & 0 & 0 & 0 & 0 & 0 & 0 & \frac{\rho^2}{r^2} \end{pmatrix}, \tag{C.3}$$

with $X = \left(1 + \frac{1}{4r^2}\right)$ and $Y = \left(1 - \frac{1}{4r^2}\right)$. The action is then expressed as

$$S_{\text{D7}} \sim \int d\rho \left(1 + \frac{1}{16(\rho^2+L^2)^2}\right)\left(1 - \frac{1}{4(\rho^2+L^2)}\right)^2 \rho^3 \sqrt{1+(\partial_\rho L)^2}. \tag{C.4}$$

The equation of motion is then

$$\frac{\partial}{\partial\rho}\left(\left(1 + \frac{1}{16(\rho^2+L^2)^2}\right)\left(1 - \frac{1}{4(\rho^2+L^2)}\right)^2 \rho^3 \frac{\partial_\rho L}{\sqrt{1+(\partial_\rho L)^2}}\right) + \left(\frac{L}{(L^2+\rho^2)^2} - \frac{L}{2\left(L^2+\rho^2\right)^3} + \frac{3L}{16\left(L^2+\rho^2\right)^4} - \frac{L}{32\left(L^2+\rho^2\right)^5}\right)\rho^3\sqrt{1+(\partial_\rho L)^2} = 0. \tag{C.5}$$

Linearising in the limit $\rho \to \infty$ and $\partial_\rho L \to 0$ we get,

$$\frac{\partial}{\partial\rho}\left(\rho^3 \partial_\rho L\right) = \frac{L}{\rho}, \tag{C.6}$$

where all but the leading first term on the right-hand side of equation C.5 are negligible. The solution to the linearised equation of motion is given by

$$L(\rho) = \frac{2c_2 I_1\left(\frac{1}{\rho}\right)}{\rho} + \frac{c_1 K_1\left(\frac{1}{\rho}\right)}{2\sqrt{\pi}\rho}, \tag{C.7}$$

where I_1 and K_1 are the modified Bessel functions of the first and second kind respectively and $c_{1,2}$ are constants. The $\rho \to \infty$ limit of equation C.7 is simply,

$$L(\rho) = C_1 + \frac{C_2}{\rho^2} - C_3 \frac{\ln \rho}{\rho^2} + \mathcal{O}\left(\frac{1}{\rho^4}\right), \tag{C.8}$$

where $C_{1,2,3}$ are constants.

Appendix D

Expanding the Dynamic AdS/QCD action

The dynamic AdS/QCD action is given by,

$$S = \int d^4x d\rho \rho^3 \mathrm{Tr}\left[\frac{1}{\rho^2+L^2}(D^M X)^\dagger (D_M X) + \frac{\Delta m^2}{\rho^2}|X|^2 + \frac{1}{2g_5^2}(F_{L,MN}F_L^{MN} + F_{R,MN}F_R^{MN})\right], \tag{D.1}$$

where

$$X = L(\rho)e^{2i\pi^a t^a}. \tag{D.2}$$

We now proceed to expand the action fully, term by term. Firstly the kinetic term of the scalar X can be written as follows:

$$\begin{aligned}(D^M X)^\dagger (D_M X) = &\underbrace{\partial_M X^\dagger \partial^M X}_{=A} \\ &\underbrace{-i(\partial_M X^\dagger)L^M X + i(\partial_M X^\dagger)R^M X + iX^\dagger L_M(\partial^M X) - iR_M X^\dagger(\partial^M X)}_{=B} \\ &\underbrace{+X^\dagger L_M L^M X - X^\dagger L_M X R^M - R_M X^\dagger L^M X + R_M X^\dagger X R^M}_{=C},\end{aligned}$$

where we assume the gauge fields are Hermitian. Also assuming $L(\rho)$ is flavour-independent, i.e. all flavours have same mass, part A simplifies to,

$$A = 4L^2 \partial_\mu \pi \partial^\mu \pi + \partial_\rho L \partial^\rho L, \tag{D.3}$$

with $\pi \equiv \pi^a \tau^a$. Writing $L^M = V^M + A^M$ and $R^M = V^M - A^M$, thereby defining the vector and axial bulk gauge fields, part B simplifies to

$$B = -8L^2 (\partial_M \pi) A^M. \tag{D.4}$$

Likewise part C simplifies to

$$C = 4L^2 A_M A^M. \tag{D.5}$$

In total the scalar kinetic term expands out as,

$$\begin{aligned} \frac{(D^M X)^\dagger (D_M X)}{\rho^2 + L^2} =& \frac{1}{\rho^2 + L^2} \left[g^{\rho\rho} (\partial_\rho L)^2 + 4L^2 g^{MM} (\partial_M \pi - A_M)^2 \right] \\ =& (\partial_\rho L)^2 + 4L^2 A_\rho^2 + \frac{4L^4}{(\rho^2 + L^2)^2} (\partial_\mu \pi - A_\mu)^2 . \end{aligned} \tag{D.6}$$

The mass term simplifies to

$$\frac{\Delta m^2}{\rho^2} X^\dagger X = \frac{\Delta m^2}{\rho^2} L^2. \tag{D.7}$$

The gauge kinetic term can be expanded in terms of the vector and axial fields, V^M and A^M, as follows

$$\begin{aligned} F_{L,MN} F_L^{MN} + F_{R,MN} F_R^{MN} =& F_{V,MN} F_V^{MN} + F_{A,MN} F_A^{MN} \\ =& (\partial_M V_N^a - \partial_N V_M^a) \left(\partial^M V^{a,N} - \partial^N V^{a,M} \right) + \\ & (\partial_M A_N^a - \partial_N A_M^a) \left(\partial^M A^{a,N} - \partial^N A^{a,M} \right), \end{aligned} \tag{D.8}$$

where we have used $t^a t^b = \frac{1}{2} \delta^{ab}$.

Appendix E

Vector-field equation of motion

Consider the bottom-up AdS/QCD action 3.23 on an AdS_5 background,

$$ds^2 = \frac{1}{z^2}\left(\eta_{ij}dx^i dx^j + dz^2\right) \equiv \frac{1}{z^2}\eta_{MN}dx^M dx^N. \tag{E.1}$$

The action of the vector fields V_M^a is given by (with $\sqrt{-g} = z^{-5}$)

$$\begin{aligned} S_V &= \int d^5x \, \frac{1}{z^5}\mathrm{Tr}\left[\frac{1}{2g_5^2}\left(\partial_M V_N^a - \partial_N V_M^a\right)\left(\partial^M V^{a,N} - \partial^N V^{a,M}\right)\right] \\ &= \int d^5x \, \mathrm{Tr}\left[\frac{1}{2g_5^2}\frac{1}{z^5}z^2\eta^{MR}z^2\eta^{NS}\left(\partial_M V_N^a - \partial_N V_M^a\right)\left(\partial_R V_S^a - \partial_S V_R^a\right)\right] \\ &= \int d^5x \, \mathrm{Tr}\left[\frac{1}{2g_5^2}\frac{1}{z}\eta^{MR}\eta^{NS}\left(\partial_M V_N^a - \partial_N V_M^a\right)\left(\partial_R V_S^a - \partial_S V_R^a\right)\right] \end{aligned} \tag{E.2}$$

The equation of motion for V_M^a can then be found by requiring that the functional change in the action, $\delta S_V^a = S_V[V^a + \delta V^a] - S_V[V^a]$, vanishes. To first order in δV_M^a,

$$\begin{aligned} \delta S_V^a = \int d^5x \, \mathrm{Tr}\Bigg[\frac{1}{2g_5^2}\frac{1}{z}\eta^{MR}\eta^{NS}\{&\left(\partial_M V_N^a - \partial_N V_M^a\right)\left(\partial_R \delta V_S^a - \partial_S \delta V_R^a\right) \\ &+ \left(\partial_M \delta V_N^a - \partial_N \delta V_M^a\right)\left(\partial_R V_S^a - \partial_S V_R^a\right)\}\Bigg]. \end{aligned} \tag{E.3}$$

Expanding the brackets and performing integration by parts to 'remove' the derivative from δV_M^a, we arrive at

$$\delta S^a = -4\int d^5x \mathrm{Tr}\left[\eta^{MR}\eta^{NS}\partial_S\left(\frac{1}{z}\left(\partial_N V_M^a - \partial_M V_N^a\right)\right)\delta V_R^a\right], \tag{E.4}$$

such that the equation of motion is simply,

$$\eta^{NR}\partial_R\left(\frac{1}{z}\left(\partial_N V_M^a - \partial_M V_N^a\right)\right) = 0. \tag{E.5}$$

Letting $V_M^a = \varepsilon_M V^a(z)e^{-iq\cdot x}$, the equation of motion is given by

$$-\frac{\eta^{\mu\nu}q_\mu q_\nu}{z}V^a - \frac{\eta^{\mu\nu}}{z}\partial_\nu\partial_\sigma V_\mu^a + \partial_z\left(\frac{1}{z}\partial_z V^a(z)\right) - \partial_z\left(\frac{1}{z}\partial_\sigma V_z^a\right) = 0. \tag{E.6}$$

Using the knowledge that V_M^a is massless and therefore transverse, $\partial^M V_M^a = 0$, the second term of equation E.6 vanishes. The last term can be gauged away by utilising the gauge freedom of the action, gauge fixing with $V_z^a = 0$, thus leaving

$$-\frac{\eta^{\mu\nu}q_\mu q_\nu}{z}V^a(z) + \partial_z\left(\frac{1}{z}\partial_z V^a(z)\right) = 0. \tag{E.7}$$

Turning our focus back to the dynamic AdS/QCD model, the metric 3.30, in the limit $\rho \to \infty$ where $\rho \gg L$, returns to that of AdS_5 with $z = \frac{1}{\rho}$. Performing this change of coordinates requires $\partial_z \to -\rho^2\partial_\rho$ and so the equation of motion becomes (dividing through by ρ^2)

$$\partial_\rho\left(\rho^3\partial_\rho V^a(\rho)\right) - \frac{q^2}{\rho}V^a(\rho) = 0. \tag{E.8}$$

The solution to this equation of motion with the boundary condition $V(\infty) = 1$, such that the solution matches on to the field theory current at the boundary, is given by

$$V^a(\rho) = \frac{2c_0}{q\rho}I_1\left(\frac{q}{\rho}\right) + \frac{q}{\rho}K_1\left(\frac{q}{\rho}\right), \tag{E.9}$$

where I_1 and K_1 are modified Bessel functions of the first and second kind respectively and c_0 is a constant. The $\rho \to \infty$ (UV) limit is then calculated to be

$$V^a(\rho) = 1 + \frac{q^2}{4\rho^2}\ln\left(\frac{q^2}{\rho^2}\right) + ... \tag{E.10}$$

Appendix F

Derivation of $\langle \bar{q}q \rangle^*$

To obtain the chiral condensate, $\langle \bar{q}q \rangle^*$, we first substitute the solution

$$L = \frac{m^*}{\rho^{\gamma^*}} + \frac{c^*}{\rho^{2-\gamma^*}}, \tag{F.1}$$

into the action

$$S = \int d^4x \; d\rho \; \rho^3 \left[(\partial_\rho L)^2 + \Delta m^2 \frac{L^2}{\rho^2} \right], \tag{F.2}$$

giving us

$$\begin{aligned} S \sim \int d\rho \Bigg\{ \rho^3 \Bigg(& -\frac{(\gamma^*)^2 (m^*)^2}{\rho^{2\gamma^*+2}} + \frac{(\gamma^*-2)^2 (c^*)^2}{\rho^{6-2\gamma^*}} - \frac{2\gamma^*(\gamma^*-2) m^* c^*}{\rho^4} \Bigg) \\ & + \Delta m^2 \rho \left(\frac{(m^*)^2}{\rho^{2\gamma^*}} + \frac{(c^*)^2}{\rho^{4-2\gamma^*}} + \frac{2m^*c^*}{\rho^2} \right) \Bigg\}. \end{aligned} \tag{F.3}$$

Grouping like powers of ρ we simplify F.3 to

$$S \sim \int d\rho \left\{ \rho^{1-2\gamma^*} \left((\gamma^*)^2 + \Delta m^2 \right) (m^*)^2 + \frac{2c^*}{\rho} \left[\gamma^*(2-\gamma^*) + \Delta m^2 \right] m^* + ... \right\} \tag{F.4}$$

where the '+...' refers to terms not-containing m^* — these c^*-only contributions will vanish when we take a functional derivative of the partition function with respect to μ^*. We next perform the integral between ρ_{IR} and Λ_{UV}. Concentrating on the diverging

UV parts, we have

$$S = \frac{\rho^{2-2\gamma^*}}{2(1-\gamma^*)}\left((\gamma^*)^2 + \Delta m^2\right)(m^*)^2 + \frac{2c^*}{\ln}(\rho)\left(\gamma^*(2-\gamma^*) + \Delta m^2\right)m^* + ... \qquad \text{(F.5)}$$

We now take $\langle\bar{q}q\rangle^* = \frac{1}{Z}\frac{\delta Z}{\delta m^*}$,

$$\langle\bar{q}q\rangle^* = \frac{(\gamma^*)^2 + \Delta m^2}{1-\gamma^*} m^* \Lambda^{2-2\gamma^*} + 2\ln(\Lambda)c^*\left(\gamma^*(2-\gamma^*) + \Delta m^2\right). \qquad \text{(F.6)}$$

Appendix G

Derivation of fixed point mass and condensate

To derive m^* and c^*, we take the two IR boundary conditions,

$$L\left(\rho = \rho_{IR}\right) = \rho_{IR} \tag{G.1}$$

and

$$\partial_\rho L|_{\rho=\rho_{IR}} = 0, \tag{G.2}$$

and apply them to the fixed point solution for the scalar L

$$L = \frac{m^*}{\rho^{\gamma^*}} + \frac{c^*}{\rho^{2-\gamma^*}}. \tag{G.3}$$

The condition G.1 gives us explicitly

$$\rho_{IR} = \frac{m^*}{\rho_{IR}^{\gamma^*}} + \frac{c^*}{\rho_{IR}^{2-\gamma^*}}, \tag{G.4}$$

implying

$$c^* = \rho_{IR}^{3-\gamma^*} - \rho_{IR}^{2-2\gamma^*} m^*. \tag{G.5}$$

The second boundary condition G.2 likewise implies

$$c^* = \frac{\rho_{IR}^{2-2\gamma^*}\gamma^* m^*}{\gamma^* - 2}. \tag{G.6}$$

Equating G.5 and G.6 allows us to find m^*,

$$m^* = \left(\frac{\gamma^* - 2}{2\gamma^* - 2}\right)\rho_{IR}^{1+\gamma^*}. \tag{G.7}$$

Rearranging G.7 as

$$\rho_{IR} = \left(\frac{2\gamma^* - 2}{\gamma^* - 2}\right)(m^*)^{\frac{1}{1+\gamma^*}}, \tag{G.8}$$

and substituting G.8 into G.1 or G.2 give us c^*:

$$c^* = \frac{\gamma^*}{2\gamma^* - 2}\left(\frac{2\gamma^* - 2}{\gamma^* - 2}\right)^{\frac{3-\gamma^*}{1+\gamma^*}}(m^*)^{\frac{3-\gamma^*}{1+\gamma^*}}. \tag{G.9}$$

Appendix H

Derivation of k

In the perturbative region ($\alpha_s \ll 1$) in the far-UV, the one-loop beta-function has a logarithmic solution

$$\alpha_s(\mu) = \frac{1}{\beta_0 \ln \mu}. \tag{H.1}$$

Since $\Delta m^2 = -2\gamma_1$ and

$$\gamma_1(\mu) = \frac{3C_2(R)}{2\pi}\alpha_s(\mu), \tag{H.2}$$

it follows that (bearing in mind that in the UV $L \ll \rho$ and so $\mu = \sqrt{\rho^2 + L^2} \approx \rho$),

$$\Delta m^2 = -\frac{3C_2(R)}{\pi}\frac{1}{\beta_0 \ln \rho}. \tag{H.3}$$

Setting

$$\xi = -\frac{3C_2(R)}{\pi\beta_0}, \tag{H.4}$$

L has the equation of motion

$$\partial_\rho \left(\rho^3 \partial_\rho L\right) - \frac{\xi}{\ln \rho}\rho L = 0. \tag{H.5}$$

Assuming the equation of motion has solutions of the form

$$L(\rho) = \frac{m}{(\ln \rho)^k}, \tag{H.6}$$

for some other constant k, by substituting H.6 into H.5 we find

$$-\frac{2\rho k m}{(\ln\rho)^{k+1}} - \frac{k(1+k)\rho m}{(\ln\rho)^{2+k}} = \frac{\rho\xi m}{(\ln\rho)^{k+1}}. \tag{H.7}$$

Since the second term on the left-handside is subleading in the UV, we can ignore it and we find the relation $\xi = -2k$. That is

$$k = \frac{3C_2(R)}{2\pi\beta_0}. \tag{H.8}$$

Appendix I

The Banks-Casher Relation

Despite the strongly coupled nature of QCD, there are a few analytical relations which can be nonetheless derived. One such is the *Banks-Casher* relation [223] which relates the value of the chiral condensate to the density of the eigenvalue of the Dirac operator in limit of vanishing eigenvalue. A derivation is as follows and is based on [25].

The QCD *partition function*:

$$\mathcal{Z}_{\text{QCD}} = \int \left(\prod_{\mu,a} \mathcal{D}A^a_\mu \right) \prod_f \mathcal{D}\bar{\psi}_f \mathcal{D}\psi_f e^{-\int d^4x \bar{\psi}_f (i\not{D} - m_f)\psi_f} e^{-S_{YM}}, \tag{I.1}$$

where,

$$S_{YM} = -\frac{1}{4g^2} \int F^a_{\mu\nu} F^{\mu\nu}_a d^4x. \tag{I.2}$$

We start by rewriting the fermion fields of QCD, $\psi(x)$ and $\bar{\psi}(x)$, in terms of the eigenfunctions of the Dirac operator $\not{D}$;

$$\psi(x) = \sum_n b_n u_n(x), \tag{I.3}$$

such that

$$\not{D} u_n(x) = \lambda_n u_n(x), \quad \int d^4x \, u^\dagger_m u_n = \delta_{mn}, \tag{I.4}$$

where b_n are Grassmann coefficients and λ are the respective eigenvalues.

The QCD *partition function* can be written down as

$$\mathcal{Z}_{\text{QCD}} = \int \left(\prod_{\mu,a} \mathcal{D}A^a_\mu \right) \prod_f \mathcal{D}\bar{\psi}_f \mathcal{D}\psi_f e^{-\int d^4x \bar{\psi}_f (i\not{D} - m_f)\psi_f} e^{-S_{YM}}, \tag{I.5}$$

where,

$$S_{YM} = -\frac{1}{4g^2} \int F^a_{\mu\nu} F^{\mu\nu}_a d^4x. \tag{I.6}$$

Re-expressing the fermion fields in terms of the Dirac eigenfunction basis I.3, the QCD partition function becomes

$$\mathcal{Z}_{\text{QCD}} = \int \prod_n db_n db^*_n \prod_{\mu,a} \mathcal{D}A^a_\mu e^{-S_{YM}} e^{-\int d^4x \; b^*_n u^\dagger_n (i\not{D} - m_f) b_m u_m},$$

where there is an intrinsic summation of m and n. This simplifies to

$$\int \prod_n db_n db^*_n \prod_{\mu,a} \mathcal{D}A^a_\mu e^{-S_{YM}} e^{-b^*_n b_n (i\lambda_n - m_f)}, \tag{I.7}$$

for which we can perform a Gaussian integral over the Grassmannian variables[1] b_n and b^*_n to leave us with

$$\int \prod_{\mu,a} \mathcal{D}A^a_\mu e^{-S_{YM}} \prod_n (i\lambda_n - m_f). \tag{I.8}$$

The quark propagator may then be expressed as

$$\langle \psi_f(x) \bar{\psi}_f(y) \rangle = \frac{1}{\mathcal{Z}_{QCD}} \int \prod_n db_n db^*_n \left(\sum_i b_i u_i(x) \right) \left(\sum_j b^*_j u^\dagger_j(y) \right) e^{-b^*_n b_n (i\lambda_n - m_f)}, \tag{I.9}$$

which becomes

$$\langle \psi_f(x) \bar{\psi}_f(y) \rangle = \frac{1}{\mathcal{Z}_{QCD}} \sum_n u_n(x) u^*_n(y) \prod_{m \neq n} (i\lambda_m - m_f) \tag{I.10}$$

after the Grassmannian integration is completed. Now using the form of $\mathcal{Z}_{QCD}$ from I.5

[1] The Gaussian integral is undertaken as

$$\int db db^* e^{-b^* M b} = \det M,$$

for any matrix operator M and Grassmannian variables b and b^*.

we reach

$$\langle \psi_f(x)\bar{\psi}_f(y)\rangle = \sum_n \frac{u_n(x)u_n^*(y)}{i\lambda_n - m_f}, \tag{I.11}$$

with all but a sole $(i\lambda_n - m_f)$ cancelling between the numerator and denominator.

In order to obtain the condensate, we must integrate over all spacetime and find the average (i.e. $\frac{1}{\text{Vol}}\int d^4x$),

$$\langle \psi\bar{\psi}\rangle_f = \frac{1}{V}\int d^4x\ \langle \psi_f(x)\bar{\psi}_f(y)\rangle = \frac{1}{V}\int d^4x\ \sum_n \frac{u_n(x)u_n^*(y)}{i\lambda_n - m_f}, \tag{I.12}$$

leaving us with

$$\langle \psi\bar{\psi}\rangle_f = \sum_n \frac{1}{i\lambda_n - m_f}. \tag{I.13}$$

Due to the relation $\{\gamma^m, \gamma^5\} = 0$ and hence $\{\not{D}, \gamma^5\} = 0$, it can be shown that for every eigenfunction u_n of $\not{D}$ having eigenvalue λ_n, there is another eigenfunction $\gamma^5 u_n$ with eigenvalue $-\lambda_n$:

$$\not{D}\left(\gamma^5 u_n\right) = -\gamma^5 \not{D} u_n = -\lambda_n \gamma^5 u_n. \tag{I.14}$$

Using this information, we can write the result in I.13 as,

$$\langle \psi\bar{\psi}\rangle_f = \sum_{\lambda_n>0}\left(\frac{1}{i\lambda_n - m_f} + \frac{1}{-i\lambda_n - m_f}\right) = \sum_{\lambda_n>0}\frac{-2m_f}{\lambda_n^2 + m_f^2}, \tag{I.15}$$

noting that the number of eigenvalues of the Dirac operator that vanish also vanishes[2]. In the thermodynamic limit, the eigenvalues become continuous so the result is of the form,

$$\langle \psi\bar{\psi}\rangle_f \int d\lambda\ g_\lambda\, \rho(\lambda)\frac{-2}{\lambda_n^2 + m_f^2}, \tag{I.16}$$

where $\rho(\lambda)$ is the density of (eigenvalue) states function and g_λ is the degeneracy factor of the states.

As per usual, one can work out the density of states by considering the number of

[2]This is because the number of vanishing eigenvalues of the Dirac operator is exactly the topological charge or Pontryagin index of the field theory, which in QCD is vanishingly small by experiment.

allowed states with a value of λ between λ and $\lambda + d\lambda$,

$$\rho(\lambda)d\lambda = \frac{\text{volume in } \lambda\text{-space of } \frac{1}{2^D} \text{ of D-dimensional spherical shell } (\lambda > 0)}{\text{volume in } \lambda\text{-space occupied per each state}}. \quad \text{(I.17)}$$

So in a D-dimensional spacetime we have

$$\rho(\lambda)d\lambda = \frac{\frac{1}{2^D} \times \frac{2\pi^{\frac{D}{2}}}{\Gamma(\frac{D}{2})}}{\frac{\pi^D}{V_D}}. \quad \text{(I.18)}$$

Or, for $D = 4$,

$$\rho(\lambda)d\lambda = \frac{\frac{1}{8}\pi^2\lambda^3 d\lambda}{\frac{\pi^4}{V_4}} = \frac{V_4\lambda^3}{8\pi^2}d\lambda. \quad \text{(I.19)}$$

This form of $\rho(\lambda)$ is only strictly valid in the non-interacting QCD theory, as we will discuss below. The degeneracy of the eigenvalues g_λ is $2N_c$ because we now have two eigenfunctions associated to each eigenvalue and have N_c variations of each fermion field.

Equation I.16 is however somewhat ill-defined. In the free ($A_\mu = 0$) case, whereby the eigenfunctions $u(x)$ can be associated to plane-wave solutions, the eigenvalues are just the momentum of the state,

$$\not{D}_{\text{free}} e^{ik\cdot x} = i\not{k} e^{ik\cdot x}.$$

But with this in mind, the integral of equation I.16 diverges as Λ_{UV} for some ultraviolet cutoff Λ_{UV}. A solution to this problem is to take the *chiral limit* in which $m_f \to 0$ much faster than $\Lambda_{\text{UV}} \to \infty$. We first recall that we can define the delta-function as the limit,

$$\delta(x) = \lim_{\varepsilon \to 0} \frac{1}{\pi} \frac{2\varepsilon}{x^2 + \varepsilon^2},$$

to write the corresponding part of the integrand of I.16 as,

$$\langle \psi\bar{\psi} \rangle = -\int d\lambda g_\lambda \rho(\lambda)\, \pi\delta(\lambda).$$

The integral is no-longer providing us with a divergence and we arrive at the famous

Banks-Casher relation

$$\langle \psi \bar{\psi} \rangle = -\pi \rho(0).$$

It is now evident that the necessary condition for the condensate to exist is $\rho(0) \neq 0$ (the free theory whereby $\rho(\lambda) \sim \lambda^3$ does not satisfy this criterion). We must conclude that whichever mechanism gives rise to chiral symmetry breaking and thus a non-zero condensate arises from the vacuum field configurations which yield a non-zero spectral density, $\rho(\lambda)$.

Appendix J

Vafa-Witten Theorem

The Vafa-Witten theorem states that in a *vector-like gauge theory*[1] (like QCD), vector symmetries cannot be spontaneously broken [207]. We show the proof of this below, again following [25].

Consider a QCD-like field theory with two *massive* quark flavours u and d: $m_u = m_d \neq 0$. Consider the set of Euclidean correlators

$$C_\Gamma(x,y) \equiv \langle J^{\bar{u}d}(x) J^{\bar{d}u}(y)\rangle, \tag{J.1}$$

where

$$J^{\bar{u}d} = \bar{u}\Gamma d, \quad J^{\bar{d}u} = \bar{d}\Gamma u, \tag{J.2}$$

for

$$\Gamma \in \{1, \gamma^5, i\gamma_\mu, \gamma_\mu\gamma^5, i\sigma_{\mu\nu}\}. \tag{J.3}$$

Inserting a complete set of states into C_Γ,

$$C_\Gamma(x,y) = \sum_n \langle 0|J^{\bar{u}d}(x,0)|n\rangle\langle n|e^{-iE_n t} J^{\bar{d}u}(y,0)|0\rangle, \tag{J.4}$$

we see that the asymptotic, late time behaviour is dominated by the lightest state (with

[1] Gauge theories are historically called 'vector-like' if Dirac mass terms can be written down in the Lagrangian without breaking the gauge symmetry. A term $-m\bar{\psi}\psi$ is written in terms of its left- and right-handed components as $-m\left(\bar{\psi}_L\psi_R + \bar{\psi}_R\psi_L\right)$ and so the left- and right-handed fields must be in the same representation of the gauge group with equal and opposite charge under that group. This is not true of the electroweak sector which is referred to as a *chiral gauge theory* and wherein masses must be generated via Yukawa terms coupled to a Higgs field.

lowest E_n) pertaining to the Γ-channel,

$$C_\Gamma \sim e^{-M_\Gamma t}. \tag{J.5}$$

We can also express the correlator in terms of the QCD partition function as

$$C_\Gamma(x,y) = -\frac{1}{\mathcal{Z}} \int \prod_{\mu,a} \mathcal{D}A^a_\mu(x) \prod_f \det|m_f - i\not{D}| e^{-S_{YM}} \mathrm{Tr}\left\{\Gamma G(x,y)\Gamma G(y,x)\right\}, \tag{J.6}$$

where $G(x,y)$ are Euclidean Greens function,

$$G(x,y) = \langle \psi(x)\bar{\psi}(y)\rangle. \tag{J.7}$$

From equation I.13, we can rewrite the Greens function as

$$G(x,y) = \sum_n \frac{u_n(x)u_n^\dagger(y)}{m_f - i\lambda_n}, \tag{J.8}$$

where u_n are eigenfunction of $\not{D}$ with eigenvalue λ_n. For every eigenfunction u_n of eigenvalue λ_n, there exists an eigenfunction $\gamma^5 u_n$ with eigenvalue $-\lambda_n$ and so we can

write

$$\gamma^5 G(x,y)\gamma^5 = \sum_n \frac{\gamma^5 u_n(x) u_n^\dagger(y)\gamma^5}{m - i\lambda_n}$$

$$= \sum_n \frac{(\gamma^5 u_n(x))(\gamma^5 u_n(y))^\dagger}{m - i\lambda_n}$$

$$= \sum_m \frac{u_m(x) u_m^\dagger(y)}{m + i\lambda_m}$$

$$= \left(\sum_m \frac{u_m(y) u_m^\dagger(x)}{m - i\lambda_m} \right)^\dagger$$

$$= G(y,x)^\dagger. \tag{J.9}$$

Using this identity inside J.6 with $\Gamma = \gamma^5$, we arrive at

$$C_{\gamma^5}(x,y) = -\frac{1}{\mathcal{Z}} \int \prod_{\mu,a} \mathcal{D}A_\mu^a(x) \prod_f \det |m_f - i\not{D}| e^{-S_{YM}} \mathrm{Tr} \left\{ |G(x,y)_G|^2 \right\}, \tag{J.10}$$

which, because of the factor of $|G|^2$ implies that

$$C_\Gamma \leq C_{\gamma^5}, \tag{J.11}$$

or from J.5,

$$M_\Gamma \geq M_{\gamma^5}. \tag{J.12}$$

This therefore implies, that the lightest *pseudoscalar* state associated with the γ_5 channel must be the lighter than any other bound state, from any other Γ-channel. So, were a vector symmetry to be spontaneously broken, massless *scalar* Goldstone particles would be present in the spectrum. However, the inequality above insists that there must also be massless *pseudoscalars* in the particle spectrum if this is the case. Since we have assumed that the quark masses are finite and therefore explicitly breaking any axial

symmetries the theory might otherwise have, no such massless pseudoscalars can exist in the spectrum. Hence, we must conclude that the spontaneous breaking of a vector symmetry in this scenario is forbidden.

Bibliography

[1] Nick Evans and Marc Scott. Hyper-Scaling Relations in the Conformal Window from Dynamic AdS/QCD. *Phys. Rev.*, D90(6):065025, 2014, 1405.5373.

[2] Johanna Erdmenger, Nick Evans, and Marc Scott. Meson spectra of asymptotically free gauge theories from holography. *Phys. Rev.*, D91(8):085004, 2015, 1412.3165.

[3] Nick Evans, Carlisson Miller, and Marc Scott. Inverse Magnetic Catalysis in Bottom-Up Holographic QCD. 2016, 1604.06307.

[4] Nick Evans, Tim R. Morris, and Marc Scott. Translational symmetry breaking in field theories and the cosmological constant. *Phys. Rev.*, D93(2):025019, 2016, 1507.02965.

[5] Nick Evans, Peter Jones, and Marc Scott. Soft walls in dynamic AdS/QCD and the technidilaton. *Phys. Rev.*, D92(10):106003, 2015, 1508.06540.

[6] J. Chadwick. The existence of a neutron. *Proceedings of the Royal Society of London A: Mathematical, Physical and Engineering Sciences*, 136(830):692–708, 1932, http://rspa.royalsocietypublishing.org/content/136/830/692.full.pdf.

[7] H. Yukawa. On the Interaction of Elementary Particles. *Proc.Phys.Math.Soc.Jap.*, 17(48), 1935.

[8] Stanley Deser. How special relativity determines the signs of the nonrelativistic, Coulomb and Newtonian, forces. *Am. J. Phys.*, 73:6, 2005, gr-qc/0411026.

[9] Seth H. Neddermeyer and Carl D. Anderson. Note on the nature of cosmic-ray particles. *Phys. Rev.*, 51:884–886, May 1937.

[10] L.M. Brown and H. Rechenberg. *The Origin of the Concept of Nuclear Forces*. Taylor and Francis, 1996.

[11] Rochester, G. D. and Butler, C. C. Evidence for the Existence of New Unstable Elementary Particles. *Nature*, 160:855–857, Dec 1947.

[12] Hopper, V. D. and Biswas, S. Evidence Concerning the Existence of the New Unstable Elementary Neutral Particle. *Physical Review*, 80:1099–1100, Dec 1950.

[13] R Armenteros, K.H. Barker, C.C. Butler, A. Cachon, and C.M. York. Lvi. the properties of charged v-particles. *The London, Edinburgh, and Dublin Philosophical Magazine and Journal of Science*, 43(341):597–611, 1952, http://dx.doi.org/10.1080/14786440608520216.

[14] Luis W. Alvarez, Philippe Eberhard, Myron L. Good, William Graziano, Harold K. Ticho, and Stanley G. Wojcicki. Neutral cascade hyperon event. *Phys. Rev. Lett.*, 2:215–219, Mar 1959.

[15] M. Meer et al. The decays of the and the mesons. In *High-energy physics. Proceedings, 11th International Conference, ICHEP'62, Geneva, Switzerland, Jul 4-11, 1962*, pages 103–107, 1962.

[16] A. Pevsner et al. Evidence for a Three Pion Resonance Near 550-MeV. *Phys. Rev. Lett.*, 7:421–423, 1961.

[17] V. E. Barnes, P. L. Connolly, D. J. Crennell, B. B. Culwick, W. C. Delaney, W. B. Fowler, P. E. Hagerty, E. L. Hart, N. Horwitz, P. V. C. Hough, J. E. Jensen, J. K. Kopp, K. W. Lai, J. Leitner, J. L. Lloyd, G. W. London, T. W. Morris, Y. Oren, R. B. Palmer, A. G. Prodell, D. Radojičić, D. C. Rahm, C. R. Richardson, N. P. Samios, J. R. Sanford, R. P. Shutt, J. R. Smith, D. L. Stonehill, R. C. Strand, A. M. Thorndike, M. S. Webster, W. J. Willis, and S. S. Yamamoto. Observation of a hyperon with strangeness minus three. *Phys. Rev. Lett.*, 12:204–206, Feb 1964.

[18] Murray Gell-Mann. The Eightfold Way: A Theory of strong interaction symmetry. 1961.

[19] Murray Gell-Mann. Symmetries of baryons and mesons. *Phys. Rev.*, 125:1067–1084, 1962.

[20] Murray Gell-Mann. A Schematic Model of Baryons and Mesons. *Phys. Lett.*, 8:214–215, 1964.

[21] Han, M. Y. and Nambu, Yoichiro. Three Triplet Model with Double SU(3) Symmetry. *Phys. Rev.*, 139:B1006–B1010, 1965.

[22] O. W. Greenberg. Spin and unitary-spin independence in a paraquark model of baryons and mesons. *Phys. Rev. Lett.*, 13:598–602, Nov 1964.

[23] E. D. Bloom, D. H. Coward, H. DeStaebler, J. Drees, G. Miller, L. W. Mo, R. E. Taylor, M. Breidenbach, J. I. Friedman, G. C. Hartmann, and H. W. Kendall. High-Energy Inelastic $e - p$ Scattering at 6^o and 10^o. *Phys. Rev. Lett.*, 23:930–934, Oct 1969.

[24] M. Breidenbach, J. I. Friedman, H. W. Kendall, E. D. Bloom, D. H. Coward, H. DeStaebler, J. Drees, L. W. Mo, and R. E. Taylor. Observed behavior of highly inelastic electron-proton scattering. *Phys. Rev. Lett.*, 23:935–939, Oct 1969.

[25] Andrei Smilga. *Lectures on quantum chromodynamics*. World Scientific, Singapore, 2001.

[26] H. Fritzsch, Murray Gell-Mann, and H. Leutwyler. Advantages of the Color Octet Gluon Picture. *Phys. Lett.*, B47:365–368, 1973.

[27] Jogesh C. Pati and Abdus Salam. Unified Lepton-Hadron Symmetry and a Gauge Theory of the Basic Interactions. *Phys. Rev.*, D8:1240–1251, 1973.

[28] Steven Weinberg. Nonabelian Gauge Theories of the Strong Interactions. *Phys. Rev. Lett.*, 31:494–497, 1973.

[29] C. N. Yang and R. L. Mills. Conservation of isotopic spin and isotopic gauge invariance. *Phys. Rev.*, 96:191–195, Oct 1954.

[30] David J. Gross and Frank Wilczek. Ultraviolet behavior of non-abelian gauge theories. *Phys. Rev. Lett.*, 30:1343–1346, Jun 1973.

[31] H. David Politzer. Reliable perturbative results for strong interactions? *Phys. Rev. Lett.*, 30:1346–1349, Jun 1973.

[32] Juan Martin Maldacena. The Large N limit of superconformal field theories and supergravity. *Int. J. Theor. Phys.*, 38:1113–1133, 1999, hep-th/9711200. [Adv. Theor. Math. Phys.2,231(1998)].

[33] Leonard Susskind. The World as a hologram. *J. Math. Phys.*, 36:6377–6396, 1995, hep-th/9409089.

[34] Murray Gell-Mann and M Levy. The axial vector current in beta decay. *Nuovo Cim.*, 16:705, 1960.

[35] Emmy Noether. Invariant Variation Problems. *Gott. Nachr.*, 1918:235–257, 1918, physics/0503066. [Transp. Theory Statist. Phys.1,186(1971)].

[36] Sidney Coleman. The invariance of the vacuum is the invariance of the world. *J-J-MATH-PHYS*, 7(5):787–787, May 1966.

[37] Yoichiro Nambu. Quasi-particles and gauge invariance in the theory of superconductivity. *Phys. Rev.*, 117:648–663, Feb 1960.

[38] J. Goldstone. Field theories with superconductor solutions. *Il Nuovo Cimento (1955-1965)*, 19(1):154–164, 1961.

[39] Stefan Scherer and Matthias R. Schindler. A Chiral perturbation theory primer. 2005, hep-ph/0505265.

[40] K. A. Olive et al. Review of Particle Physics. *Chin. Phys.*, C38:090001, 2014.

[41] Michael E. Peskin and Daniel V. Schroeder. *An Introduction to quantum field theory*. 1995.

[42] Curtis G. Callan. Broken scale invariance in scalar field theory. *Phys. Rev. D*, 2:1541–1547, Oct 1970.

[43] K. Symanzik. Small distance behaviour in field theory and power counting. *Communications in Mathematical Physics*, 18(3):227–246, 1970.

[44] Dennis D. Dietrich and Francesco Sannino. Conformal window of SU(N) gauge theories with fermions in higher dimensional representations. *Phys. Rev.*, D75:085018, 2007, hep-ph/0611341.

[45] William E. Caswell. Asymptotic behavior of non-abelian gauge theories to two-loop order. *Phys. Rev. Lett.*, 33:244–246, Jul 1974.

[46] Tom Banks and A. Zaks. On the Phase Structure of Vector-Like Gauge Theories with Massless Fermions. *Nucl. Phys.*, B196:189–204, 1982.

[47] Kenneth G. Wilson. Confinement of quarks. *Phys. Rev. D*, 10:2445–2459, Oct 1974.

[48] Siegfried Bethke. Experimental tests of asymptotic freedom. *Prog. Part. Nucl. Phys.*, 58:351–386, 2007.

[49] Thomas Appelquist, John Terning, and L. C. R. Wijewardhana. Zero temperature chiral phase transition in su(N) gauge theories. *Phys. Rev. Lett.*, 77:1214–1217, Aug 1996.

[50] Thomas Appelquist, Anuradha Ratnaweera, John Terning, and L. C. R. Wijewardhana. Phase structure of an SU(n) gauge theory with N_f flavors. *Phys. Rev. D*, 58:105017, Oct 1998.

[51] Thomas A. Ryttov and Francesco Sannino. Supersymmetry inspired qcd beta function. *Phys. Rev. D*, 78:065001, Sep 2008.

[52] Thomas A. Ryttov and Francesco Sannino. Conformal windows of su(n) gauge theories, higher dimensional representations, and the size of the unparticle world. *Phys. Rev. D*, 76:105004, Nov 2007.

[53] Francesco Sannino and Joseph Schechter. Chiral phase transition for SU(n) gauge theories via an effective lagrangian approach. *Phys. Rev. D*, 60:056004, Aug 1999.

[54] Adi Armoni. The Conformal Window from the Worldline Formalism. *Nucl. Phys.*, B826:328–336, 2010, 0907.4091.

[55] Holger Gies and Joerg Jaeckel. Chiral phase structure of QCD with many flavors. *Eur. Phys. J.*, C46:433–438, 2006, hep-ph/0507171.

[56] Thomas DeGrand. Finite-size scaling tests for SU(3) lattice gauge theory with color sextet fermions. *Phys. Rev.*, D80:114507, 2009, 0910.3072.

[57] Gerard 't Hooft. A Planar Diagram Theory for Strong Interactions. *Nucl. Phys.*, B72:461, 1974.

[58] Ofer Aharony, Steven S. Gubser, Juan Martin Maldacena, Hirosi Ooguri, and Yaron Oz. Large N field theories, string theory and gravity. *Phys. Rept.*, 323:183–386, 2000, hep-th/9905111.

[59] T. Frankel. *The Geometry of Physics: An Introduction*. Cambridge University Press, 2004.

[60] V. N. Gribov. *The Theory of Complex Angular Momenta*. 2003.

[61] M.B. Green, J.H. Schwarz, and E. Witten. *Superstring Theory: Volume 1, Introduction*. Cambridge Monographs on Mathematical Physics. Cambridge University Press, 1988.

[62] J. Polchinski. *String Theory: Volume 1, An Introduction to the Bosonic String*. Cambridge Monographs on Mathematical Physics. Cambridge University Press, 1998.

[63] K. Becker, M. Becker, and J.H. Schwarz. *String Theory and M-Theory: A Modern Introduction*. Cambridge University Press, 2006.

[64] E. Kiritsis. *String Theory in a Nutshell*. In a Nutshell. Princeton University Press, 2011.

[65] D.Z. Freedman and A. Van Proeyen. *Supergravity*. Cambridge University Press, 2012.

[66] Eric D'Hoker and Daniel Z. Freedman. Supersymmetric gauge theories and the AdS / CFT correspondence. In *Strings, Branes and Extra Dimensions: TASI 2001: Proceedings*, pages 3–158, 2002, hep-th/0201253.

[67] F. Gliozzi, J. Scherk, and D. Olive. Supersymmetry, supergravity theories and the dual spinor model. *Nuclear Physics B*, 122:253–290, April 1977.

[68] Wieland Staessens and Bert Vercnocke. Lectures on Scattering Amplitudes in String Theory. In *5th Modave Summer School in Mathematical Physics Modave, Belgium, August 17-21, 2009*, 2010, 1011.0456.

[69] C.V. Johnson. *D-Branes*. Cambridge Monographs on Mathematical Physics. Cambridge University Press, 2006.

[70] P. Candelas, G. T. Horowitz, A. Strominger, and E. Witten. Vacuum configurations for superstrings. *Nuclear Physics B*, 258:46–74, 1985.

[71] Enrique Alvarez, Luis Alvarez-Gaume, and Yolanda Lozano. An Introduction to T duality in string theory. *Nucl. Phys. Proc. Suppl.*, 41:1–20, 1995, hep-th/9410237.

[72] Stefan Forste. Strings, branes and extra dimensions. *Fortsch. Phys.*, 50:221–403, 2002, hep-th/0110055.

[73] M. Ammon and J. Erdmenger. *Gauge/Gravity Duality*. Cambridge University Press, 2015.

[74] H. Năstase. *Introduction to AdS/CFT Correspondence*. Cambridge University Press, 2015.

[75] E. Papantonopoulos. *From Gravity to Thermal Gauge Theories: The AdS/CFT Correspondence*. Lecture Notes in Physics. Springer Berlin Heidelberg, 2011.

[76] P. Kerner. *Gauge/Gravity Duality: A Road Towards Reality*. Omniscriptum Gmbh & Company Kg., 2012.

[77] B. Zwiebach. *A First Course in String Theory*. Cambridge University Press, 2009.

[78] A. Gomberoff and D. Marolf. *Lectures on Quantum Gravity*. Series of the Centro De Estudios Científicos. Springer US, 2006.

[79] Charles B. Thorn. Reformulating string theory with the 1/N expansion. In *The First International A.D. Sakharov Conference on Physics Moscow, USSR, May 27-31, 1991*, pages 0447–454, 1991, hep-th/9405069.

[80] Jacob D. Bekenstein. Black holes and entropy. *Phys. Rev. D*, 7:2333–2346, Apr 1973.

[81] Edward Witten. Anti-de Sitter space and holography. *Adv. Theor. Math. Phys.*, 2:253–291, 1998, hep-th/9802150.

[82] Joshua Erlich, Emanuel Katz, Dam T. Son, and Mikhail A. Stephanov. QCD and a holographic model of hadrons. *Phys. Rev. Lett.*, 95:261602, 2005, hep-ph/0501128.

[83] Edward Witten. Anti-de Sitter space and holography. *Adv. Theor. Math. Phys.*, 2:253–291, 1998, hep-th/9802150.

[84] S. S. Gubser, Igor R. Klebanov, and Alexander M. Polyakov. Gauge theory correlators from noncritical string theory. *Phys. Lett.*, B428:105–114, 1998, hep-th/9802109.

[85] Tadakatsu Sakai and Shigeki Sugimoto. Low energy hadron physics in holographic QCD. *Prog. Theor. Phys.*, 113:843–882, 2005, hep-th/0412141.

[86] Martin Kruczenski, David Mateos, Robert C. Myers, and David J. Winters. Meson spectroscopy in AdS / CFT with flavor. *JHEP*, 07:049, 2003, hep-th/0304032.

[87] Andreas Karch and Emanuel Katz. Adding flavor to AdS / CFT. *JHEP*, 06:043, 2002, hep-th/0205236.

[88] Leandro Da Rold and Alex Pomarol. Chiral symmetry breaking from five dimensional spaces. *Nucl. Phys.*, B721:79–97, 2005, hep-ph/0501218.

[89] Timo Alho, Nick Evans, and Kimmo Tuominen. Dynamic AdS/QCD and the Spectrum of Walking Gauge Theories. *Phys. Rev.*, D88:105016, 2013, 1307.4896.

[90] Matti Jarvinen and Elias Kiritsis. Holographic Models for QCD in the Veneziano Limit. *JHEP*, 03:002, 2012, 1112.1261.

[91] Johanna Erdmenger, Nick Evans, Ingo Kirsch, and Ed Threlfall. Mesons in Gauge/Gravity Duals - A Review. *Eur. Phys. J.*, A35:81–133, 2008, 0711.4467.

[92] Andreas Karch and Lisa Randall. Open and closed string interpretation of SUSY CFT's on branes with boundaries. *JHEP*, 06:063, 2001, hep-th/0105132.

[93] Oliver DeWolfe, Daniel Z. Freedman, and Hirosi Ooguri. Holography and defect conformal field theories. *Phys. Rev.*, D66:025009, 2002, hep-th/0111135.

[94] Johanna Erdmenger, Zachary Guralnik, and Ingo Kirsch. Four-dimensional superconformal theories with interacting boundaries or defects. *Phys. Rev.*, D66:025020, 2002, hep-th/0203020.

[95] Kostas Skenderis and Marika Taylor. Branes in AdS and p p wave space-times. *JHEP*, 06:025, 2002, hep-th/0204054.

[96] Neil R. Constable and Robert C. Myers. Exotic scalar states in the AdS / CFT correspondence. *JHEP*, 11:020, 1999, hep-th/9905081.

[97] J. Babington, J. Erdmenger, Nick J. Evans, Z. Guralnik, and I. Kirsch. A Gravity dual of chiral symmetry breaking. *Fortsch. Phys.*, 52:578–582, 2004, hep-th/0312263.

[98] Andreas Karch, Emanuel Katz, Dam T. Son, and Mikhail A. Stephanov. Linear confinement and AdS/QCD. *Phys. Rev.*, D74:015005, 2006, hep-ph/0602229.

[99] M.A. Shifman, A.I. Vainshtein, and V.I. Zakharov. Qcd and resonance physics. theoretical foundations. *Nuclear Physics B*, 147(5):385 – 447, 1979.

[100] Peter Breitenlohner and Daniel Z Freedman. Stability in gauged extended supergravity. *Annals of Physics*, 144(2):249 – 281, 1982.

[101] Nathan Seiberg. Notes on theories with 16 supercharges. *Nucl. Phys. Proc. Suppl.*, 67:158–171, 1998, hep-th/9705117.

[102] V. G. Kac. Representations of Classical Lie Superalgebras. In *2nd Conference on Differential Geometrical Methods in Mathematical Physics. Bonn, Germany, July 13-16, 1977*, pages 597–626, 1977.

[103] V. K. Dobrev and V. B. Petkova. Group Theoretical Approach to Extended Conformal Supersymmetry: Function Space Realizations and Invariant Differential Operators. *Fortsch. Phys.*, 35:537, 1987.

[104] V. K. Dobrev and V. B. Petkova. All Positive Energy Unitary Irreducible Representations of Extended Conformal Supersymmetry. *Phys. Lett.*, B162:127–132, 1985.

[105] Shiraz Minwalla. Restrictions imposed by superconformal invariance on quantum field theories. *Adv. Theor. Math. Phys.*, 2:781–846, 1998, hep-th/9712074.

[106] Thomas Appelquist, Kenneth Lane, and Uma Mahanta. Ladder approximation for spontaneous chiral-symmetry breaking. *Phys. Rev. Lett.*, 61:1553–1556, Oct 1988.

[107] Andrew Cohen and Howard Georgi. Walking beyond the rainbow. *Nuclear Physics B*, 314(1):7 – 24, 1989.

[108] Yasumichi Aoki, Tatsumi Aoyama, Masafumi Kurachi, Toshihide Maskawa, Keiichi Nagai, Hiroshi Ohki, Akihiro Shibata, Koichi Yamawaki, and Takeshi Yamazaki. Many flavor QCD as exploration of the walking behavior with the approximate IR fixed point. *PoS*, LATTICE2011:080, 2011, 1202.4712.

[109] Yasumichi Aoki, Tatsumi Aoyama, Masafumi Kurachi, Toshihide Maskawa, Keiichi Nagai, Hiroshi Ohki, Akihiro Shibata, Koichi Yamawaki, and Takeshi Yamazaki. Lattice study of conformality in twelve-flavor QCD. *Phys. Rev.*, D86:054506, 2012, 1207.3060.

[110] Yasumichi Aoki, Tatsumi Aoyama, Masafumi Kurachi, Toshihide Maskawa, Keiichi Nagai, Hiroshi Ohki, Enrico Rinaldi, Akihiro Shibata, Koichi Yamawaki, and Takeshi Yamazaki. Light composite scalar in twelve-flavor QCD on the lattice. *Phys. Rev. Lett.*, 111(16):162001, 2013, 1305.6006.

[111] Anqi Cheng, Anna Hasenfratz, Gregory Petropoulos, and David Schaich. Scale-dependent mass anomalous dimension from Dirac eigenmodes. *JHEP*, 07:061, 2013, 1301.1355.

[112] Albert Deuzeman, Maria Paola Lombardo, Tiago Nunes da Silva, and Elisabetta Pallante. Bulk transitions of twelve flavor QCD and $U_A(1)$ symmetry. *PoS*, LATTICE2011:321, 2011, 1111.2590.

[113] T. Appelquist, G. T. Fleming, M. F. Lin, E. T. Neil, and D. A. Schaich. Lattice Simulations and Infrared Conformality. *Phys. Rev.*, D84:054501, 2011, 1106.2148.

[114] Anna Hasenfratz. Conformal or Walking? Monte Carlo renormalization group studies of SU(3) gauge models with fundamental fermions. *Phys. Rev.*, D82:014506, 2010, 1004.1004.

[115] Zoltan Fodor, Kieran Holland, Julius Kuti, Daniel Nogradi, and Chris Schroeder. Nearly conformal gauge theories in finite volume. *Phys. Lett.*, B681:353–361, 2009, 0907.4562.

[116] Thomas Appelquist, George T. Fleming, and Ethan T. Neil. Lattice Study of Conformal Behavior in SU(3) Yang-Mills Theories. *Phys. Rev.*, D79:076010, 2009, 0901.3766.

[117] Thomas Appelquist, George T. Fleming, and Ethan T. Neil. Lattice study of the conformal window in QCD-like theories. *Phys. Rev. Lett.*, 100:171607, 2008, 0712.0609. [Erratum: Phys. Rev. Lett.102,149902(2009)].

[118] A. Deuzeman, M. P. Lombardo, and E. Pallante. Evidence for a conformal phase in SU(N) gauge theories. *Phys. Rev.*, D82:074503, 2010, 0904.4662.

[119] Yigal Shamir, Benjamin Svetitsky, and Thomas DeGrand. Zero of the discrete beta function in SU(3) lattice gauge theory with color sextet fermions. *Phys. Rev.*, D78:031502, 2008, 0803.1707.

[120] Y. Iwasaki, K. Kanaya, S. Kaya, S. Sakai, and T. Yoshie. Phase structure of lattice QCD for general number of flavors. *Phys. Rev.*, D69:014507, 2004, hep-lat/0309159.

[121] Luigi Del Debbio and Roman Zwicky. Hyperscaling relations in mass-deformed conformal gauge theories. *Phys. Rev.*, D82:014502, 2010, 1005.2371.

[122] Raul Alvares, Nick Evans, and Keun-Young Kim. Holography of the Conformal Window. *Phys. Rev.*, D86:026008, 2012, 1204.2474.

[123] David Kutasov, Jennifer Lin, and Andrei Parnachev. Holographic Walking from Tachyon DBI. *Nucl. Phys.*, B863:361–397, 2012, 1201.4123.

[124] Veselin G. Filev, Clifford V. Johnson, R. C. Rashkov, and K. S. Viswanathan. Flavoured large N gauge theory in an external magnetic field. *JHEP*, 10:019, 2007, hep-th/0701001.

[125] Kazumoto Haba, Shinya Matsuzaki, and Koichi Yamawaki. Holographic Technidilaton. *Phys. Rev.*, D82:055007, 2010, 1006.2526.

[126] Shinya Matsuzaki and Koichi Yamawaki. Holographic techni-dilaton at 125 GeV. *Phys. Rev.*, D86:115004, 2012, 1209.2017.

[127] Nick Evans and Kimmo Tuominen. Holographic modelling of a light technidilaton. *Phys. Rev.*, D87(8):086003, 2013, 1302.4553.

[128] Daniel Elander and Maurizio Piai. The decay constant of the holographic technidilaton and the 125 GeV boson. *Nucl. Phys.*, B867:779–809, 2013, 1208.0546.

[129] Daniel Elander, Carlos Nunez, and Maurizio Piai. A Light scalar from walking solutions in gauge-string duality. *Phys. Lett.*, B686:64–67, 2010, 0908.2808.

[130] Thomas Appelquist and Francesco Sannino. The Physical spectrum of conformal SU(N) gauge theories. *Phys. Rev.*, D59:067702, 1999, hep-ph/9806409.

[131] Dennis D. Dietrich, Francesco Sannino, and Kimmo Tuominen. Light composite Higgs from higher representations versus electroweak precision measurements: Predictions for CERN LHC. *Phys. Rev.*, D72:055001, 2005, hep-ph/0505059.

[132] V. A. Miransky. Dynamics in the conformal window in QCD like theories. *Phys. Rev.*, D59:105003, 1999, hep-ph/9812350.

[133] Biagio Lucini. Strongly Interacting Dynamics beyond the Standard Model on a Spacetime Lattice. *Phil. Trans. Roy. Soc. Lond.*, A368:3657–3670, 2010, 0911.0020.

[134] Luigi Del Debbio, Biagio Lucini, Agostino Patella, Claudio Pica, and Antonio Rago. The infrared dynamics of Minimal Walking Technicolor. *Phys. Rev.*, D82:014510, 2010, 1004.3206.

[135] Luigi Del Debbio, Biagio Lucini, Agostino Patella, Claudio Pica, and Antonio Rago. Mesonic spectroscopy of Minimal Walking Technicolor. *Phys. Rev.*, D82:014509, 2010, 1004.3197.

[136] Gunnar S. Bali, Francis Bursa, Luca Castagnini, Sara Collins, Luigi Del Debbio, Biagio Lucini, and Marco Panero. Mesons in large-N QCD. *JHEP*, 06:071, 2013, 1304.4437.

[137] Andreas Karch, Andy O'Bannon, and Kostas Skenderis. Holographic renormalization of probe D-branes in AdS/CFT. *JHEP*, 04:015, 2006, hep-th/0512125.

[138] K.C. Bowler, D.L. Chalmers, A. Kenway, R.D. Kenway, G.S. Pawley, and D.J. Wallace. A critique of quenched hadron mass calculations. *Physics Letters B*, 162(4):354 – 356, 1985.

[139] Huey-Wen Lin et al. First results from 2+1 dynamical quark flavors on an anisotropic lattice: Light-hadron spectroscopy and setting the strange-quark mass. *Phys. Rev.*, D79:034502, 2009, 0810.3588.

[140] S. Aoki et al. 2+1 Flavor Lattice QCD toward the Physical Point. *Phys. Rev.*, D79:034503, 2009, 0807.1661.

[141] C. Allton et al. 2+1 flavor domain wall QCD on a (2 fm)*83 lattice: Light meson spectroscopy with L(s) = 16. *Phys. Rev.*, D76:014504, 2007, hep-lat/0701013.

[142] J. T. Londergan, J. Nebreda, J. R. Pelaez, and A. Szczepaniak. Identification of non-ordinary mesons from the dispersive connection between their poles and their Regge trajectories: The $f_0(500)$ resonance. *Phys. Lett.*, B729:9–14, 2014, 1311.7552.

[143] Michael Teper. What lattice calculations tell us about the glueball spectrum. In *High-energy physics. Proceedings, International Europhysics Conference, Jerusalem, Israel, August 19-25, 1997*, pages 384–387, 1997, hep-ph/9711299.

[144] T. Vachaspati. Magnetic fields from cosmological phase transitions. *Phys. Lett.*, B265:258–261, 1991.

[145] Kari Enqvist and Poul Olesen. On the evolution of magnetic fields in the early universe. 1994, hep-ph/9405316.

[146] V. Skokov, A. Yu. Illarionov, and V. Toneev. Estimate of the magnetic field strength in heavy-ion collisions. *Int. J. Mod. Phys.*, A24:5925–5932, 2009, 0907.1396.

[147] S. Ejiri, F. Karsch, E. Laermann, C. Miao, S. Mukherjee, P. Petreczky, C. Schmidt, W. Soeldner, and W. Unger. On the magnetic equation of state in (2+1)-flavor QCD. *Phys. Rev.*, D80:094505, 2009, 0909.5122.

[148] Y. Aoki, G. Endrodi, Z. Fodor, S. D. Katz, and K. K. Szabo. The Order of the quantum chromodynamics transition predicted by the standard model of particle physics. *Nature*, 443:675–678, 2006, hep-lat/0611014.

[149] G. S. Bali, F. Bruckmann, G. Endrodi, Z. Fodor, S. D. Katz, S. Krieg, A. Schafer, and K. K. Szabo. The QCD phase diagram for external magnetic fields. *JHEP*, 02:044, 2012, 1111.4956.

[150] G. S. Bali, F. Bruckmann, G. Endrodi, Z. Fodor, S. D. Katz, and A. Schafer. QCD quark condensate in external magnetic fields. *Phys. Rev.*, D86:071502, 2012, 1206.4205.

[151] Gergely Endrodi. Critical point in the QCD phase diagram for extremely strong background magnetic fields. *JHEP*, 07:173, 2015, 1504.08280.

[152] S. P. Klevansky and R. H. Lemmer. Chiral-symmetry restoration in the nambu ˘ jona-lasinio model with a constant electromagnetic field. *Phys. Rev. D*, 39:3478–3489, Jun 1989.

[153] I.A. Shushpanov and A.V. Smilga. Quark condensate in a magnetic field. *Physics Letters B*, 402(3):351 – 358, 1997.

[154] Eduardo S. Fraga and Ana Julia Mizher. Can a strong magnetic background modify the nature of the chiral transition in QCD? *Nucl. Phys.*, A820:103C–106C, 2009, 0810.3693.

[155] Ana Julia Mizher, M. N. Chernodub, and Eduardo S. Fraga. Phase diagram of hot QCD in an external magnetic field: possible splitting of deconfinement and chiral transitions. *Phys. Rev.*, D82:105016, 2010, 1004.2712.

[156] Raoul Gatto and Marco Ruggieri. Deconfinement and Chiral Symmetry Restoration in a Strong Magnetic Background. *Phys. Rev.*, D83:034016, 2011, 1012.1291.

[157] Dmitri Kharzeev, Karl Landsteiner, Andreas Schmitt, and Ho-Ung Yee. Strongly Interacting Matter in Magnetic Fields. *Lect. Notes Phys.*, 871:pp.1–624, 2013.

[158] Vladimir A. Miransky and Igor A. Shovkovy. Quantum field theory in a magnetic field: From quantum chromodynamics to graphene and Dirac semimetals. *Phys. Rept.*, 576:1–209, 2015, 1503.00732.

[159] Eduardo S. Fraga, Jorge Noronha, and Leticia F. Palhares. Large N_c Deconfinement Transition in the Presence of a Magnetic Field. *Phys. Rev.*, D87(11):114014, 2013, 1207.7094.

[160] Kenji Fukushima and Yoshimasa Hidaka. Magnetic Catalysis Versus Magnetic Inhibition. *Phys. Rev. Lett.*, 110(3):031601, 2013, 1209.1319.

[161] Toru Kojo and Nan Su. The quark mass gap in a magnetic field. *Phys. Lett.*, B720:192–197, 2013, 1211.7318.

[162] G. Endroedi. QCD equation of state at nonzero magnetic fields in the Hadron Resonance Gas model. *JHEP*, 04:023, 2013, 1301.1307.

[163] Falk Bruckmann, Gergely Endrodi, and Tamas G. Kovacs. Inverse magnetic catalysis and the Polyakov loop. *JHEP*, 04:112, 2013, 1303.3972.

[164] Jingyi Chao, Pengcheng Chu, and Mei Huang. Inverse magnetic catalysis induced by sphalerons. *Phys. Rev.*, D88:054009, 2013, 1305.1100.

[165] Marcio Ferreira, Pedro Costa, Debora P. Menezes, Constanca Providencia, and Norberto Scoccola. Deconfinement and chiral restoration within the SU(3) Polyakov–Nambu–Jona-Lasinio and entangled Polyakov–Nambu–Jona-Lasinio models in an external magnetic field. *Phys. Rev.*, D89(1):016002, 2014, 1305.4751. [Addendum: Phys. Rev.D89,no.1,019902(2014)].

[166] Jens O. Andersen, William R. Naylor, and Anders Tranberg. Chiral and deconfinement transitions in a magnetic background using the functional renormalization group with the Polyakov loop. *JHEP*, 04:187, 2014, 1311.2093.

[167] Niklas Mueller, Jacqueline A. Bonnet, and Christian S. Fischer. Dynamical quark mass generation in a strong external magnetic field. *Phys. Rev.*, D89(9):094023, 2014, 1401.1647.

[168] M. Ruggieri, L. Oliva, P. Castorina, R. Gatto, and V. Greco. Critical Endpoint and Inverse Magnetic Catalysis for Finite Temperature and Density Quark Matter in a Magnetic Background. *Phys. Lett.*, B734:255–260, 2014, 1402.0737.

[169] R. L. S. Farias, K. P. Gomes, G. I. Krein, and M. B. Pinto. Importance of asymptotic freedom for the pseudocritical temperature in magnetized quark matter. *Phys. Rev.*, C90(2):025203, 2014, 1404.3931.

[170] M. Ferreira, P. Costa, O. Lourenco, T. Frederico, and C. Providencia. Inverse magnetic catalysis in the (2+1)-flavor Nambu-Jona-Lasinio and Polyakov-Nambu-Jona-Lasinio models. *Phys. Rev.*, D89(11):116011, 2014, 1404.5577.

[171] Alejandro Ayala, M. Loewe, Ana Julia Mizher, and R. Zamora. Inverse magnetic catalysis for the chiral transition induced by thermo-magnetic effects on the coupling constant. *Phys. Rev.*, D90(3):036001, 2014, 1406.3885.

[172] E. J. Ferrer, V. de la Incera, and X. J. Wen. Quark Antiscreening at Strong Magnetic Field and Inverse Magnetic Catalysis. *Phys. Rev.*, D91(5):054006, 2015, 1407.3503.

[173] Lang Yu, Jos Van Doorsselaere, and Mei Huang. Inverse Magnetic Catalysis in the three-flavor NJL model with axial-vector interaction. *Phys. Rev.*, D91(7):074011, 2015, 1411.7552.

[174] Jens Braun, Walid Ahmed Mian, and Stefan Rechenberger. Delayed Magnetic Catalysis. *Phys. Lett.*, B755:265–269, 2016, 1412.6025.

[175] Niklas Mueller and Jan M. Pawlowski. Magnetic catalysis and inverse magnetic catalysis in QCD. *Phys. Rev.*, D91(11):116010, 2015, 1502.08011.

[176] Alejandro Ayala, C. A. Dominguez, L. A. Hernandez, M. Loewe, and R. Zamora. Magnetized effective QCD phase diagram. *Phys. Rev.*, D92(9):096011, 2015, 1509.03345. [Addendum: Phys. Rev.D92,no.11,119905(2015)].

[177] Alejandro Ayala, C. A. Dominguez, L. A. Hernandez, M. Loewe, and R. Zamora. Inverse magnetic catalysis from the properties of the QCD coupling in a magnetic field. *Phys. Lett.*, B759:99–103, 2016, 1510.09134.

[178] Koichi Hattori, Toru Kojo, and Nan Su. Mesons in strong magnetic fields: (I) General analyses. *Nucl. Phys.*, A951:1–30, 2016, 1512.07361.

[179] Aftab Ahmad and Alfredo Raya. Inverse magnetic catalysis and confinement within a contact interaction model for quarks. *J. Phys.*, G43(6):065002, 2016, 1602.06448.

[180] Shijun Mao. Inverse magnetic catalysis in NambuJona-Lasinio model beyond mean field. *Phys. Lett.*, B758:195–199, 2016, 1602.06503.

[181] Johanna Erdmenger, Rene Meyer, and Jonathan P. Shock. AdS/CFT with flavour in electric and magnetic Kalb-Ramond fields. *JHEP*, 12:091, 2007, 0709.1551.

[182] Nick Evans, Astrid Gebauer, Keun-Young Kim, and Maria Magou. Holographic Description of the Phase Diagram of a Chiral Symmetry Breaking Gauge Theory. *JHEP*, 03:132, 2010, 1002.1885.

[183] N. Callebaut and D. Dudal. Transition temperature(s) of magnetized two-flavor holographic QCD. *Phys. Rev.*, D87(10):106002, 2013, 1303.5674.

[184] Niko Jokela, Alfonso V. Ramallo, and Dimitrios Zoakos. Magnetic catalysis in flavored ABJM. *JHEP*, 02:021, 2014, 1311.6265.

[185] Romulo Rougemont, Renato Critelli, and Jorge Noronha. Holographic calculation of the QCD crossover temperature in a magnetic field. *Phys. Rev.*, D93(4):045013, 2016, 1505.07894.

[186] D. Dudal, Diego R. Granado, and Thomas G. Mertens. No inverse magnetic catalysis in the QCD hard and soft wall models. *Phys. Rev.*, D93(12):125004, 2016, 1511.04042.

[187] Nick Evans, Astrid Gebauer, Maria Magou, and Keun-Young Kim. Towards a Holographic Model of the QCD Phase Diagram. *J. Phys.*, G39:054005, 2012, 1109.2633.

[188] Riccardo Apreda, Johanna Erdmenger, Nick Evans, and Zachary Guralnik. Strong coupling effective Higgs potential and a first order thermal phase transition from AdS/CFT duality. *Phys. Rev.*, D71:126002, 2005, hep-th/0504151.

[189] David Mateos, Robert C. Myers, and Rowan M. Thomson. Holographic phase transitions with fundamental matter. *Phys. Rev. Lett.*, 97:091601, 2006, hep-th/0605046.

[190] Carlos Hoyos-Badajoz, Karl Landsteiner, and Sergio Montero. Holographic meson melting. *JHEP*, 04:031, 2007, hep-th/0612169.

[191] M. Vojta. Lattice symmetry breaking in cuprate superconductors: stripes, nematics, and superconductivity. *Advances in Physics*, 58:699–820, November 2009, 0901.3145.

[192] D. V. DERYAGIN, D. YU. GRIGORIEV, and V. A. RUBAKOV. Standing wave ground state in high density, zero temperature qcd at large nc. *International Journal of Modern Physics A*, 07(04):659–681, 1992, http://www.worldscientific.com/doi/pdf/10.1142/S0217751X92000302.

[193] E. Shuster and D. T. Son. On finite density QCD at large N(c). *Nucl. Phys.*, B573:434–446, 2000, hep-ph/9905448.

[194] Mark G. Alford, Jeffrey A. Bowers, and Krishna Rajagopal. Crystalline color superconductivity. *Phys. Rev.*, D63:074016, 2001, hep-ph/0008208.

[195] Shin Nakamura, Hirosi Ooguri, and Chang-Soon Park. Gravity Dual of Spatially Modulated Phase. *Phys. Rev.*, D81:044018, 2010, 0911.0679.

[196] Hirosi Ooguri and Chang-Soon Park. Spatially Modulated Phase in Holographic Quark-Gluon Plasma. *Phys. Rev. Lett.*, 106:061601, 2011, 1011.4144.

[197] C. A. Ballon Bayona, Kasper Peeters, and Marija Zamaklar. A Non-homogeneous ground state of the low-temperature Sakai-Sugimoto model. *JHEP*, 06:092, 2011, 1104.2291.

[198] Oren Bergman, Niko Jokela, Gilad Lifschytz, and Matthew Lippert. Striped instability of a holographic Fermi-like liquid. *JHEP*, 10:034, 2011, 1106.3883.

[199] Aristomenis Donos and Jerome P. Gauntlett. Holographic striped phases. *JHEP*, 08:140, 2011, 1106.2004.

[200] Benjamin Withers. Holographic Checkerboards. *JHEP*, 09:102, 2014, 1407.1085.

[201] V. Alan Kostelecky and Stuart Samuel. Spontaneous Breaking of Lorentz Symmetry in String Theory. *Phys. Rev.*, D39:683, 1989.

[202] Anthony W. H. Preston and Tim R. Morris. Cosmological back-reaction in modified gravity and its implications for dark energy. *JCAP*, 1409:017, 2014, 1406.5398.

[203] Anthony W. H. Preston. Cosmological backreaction in higher-derivative gravity expansions. *JCAP*, 1608(08):038, 2016, 1605.06121.

[204] M. Pospelov and M. Romalis. Lorentz invariance on trial. *Phys. Today*, 57N7:40–46, 2004.

[205] T. Pruttivarasin, M. Ramm, S. G. Porsev, I. I. Tupitsyn, M. Safronova, M. A. Hohensee, and H. Haeffner. A Michelson-Morley Test of Lorentz Symmetry for Electrons. *Nature*, 517:592, 2015, 1412.2194.

[206] Ian Low and Aneesh V. Manohar. Spontaneously broken space-time symmetries and Goldstone's theorem. *Phys. Rev. Lett.*, 88:101602, 2002, hep-th/0110285.

[207] C. Vafa and E. Witten. Restrictions on symmetry breaking in vector-like gauge theories. *Nuclear Physics B*, 234(1):173 – 188, 1984.

[208] Cumrun Vafa and Edward Witten. Parity conservation in quantum chromodynamics. *Phys. Rev. Lett.*, 53:535–536, Aug 1984.

[209] Syksy Rasanen. Dark energy from backreaction. *JCAP*, 0402:003, 2004, astro-ph/0311257.

[210] Dominik J. Schwarz. Cosmological backreaction. In *On recent developments in theoretical and experimental general relativity, astrophysics and relativistic field theories. Proceedings, 12th Marcel Grossmann Meeting on General Relativity, Paris, France, July 12-18, 2009. Vol. 1-3*, pages 563–577, 2010, 1003.3026.

[211] Chris Clarkson, George Ellis, Julien Larena, and Obinna Umeh. Does the growth of structure affect our dynamical models of the universe? The averaging, backreaction and fitting problems in cosmology. *Rept. Prog. Phys.*, 74:112901, 2011, 1109.2314.

[212] Boudewijn F. Roukema, Jan J. Ostrowski, and Thomas Buchert. Virialisation-induced curvature as a physical explanation for dark energy. *JCAP*, 1310:043, 2013, 1303.4444.

[213] Thomas Buchert and Jurgen Ehlers. Averaging inhomogeneous Newtonian cosmologies. *Astron. Astrophys.*, 320:1–7, 1997, astro-ph/9510056.

[214] Thomas Buchert. On average properties of inhomogeneous fluids in general relativity. 1. Dust cosmologies. *Gen. Rel. Grav.*, 32:105–125, 2000, gr-qc/9906015.

[215] Xavier Roy, Thomas Buchert, Sante Carloni, and Nathaniel Obadia. Global gravitational instability of FLRW backgrounds — interpreting the dark sectors. *Class. Quant. Grav.*, 28:165004, 2011, 1103.1146.

[216] Thomas Buchert and Syksy Rasanen. Backreaction in late-time cosmology. *Ann. Rev. Nucl. Part. Sci.*, 62:57–79, 2012, 1112.5335.

[217] G. Hinshaw et al. Nine-Year Wilkinson Microwave Anisotropy Probe (WMAP) Observations: Cosmological Parameter Results. *Astrophys. J. Suppl.*, 208:19, 2013, 1212.5226.

[218] Stephen R. Green and Robert M. Wald. A new framework for analyzing the effects of small scale inhomogeneities in cosmology. *Phys. Rev.*, D83:084020, 2011, 1011.4920.

[219] Stephen R. Green and Robert M. Wald. Examples of backreaction of small scale inhomogeneities in cosmology. *Phys. Rev.*, D87(12):124037, 2013, 1304.2318.

[220] A.A. Starobinsky. A new type of isotropic cosmological models without singularity. *Physics Letters B*, 91(1):99 – 102, 1980.

[221] P. C W Davies, S. A. Fulling, S. M. Christensen, and T. S. Bunch. Energy-momentum tensor of a massless scalar quantum field in a robertson-walker universe. *Annals of Physics*, 109(1):108–142, 1977.

[222] P. A. R. Ade et al. Planck 2015 results. XX. Constraints on inflation. 2015, 1502.02114.

[223] T. Banks and A. Casher. Chiral symmetry breaking in confining theories. *Nuclear Physics B*, 169(1):103 – 125, 1980.